

214

**THE MECHANICAL EFFECTS
OF SHORT-CIRCUIT CURRENTS
IN OPEN AIR SUBSTATIONS
(PART II)**

**Working Group
23.03**

October 2002



THE MECHANICAL EFFECTS OF SHORT-CIRCUIT CURRENTS IN OPEN AIR SUBSTATIONS (PART II)

A companion book of the CIGRE brochure 105

PREFACE

This brochure is a companion of the former one published in 1996 by CIGRE (N°105) "The mechanical effects of short-circuit currents in open-air substations" which is in fact the "PART I". That brochure had been a revision of another brochure written in 1987 under the leadership of Zbigniew Nartowski (Energoprojekt, Cracow, Poland) the former chairman of the CIGRE working group dealing with that subject. Many ideas and proposal had already been described in the original 1987 brochure.

In 1992 CIGRE SC23 decided to restart the activity in short-circuit mechanical effects in open-air substations. This was due to the increase of knowledge in this field, especially in the field of the impact of dynamics forces on structural design. In fact electromagnetic forces induced large displacement and dynamic behaviour of cables and supports.

The first step, published in 1996 (CIGRE thematic brochure N°105), concerned simplified methods. Brochure 105 explains the background of IEC 60865-1 and gives access to a data base of 40 short-circuit tests performed in the world, with data and oscillogramms.

Actual IEC 60865 (part 1 and 2) helps to define maximum loads and minimum clearances which have to be taken into account as static load and distances for design. By this, the design of towers can be either too conservative or, rarely, in the opposite site.

This brochure will detail why and how to go further in these methods. Moreover, there is no actual IEC recommendation for short-circuit mechanical loads on apparatus which are connected to the main bus at upper level by slack cable. Some hypothesis of actual IEC rules like neglecting the reclosure in flexible busbars will be analysed in more details on the base of actual full scale tests.

Advanced methods will be shortly presented as well as an introduction to probabilistic approach.

This brochure has been written by the members of the CIGRE ESCC (effects of short-circuit current) task force and revised by WG 23-03 (chairman H. Böhme (ABB, Heidelberg), followed recently by A-M Sahazizian from (One, Canada) and SC 23 of CIGRE. Many members of this CIGRE activity are also members of IEC TC73 as well as CIGRE SC23 and D. Tsanakas (Univ. of Patras, Greece) was our official liaison to both SC23 and IEC TC73 as

member and convener of WG2 "short-circuit effects".

This brochure follows the main chapters of the former brochure.

An alphabetical list of the authors of this brochure follows :

G. Declercq	RTE, France
M. El Adnani	Univ. Marrakech, Morocco
J.L. Lilien (Convener)	Univ. Liège, Belgium
W. Meyer	Univ. of Erlangen-Nürnberg, Germany
A.M. Miri	Univ. Karlsruhe, Germany
K.O. Papailiou	SEFAG, Switzerland
D. Roeder	Siemens, Germany
N. Stein (Secretary)	FGH, Germany
D. Tsanakas	Univ. of Patras, Greece

This document has been approved by :

M. Pettersson., convener of CIGRE SC 23

Mrs. Sahazizian, convener of CIGRE WG 23-03

M. Oeding chairman of IEC TC 73

M. Lilien, convener of CIGRE ESCC task force

The target groups for this brochure can be defined as follows :

- IEC, the CIGRE brochure being the technical base for the methods to be suggested in substation design against short-circuit mechanical loading
- Substations engineers, to understand the technical background existing behind IEC methods from one side, to think about system design taking into consideration SCC loads at early stage and not simply to verify structures against SCC loads, to give them trends to decrease SCC loading for uprating, refurbishment as well as designing new substations
- Technical group like equipment suppliers, to help them providing new design, not only for static loads but also for dynamic loading.

The authors gratefully acknowledge G. Declercq, E. Janvier (RTE) for his wonderful editorial task and A-M Sahazizian (Hydro One, Canada) for her English language revision.

CONTENTS

1. INTRODUCTION	5
1.1. General presentation of the book content	5
1.2. General presentation of the main problem	6
1.3. Substations mechanical characteristics	7
1.3.1. Insulator support dynamic behaviour	7
1.3.2. Typical apparatus dynamic behaviour.....	7
1.3.3. Rough evaluation of the basic frequency of insulators apparatus and supporting structures.	8
1.3.4. Main busbars frequencies.....	9
2. RIGID BUSBARS	10
2.1. Introduction.....	10
2.2. Short-circuit Strength according to IEC 60865-1 and EN 60865-1	10
2.2.1. Method	10
2.2.2. Short-circuit current forces.....	11
2.2.3. Bending stresses in the conductors taking into account plastic effects and forces on the substructures 13	
2.2.4. Relevant natural frequencies of main- and sub-conductors.....	20
2.2.5. Section moduli of main and sub-conductors	24
2.2.6. Superposition of stresses in conductors.....	27
2.3. Special Configurations.....	28
2.3.1. Associated phase structures busbar on a common support.....	28
2.3.2. Influence of two busbars	31
3. FLEXIBLE BUSBARS.....	36
3.1. Introduction.....	36
3.2. Typical Oscillograms and Calculations.....	37
3.2.1. Typical oscillograms of forces in the bus.....	37
3.2.2. Application of advanced method on high voltage busbar system	39
3.3. The dropper behaviour.....	42
3.3.1. Introduction.....	42
3.3.2. Typical oscillograms	42
3.3.3. Advanced computation results	44
3.3.4. Simplified methods	46
3.4. The bundle pinch.....	52
3.4.1. Introduction.....	52
3.4.2. Advanced computation results	53
3.4.3. Dynamic behaviour of close and various degrees of wide bundling.....	54
3.5. Load on Portals, apparatus terminals and equivalent static load.....	58
3.5.1. Introduction.....	58
3.5.2. Maximum instantaneous load and equivalent static load for dropper stretch.....	58
3.5.3. Maximum instantaneous load and equivalent static load for bundle pinch.....	58
3.5.4. Maximum instantaneous load and equivalent static load for Ft, Ff.....	59
3.6. ESL factors from numerical simulations.	60

3.7.	Special problems	61
3.7.1.	Auto-reclosing.....	61
3.7.2.	Interphase-Spacer.....	62
3.7.3.	A new simplified method for spacer compression evaluation.....	65
3.7.4.	Jumpers	68
3.7.5.	Springs in strained spans.....	68
4.	GUIDELINES FOR DESIGN AND UPRATING	69
4.1.	Introduction.....	69
4.2.	Limitation of magnitude and duration of short-circuit current.....	69
4.3.	Flexible conductors	69
4.4.	Supporting Structures	70
4.5.	Foundations	70
4.6.	Safety factors and load combinations.....	70
4.6.1.	Substations	71
4.7.	Clearances.....	71
5.	PROBABILISTIC APPROACH TO SHORT-CIRCUIT EFFECTS.....	73
5.1.	THE VARIOUS POSSIBLE APPROACHES	73
5.1.1.	Deterministic Methods.....	74
5.1.2.	First Level Probabilistic Method.....	74
5.1.3.	Second Level Probabilistic Method	74
5.1.4.	Optimization.....	75
5.2.	SECOND LEVEL PROBABILISTIC METHOD.....	77
5.2.1.	Stress and strength relationship for supporting insulators.....	77
5.2.2.	A global Approach	80
5.2.3.	A Calculation Method.....	80
5.3.	CONCLUSIONS	96
6.	D.C. CONFIGURATIONS.....	97
6.1.	Introduction.....	97
6.2.	Short-circuit Currents and Electromagnetic Forces.....	97
6.2.1.	Short-circuit current characteristics measured	97
6.2.2.	Standardised characteristics of short-circuit currents and electromagnetic forces	99
6.3.	Mechanical and Thermal Stress.....	100
6.3.1.	Conditions for the equivalent function.....	100
6.3.2.	Calculation of the parameters of the equivalent functions	101
6.3.3.	Mechanical stress	104
6.3.4.	Thermal stress	105
6.4.	Conclusion	105
7.	REFERENCES.....	106
8.	ANNEX	112

8.1.	The Equivalent Static Load and equivalent static load factor	112
8.1.1.	Definition of ESL (Equivalent Static Load) and ESL factor	112
8.1.2.	Concerned structures	113
8.1.3.	Concerned loadings	113
8.1.4.	How to use ESL in design together with simplified method of actual IEC 60865	113
8.1.5.	Validation of the method : How to evaluate ESL during tests or advanced simulations	113
8.1.6.	Examples	113
8.2.	Clamped-free beam dynamic response to a top load identical to a short-circuit force. ESL value, ESL factor for different structural data of the support.....	116
8.2.1.	The geometry	116
8.2.2.	Excitation	116
8.2.3.	Examples	116
8.3.	Comparison of Test Results and Calculation According to IEC Publication 60865-1	119
8.3.1.	Slack conductors on supporting insulators	119
8.3.2.	Strained conductors	120
8.3.3.	Bundle pinch effect	126
8.3.4.	Conclusions	127
8.4.	INFLUENCE OF THE RECLOSURE	128
8.5.	EXAMPLE OF RECLOSURE CALCULATION.....	131
8.6.	Flow Charts to the Standardised Method for rigid busbars	133
8.7.	Errata to Brochure No 105.....	140

1. INTRODUCTION

1.1. GENERAL PRESENTATION OF THE BOOK CONTENT

This brochure is a companion to CIGRE thematic publication 105 published in 1996 [Ref 101] on the same subject.

Publication 105 can be considered as a very useful tool for defining the problem of short-circuit mechanical effects in substations with rigid or flexible busbars. The content has been transposed to IEC recommendation 60865 [Ref 2].

This book is divided in several parts. Some of one being considered as a definitive proposal (like rigid conductors), others are completely new approach (like equivalent static load in flexible conductors), considered as enough mature to be included in IEC and others are proposal for future trends (probabilistic approach).

In the past only the static behaviour of the support has been taken into account. Recent development concerns a more comprehensive approach of bundle pinch effect, dropper stretch and other features and their true impact on design as dynamic loading.

The new approach for flexible busbars is closely related to the dynamics of structures. The reader, not expert in that field, will find in annex 1 some basics.

This brochure is focused on dynamic effects and corresponding methods to define actual design loads for substations. A very good tentative has already been described in brochure 105 [Ref 101] as far as it concerns rigid busbars (see also chapter 2 hereafter). However, flexible busbars had not been evaluated in a similar way. The existing methods define maximal tensile load in the conductor but there are no detailed methods to define corresponding design loads. In a sense these loads have to be considered as acting in a quasi-steady regime, which is not true in most of the actual cases.

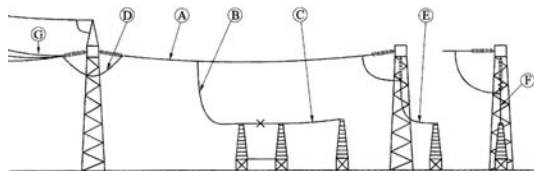


Figure 1.1 Flexible bus configuration for calculation and tests
A) horizontal strain bus connected by insulator chains to steel structures
B) vertical dropper between strained bus and apparatus
C) horizontal connection between components
D) jumper connecting two strained conductor sections
E, F) end-span droppers (classical or spring loaded).

The Figure 1.1 details typical flexible busbars layout. Only case A has been evaluated in the former brochure. And even in the treated cases, the evaluation was restricted to estimate tension in the main bus (A on the Figure 1.1) in case of single and bundle conductors. Maximum tension in the cable is not necessary a design load for the supporting structure.

Annex 8.3 details what is possible to evaluate using former brochure 105.

Moreover, to evaluate correctly the design load, we will also consider new cases, like dropper (case B (in-span dropper), E (end-span dropper), D (jumper)).

The relationship between forces and design loads is strongly related to dynamic behaviour of structures. As power engineers are not generally familiar with such problems, some detailed informations will be given.

The content of the brochure is divided in 6 chapters, one annex, references and a detailed new data base on short-circuit tests (new cases supplement brochure 105, volume 2).

Chapter 2 deals with rigid busbars. In the 105 brochure [Ref 101], the electromagnetic forces on the conductors are discussed and their dynamic effects on the arrangements shown. In this paper, first the simplified method stated in the IEC Publication 60865-1 [Ref 2] and the European Standard EN 60865-1 [Ref 3] is described and it is shown that a permitted use of plastic deformation allows a higher loading. In the second part, the calculation of forces and stresses in special configurations is derived such as associated phase structures busbar on a common support, parallel busbars.

Chapter 3 deals with flexible bus systems.

Chapter 4 is giving extra recommendations (see also brochure 105) for design and uprating.

Chapter 5 is giving a new trend in the design approach, taking into account probabilistic aspects. There is not yet a consensus of using such methods mainly because of the lack of data's needed to use them. However, they can bring substantial benefit in substation design and such approaches have merit to be presented and this brochure is addressing them.

In power plants and substations, dc auxiliary systems are used to supply motors, measuring devices and other kind of loads. Power converters, storage batteries, smoothing capacitors and motors can cause high short-circuit currents which lead to high mechanical and thermal stresses. Therefore in chapter 6, the variety of short-circuit currents occurring in dc configurations are presented and

standardized characteristics for the currents and electromagnetic forces are introduced. With this, simplified methods are derived to calculate the mechanical and thermal effects which are stated in IEC 61660-1 and IEC 61660-2 [Ref 59, Ref 61].

In the Annex, the equivalent static load and the equivalent static load factor are defined and evaluated for different kinds of supporting and short-circuit loading, the calculation according to IEC 60865-1 are compared with test results, the influence of reclosure is shown and a simplified method for calculation is derived, and flow charts to the standardized method for rigid busbars is given. Errata to the brochure 105 complete this part.

1.2. GENERAL PRESENTATION OF THE MAIN PROBLEM

Let's recall some basic of physics in relation with short-circuit mechanical effects, in the case of a flexible busbar. This understanding is favourably accompanied by the observation of the video which detailed some short-circuit tests on rigid and flexible busbar (available at CIGRE central office).

After short-circuit inception, the flexible bus starts to swing. If both currents are flowing in opposite direction (typical two-phase fault) the conductors will separate from each other. If both currents are flowing in the same direction (two conductor of one bundle for example) the conductors will come together. After a short while, there is not only kinetic, potential and electromagnetic energy (this last disappearing at the end of the short-circuit), but some deformation energy (elongation of the cable which causes tension fluctuations and strain energy in support) and thermal energy (due to heating effects). Of course damping is present (structural damping and aerodynamic damping) but it is negligible at the beginning compared to other energies.

Thus after short-circuit inception, there is a big mixture and exchange of energy which finally disappears due to damping.

Typical maximum loads for design, generally appear when global energy has to be mostly converted into deformation energy. This is especially the case during maximum swing out (very low kinetic and potential energy so that a large part is converted in deformation energy, which means a large increase of tension), the falling down maxima (same reason, generally more critic because of the loss of potential energy due to cable position at that moment), and the pinch effect (same reason also, but at that time we have the full electromagnetic energy, especially during asymmetrical part of the current, and the other

kinds of energy have not yet started to take their part). On the following figures you can see the three typical maxima during short-circuit on a flexible bus-bars.

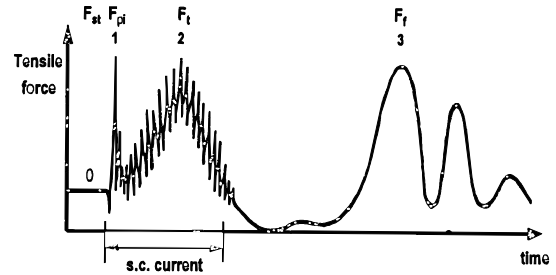


Figure 1.2 Measured tensile force of a flexible bundle conductor during and after a line-to-line short-circuit (F_{st} , static force, F_{pi} , pinch force, F_i , tensile force, F_f drop force)

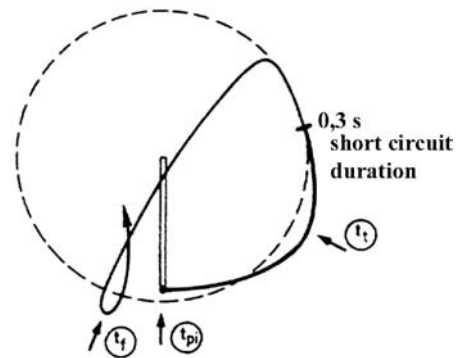


Figure 1.3 Movement of a flexible conductor during and after a line-to-line short-circuit

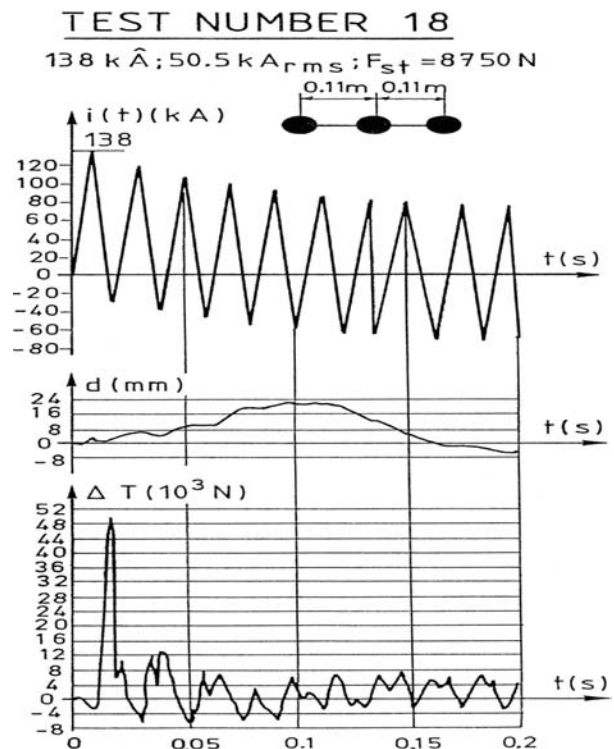


Figure 1.4 Schematic short-circuit current wave shape ($i(t)$, portal displacement (d) and tension increase (ΔT) (pinch effect) in the bus. There is a 50 kN increase over an initial 8.7 kN.

The pinch (first maximum) can be very high (up to 6 times the static value) and this has been observed during tests. It must be noted that supporting structure (d) did not move at all as tension (ΔT) varied in the cable (Figure 1.4), the maximum tension occurring when the structure has not yet really moved. It is a clear dynamic effect.

Is there any real need to design for such a high load value ? The answer is certainly positive for spacer compression and attachment clamps, but probably not for supporting structures and apparatus, which have large inertia and which could be unaffected to such instantaneous loads. Coming back to Figure 1.4, it is clear that supporting structure design is more related to its top displacement than to the applied forces.

Another clear known case is the movement of the cable (or the rigid bus), which is obviously not affected by the 50 Hz component of the electromagnetic loads. Sometimes the cable does not even move (or it moves so little) that the short-circuit is already finished. But after that the cable starts to move and the movement can be quite large. Corresponding frequency at the movement is clearly free vibration frequency of the cable alone. In such cases, the study of the movement can be done by completely neglecting frequency component of the forces, and only taking into account the pseudo-continuous component of the electromagnetic forces. That is for example why, in a three phase short-circuit, the middle phase remains more or less stable despite the fact that higher peak forces are acting on it. In such a case, there are no or very limited pseudo-continuous component of the middle phase.

Why some structure are not reacting against applied loads following their temporal evolution ?

This is because a supporting structure will not react to such a dynamic load as it is the case for slow time evolution loads (so called quasi-static loads).

The question is what is a quick load, what is a quasi-static load.

And finally how to take these loads into account for the design, this is one of the goals of this brochure.

But first let's remember what kind of problems have been solved in the former brochure.

The methods described in the former brochure give access to typical maximum forces that occur during short-circuit in most classical dispositions.

To design a substation, one needs to define a new step to go from applied forces to stresses created in the bus, attachments and in the supporting or anchoring structure.

For static loads, the relationship between forces and stresses can easily be managed, but for dynamic loading, inertial forces can induce dramatic changes for the design (see annex 8.1 for some basic tutorial on the subject).

1.3. SUBSTATIONS MECHANICAL CHARACTERISTICS

This chapter is presenting basic data for a typical portal and insulator stiffness and dynamic behaviour of supports and apparatus.

1.3.1. Insulator support dynamic behaviour

Next figure is a typical frequency response of a bus supporting insulator :

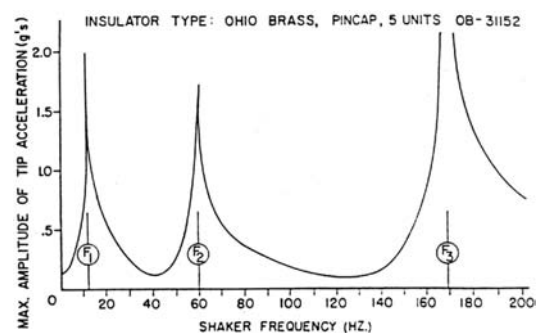


Figure 1.5 Ohio Brass cap and pin, 5 units, 550 kV, 1,84 m Graph of the dynamic response of insulator tip versus the frequency of the applied excitation force. ($f_1 = 10,2$ Hz ; critical damping = 0,025 ; $f_2 = 63$ Hz ; $f_3 = 172$ Hz)

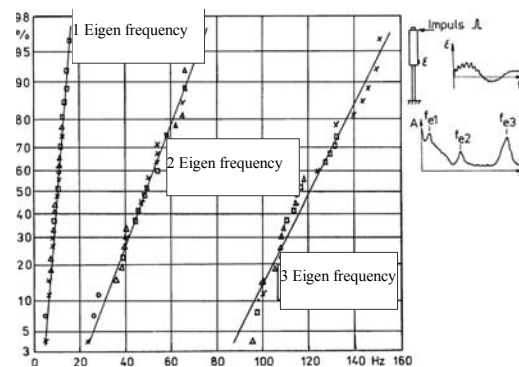


Figure 1.6 This fig. details the distribution of frequencies for similar 110 kV supporting insulators. It is clear from this fig. that the knowledge of a frequency must be considered inside a range.

1.3.2. Typical apparatus dynamic behaviour

The next figures represent modal shapes of typical substation apparatus (obtained by computer modelling) :

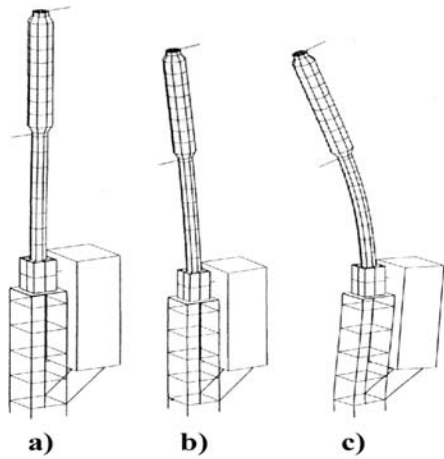


Figure 1.7 a) 245 kV **circuit breaker**
 b) first modal shape (3,4 Hz)
 c) second modal shape (20,3 Hz)

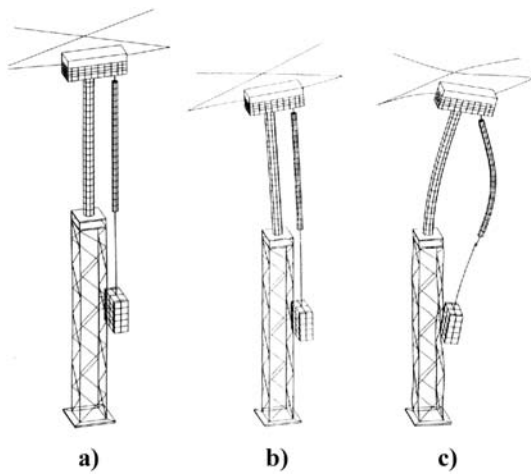


Figure 1.8 a) 245 kV Pantograph disconnector
 b) first modal shape (3,8 Hz)
 c) second modal shape (26,5 Hz)

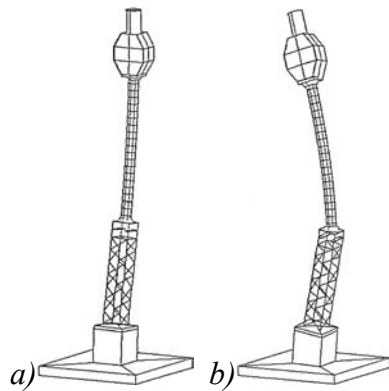


Figure 1.9 550 kV **current transformer**
 a) Eigenfrequency 1,840 Hz
 b) Eigenfrequency 7,603 Hz

1.3.3. Rough evaluation of the basic frequency of insulators apparatus and supporting structures.

1.3.3.1 Insulator support and apparatus

We can try to make a rough estimation of basic frequencies for typical apparatus: In the absence of data, Figure 1.12 can be used for a first rough estimate of any structures in substations. The middle dotted straight line can be used for supporting insulators, the upper straight line is upper border for insulator support and the lower straight line is the bottom border for insulator support (mainly composite). This can also be used for any apparatus (current transformer, circuit breaker, isolator, surge arrester). The height includes supporting structure.

The figure gives access to the main first eigenfrequency, which will be used in this brochure to evaluate the Equivalent Static Load (see further). The horizontal shaded areas highlight the resonance risk areas for a 50 Hz network. There are three zones corresponding to the cases of resonance on the first eigenmode and the second eigenmode in relation with either 50 or 100 Hz component of excitation frequencies. There is evidence that 400 kV range is free of resonance problems and that 123 kV up to 245 kV is certainly more prone to such problems.

It is not just a coincidence that all these different kind of supports have similar eigenfrequencies with only one main parameter: the height (means the voltage). You have to remember that the eigenfrequency of a clamped-free beam is inversely proportional to the square of its length and proportional only to the square root of its young's modulus (more or less the same for all apparatus, except for fiber glass) and of its moment of inertia (means mainly its outside diameter, also very similar for all cases).

Table 1.1 gives the range of basic data for typical substation structures like post insulators and gantries.

		Rated Voltage/ nominal voltage (kV)		
		123/ 110	245/ 220	420/ 380
Post insulators				
Height	m	1..7	2,1..2,5	3,15..4,5
Mass	kg	35..200	120..400	250..650
Cantilever strength	kN	4..16	8..16	8..16
Stiffness	N/mm	300..2500	40..200	40..140
First natural frequency	Hz	20..60	7..14	4..12
Damping log decr.	%	2	2	2
Supporting structures for flexible bus (gantries)				
Height	m	5..6	8..10	12..15
Stiffness	N/mm	150..1300	500..800	600..3500
First natural frequency	Hz	3..6	3..5	1..4

Table 1.1 Basic data for typical substation structures

1.3.3.2 Supporting structures

Similar tests have been performed on truss supporting structure. The structure used for FGH tests (see volume 2 of this brochure) has been thoroughly studied as far as it concerns its dynamic properties. Some of the results are detailed below.

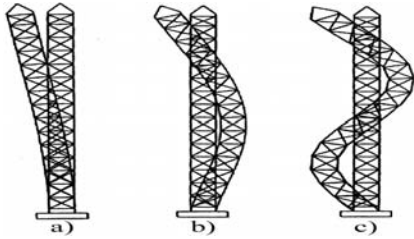


Figure 1.10 North portal eigenfrequencies
 a) calculated 3,42 Hz, measured 3,40 Hz
 b) calculated 13,19 Hz
 c) calculated 24,97 Hz

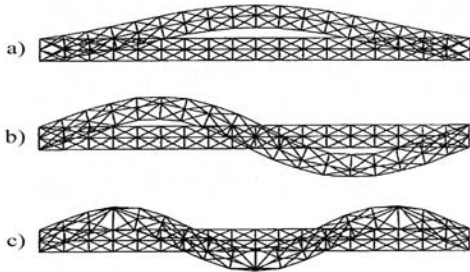


Figure 1.11 Crossarm eigenfrequencies
 a) calculated 10,74 Hz, measured 9,62 Hz
 b) calculated 26,46 Hz
 c) calculated 59,24 Hz

The first eigenfrequency of the whole structure is obviously less than the slowest one and it is obviously related to vertical frame which is in this case around 4 Hz (see exact data in volume 2).

1.3.4. Main busbars frequencies

- rigid conductors : see chapter2, generally in the range 3-5 Hz
- Flexible conductors: Cable structure in substation, for busbars, is generally a leveled span made of single or bundle conductors. The basic oscillation frequency is given by the inverse of (*23) (References to clauses, equations and figures of IEC60865-[Ref 2] are marked by an asterisk (*)), generally in the range 0.3 – 0.5 Hz, ten times lower than rigid busbar.

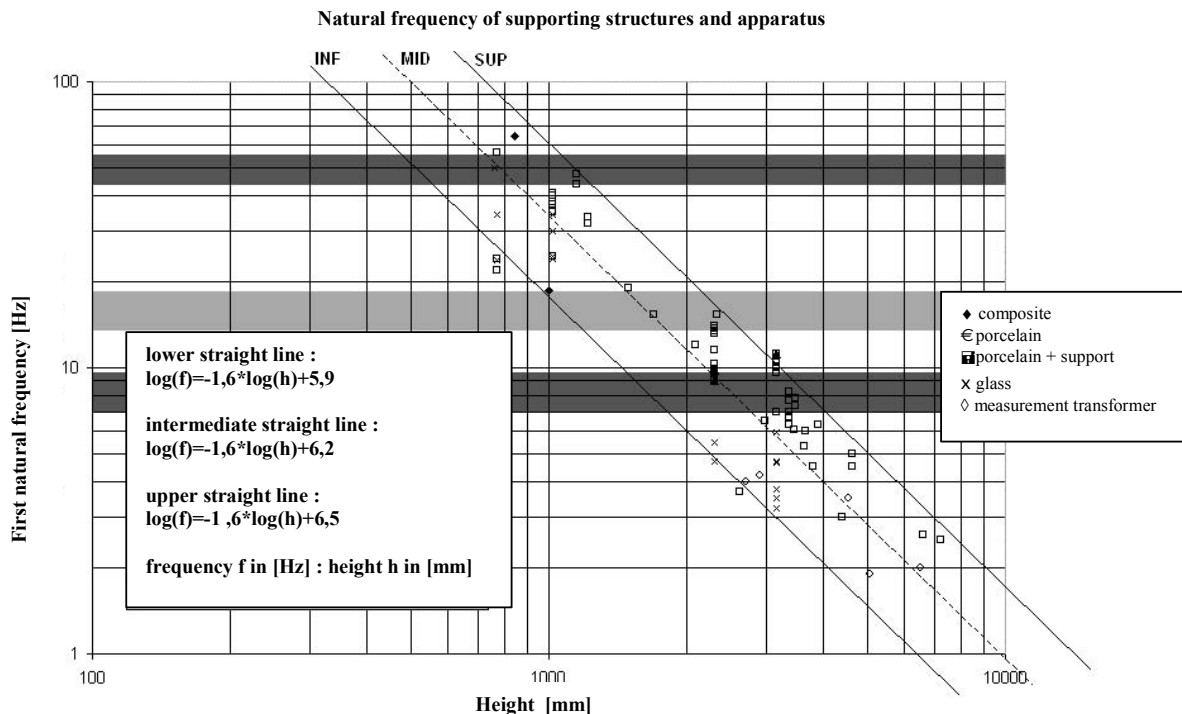


Figure 1.12 Insulator support glass, porcelain or composite and measuring transformer from 63 to 765 kV (Courtesy RTE, Rosenthal, Ceralep, Sediver, Groupe Schneider, Alstom (Balteau))

2. RIGID BUSBARS

2.1. INTRODUCTION

Rigid busbars are used at all voltage and current levels and distinguish themselves in need of less space in contrast to busbars with flexible conductors. Conductors used usually have tubular or rectangular profile and are mounted on supporting structures mainly composed of insulators and steel structures.

In the brochure No 105 [Ref 1], the electromagnetic forces on the conductors in one plane are derived and discussed, and their dynamic effects on the arrangements are shown. This section continues the presentation on rigid busbars and is divided in two parts. In sub-section 2.2, the simplified method stated in the IEC Publication 60865-1 [Ref 2] and the European Standard EN 60865-1 [Ref 3] is described and shown that a permitted use of plastic deformation allows a higher loading. In sub-section 2.3, special configurations are regarded such as parallel busbars, associated phase structures on a common support, the influence of two busbars.

2.2. SHORT-CIRCUIT STRENGTH ACCORDING TO IEC 60865-1 AND EN 60865-1

Advanced methods allow to evaluate time histories of stresses, forces and displacements caused by short-circuit currents with high accuracy in any structure of substations with rigid conductors. But this needs many detail data for input. Very often busbars are built with conductors side by side in one plane. For this purposes, simplified methods are very useful. The short-circuit strength of three-phase systems and single-phase two-line systems can be established with the IEC Publication 60865-1 [Ref 2] and the European standard EN 60865-1 [Ref 3]; both have an identical wording.

The method used with rigid busbars had been described first in 1955 by W. Lehmann [Ref 4] and in 1961 it had been taken over in the first edition of the German standard VDE 0103 [Ref 5]. New investigations had been dropped in the following editions. In 1986, the first IEC Publication 865 [Ref 6] had been published and in 1993 the actual standard IEC/EN 60865-1 [Ref 2, Ref 3] was approved.

This method stated in the standard determines the short-circuit stresses and forces with the rules of statics and the dynamic of the system is taken into account by 'dynamic factors'. The permission to restrict stresses not only to elasticity of the material but also to allow plastic deformations makes possible a better utilisation of the material and therefore a more economical design.

The derivation of the method and the background are written in many publications and internal reports in

which, however, only aspects of the method are given. A complete presentation has not been available until now. To explain the background of the standard it is necessary to look at the totality of all substations with different types of conductors, supports and so on. That means all voltage levels have to be regarded: High voltage HV as well as medium voltage MV and low voltage LV.

2.2.1. Method

The electromagnetic forces on the conductors caused by the short-circuit currents in the conductors act on arrangements, which are called supporting framework made from elastic beams. The time dependent current forces induce oscillations, and there are maximum values of effects in certain locations at certain times: maximum deflection, maximum stress in the conductor, maximum forces on sub-structures. If the last two mentioned force are known, the short-circuit strength of an arrangement can be usually assessed with sufficient accuracy. Normally only the values of the maxima are needed and not the location or time.

Therefore IEC/EN 60865-1 calculates maximum values for the conductor stress including its strength and the forces on the substructures; the maximum deflection is not of interest. The method is adjusted to practical requirements and contains simplifications with safety margins.

The calculations are done in two steps according to the rules of statics:

- The maximum of the short-circuit current force acts as a static force F on the conductors and from this the relevant quantities are calculated.
- The dynamic response of the structure due to the time dependent excitation is described by the factors :

$$(2.1) \quad V = \frac{\text{response caused by dynamic load}}{\text{response caused by static load}}$$

- They are different for conductor stresses and forces on the substructures. With these factors the static calculated quantities are multiplied to get the actual dynamic response of the structure.

These steps can also be read as follows: The static force F is multiplied with the dynamic factor V and this force $V \cdot F$ acts as an equivalent static load ESL on the arrangement and gives the relevant quantities for design.

Remains be proven whether the maximum permissible stresses are exceeded or not.

There has been a great effort to get the factors V : Tests with actual arrangements, analytical and numerical calculations were required.

This method allows to state the short-circuit strength of usual arrangements with acceptable effort and makes it possible without a lot of parameter investigations to define the optimal design. Using pc-programs, e.g. [Ref 7], the evaluation can be done quickly and comfortably.

The calculation runs in the following steps:

- Calculation of the peak value of the forces between conductors during a three-phase short circuit

$$(2.2) \quad F_{m3} = \frac{\mu_0}{2\pi} \frac{\sqrt{3}}{2} i_{p3}^2 \frac{l}{a_m}$$

during a line-to-line short circuit in single-phase systems

$$(2.3) \quad F_{m2} = \frac{\mu_0}{2\pi} i_{p2}^2 \frac{l}{a_m}$$

and the peak value of the forces between sub-conductors during a three-phase or a line-to-line short circuit

$$(2.4) \quad F_s = \frac{\mu_0}{2\pi} \left(\frac{i_p}{n} \right)^2 \frac{l_s}{a_s}$$

i_{p3} , i_{p2} , i_p are the peak values of the short-circuit currents, l is the centre-line distance of the supports, l_s is the centre-line distance between two spacers, a_m , a_s the effective distances between main conductors and sub-conductors and n the number of sub-conductors. In the following, for F_m is to be inserted either F_{m3} or F_{m2} .

- Calculation of the conductor stress caused by the force F_m between main conductors

$$(2.5) \quad \sigma_m = V_\sigma V_r \beta \frac{F_m l}{8Z_m}$$

and the conductor stress caused by the force F_s between sub-conductors

$$(2.6) \quad \sigma_s = V_{\sigma s} V_{r s} \frac{F_s l_s}{16Z_s}$$

The factors V_σ , $V_{\sigma s}$ take into account the dynamic of the system, V_r the increase of the stress due to unsuccessful three-phase automatic reclosing and β the type and number of supports of the conductor. Z_m , Z_s are the section moduli of the main and sub-conductor respectively.

- Both conductor stresses shall not be greater than limitations given by material and geometry properties

$$(2.7) \quad \sigma_{\text{tot}} = \sigma_m + \sigma_s \leq qR_{p0,2}$$

and in the sub-conductor

$$(2.8) \quad \sigma_s \leq R_{p0,2}$$

with the factor of plasticity q and the stress corresponding to the yield point $R_{p0,2}$.

- Calculation of the forces on the supports due to the force F_m between main conductors

$$(2.9) \quad F_d = V_F V_r \alpha F_m$$

V_F and V_r are due to the dynamic forces and α is the distribution of the forces on to the supports.

- For $V_\sigma V_r$, $V_{\sigma s} V_r$ and $V_F V_r$ maximum values can be used. Lower values are possible if they are estimated as a function of the relevant natural frequency of the conductor. This becomes for main conductor consisting of a single conductor

$$(2.10) \quad f_c = \frac{\gamma}{l^2} \sqrt{\frac{EJ_m}{m'}}$$

for a main conductor consisting of sub-conductors

$$(2.11) \quad f_c = c \frac{\gamma}{l^2} \sqrt{\frac{EJ_s}{m'_s}}$$

for a sub-conductor

$$(2.12) \quad f_{cs} = \frac{3,56}{l_s^2} \sqrt{\frac{EJ_s}{m'_s}}$$

The factor γ considers the type and number of supports, c the location and the mass of the spacers. E is the Young's modulus; J_m , J_s are the moments of area, m' , m'_s the masses per unit length.

The detailed flow-chart of the procedure is given in the Annex 8.6 for calculation without and with relevant natural frequency.

Arrangements which cannot be calculated with the simplified method stated above or if the time histories of the stresses, forces, displacements are needed to detect weak points then the investigation can be done by use of e.g. Finite-Element-Method.

2.2.2. Short-circuit current forces

Short-circuit currents in the conductors give electromagnetic forces acting on the conductors. On a single main conductor there are only the forces caused by the other main conductors. If the main conductor consists of two and more sub-conductors, in addition, the forces between the sub-conductors of the same main-conductor are to be regarded. Due to the different distances between the sub-conductor referred to and all other sub-conductors, the maxima of the time functions depend on the effective distances between the conductors. The calculation can be extensive even if constant current density is assumed. The consideration of current displacement is only possible by use of Current-Splitting-Method or Finite-Element-Method. For standardisation Such a procedure is not possible for standardization and simplifications have to be done.

In HV-substations, mainly single conductors with tubular profiles are used and the effective distances between the conductors coincide with the center-line distances. For this arrangements of conductors in one plane, the electromagnetic forces are analysed in detail in [Ref 1, Ref 8, Ref 9, Ref 10]. Here are given only the results.

The time functions of the electromagnetic forces consist of four partial functions:

$$(2.13) \quad F(t) = \underbrace{F_0 + F_{2\omega}(t)}_{\text{steady state}} + \underbrace{F_g(t) + F_\omega(t)}_{\text{decaying}}$$

- constant term F_0 , arithmetic mean of $F(t)$ in steady state;
- undamped oscillation $F_{2\omega}(t)$ at double the electrical frequency;
- exponential term $F_g(t)$, decaying with $\tau/2$;
- oscillation $F_{2\omega}(t)$ with electrical frequency, decaying with τ .

τ is the time constant of the electrical network.

The maximum values are:

- three-phase short-circuit, inner conductor L2:

$$(2.14) \quad F_{m3,L2} = \frac{\mu_0}{2\pi} \frac{\sqrt{3}}{2} i_{p3}^2 \frac{l}{a_m} = 0,866 \frac{\mu_0}{2\pi} i_{p3}^2 \frac{l}{a_m}$$

- three-phase short-circuit, outer conductors L1 and L3:

$$(2.15) \quad \begin{aligned} F_{m3,L1} = F_{m3,L3} &= \frac{\mu_0}{2\pi} \frac{3 + 2\sqrt{3}}{8} i_{p3}^2 \frac{l}{a_m} \\ &= 0,808 \frac{\mu_0}{2\pi} i_{p3}^2 \frac{l}{a_m} \end{aligned}$$

- line-to-line short-circuit:

$$(2.16) \quad \begin{aligned} F_{m2} &= \frac{\mu_0}{2\pi} i_{p2}^2 \frac{l}{a_m} = \frac{\mu_0}{2\pi} \left(\frac{\sqrt{3}}{2} i_{p3} \right)^2 \frac{l}{a_m} \\ &= 0,750 \frac{\mu_0}{2\pi} i_{p3}^2 \frac{l}{a_m} \end{aligned}$$

i_{p3} and i_{p2} are the peak short-circuit currents during three-phase respective line to-line short-circuits. They can be calculated from the initial short-circuit current I_k'' : $i_p = \kappa \sqrt{2} I_k''$ [Ref 11, Ref 12].

The time patterns of the forces and the investigations of the partial functions drive to the following comments:

- a) Comparison of the forces at the inner conductor L2 with those at the outer conductors L1, L3 during three-phase short-circuit:

- The constant term F_0 is of considerable magnitude at L1 and L3 and not present for L2.
- The maxima of steady-state oscillation $F_{2\omega}(t)$ are twice as large for L2 as they are for L1, L3. The maxima of F_ω and F_g are somewhat larger for L2 than for L1, L3.
- The time histories for the resultant forces show a noticeable difference, however the maxima at L2 are always about 7 % higher than at L1, L3 for all R/X , both at transient and steady state.

Considering only the forces it cannot be said which conductor will be stressed higher: L1 and L3, or L2, although the maximum is greater at L2 than at L1,

L3. Section 2.2.3 describes that with HV-arrangements with conductor frequency much lower than the system frequency the stresses on conductors L1, L3 are higher than L2, where as for MV- and LV-arrangements with frequencies equal or greater than system frequency the stress in L2 is decisive.

- b) Comparison of the forces during line-to-line short-circuit with those at the outer conductors L1, L3 during three-phase short-circuit:

- The constant terms F_0 are equal.
- The maxima of all partial functions are somewhat smaller in the case of a line-to-line short-circuit.
- The time histories of the resultant forces are very similar. In the case of a line-to-line short-circuit, the maxima are 7 % smaller.

The line-to-line short-circuit stress is somewhat lower than three-phase short-circuit; Therefore the line-to-line short-circuit needs no additional investigation.

The maximum force has the highest value at the inner conductor L2 during three-phase short-circuit and is used as static force in equation (2.2) and in the standard. The static force during a line-to-line short-circuit is equation (2.3).

In the case of conductors not having circular or tubular profiles, the effective distances a_m of the main conductors differ from the center-line distances. a_m can be calculated according to the standard; further information is given in [Ref 4, Ref 13, Ref 14].

The influence of the current displacement in the conductors can be calculated with Current-Splitting-Method [Ref 15]. As shown in [Ref 16], it is of low importance; therefore equations (2.2) and (2.3) are valid with sufficient accuracy.

The stress due to the forces between the sub-conductors is calculated separately and superposed according to section 2.2.6. In each of the sub-conductors, the current i_L/n flows in the same direction. The greatest force acts on the outer sub-conductors where the forces due to the $n - 1$ sub-conductors are added:

$$(2.17) \quad \begin{aligned} F_1 &= \frac{\mu_0}{2\pi} \left(\frac{i_L}{n} \right)^2 \left[\frac{1}{a_{s,12}} + \frac{1}{a_{s,13}} + \dots + \frac{1}{a_{s,1n}} \right] l_s \\ &= \frac{\mu_0}{2\pi} \left(\frac{i_L}{n} \right)^2 \frac{l_s}{a_s} \end{aligned}$$

l_s is the distance between two spacers and $a_{s,1i}$ the effective distance between conductors 1 and i . The term in brackets can be summarised in the effective distance a_s . The maximum value is equivalent to those of the line-to-line short-circuit according to equation (2.16):

$$(2.18) \quad F_s = \frac{\mu_0}{2\pi} \left(\frac{i_p}{n} \right)^2 \frac{l_s}{a_s}$$

and becomes the static force in equation (2.4).

2.2.3. Bending stresses in the conductors taking into account plastic effects and forces on the substructures

The determination of the short-circuit strength according to the rules of statics and under the assumption that deformations occur in the elastic range leads to a design of the busbar which requires less supporting distances, higher cross-sections and /or more robust supports, meaning higher costs. If small permanent plastic deformations are permitted after short-circuit a favourable design is obtained. Therefore the verification of safe loading is done taking advantage of plastic load capacity. The calculation is done according to the theory of plastic hinges similar to the one done for steel structures [Ref 17, Ref 18].

2.2.3.1 Short-circuit strength of conductors

The static load F_m cause in a beam a static stress

$$(2.19) \quad \sigma_{m,stat} = \frac{M_{pl,max}}{Z_m} = \beta \frac{F_m l}{8Z_m}$$

with the moment $M_{pl,max}$ according to Table 2.1. With different factor β the same equation can be used for different types and numbers of supports. The dynamic response of the structure is considered by the use of the factors V_σ and V_r [Ref 1, Ref 4, Ref 8, Ref 9, Ref 19, Ref 20]. Hence the rating value is as follows:

$$(2.20) \quad \sigma_m = V_\sigma V_r \sigma_{m,stat} = \beta V_\sigma V_r \frac{F_m l}{8Z_m}$$

Sub-conductors are fixed by connecting pieces in the span. The outer sub-conductors oscillate towards each other and can be handled as a single span beam fixed in the connecting pieces. According to the equations (2.19) and (2.20) the structure response due to the forces between the sub-conductors leads to the rating stress in the sub-conductor:

$$(2.21) \quad \sigma_s = V_{\sigma s} V_r \sigma_{s,stat} = V_{\sigma s} V_r \frac{M_{pl,max}}{Z_s} = V_{\sigma s} V_r \frac{F_s l}{16Z_s}$$

Conductors are assumed to withstand a short-circuit if they do not show a remarkable permanent deformation [Ref 4, Ref 21]. In the case of short actions this is true if the conductor is not stressed with higher stress than with twice the stress corresponding to the yielding point of the material taking advantage of its plasticity:

$$(2.22) \quad \sigma_{zul} = 2R_{p0,2}$$

Tests show the occurrence of a permanent deformation of 0,3 ... 0,5 % of the supporting distance which is

equivalent to a conductor lengthening of about 0,03 %¹. In equation (2.22), the factor 2 of plasticity arises when a beam fixed at both ends has plastic deformations within the span and in addition there is buckling in the rigid supporting points; it changes from a fix support to a partial one.

In steel construction the maximum capacity is reached when a plastic hinges are used. This means that the stress at the fix points and in the span is at the yielding point and there is full plasticity. The factor β considers the plastic hinges at the rigid support point and the factor q the plastic hinge in the span.

When going from complete to partial fixation the maximum moment $M_{pl,max}$ occurs in the fixation before the maximum elastic moment $M_{el,max}$ is reached. By this the maximum moment at the fixation is decreased. Both moments are given in Table 2.1 and the comparison show that a greater loading is possible. In the case of a beam fixed at both ends 33 % can be gained:

$$(2.23) \quad \frac{M_{el,max}}{M_{pl,max}} = \frac{F_m l / 12}{F_m l / 16} = \frac{4}{3} = 1,33$$

The single span beam supported at both ends has no plastic hinges in the supports. The spans with continuous beams are calculated separately and the moments are estimated. Arrangements with two spans are equivalent to a beam supported/fixated. With three and more spans the outer spans are nearly equivalent to a beam supported/fixated and the inner spans to a beam fixed/fixated; the moments are greater in the outer spans than in the inner ones, which can be found by comparison with a single span: The outer spans are decisive.

The plastic moments for different types of beams and supports are related to the moment in a beam supported at both ends. Hence the factor β is calculated, which is also given in Table 2.1:

$$(2.24) \quad \beta = \frac{M_{pl,max}}{M_{el,max, supported/ supported}}$$

The plastic behaviour in the span can be explained best with materials having a distinctive yielding point. This is not existent neither for aluminum nor for copper, as shown in Figure 2.1a. It is substituted by an ideal elastic-plastic characteristic. The following is shown in the case of an rectangular profile, which is easier to demonstrate and is analogous to other profiles.

¹ The tests have been performed in 1942 and 1944 by Siemens-Schuckert factory in Berlin

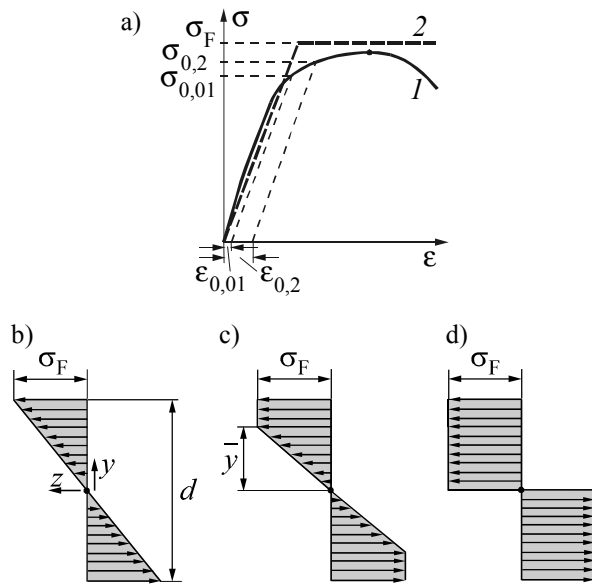


Figure 2.1 Stress-strain diagram and stress distribution in a rectangular cross-section
 a) Stress-strain;
 1 copper, aluminium;
 2 ideal elastic-plastic
 b) Stress in the elastic range
 c) Stress in the elastic-plastic range
 d) Stress in the full plastic range

The rectangular beam is loaded by a force F_m per unit length. In the elastic range the stress increases linearly from the neutral axis to the outer fibre, Figure 2.1b. The inner moment is

$$M_{el} = \int_A \sigma(x, y) y \, dA = \int_{-d/2}^{d/2} \sigma_m \frac{y}{d/2} y b \, dy \quad (2.25)$$

$$= \frac{d^2 b}{6} \sigma_m = Z_m \sigma_m$$

An outer moment acts in opposite direction, e.g. $F_l/8$ in the case of a beam with both ends supported. The outer moment is now increased until the yielding point σ_F is reached. Because all other fibres are in the elastic range, the outer fibre is prevented from yielding, and high deformations are not allowed to occur. For better usage, a further propagation of the flow stress over the cross section is permitted, Figure 2.1c. The areas $|y| < d/2$ are not fully stretched and are able to take part in the weight-carrying. During partial plasticity the inner moment becomes

Table 2.1: Factors β and α for different supports
 Maximum moment $M_{pl,max}$ with plastic hinges at the fixing points in the case of single span beams or at the inner supports of continuous beams, maximum moment $M_{el,max}$ in the elastic range

type of beam and support		$M_{pl,max}$	$M_{el,max}$	β	α
single span beam	A and B: supported 	-	$\frac{F_m l}{8}$	1,0	A: 0,5 B: 0,5
	A: fixed B: supported 	$\frac{F_m l}{11}$	$\frac{F_m l}{8}$	$\frac{8}{11} = 0,73$	A: 0,625 B: 0,375
	A and B: fixed 	$\frac{F_m l}{16}$	$\frac{F_m l}{12}$	$\frac{8}{16} = 0,5$	A: 0,5 B: 0,5
continuous beam with equidistant supports	two spans 	$\frac{F_m l}{11}$	$\frac{F_m l}{8}$	$\frac{8}{11} = 0,73$	A: 0,375 B: 1,25
	3 or more spans 	$\frac{F_m l}{11}$	$\frac{F_m l}{8}$	$\frac{8}{11} = 0,73$	A: 0,4 B: 1,1

$$\begin{aligned}
 (2.26) \quad M_{\text{el-pl}} &= 2 \left[\int_0^{\bar{y}} \sigma_F \frac{y}{y} yb \, dy + \int_{\bar{y}}^{d/2} \sigma_F yb \, dy \right] \\
 &= \sigma_F \left[\left(\frac{d}{2} \right)^2 - \frac{\bar{y}^2}{3} \right] b
 \end{aligned}$$

When $|\bar{y}| = 0$ the flow stress is in the complete cross section, Figure 2.1d. With a permanent lengthening in the outer fibre of $\epsilon_{0,2} = 0,2 \%$, an outer moment M_{Tr} acts which is called realistic ultimate load. It is equal to the inner moment $M_{\text{el-pl}}$ according to equation (2.26):

$$\begin{aligned}
 (2.27) \quad M_{\text{Tr}} &= M_{\text{el-pl}}(\bar{y} = 0) = \frac{d^2 b}{4} \sigma_{0,2} \\
 &= 1,5 Z_m \sigma_{0,2} = q Z_m \sigma_{0,2}
 \end{aligned}$$

In contrast to the pure elastic limit the outer moment can be increased about 50 %. Then the load capacity is exhausted. The perfect plastic factor is $q = 1,5$ for rectangular profiles. With other profiles factor q deviates and is given in Table 2.2 [Ref 21, Ref 22].

The permanent deformation of $\epsilon_{0,2} = 0,2 \%$ is equivalent to the yielding point $R_{p0,2}$. The maximum value of the stresses σ_m respectively σ_{tot} shall not be greater than given by the realistic ultimate load in equation (2.27):

$$(2.28) \quad \sigma_m \leq q R_{p0,2} \quad \text{resp.} \quad \sigma_{\text{tot}} \leq q R_{p0,2}$$

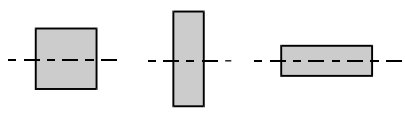
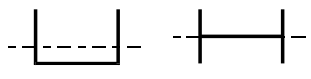
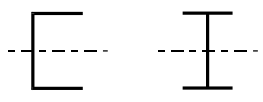
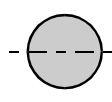
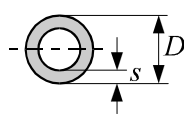
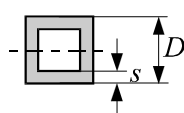
It is recommended not to exceed the yielding point in the case of sub-conductor stress σ_s in order to hold the distance between the sub-conductors nearly constant:

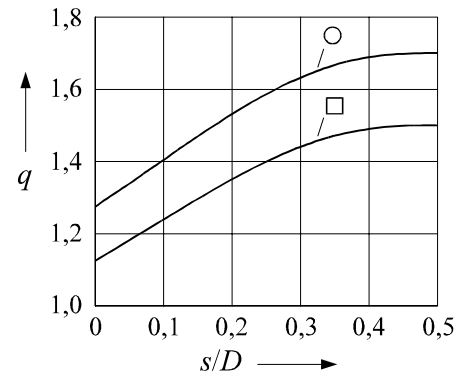
$$(2.29) \quad \sigma_s \leq R_{p0,2}$$

If ranges for the value $R_{p0,2}$ according to the yielding point are available, the minimum limit $R_{p0,2}$ should be used in equations (2.28) and (2.29) to get a permanent deformation which is not too large.

To regard the plasticity under consideration of the transition from complete to partial fixation a higher loading is possible in contrast to the calculation only in the elastic range, if a little permanent deformation is permitted. In the case of beams fixed/ fixed it becomes $4/3 \cdot 1,5 = 2$ which agrees with the measured value in equation (2.22). In substations, normally tubes with $s/D = 0,02 \dots 0,3$ over two or more spans are used. In this case the loading can be increased by the factor 1,8 ... 2,3.

Table 2.2: Factor q for different cross-sections
The bending axis are dotted, and the forces are perpendicular to it

	$q = 1,5$
	$q = 1,83$
	$q = 1,19$
	$q = 1,7$
	$q = 1,7 \frac{1 - (1 - 2s/D)^3}{1 - (1 - 2s/D)^4}$
	$q = 1,5 \frac{1 - (1 - 2s/D)^3}{1 - (1 - 2s/D)^4}$



2.2.3.2 The factors V_α and V_σ

Figure 2.2 shows the factor V_σ for the outer conductors L1 and L3 as function of the mechanical relevant natural frequency f_c of the conductors for two damping decrements Λ and fixed supports. V_σ depends on f_c because the loading is composed from four partial functions according to equation (2.13). With f_c much lower than the system frequency f , V_σ is determined by the constant terms in the electromagnetic force, it follows $V_\sigma < 1$. Is f_c much higher than f , the conductor movement follows the electromagnetic force and therefore $V_\sigma = 1$. Intermediate amplifications occur if the mechanical relevant frequency or one of the higher eigenfrequencies is in the range of f or $2f$; the amplifications with $2f$ are higher than with f . They decrease with increasing damping; outside the resonances the damping is of minor influence. Other fixations of the conductor shift the resonances.

Only at the resonances with $2f$ and for $f_c/f > 1$, V_σ is greater for the inner conductor L2, because the term of

the electromagnetic force at $2f$ is two times higher and the constant term is zero. For $f_c/f < 1$ outside the resonances, the stress for the outer phases L1, L3 is higher caused by the constant term.

The amplifications due to resonance require that the stress in the conductor is always in the elastic range. In fact, during or near resonance the stress will increase as far as plasticity is reached. By this the mechanical frequency of the conductor is shifted to lower values and the condition for resonance which is only valid in the elastic range is no longer met. Because the increase of the stress due to resonance needs a constant eigenfrequency resonance, resonance phenomena cannot occur in plastic limit state [Ref 23]. The factor V_σ cannot become greater than 1. The dynamic calculation is equivalent to a static calculation with the maximum values of the electromagnetic force as a static equivalent force which cause the ultimate load M_{Tr} according to equation (2.27). Lower outer moments give elastic or elastic-plastic deformations lower than the ultimate load, but equations (2.28) and (2.29) are always fulfilled.

Figure 2.2 is calculated for beams fixed at both ends. In substations, the conductors are mounted on insulators which are elastic and can oscillate. Thus there are no fixed supports. For $f_c > f$, the amplifications by resonance are clearly reduced and also the range in between [Ref 20, Ref 24]. For the simplified method it is sufficient to state a curve which lies near the minima in Figure 2.2. Attention should be paid to the fact, that the calculated curves are related to the maximum force at L1, L3 and the standardised one is related to the maximum force at L2, which differ by about 7 %.

If the verification for the short-circuit strength is done without consideration of the conductor frequency, a calculation with the maximum $V_\sigma = 1$ can be done, this value is stated in Table 2 of the standard. The use of values $V_\sigma < 1$ especially with HV-arrangements needs the knowledge of the conductor frequency, which is shown in sub-section 2.2.4.

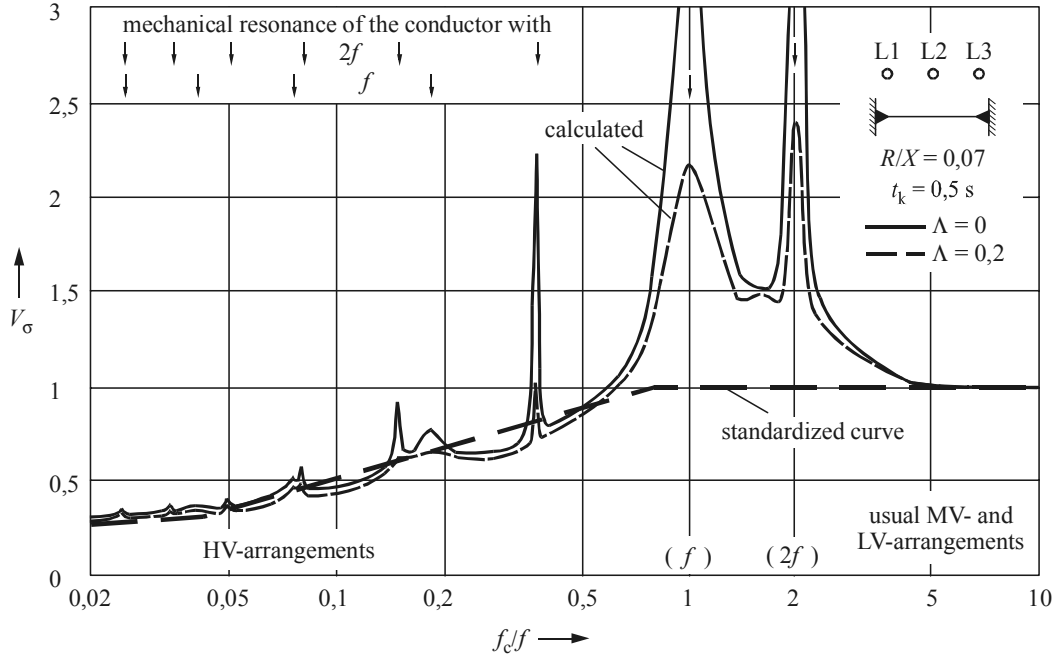


Figure 2.2 Calculated factors V_{σ} in the outer conductors L1 and L3 in the case of a three-phase short circuit as function of the related relevant natural frequency f_c/f of the conductor and the logarithmic damping Λ , both ends fixed [Ref 8, Ref 9, Ref 19]. Also the standardised curve is given

In Figure 2.2, R/X is 0,07, resp. $\kappa = 1,81$. When κ decreases, the maxima of the electromagnetic forces in equations (2.15), (2.16), (2.18) decrease proportional to κ^2 , the decaying and the frequent term decrease too, whereas the constant and the double frequent term are independent. That means V_{σ} increases. The curves in Figure 2.2 move to higher values while the standardised curve follows the minima. In the case of $R/X \leq 0,15$ resp. $\kappa \geq 1,64$ the results are not very different.

Sub-conductors are treated as beams with both ends fixed. They act as main conductors but with other frequencies. To calculate the stress in the sub-conductors, the factor V_{σ_s} is set to unity ($= 1$) without consideration of the relevant natural frequency f_{cs} . With consideration of the relevant natural frequency f_{cs} the same figures can be used as for V_{σ} , but f_c is to be replaced by f_{cs} .

Single-phase systems are to be handled in the same way.

2.2.3.3 Forces on the sub-structures

The forces on the sub-structures of the conductors are also calculated from the static short-circuit load F_m [Ref 1, Ref 4, Ref 8, Ref 9, Ref 19, Ref 20]:

$$(2.30) \quad F_d = V_F V_r \alpha F_m$$

V_F considers the dynamic response and α the distribution on the sub-structures.

F_d acts at the clamp on the top of the insulator. If the supports assumed to be rigid, the moment along the insulator is linear. Supports in LV- and MV-substations

fulfil this. Supports in HV-arrangements have a lower stiffness and influence the oscillation of the system. Along sub-structures of 110-kV-, 220-kV- and 380-kV-substations, the maximum dynamic moments are calculated by means of Transfer-Matrix-Method [Ref 20, Ref 24]. Figure 2.3 shows the results for the arrangement with two spans, described in [Ref 1, Volume 2, Case 1]. The measured values are also drawn and show a good agreement. The dynamic moment is nearly linear. In addition, the moment is given which follows from a static load with the maximum value of the electromagnetic force; it is linear. In both cases, the maxima of the moments and with this the maximum stresses occur in the bottom of the insulators and steel support structures. This justifies to take F_d as an equivalent static force at the clamp which gives the same moments as the dynamic force.

The stress at the bottom of the insulator by F_d must not be higher than the minimum failing load of the insulator which is given as a force F_1 at the top of the insulator. Therefore the moments have to fulfil the following equation

$$(2.31) \quad F_d (h_1 + h_c) \leq F_1 h_1$$

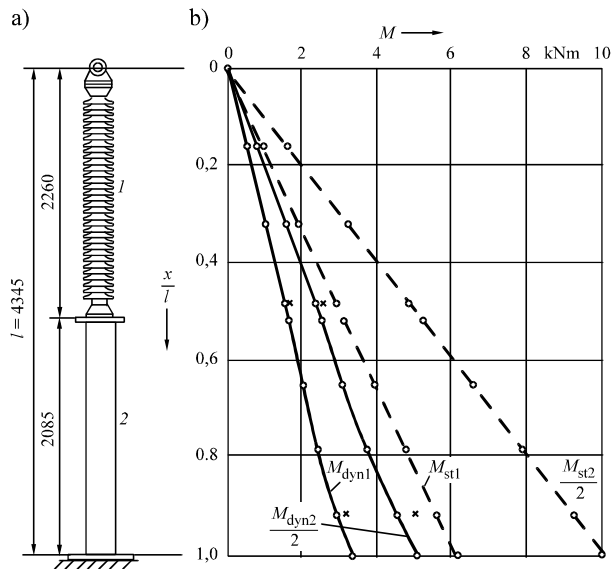


Figure 2.3 Bending moment along a 220-kV-support [Ref 20]

- a) Support: 1 insulator, 2 steel pillar
 - b) Maximum dynamic moments M_{dyn1} , M_{dyn2} and static moments M_{st1} , M_{st2}
- Index 1: outer supports
Index 2: inner supports
- calculated
 - × measured by FGH

where h_1 is the insulator height and h_c is the distance between the top of the insulator and the center of the conductor in the clamp.

The strength of the conductors can be calculated with the rules of statics and stresses according to the plastic limit, and from this an upper limit $V_\sigma = V_{\sigma s} = 1$ follows. In this case, V_F becomes equal to 1. Forces on supports can only be higher than calculated with $V_F = 1$ according to the rules of statics, if the conductor stresses are within the elastic limit $R_{p0,01}$. $R_{p0,01}$ is not very often used. Usually, ranges with a minimum value $R_{p0,2}$ and a maximum value $R'_{p0,2}$ are given, or only one value $R_{p0,2}$ is given. Therefore the elastic limit is set to $0,8R'_{p0,2} > R_{p0,01}$.

Figure 2.4 shows the maximum possible values of V_F depending on the conductor stress σ_{tot} . In range 1, $\sigma_{tot} > 0,8R'_{p0,2}$ holds and with this $V_F = 1$ due to plasticity effects. When σ_{tot} becomes less than $0,8R'_{p0,2}$, in range 2, the conductor oscillates but with noticeable damping due to the still not complete relieved from plastic hinges, which also shifts the resonance frequency. The forces on the sub-structures increase with decreasing conductor stresses. In Figure 2.4, for V_F linearity is assumed in range 2. For $0,8R'_{p0,2}/\sigma_{tot} = 2,7$ the

maximum of V_F is reached in range 3. Figure 2.4 does not depend on the conductor frequency and is valid for all arrangements.

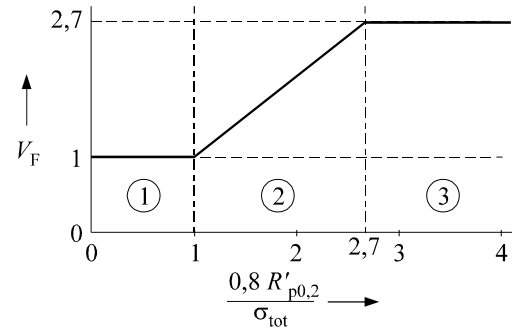


Figure 2.4 Maximum possible values of V_F depending on the stress σ_{tot}

The conductor frequency factors V_F can be calculated as shown in Figure 2.5 for a beam with both ends fixed. This is done similar to Figure 2.2. Again it is required that the conductor is deformed only elastic. Under this assumption, a curve can be drawn which lies near the minima for $f/f_c < 0,6$; within $0,6 < f/f_c < 6$ resonance with f and $2f$ and mechanical damping is considered; this becomes one for $f/f_c > 6$. The maximum is 2,7 and taken over to Figure 2.4.

The factors V_F are different for L2 and L1, L3 as written above for V_σ , and also the values on which the calculated curves and the standardized one are based.

In HV-substations where f_c/f is noticeably less than one, the calculation with the maximum value according to Figure 2.4 leads to a too conservative design. From Figure 2.5 it follows $V_F < 1$. In these cases it is recommended to calculate the relevant natural frequency to get a more precise design or to take advantage of reserves. Also with MV- and LV-busbars the consideration of the frequency can lead to values of V_F lower than those according to Figure 2.4; if not, Figure 2.4 is decisive.

V_F also depends on κ as shown for V_σ above.

Single-phase systems are treated as three-phase-systems but with restriction $V_F = 1,8$ if $f_c/f \approx 2$.

With the knowledge of the static load $V_F V_r F_m$ the forces on the supports can be calculated by use of the α factor.

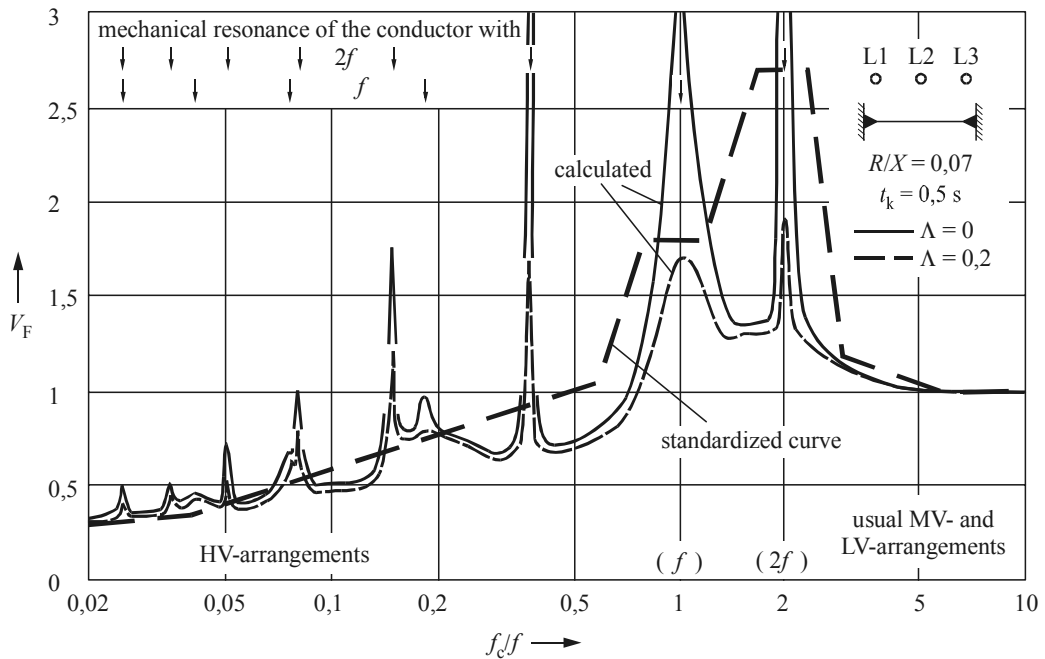


Figure 2.5 Calculated factors V_F in the outer conductors L1 and L3 in the case of a three-phase short circuit as function of the related relevant natural frequency f_c/f of the conductor and the logarithmic damping Λ , both ends fixed [Ref 8, Ref 9, Ref 19]. Also the standardised curve is given.

In the case of single span beams and continuous beams with two spans, Table 2.1 gives the values α known from statics. If there are three or more spans the force at the first support is a little bit higher and at the second support a little bit lower compared to a two-span bus. This is confirmed by numerical calculations of 110-kV-, 220-kV- and 380-kV-busbars [Ref 8, Ref 10]. The remaining supports will be subjected by lower forces.

Due to resonances, different distances between the supports can cause up to 20% higher forces at the supports compared to the case of equal distances, if the length of the shorter span is 15 % to 100 % of the other spans. Less than 15 % and more than 100 % give a further increase [Ref 8, Ref 10, Ref 24]. Numerical dynamic and static evaluations confirm this. Therefore it is recommended to avoid span length less than 20 % of the adjacent ones; if this is not possible, the conductors shall be decoupled using flexible joints at the supports.

2.2.3.4 Factor V_r

In most 110-kV-systems and in all systems with voltages above, single-phase automatic reclosing is used; this does not result in higher stresses compared to the three-phase short-circuit. In MV- and LV-systems, the three-phase automatic reclosing is used. This could also sometimes be used in a 110-kV-system. If the reclosing is unsuccessful, a three-phase short-circuit happens again. An increase of the conductor stress and the forces on the supports can occur. The worst case

follows if the first current flow ends at maximum moment and the beginning of the second current flow coincides with a maximum moment during free vibration of the conductor [Ref 8, Ref 10, Ref 25]. For this purposes, the factor V_r is introduced as the ratio of two dynamic load responses:

$$(2.32) V_r = \frac{\text{response with automatic reclosing}}{\text{response without automatic reclosing}}$$

V_r depends on the conductor frequency and increases for $f_c/f < 2$, Figure 2.6; V_r becomes one for $f_c/f > 2$. During longer dead times the free oscillation of the conductors is damped which results in lower V_r . The calculated curves are approached by the dotted curve for the standard.

When estimating without conductor frequency, the stresses σ_m and σ_s are to be calculated by use of $V_r = 1,8$ to get results on the safe side.

In Figure 2.4, V_F is to be replaced by $V_F V_r$ with three-phase automatic reclosing.

If there is no three-phase automatic reclosing $V_r = 1$ is to be used in the corresponding equations when considering the conductor frequency.

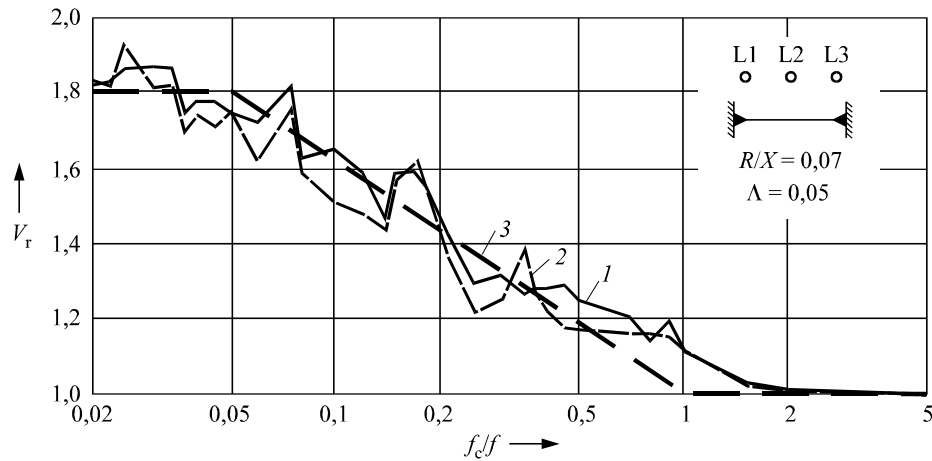


Figure 2.6 Calculated factors V_r in the outer conductors L1 and L3 in the case of a three-phase short circuit as function of the related relevant natural frequency f_c/f of the conductor, both ends fixed [Ref 8]. Dead time $t_u = 0,3$ s.
 1 conductor stress 2 forces on the supports 3 standardised curve

If the three-phase automatic reclosing is used and the calculation is carried out only according to Table 2 of the standard without estimating the conductor frequency, an additional calculation without reclosing has to be performed; the conductor stresses are lower during the first current flow which can result in higher values for V_F V_r and therefore in higher forces at the supports. With consideration of the frequency this is also true even if $V_F V_r > 1$ with automatic reclosing.

2.2.4. Relevant natural frequencies of main- and sub-conductors

An economic design of busbars is only possible when the dynamic of the system is regarded. With this remark, reduction of stresses and forces can be achieved in HV-arrangements. On the other side, in MV- and LV-arrangements resonances with the frequent and double-frequent parts of the electromagnetic forces can be avoided. In section 2.2.3 it is shown that the relevant natural frequency of the busbar is the decisive factor. In the following is described the estimation of the relevant natural frequency of main conductors, which can be single conductors or consist of sub-conductors, and of the sub-conductors.

2.2.4.1 Relevant natural frequency of a single conductor

If the main conductor is a single conductor, its eigenfrequencies follow from the solution of the eigenvalue equation

$$(2.33) \quad f_{ci} = \frac{\gamma_i}{l^2} \sqrt{\frac{EJ_m}{m'}}$$

The factor γ_i depends on the order of the harmonics and also on the boundary conditions of the beam.

The relevant natural frequency of single span beams is identical with the basic frequency and follows from equation (2.33) with $\gamma_1 = \gamma$ from Table 2.3:

$$(2.34) \quad f_c = \frac{\gamma}{l^2} \sqrt{\frac{EJ_m}{m'}}$$

where J_m is to be taken with respect to the main conductor axis perpendicular to the direction of F_m .

In continuous beams with n spans and equidistant or nearly equidistant supports, the modes with number n have horizontal or nearly horizontal bending tangent at the inner supports and therefore a predominant positive elastic line. Figure 2.7 shows the eigenmodes of the numbers one to five of a three-span beam; the modes with even numbers are symmetrical to the middle axis and those with odd numbers symmetric to the central point. The third mode is the lowest one with horizontal bending tangent near the inner supports, it looks like a static elastic line and has the relevant natural frequency. In two-span beams, the second mode has a horizontal tangent at the inner support and the elastic line of one of the spans is the same as the elastic line of the first mode of a single span-beam fixed/supported: $\gamma = 2,45$ according to Table 2.3. Three and more spans need the solution of the eigenvalue problem for number n . $n \rightarrow \infty$ leads to a mode of number n which coincides between the inner supports with the first mode of a single-span beam fixed/ fixed and $\gamma = 3,56$ can be taken. The actual frequency of busbars with an usual number of spans is somewhat lower as shown in Figure 2.8; $f_{c,n}$, calculated by Finite-Element-Method.

The described frequency estimation is based on ideal rigid supports. But the supports in a substation are elastic and the relevant natural frequency is shifted to lower values which could be noticed when f_c is near to system frequency f or $2f$, see section 2.2.3 and [Ref 26].

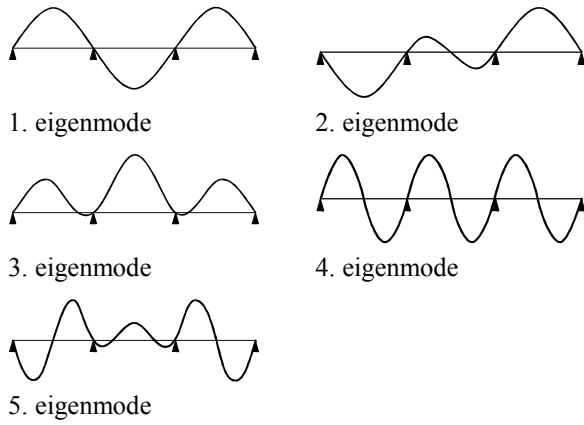


Figure 2.7 Continuous beam with three spans: eigenmodes 1 to 5

2.2.4.2 Relevant natural frequency of main conductor consisting of sub-conductors

If there are not connecting pieces within the span the sub-conductors oscillate with the frequency

$$(2.35) \quad f_0 = \frac{\gamma}{l^2} \sqrt{\frac{EJ_s}{m'_s}}$$

where J_s is to be taken with respect to the main conductor axis perpendicular to the direction of F_m .

The fitting of k connecting pieces according to Figure 2.9 increases the continuous conductor mass by additional masses at their locations. By this the relevant frequency decreases compared to the span without connecting pieces; except the connecting pieces have a

stiffening effect (stiffening elements) and the oscillation is perpendicular to the surface. The stiffening causes an increase of the frequency.

A sufficient accurate calculation of the relevant frequency can only be done when the additional mass of the connecting pieces is taken into account as well as their stiffening effects which is pointed out by tests [Ref 27, Ref 28]. Therefore equation (2.35) is multiplied by a factor c ; the main conductor frequency f_c with connecting pieces is calculated from the frequency f_0 of a sub-conductor without connecting pieces

$$(2.36) \quad f_c = cf_0 = c \frac{\gamma}{l^2} \sqrt{\frac{EJ_s}{m'_s}}$$

The factor c consists of the factor c_m affected by the mass of connecting pieces and the factor c_c affected by their stiffening effect:

$$(2.37) \quad c = c_m c_c$$

At first it is looked at the influence of the mass. Due to the connecting pieces the sub-conductors oscillate with the same basic frequency as monophase. The eigen-angular frequency of a spring-mass-system can be determined from the stiffness c_F and the mass m of the spring:

$$(2.38) \quad \omega^2 = \frac{c_F}{m}$$

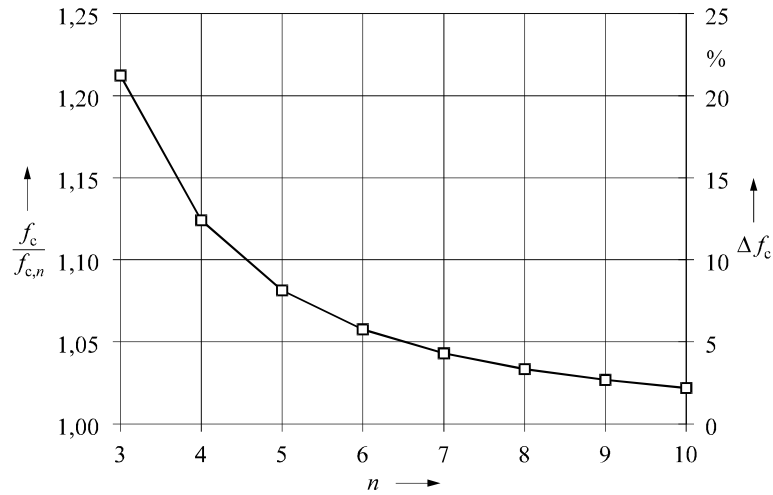

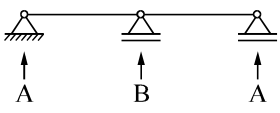
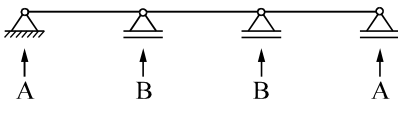


Figure 2.8 Frequency f_c calculated according to equation (2.34) related to the actual frequency $f_{c,n}$ of a continuous beam with n spans, and error $\Delta f_c = f_c / f_{c,n} - 1$

Table 2.3: Factor γ for different supports

type of beam and support		γ
single span beam	continuous beam with equidistant supports	
A and B: supported		1,57
A: fixed B: supported	two spans 	2,45
A and B: fixed	3 or more spans 	3,56

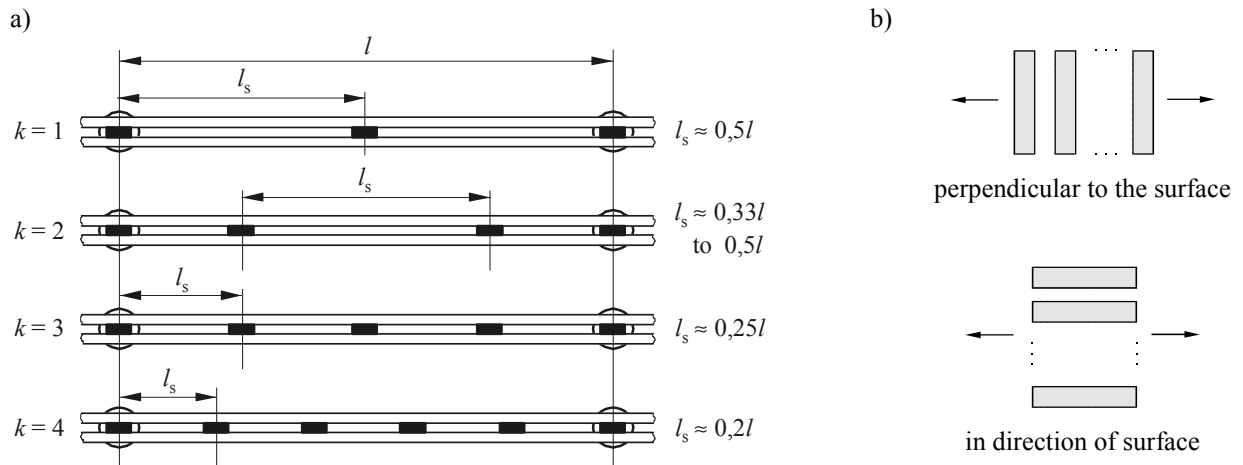


Figure 2.9 Main conductor consisting of sub-conductors

a) Arrangement of connecting pieces within the span

b) Direction of oscillation

The connecting pieces are taken into account by additional masses m_z which are distributed over the n sub-conductors and weighted by the influence factor ξ_m :

$$(2.39) \quad \omega^2 = \frac{c_F}{m'_s + \xi_m \frac{m_z}{n}} = \frac{1}{1 + \xi_m \frac{m_z}{nm'_s l}} \frac{c_F}{m'_s}$$

$$= \frac{1}{1 + \xi_m \frac{m_z}{nm'_s l}} \omega_0^2$$

with $\omega = 2\pi f_0$. Hence the frequency f follows with the factor c_m :

$$(2.40) \quad f = \frac{\omega}{2\pi} = \frac{1}{\sqrt{1 + \xi_m \frac{m_z}{nm'_s l}}} f_0 = c_m f_0$$

ξ_m depends on the number k and the position l_s/l of connecting pieces; m_z is the total mass of one piece. ξ_m is now calculated from the actual frequency of the main conductor. An upper limit can be gained analytically by use of the Rayleigh-quotient [Ref 29, Ref 30], which compares the maximum kinetic energy U_{\max} when passing the rest position with the maximum energy E_{\max} in the reversal of direction of movement during the undamped oscillation [Ref 31]

$$(2.41) \quad U_{\max} = E_{\max} = \omega^2 \bar{E}_{\max}$$

Hence the Rayleigh-quotient is :

$$(2.42) \quad R = \omega^2 = \frac{U_{\max}}{\bar{E}_{\max}}$$

where

$$(2.43) \quad U_{\max} = \frac{1}{2} \int_0^l \frac{M_b^2(x)}{EJ_s} dx$$

$$\bar{E}_{\max} = \frac{1}{2} \int_0^l \omega^2(x) dm$$

$w(x)$ and $M_b(x) = EJ_s w''(x)$ are the elastic line and line of the bending moment during the oscillation. Inserting the eigenmode, R becomes its minimum. Any elastic line or bending moment leads to a sufficient approximation of the basic frequency, e.g. as a result of the dead load. This approximation is always higher than the actual value. Other methods are finite elements or transfer matrices.

In extensive investigations by use of the above mentioned methods, the frequencies were calculated of a bus with two rectangular sub-conductors and both ends fixed or supported and hence the factor ξ_m estimated. [Ref 31]. ξ_m is listed in Table 2.4 and the influence of the connecting pieces on the factor c_m is given in Figure 2.10. For $k > 6$, $\xi_m = 1/(k+1)$ can be set. The results are also valid with good accuracy, for more than two sub-conductors.

A stiffening effect of the connecting pieces is only possible under ideal conditions when the sub-conductors are rigidly fixed together. In practice, this is ensured for the usual length of the stiffening elements compared to the conductor length and the usual sub-conductor distances. Friction, internal clearance or displacement in axial direction can reduce the ideal rigidity. In addition, the direction of oscillation must be perpendicular to the surface, see Figure 2.9. The frequency is also calculated from f_0 in equation (2.35) and the factor c_c :

$$(2.44) \quad f = c_c f_0$$

with these conditions, $c_c \geq 1$ is to be expected; in all other cases $c_c = 1$ holds.

The test results in [Ref 27, Ref 28] include the influence of the masses of the connecting pieces besides the stiffening effects for conductor with both ends fixed. The stiffening can be eliminated with c_m according to equation (2.40) and ξ_m from Table 2.4. The evaluation of the tests are completed by calculation with Finite-Element- and Transfer-Matrix-Method for beams with both end supported [Ref 31]. The factors c_c considered are also listed in Table 2.4. The calculation of the relevant natural frequencies for a sub-conductor with stiffening elements according to equation (2.33) using the reduced moments of area given in section 2.2.5 leads to values much higher than the results from equation (2.44); This can be explained by the fact that the dynamic stiffness is lower than the static stiffness.

Table 2.4: Factors ξ_m and c_c

k	0	1	2	2
l_s/l	1,00	0,50	0,33	0,50
ξ_m	0,0	2,5	3,0	1,5
c_c	1,00	1,00	1,48	1,75
k	3	4	5	6
l_s/l	0,25	0,2	0,17	0,14
ξ_m	4,0	5,0	6,0	7,0
c_c	1,75	2,15	2,46	2,77

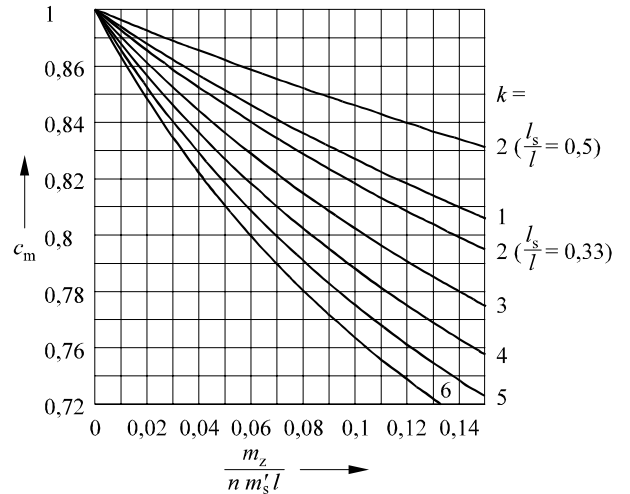


Figure 2.10 Influence of the masses of connecting pieces on the factor c_m

2.2.4.3 Relevant natural frequencies of a sub-conductor

The sub-conductors oscillate as a single-span beam fixed at the connecting pieces. The relevant natural frequency can be calculated with equation (2.34) after replacing l by l_s , J_m by J_s , m' by m'_s , and $\gamma = 3,56$ according Table 2.3:

$$(2.45) \quad f_{cs} = \frac{\gamma}{l^2} \sqrt{\frac{EJ_s}{m'_s}}$$

This equation is exact only for the inner spans if the distances between the connecting pieces and the supports are equal. In other cases the frequencies of each segment is different; for simplification of the method, it is recommended to use equation (2.34).

2.2.4.4 Relevant natural frequencies of cantilever beams, beams with additional masses and swan-neck bends

Above, it is described how to calculate the relevant natural frequencies of single-span beams with/without torsion-free ends as well as continuous beams. Distinguish marks are the static lines. From this, the results could be extrapolated to other arrangements.

Typical examples are the conductors shown in Figure 2.11a. At one end a flexible connection to another equipment can be fastened, or in the span there could be an additional mass, e.g. the contact of a disconnector. For the cantilever ends and the drawn kind of supports, the factor γ lies between the specified limits; the value to be taken depends on the lengths of the cantilever end and the freedom of movement of that end. In the case of the additional mass in the span, the frequency can be calculated with the factor c_m stated above. Alternatively, in all cases the relevant natural frequency can be estimated according to the equation (2.38) from the maximum displacement $\max y$ due to dead load:

$$(2.46) \quad \begin{aligned} f_c &= \frac{1}{2\pi} \sqrt{\frac{c_F}{m}} \approx \frac{1}{2\pi} \sqrt{\frac{1}{m} \frac{F}{\max y}} \\ &= \frac{1}{2\pi} \sqrt{\frac{F}{mg_n} \frac{g_n}{\max y}} = \frac{1}{2\pi} \sqrt{\frac{g_n}{\max y}} \end{aligned}$$

where c_F is the spring coefficient, m the overall mass, F the dead load due to m and $g_n = 9,81 \text{ m/s}^2$ the acceleration of gravity. From this the numerical equation follows which is given in Figure 2.11.

More complicated connections, e.g. swan-neck bends between different levels in Figure 2.11b, can be investigated with sufficient accuracy. Lets assume that the sides have equal lengths and are full stiff against torsion; in this case the static line perpendicular to the conductor plane for $\varphi = 180^\circ$, i.e. straight beam both ends fixed, fits also for $90^\circ \leq \varphi < 180^\circ$, the frequency is correct. The other extreme is no stiffness against torsion, the sides will sag like cantilever beams for $\varphi = 90^\circ$; the frequency will be reduced to 63 % compared with the ideal stiff conductor. Both limits are used in substations: Tubes in HV-substations are stiff whereas rectangular profiles in MV- LV-substations are not stiff. For frequency-estimation, tubes can be 'straightened' and good results can be obtained after reduction of 5 % to 15 % depending on the length of the sides .

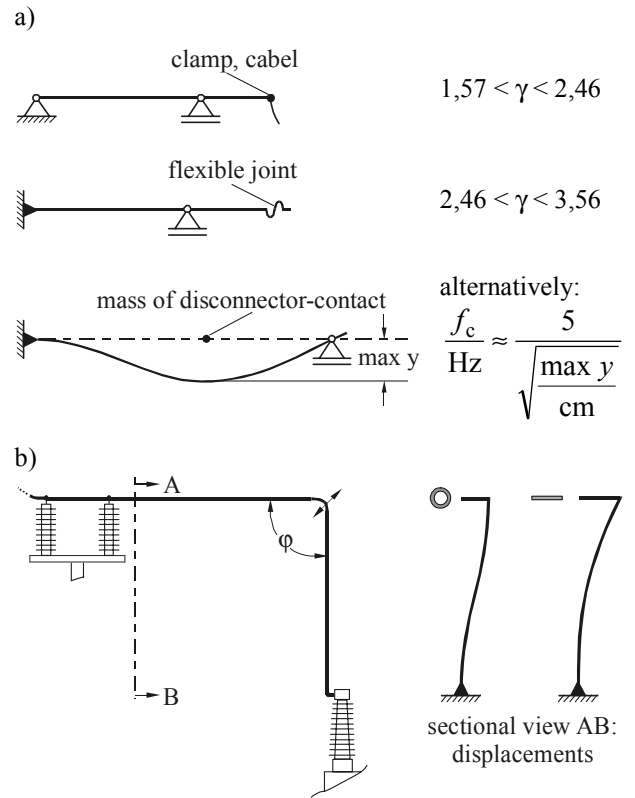


Figure 2.11 Estimation of relevant frequency

- a) Cantilever beam and beam with additional masses
- b) swan-neck bend

2.2.5. Section moduli of main and sub-conductors

The stresses σ_m and σ_s according to equations (2.5) and (2.6) depend on the section moduli Z_m of the main conductor and Z_s of the sub-conductor. For Z_m it is to distinguish whether the main conductor is a single conductor, or consists of two or more sub-conductors with rectangular profile or of two sub-conductors with U-profile. If the main conductor is made up of sub-conductors, there can be either no connecting piece or the connecting pieces act as spacers or as stiffening elements. In addition, the direction of the electromagnetic force is important.

For calculation of section moduli the distribution of bending stresses has to be taken into account. Axial forces do not occur, the conductors are assumed to move free in the clamps.

2.2.5.1 Section modulus of a single conductor

Figure 2.12a shows a single conductor, for example with rectangular cross section A_m . The vector \vec{M}_m is the outer moment caused by the force F_m on the main conductor. It lies in the centre S_m and makes compressive stress above the neutral fibre $O-O$ and tensile stress below. The maximum stress σ_m in the outer fibres at $\pm d_m/2$ follows from equation (2.25)

$$(2.47) \quad M = \frac{J_m}{d_m/2} \sigma_m = Z_m \sigma_m$$

where M is the inner moment, J_m the second moment of area with respect to the axis $O-O$. J_m and Z_m can be found in handbooks for all used profiles.

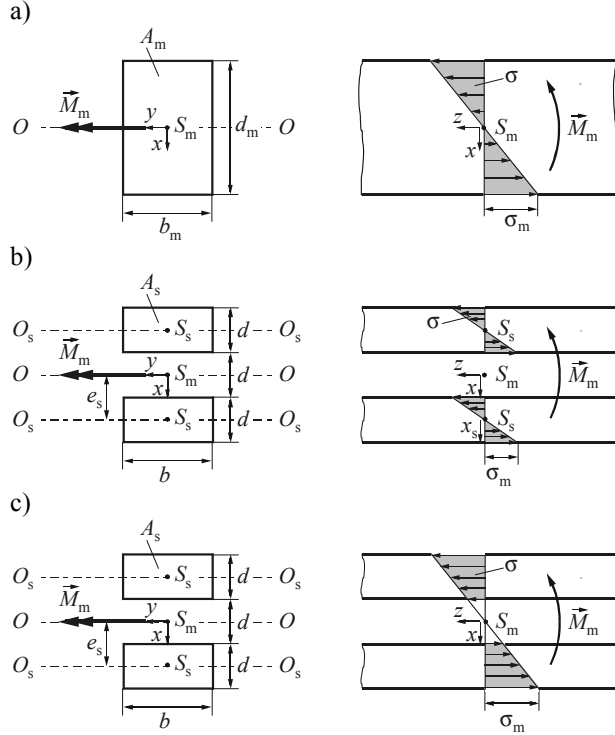


Figure 2.12 Stresses in main conductors

- Single conductor
- No connection of sub-conductors
- Rigid connection of sub-conductors

2.2.5.2 Section moduli of main-conductors consisting of sub-conductors

Different number and type of connecting pieces and direction of force on the main conductor result in different values of J_m and Z_m . Three possibilities are dealt with in the following.

1. No connection of sub-conductors and main conductor force perpendicular to surface:

The sub-conductors are independently displaced by the outer moment \vec{M}_m . Figure 2.12b shows the stresses in the sub-conductors. The opposite surfaces move axial against each other. One is subjected to compressive stress with shortened fibres, the other one is subjected to tensile stress with elongated fibres. The movement have their maxima at the supports and are zero at the middle of the span. The independent displacements are possible if

- there are no connecting pieces or
- the connecting pieces act as spacers or
- there is one stiffening element in the middle of the span.

It is assumed that the connecting pieces do not increase the stiffness. On each sub-conductor the moment $M_m/2$

acts and the inner moment M in each sub-conductor becomes:

$$(2.48) \quad M_m = 2M = 2 \frac{J_s}{d_m/2} \sigma_m = 2Z_s \sigma_m = Z_m \sigma_m$$

J_s and Z_s are to be taken with respect to the axis O_s-O_s of the sub-conductors. Therefore the section modulus Z_m of the main conductor with respect to the axis $O-O$ is the sum of section moduli Z_s .

n sub-conductors in a main conductor in Figure 2.13a leads to

$$(2.49) \quad Z_m = nZ_s$$

2. Rigid connection of sub-conductors and main conductor force perpendicular to surface:

With rigid connection, the sub-conductors are not able to move towards each other; the upper conductor is compressed, the lower one elongated, see Figure 2.12c. This can be obtained using two or more stiffening elements. The distribution of the stress is similar to the single conductor in Figure 2.12a. The second moment of area with respect to the axis $O-O$ is to be calculated by Steiner's law:

$$(2.50) \quad J_m = 2(J_s + e_s^2 A_s)$$

and equation (2.47) holds. For n sub-conductors in Figure 2.13a, J_m becomes

$$(2.51) \quad J_m = 2(J_s + e_1^2 A_s) + 2(J_s + e_2^2 A_s) + \dots + 2(J_s + e_{n/2}^2 A_s) = nJ_s + 2A_s \sum_{i=1}^{n/2} e_i^2$$

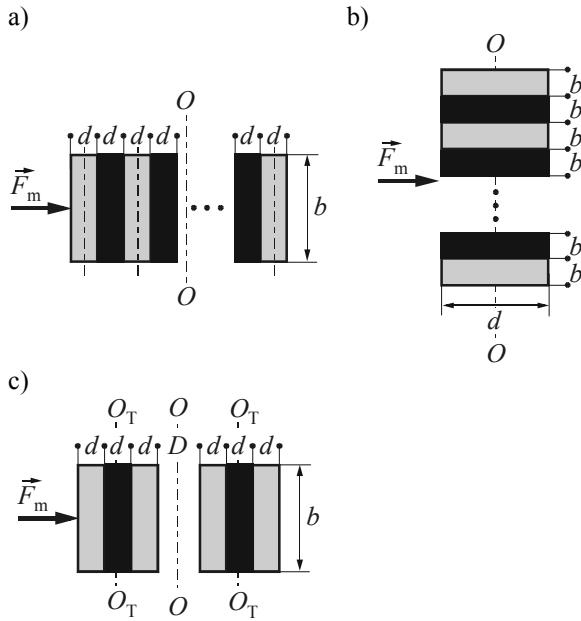


Figure 2.13 Stresses in main conductors

The connecting pieces are black

- Force perpendicular to surface
- Force in direction of surface
- Four connecting pieces, two and two connected

where n is an even number and e_i is the distance between the centre of sub-conductor i and axis $O-O$. If the spacings of the sub-conductors are equal to the thickness d , the sum can be written:

$$(2.52) \quad \sum_{i=1}^{n/2} e_i^2 = d^2 + (3d)^2 + (5d)^2 + \dots + \left(\left(2 \frac{n}{2} - 1 \right) d \right)^2 = \frac{n(n^2 - 1)}{6} d^2$$

If n is an odd number, the result is the same as the one given by the equation (2.52). Hence for all n :

$$(2.53) \quad J_m = nJ_s + 2A_s \frac{n(n^2 - 1)}{6} d^2 = n(4n^2 - 3)J_s$$

The distance of the outer fibre from axis $O-O$ is $(2n - 1)d/2$. Z_m becomes:

$$(2.54) \quad Z_m = \frac{J_m}{(2n - 1)d/2} = \frac{n(4n^2 - 3)}{2n - 1} \frac{J_s}{d/2} = \frac{n(4n^2 - 3)}{2n - 1} Z_s$$

where

$$(2.55) \quad J_s = \frac{d^3 b}{12} \quad Z_s = \frac{d^2 b}{6}$$

In Figure 2.13c there are four sub-conductors, two by two connected with stiffening elements. The pairs are

not connected, therefore Z_m follows from equation (2.48); the section modulus of each pair is to be taken with respect to the axis O_T-O_T according to equation (2.54) and $n = 2$:

$$(2.56) \quad Z_m = 2Z_{sT} = 2 \cdot \frac{26}{3} Z_s = \frac{52}{3} Z_s$$

It is independent from the spacing of the pairs.

U- and I-profiles can be treated in similar manner.

In equations (2.54) and (2.56) it is assumed an ideal rigid connection between the sub-conductors. However, the stiffening elements are mounted at discrete spots and no continuous stiffening is reached. Therefore the actual section modulus are lower. [Ref 32] reports about tests with two sub-conductors Al 80 mm × 10 mm with spacing of the thickness. The results can be summarised as follows:

- one stiffening element practically does not increase the stiffness;
 - with two or three stiffening elements, the actual section modulus is about 60 % of the value according to equation (2.54);
 - with four elements, the actual value is about 80 %.
- Tests concerning U- and I-profiles are not known. Section 2.2.2.3 and Table 5 of the standard recommend the following section moduli for main conductors:
- with rectangular profiles 60 %
 - with U- and I-profiles 50 %
- of the value of ideal rigid connection.

3. Main conductor force in the direction of the surface

If the electromagnetic force F_m is as shown in Figure 2.13b, the connecting pieces have non-essential influence on the stiffness; they may be spacers or stiffening elements. However, the sum of the lengths of the elements has to be much smaller than the span length. The main conductor axis $O-O$ coincides with the sub-conductor axis O_s-O_s . In each sub-conductor the outer moment M_m/n results in the inner moment M :

$$(2.57) \quad M_m = nM = n \frac{J_s}{d/2} \sigma_m = nZ_s \sigma_m = Z_m \sigma_m$$

The section modulus Z_m of the main conductor is the sum of the section moduli Z_s :

$$(2.58) \quad Z_m = nZ_s$$

2.2.5.3 Section modulus of sub-conductors

Besides the force F_m between the main conductors, on each sub-conductor the force F_s according to equation (2.4) which gives the outer moment M_s , Figure 2.14. The sub-conductors move towards each other and they behave like single conductors fixed at both ends. J_s and Z_s of a sub-conductor is equal to the correspondent values of a single conductor having the same dimensions and bending axis. For the rectangular

profiles in Figure 2.14 it follows with respect to the axis O_s-O_s :

$$(2.59) \quad J_s = \frac{d^3 b}{12} \quad Z_s = \frac{d^2 b}{6}$$

Figure 2.14 Stresses in sub-conductors

2.2.6. Superposition of stresses in conductors

2.2.6.1 Superposition of the stresses in main and sub-conductor.

The time scale of the forces between the main conductors and the forces between the sub-conductors as well as the relevant frequencies of main and sub-conductor differ. The maximum of the total stress in the conductor follows from the time scale of the stress caused by the forces in the dynamic system. To make the method suitable for practical use in the standard, stresses σ_m and σ_s are calculated separately in the equations (2.5) and (2.6) and superposed according to Figure 2.15. In sub-conductor 1, the stresses σ_m and σ_s are subtracted; in sub-conductor 2, they are added up to the total stress σ_{tot} :

$$(2.60) \quad \sigma_{tot} = \sigma_m + \sigma_s$$

In the main conductor in Figure 2.15 with both ends supported and one spacer in the span and also with both

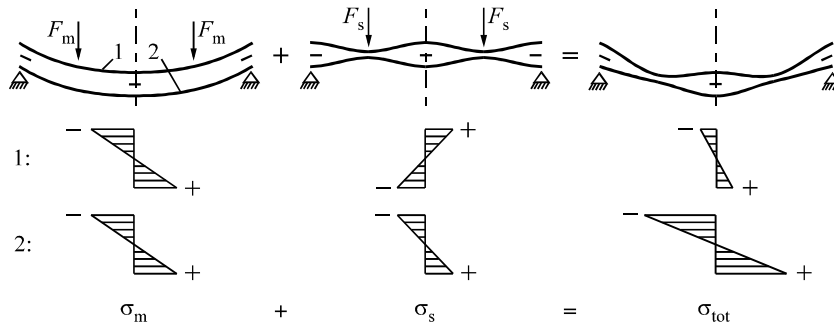


Figure 2.15 Superposition of stresses in main and sub-conductors

ends fixed, σ_m and σ_s occur at the same locations. Other types of supports or continuous beams or asymmetrically mounted spacers will give different locations for σ_m and σ_s . Nevertheless equation (2.60) is used and the results are on the safe side. Although in equations (2.5) and (2.6) plasticity is considered, the superposition is done.

2.2.6.2 Superposition of the stresses caused by orthogonal moments

The force between main conductors perpendicular to the force between sub-conductors or the consideration of dead load, ice, wind in addition to the short-circuit forces give orthogonal moments M_1 and M_2 in the conductors. Figure 2.16 shows the situation for conductors with rectangular and circular profiles.

The stresses σ_1 and σ_2 are perpendicular to the cross-sectional area and are moved into the plane. In the neutral fibre, $\sigma_1 + \sigma_2 = 0$ holds, e. g. in point A . The maximum stress is in the points H^+ and H^- which have maximum distance from the neutral fibre:

– rectangular profile, Figure 2.16a:

$$(2.61) \quad \sigma_{max} = \pm(\sigma_{1max} + \sigma_{2max})$$

– circular profile, Figure 2.16b:

$$(2.62) \quad \sigma_{max} = \pm(\sigma'_1 + \sigma'_1)$$

Equation (2.61) is valid for U- and I-profiles, equation (2.62) for tubes.

In circular profiles, every axis through the center of gravity can be axis of inertia, also the drawn axis $O-O$ in which the vector $\vec{M} = \vec{M}_1 + \vec{M}_2$ lies and is simultaneously the neutral axis. The absolute value of \vec{M} is given by the equation (2.63):

$$(2.63) \quad |\vec{M}| = M = \sqrt{|\vec{M}_1|^2 + |\vec{M}_2|^2}$$

With $\sigma_{1\max} = M_1/Z$, $\sigma_{2\max} = M_2/Z$ and $\sigma_{\max} = M/Z$ the maximum stress becomes:

$$(2.64) \quad \sigma_{\max} = \pm \sqrt{\sigma_{1\max}^2 + \sigma_{2\max}^2}$$

Equation (2.64) is also valid for tubes.

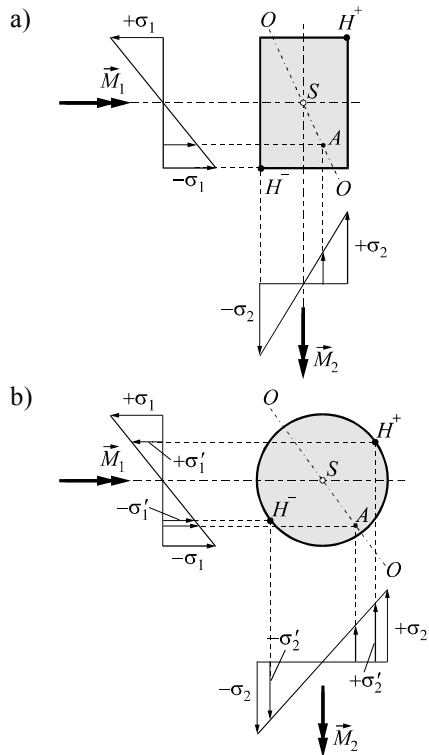


Figure 2.16 Stresses caused by orthogonal moments
a) rectangular profile
b) circular profile

2.3. SPECIAL CONFIGURATIONS

2.3.1. Associated phase structures busbar on a common support

In the associated phase structures, the busbar is often set horizontally on a common support as shown on the Figure 2.17.

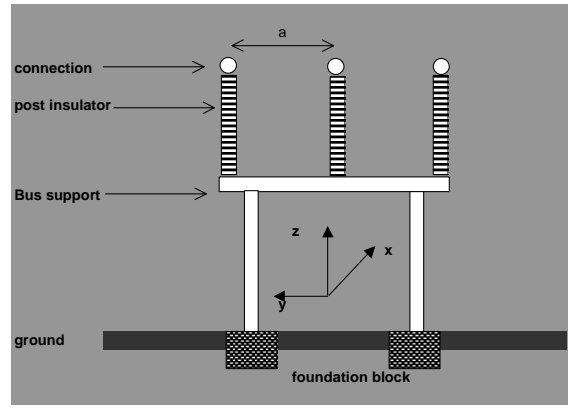


Figure 2.17 Common support of busbar

The dynamic response of the tubes obeys the following law :

$$(2.65) \quad (\rho S)_{tube} \frac{\partial^2 u_i^{tube}}{\partial t^2} + c_{tube} \frac{\partial u_i^{tube}}{\partial t} + (EI)_{tube} \frac{\partial^4 u_i^{tube}}{\partial x^4} = F_i^y(t)$$

where u_i is the displacement function of a tube,
E modulus of elasticity,
I moment of inertia,
 $(\rho S)_{tube}$ own weight per unit length.

In the case of two- or three-phase faults, instant LAPLACE's forces meet the following equations :

$$(2.66) \quad \sum_{i=1,3} \vec{F}_i^y = \vec{0}$$

If, in fact, we call i_1, i_2, i_3 the instant currents in phases 1, 2, 3, these forces can be written as follows :

$$(2.67) \quad F_1^y = \frac{\mu_0}{2\pi a} i_1 \left(i_2 + \frac{i_3}{2} \right)$$

$$(2.68) \quad F_2^y = \frac{\mu_0}{2\pi a} i_2 (i_3 - i_1)$$

$$(2.69) \quad F_3^y = -\frac{\mu_0}{2\pi a} i_3 \left(i_2 + \frac{i_1}{2} \right)$$

By using the differential operator's linearity properties and posing :

$$(2.70) \quad U^{tube} = \sum_i u_i^{tube}$$

one could easily check the following differential equation independent of the shape of the current chosen (phase to earth, earthed or insulated phase to phase, three-phase):

$$(2.71) \quad (\rho S)_{tube} \frac{\partial^2 U^{tube}}{\partial x^2} + c_{tube} \frac{\partial U^{tube}}{\partial x} + (EI)_{tube} \frac{\partial^4 U^{tube}}{\partial x^4} = \sum_{i=1..3} F_i^y = 0$$

Consequently : $U^{tube} = 0 = \sum_i u_i^{tube} \forall t \forall x$

if the sequence of the connecting pieces are the same on each phase.

This relation of functions u_i being true at any moment, whatever the value of x , one could easily deduce that the forces and moments deduced from the function derivated at connection level also meet the relations below :

$$(2.72) \quad \sum_{i=1..3} f_{i,k}^y = 0$$

$$(2.73) \quad \sum_{i=1..3} M_{i,k}^z = 0$$

This is true for any tube k .

Consequently, as the **efforts at top of the column** are the vectorial addition of the contributions of tubes set on each side, they meet similar relations.

$$(2.74) \quad \sum_{i=1..3} f_i^y = 0$$

$$(2.75) \quad \sum_{i=1..3} M_i^z = 0$$

Dynamic response of insulator column :

With respect to the **bending of the jth column of phase i**, one has the following equation available to calculate the dynamic response of the system :

$$(2.76) \quad (\rho S)_{column} \frac{\partial^2 u_j^{column}}{\partial x^2} + c_{column} \frac{\partial u_j^{column}}{\partial x} + (EI)_{column} \frac{\partial^4 u_j^{column}}{\partial x^4} = f_{i,j}^y \delta(z - z_0)$$

z_0 being the point of application in the middle of the connection.

At bottom of the j th column, it will also be possible to check the following relations :

$$(2.77) \quad \sum_{i=1..3} F_{i,j}^y = 0$$

$$(2.78) \quad \sum_{i=1..3} M_{i,j}^x = 0$$

With respect to the **torsion of the jth column of phase i**, one has the following equation to calculate the dynamic response of the system :

$$(2.79) \quad (I_\theta)_{column} \frac{\partial^2 \theta_j^{column}}{\partial x^2} + c'_{column} \frac{\partial \theta_j^{column}}{\partial x} + (GJ)_{column} \frac{\partial^2 \theta_j^{column}}{\partial x^2} = M_{i,j}^z \delta(z - z_0)$$

z_0 being the point of application in the middle of the connection.

I_θ : Mass inertia relative to the axis per unit of length,
 G : Coulomb or torsion modulus,
 J : Polar inertia of straight section.

At bottom of the j th column of phase i , one could also check the following relations :

$$(2.80) \quad \sum_{i=1..3} M_{i,jbase}^z = 0$$

Conclusions :

The wrenches (force and moment) at bottom of two columns in which the phases differ determine the third wrench. The other contributions of each phase are consequently linked to stresses other than electrodynamic (dead weight, wind, ...) The supporting structures are subject to differential loadings. Their sizing will most often depend on the other design hypotheses (wind, ice, earthquake, etc.)

Example :

Considering a structure as illustrated in Figure 2.18, we have plotted in Figure 2.19 the time variations vs. time, forces and moments in the three directions.

The dimensional data for this structure are as follows :

$a = 5$ m, $I_{cc} = 31.5$ kA,

busbar:

bar length = 15 m, diameter = 120 mm, thickness = 8 mm, material : Aluminium,

connection : clamped, pinned on each post insulator,

insulating glass column. C4

One can easily check on Figure 2.19 that, at bottom of the column :

- the sum of the moments in the direction x is zero (electrodynamic load),
- the moments in the direction y are practically constant (they correspond to the dead weight),
- the sum of the moments to z is zero (electrodynamic load),
- the efforts to x are zero (electrodynamic load),
- the sum of the forces to y is zero (electrodynamic load),
- the forces to z are practically constant (they correspond to the dead weight).

For the supporting structure given below, we have calculated the loads under static conditions from the maximum dynamic values and dead weight. The results are as follows :

Electrodynamic loads and dead weight*

	point No.1	point No.2	point No.3
Fx	29 N	20 N	9 N
Fy*	-1290 N	557 N	733 N
Fz	-4034 N	-4034 N	-4034 N
Mx*	2989 N.m	-1337 N.m	-1652 N.m
My	1457 N.m	1437 N.m	1412 N.m
Mz*	-1463 N.m	695 N.m	768 N.m

Support element internal stresses

N/m ²	ICC	ICC+ PP
Column	1.32 e7	1.37 e8
Column spacers	1 e7	7.5 e7
Beam	1.65 e7	1.29 e8
Beam spacers	2.27 e5	1.71 e7
Post insulator support spacers	8.94 e6	1.69 e8

The location of points 1, 2, 3 is shown on the Figure 2.18.

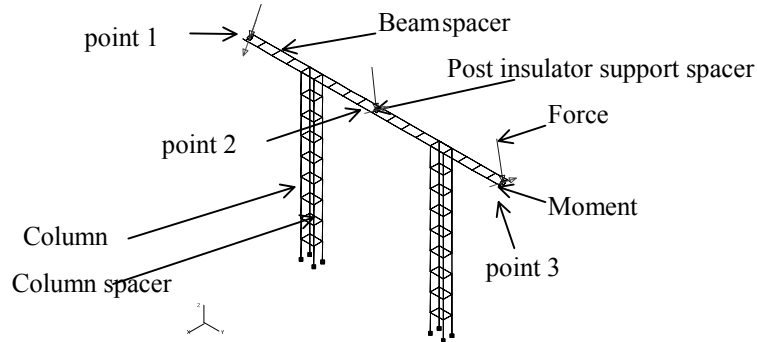


Figure 2.18 Location of forces and moments

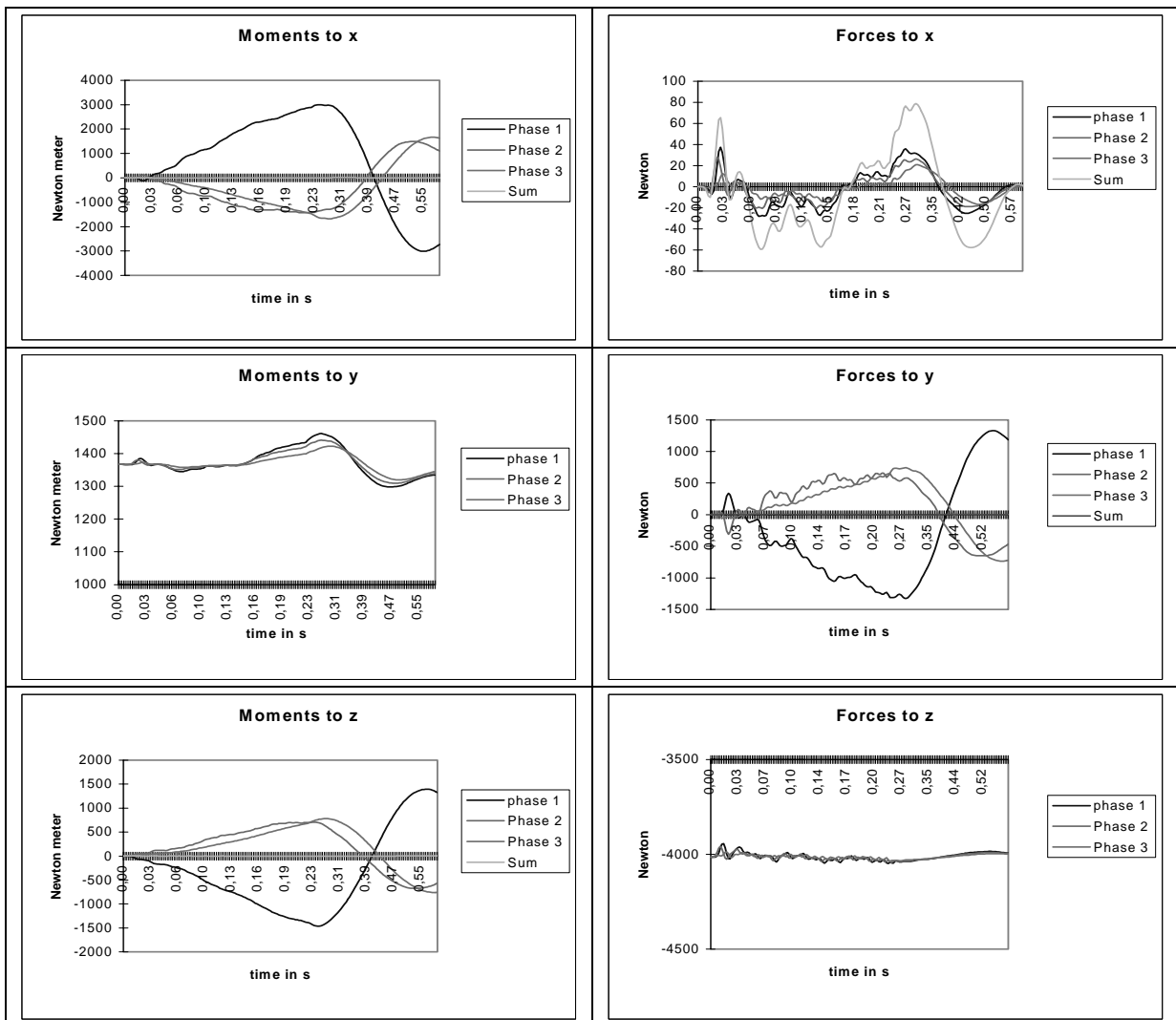


Figure 2.19 Forces and moments at bottom of the column

2.3.2. Influence of two busbars

a). Introduction

Many substations have several busbars in parallel. To handle three-phase or phase to phase faults on 1 or 2 busbars, a special analyses is done in this section to approach the maximum amplitude of stresses to define the withstanding capability of the structures.

For example, RTE takes the following fault situation named « transfer situation » into account when only one line is temporarily protected by the « coupling bay » protections :

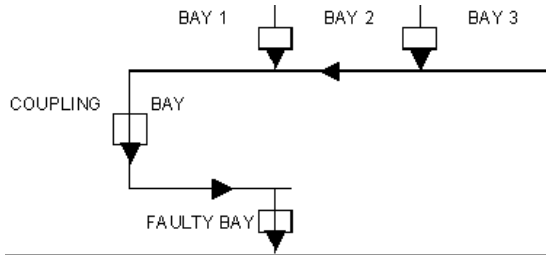


Figure 2.20 Two busbars in parallel

An amplification coefficient is introduced which allows one to step from a reference situation to the actual configuration depending on the type of substation (separated or associated phase layout) and of the fault to be analysed. This approach gives also the maximum asymmetry for these cases.

b). General considerations

The amplitude of the LAPLACE's force depends on the location of the considered phase, the type of fault and the characteristic of the fault.

Phase to phase fault and phase to earth fault

Due to the linear properties of the mechanical equations, the maximum of the force corresponding to the maximum asymmetry is obtained when the phase voltage is zero at the beginning of the fault. The amplification coefficients are given below and are without approximation.

Three-phase fault

If the instant expression of LAPLACE's force is given by an expression of the type :

$$(2.81) \quad F = \frac{\mu_0}{2\pi} i_2 (\alpha i_1 + \beta i_2 + \gamma i_3)$$

let us suppose that :

$$(2.82) \quad K = \alpha a + \beta + \gamma a^2 = \|K\| e^{j\Phi} \text{ where } a = e^{j\frac{2\pi}{3}}$$

In this paragraph, Re(K) is the real part of K.

The maximum force is reached after $\frac{1}{2}$ period and its value is :

$$(2.83) \quad \hat{F} = \frac{\mu_0}{2\pi} (I_k'' \sqrt{2} \kappa)^2 \|K\| \text{MAX} \left(\cos^2 \left(\frac{\Phi}{2} \right), \sin^2 \left(\frac{\Phi}{2} \right) \right)$$

$$\hat{F} = \frac{\mu_0}{2\pi} (I_k'' \sqrt{2} \kappa)^2 \frac{\|K\| + |\text{Re}(K)|}{2}$$

$$(2.84) \quad \kappa = 1.02 + 0.98 e^{\frac{-3R}{X}}$$

κ : factor for the calculation of the peak short-circuit current [Ref 11].

The main steps which allow one to obtain this relation are given in [Ref 99]. The solution to this problem seemingly allows the main situations met to be handled (separated phases and associated phases . . .).

The amplification coefficient in this case is not exact because this optimization is done on the force not on the dynamic response of the system. All components defined in paragraph 2.2 of Ref 1 are taken into account same as in the IEC standard. The dynamic behavior can differ likely like for the central busbar for an associated-phase layout in a three-phase fault in comparison with this optimization [Ref 8].

If the reference situation is calculated with an advanced method taking into account time constant and fault clearance time, the amplification coefficient is applied to the maximum $F_{\text{reference}}$.

$$(2.85) \quad \hat{F} = F_{\text{reference}} K_{xp}^{xb}$$

The tables given below can be used to find the maximum of asymmetry on a bar during a three-phase fault on two busbars. This asymmetry is given on phase 1 of the busbar 1.

c). Laplace's force due to the short-circuit

There are three possible layouts :

- separate-phase layout,
- asymmetrical associated-phase layout,
- symmetrical associated-phase layout.

For the *separate-phase layout*, the maximum LAPLACE force named reference in Table 2.5 is given by :

$$(2.86) \quad F_{\text{reference}} = \frac{\mu_0}{2\pi} \frac{(I_{k1}'' \sqrt{2} \kappa)^2}{d}$$

corresponding to a phase to earth fault in transfer situation.

For the *associated-phase layouts*, the maximum LAPLACE force named reference in Table 2.6 and Table 2.7 is given by :

$$(2.87) \quad F_{\text{reference}} = \frac{\mu_0}{2\pi} \frac{(I_k'' \sqrt{2} \kappa)^2}{d} \frac{3}{4}$$

corresponding to a phase to phase fault on one busbar.

Both these values can be calculated by advanced methods.

Separate-phase layout

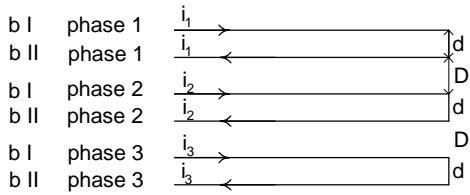


Figure 2.21 b= busbar

The following expression of LAPLACE's force on phase 2 of busbar 1 corresponds to separate-phase layout given above :

$$(2.88) F = \frac{\mu_0}{2\pi} i_2 \left(\frac{i_1}{D+d} - \frac{i_1}{D} + \frac{i_2}{d} - \frac{i_3}{D+d} + \frac{i_3}{D+2d} \right)$$

SEPARATE PHASE LAYOUT

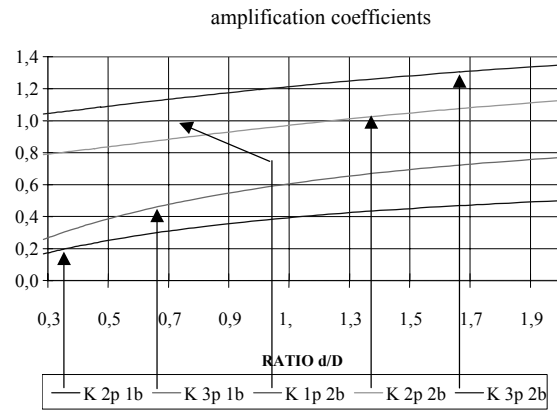


Figure 2.22 Comparison of stresses versus type of faults

Type of fault	block diagram analysed	Amplification Coefficients	Maximum Asymmetry	Remarks
single-phase fault developing through two busbars		$K_{1p}^{2b} = 1$	$\varphi_u = 0$	calculated by IEC 60865 or by advanced method.
two-phase fault developing through two busbars		$K_{2p}^{2b} = \frac{3}{4} \left(1 + \frac{d}{D} - \frac{d}{d+D} \right)$	$\varphi_u = 0$	if $I_{mono} = I_{tri}$
three-phase fault developing through two busbars		$K_{3p}^{2b} = \frac{\ K\ + Re(K) }{2}$ phase 1 busbar 2 $\alpha = 1$ $\beta = -\frac{d}{D} + \frac{d}{D+d}$ $\gamma = -\frac{d}{2D+d} + \frac{d}{2D+2d}$ $K = \alpha + \beta a^2 + \gamma a = \ K\ e^{j\phi}$ phase 2 busbar 1 or 2 $\alpha = \frac{d}{D+d} - \frac{d}{D}$ $\beta = 1$ $\gamma = -\frac{d}{D+d} + \frac{d}{D+2d}$ $K = \alpha a + \beta + \gamma a^2 = \ K\ e^{j\phi}$	$-\frac{\phi}{2} \pm v\pi$ $\frac{2\pi}{3} - \frac{\phi}{2} \pm v\frac{\pi}{2}$ where v is integer	if $I_{mono} = I_{tri}$

Table 2.5 Separated-phase layout Amplification Coefficients

Asymmetrical associated-phase layout

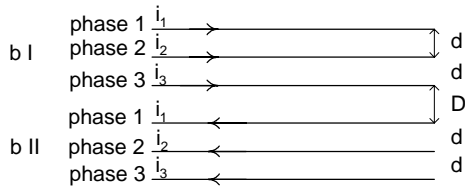


Figure 2.23 b=busbar

The following expression of Laplace's force on phase 2 of busbar 1 corresponds to the asymmetrical associated-phase layout represented above :

$$(2.89) F = \frac{\mu_0}{2\pi} i_2 \left(\frac{i_1}{d} - \frac{i_3}{d} + \frac{i_1}{D+d} + \frac{i_2}{D+2d} + \frac{i_3}{D+3d} \right)$$

ASYMMETRICAL ASSOCIATED PHASE LAYOUT

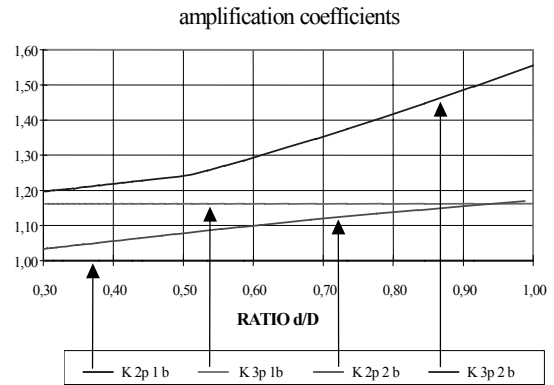


Figure 2.24 Comparison of stresses versus type of faults

Type of fault	block diagram analysed	Amplification Coefficients	Maximum Asymmetry	remarks
phase to phase fault		$K_{2p}^{1b} = 1$	$\varphi_u = 0$	calculated by IEC 60865 or by advanced method.
two-phase fault developing through two busbars		$K_{2p}^{2b} = 1 + \frac{d}{d+D} - \frac{d}{2d+D}$	$\varphi_u = 0$	
three-phase fault developing through two busbars		$K_{3p}^{2b} = \frac{4}{3} \frac{\ K\ + Re(K) }{2}$ <p>phase 2 busbar 1</p> $\alpha = 1 + \frac{d}{d+D}$ $\beta = \frac{d}{D+2d}$ $\gamma = -1 + \frac{d}{D+3d}$ $K = \alpha\alpha + \beta + \gamma^2 = \ K\ e^{j\phi}$ <p>phase 3 busbar 1</p> $\alpha = \frac{1}{2} + \frac{d}{D}$ $\beta = 1 + \frac{d}{d+D}$ $\gamma = \frac{d}{2d+D}$ $K = \alpha\alpha^2 + \beta\alpha + \gamma = \ K\ e^{j\phi}$	$\frac{2\pi}{3} - \frac{\phi}{2} \pm \nu \frac{\pi}{2}$ <p>where ν is integer</p> $\frac{\pi}{3} - \frac{\phi}{2} \pm \nu \frac{\pi}{2}$	

Table 2.6 Asymmetrical associated-phase layout Amplification Coefficients

Symmetrical associated-phase layout

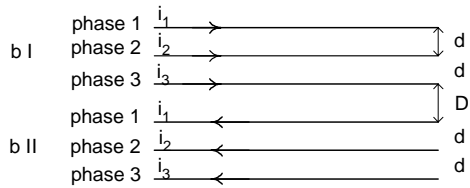


Figure 2.25 b=busbar

The following expression of Laplace's force on phase 2 of busbar 1 corresponds to the symmetrical associated-phase layout represented above :

$$(2.90) F = \frac{\mu_0}{2\pi} i_2 \left(\frac{i_1}{d} - \frac{i_3}{d} + \frac{i_3}{D+d} + \frac{i_2}{D+2d} + \frac{i_1}{D+3d} \right)$$

SYMMETRICAL ASSOCIATED PHASES

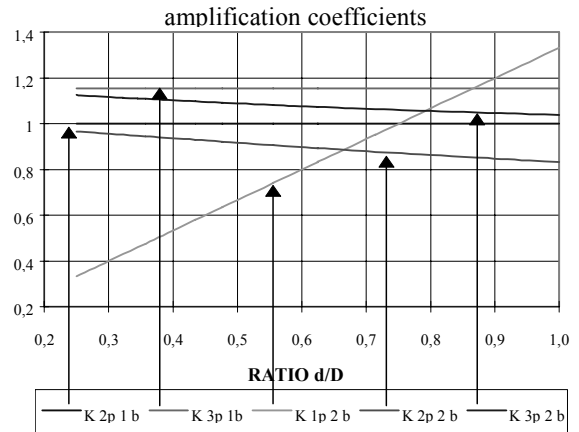


Figure 2.26 Comparison of stresses versus type of faults

Type of fault	block diagram analyzed	Amplification Coefficients	Maximum Asymmetry	remarks
phase to phase fault developing through one busbar		$K_{2p}^{1b} = 1$	$\varphi_u = 0$	calculated by IEC 60865 or by advanced method.
two-phase fault developing through two busbars		$K_{2p}^{2b} = 1 - \frac{d}{d+D} + \frac{d}{2d+D}$	$\varphi_u = 0$	$K_{2p}^{2b} < 1$
phase to earth fault developing through two busbars		$K_{1p}^{2b} = \frac{d}{D} \frac{4}{3}$	$\varphi_u = 0$	if $I_{mono} = I_{tri}$
three-phase fault developing through two busbars		$K_{3p}^{2b} = \frac{4}{3} \frac{\ K\ + Re(K) }{2}$ phase 2 busbar 1 or 2 $\alpha = 1 + \frac{d}{3d+D}$ $\beta = \frac{d}{D+2d}$ $\gamma = -1 + \frac{d}{D+d}$ $K = \alpha\alpha + \beta + \gamma\alpha^2 = \ K\ e^{j\phi}$	$\frac{2\pi}{3} - \frac{\phi}{2} \pm v \frac{\pi}{2}$ where v is integer	

Table 2.7 Symmetrical associated-phase layout Amplification Coefficients

d) Methods used

IEC 60865 method :

- Calculation of amplification factor,
- IEC Calculation on the reference case and application of amplification factor to :
 - * force on support of rigid conductors (Fd),
 - * resulting conductor stress (σ_{tot}).

Advanced method :

The amplification factor applies, for the calculation, on the same bases (τ and t_e) between the reference case and the considered situation (for example a three-phase fault on two busbars). Designers have to determine the bar and the phase for which the stress is maximum.

e) Examples

	Separate phase (1)	Asymmetrical phase (2)	Symmetrical phase (3)
d (m)	8.8	2	2
D (m)	4.8	2	2
α	-1.186	1.5	0.2
β	1	1.5	-0.750
γ	-0.254	0.333	-0.167
ϕ	-25.1°	180°	37.5°
$\ K\ $	1.9	1.167	0.83
ϕ_{max}	132.57°	60°	161.2°
ϕ_{min}	42.57°	-30°	71.2°
K	1.8102	1.5556	0.9921
ϕ_{max} Aster (4)	132.6°	60°	165°
K_{aster} (4)	1.78	1.5552	0.9477
%	1.67	0.02	4.47

Table 2.8 Example of calculation for various structure types, for three-phases fault on two busbars.

(1) : The maximum response is obtained for a three-phases fault on two busbars on phase 2 bar 1.

(2) : As for (1), the maximum response is for a three-phases fault on two busbars on phase 3 bar 1.

(3) : In the case of phase 1 bar 1 and $I_{mono} = I_{tri}$, for $\frac{d}{D} < \frac{\sqrt{3}}{2}$, the maximum response is obtained for a three-phase fault on one busbar. For $\frac{d}{D} > \frac{\sqrt{3}}{2}$, the phase to earth fault on two busbars has the maximum response.

(4) : Results obtained by the Code ASTER. Given a fault flowing on two busbars, the Code ASTER of E.D.F. allows one to compute the influence of the phase variation over the force applied to the central bar. The results have been noted on the Figure 2.27, Figure 2.28 and Figure 2.29.

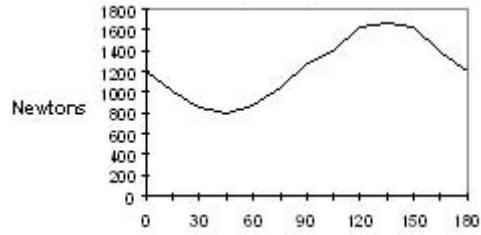


Figure 2.27 **Separate-phase layout**
Force on central bar during a three-phase fault on two busbars.

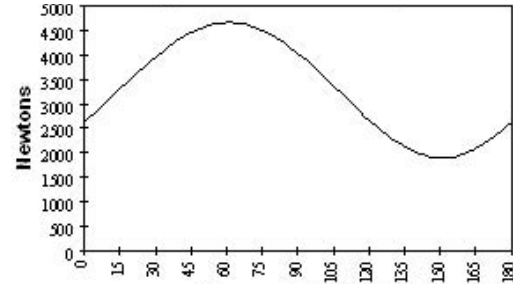


Figure 2.28 **Asymmetrical associated phase layout**
Maximum force during a three-phase fault on two busbars

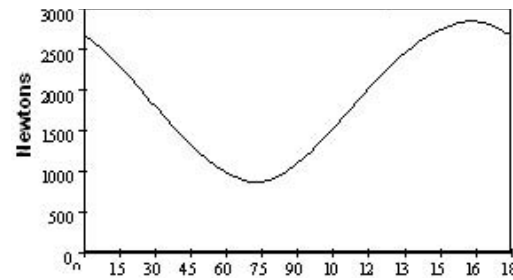


Figure 2.29 **Symmetrical associated phase layout**
Force on outside bar during a three-phase fault on two busbars.

3. FLEXIBLE BUSBARS

3.1. INTRODUCTION

In the past, extensive tests had been carried out to study the behaviour of arrangements with flexible conductors in substations and to evaluate methods for design purposes. At first simplified methods for calculation by hand had been developed for typical cases and later on analytical and numerical methods or a combination of both on computers. Nowadays two different methods are used depending on the task, the situation and the arrangement: simplified and advanced methods.

Simplified methods allow calculations by hand or personal computers [Ref 7] with analytical equations and figures. They are helpful for typical design cases with single or bundled conductors. Only general input data are necessary and the results are maximum values of tensile forces and displacements. The procedures are adjusted to practical requirements and contain simplifications with safety margins. Parameter sensitive investigations can be done in a very short time.

Advanced methods use finite element or finite difference modelling and powerful software is available for workstations and personal computers. They can be applied to any structural configuration with single and bundled conductors. Detailed modelling and basic structural data are necessary. The computation of the dynamic response of the complete structure including their non-linear behaviour is possible and accurate results can be obtained. The results are limited only by the degree of detail in the modelling and the availability of reliable basic structural data. The calculation of eigenfrequencies, time histories of forces, moments and deformations allow to study the system behaviour, to detect and improve weak points or to ascertain the short-circuit strength even for complex cases. Advanced methods will always be very helpful to better simulate actual loading, to limit safety factor used for inaccurate evaluation, to evaluate special cases, actual geometry, etc. Also the range of validity of simplified methods can be investigated.

In the International Standard IEC 60865-1 [Ref 2], which is identical with the European Standard EN 60865-1 [Ref 3], a simplified method is stated for the calculation of maximum values of the

- short-circuit tensile force F_t during or at the end of the short-circuit current flow,
- drop force F_f when the span falls down from its highest point of movement,

- pinch force F_{pi} in the case of bundled conductors, when the sub-conductors clash or reduce their distance without clashing,
- horizontal displacement b_h during the swing out of the span.

The physical background of the method, the assumptions and the derivation of the equations are given in detail in sections 4.2 and 4.3 of [Ref 1]. The good agreement of the calculation according to IEC 60865-1 with test results is shown in Annex 8.3 IEC 60865-2 [Ref 35] gives calculation examples.

Figure 1.1 shows seven different arrangements of flexible conductors which are predominant in substations; they are described in detail in clause 1.4 of [Ref 1]. IEC/EN 60865-1 [Ref 2, Ref 3] is applicable to the following horizontal spans in side-by-side configuration:

- Strain bus connected by insulator chains to steel structures (case A) without droppers in the span (case B).
- Strain bus, when the droppers are close to the insulator chains. The droppers may be neglected in the calculation.
- Connection between components or horizontal slack bus connected to support insulators (case C).
- Inclining span (case G).

In the standard, the span length is restricted to $l \leq 60$ m. However, the calculation is in good agreement with test results, even for strain bus with $l > 60$ m, see Annex 8.3.

As far as new developments concerned are concern, compared to IEC/EN 60865-1 [Ref 2, Ref 3], and CIGRE/IEC Brochure [Ref 1], there are some more steps to evaluate for understanding of the phenomena and getting new rules for design:

- the effects caused by droppers,
- the bundle pinch effect including spacer compression,
- the definition of equivalent static design loads taking into account structural dynamics
- and special problems.

First, Section 3.2 gives a survey of typical oscillograms of forces in substations and the application of advanced methods including foundations.

Section 3.3 deals with the behaviour of the droppers. It exemplifies by typical oscillograms and gives the results of advanced calculations. Calculations for a strain bus with dropper in the span (case A and B in Figure 1.1) as well as vertical droppers (cases E, F) cannot be actually done by applying IEC/EN 60865-1. Section 3.3 shows how to extend the method based on IEC/EN 60865-1 and new procedures are evaluated.

Section 3.4 deals with the effects of close and wide bundling. Typical oscillograms are shown and results of advanced calculations are given.

Design loads suggested in IEC/EN 60865-1 take the maximum instantaneous values of F_t , F_f , F_{pi} as static load for design purposes. The aim of Section 3.5 is to define the limits in which such design recommendations are valid and in which some correcting factors including dynamics of structure must be taken into account. Also new design loads are evaluated.

In Section 3.5.4, special problems are discussed. Interphase spacers allow to reduce the horizontal movement of the spans. The extension of IEC/EN 60865-1 on three-phase automatic reclosing, spacer compression and jumpers are described and it shows how to handle spans with springs.

3.2. TYPICAL OSCILLOGRAMS AND CALCULATIONS

3.2.1. Typical oscillograms of forces in the bus

Below are typical oscillograms for the short-circuit mechanical effects in the buses: forces in the supporting structure of slack conductors and tensile forces in strained conductors. A detailed description of the test structures and further informations are given in Volume two of this brochure and Volume two of [Ref 1]².

Typical forces in droppers are reproduced in Section 3.3.

The first effect is caused by the short-circuit forces between the phase conductors. In the upper oscillogram of Figure 3.1, the span of a slack conductor rotates several times and leads to nearly equal maxima during swing out and when it passes its initial static position.

In the lower oscillogram of Figure 3.1 and Figure 3.2 to Figure 3.4, mainly the two tensile force maxima caused by the movement of the span can be clearly pointed out; the first one due to swing out and the second one due to falling down. The basic frequency content of the time scale is the swing frequency of the busbars, with its sag according to the equation in section 1.3.3 of [Ref 1].

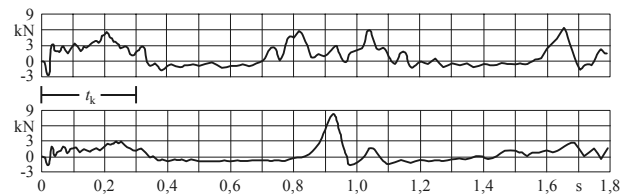


Figure 3.1 Single slack conductor: equivalent dynamic force at the clamp representing the stress at the bottom of the insulator (15-m-span); case 2, Figure 3.1 of the volume 2.

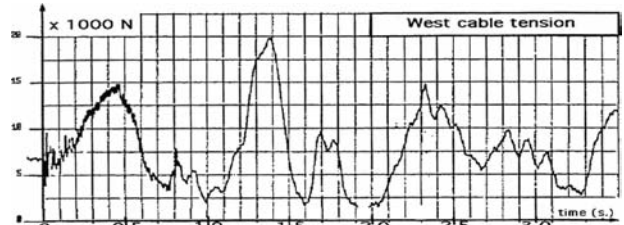


Figure 3.2 Single strained conductor (40-m-span); case *6, Figure 6.6

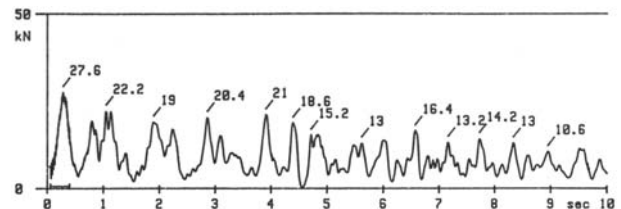


Figure 3.3 Single strain conductor (40-m-span); case *8, Figure 8.5

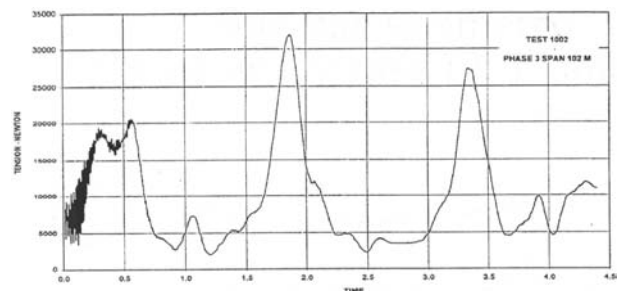


Figure 3.4 Single strain conductor (102-m-span); case *11, Figure 11.11

The pinch is another effect due to bundle collapse and the presence of spacers which impede conductors to come together near their location. In the subspan between two adjacent spacers, the sub-conductors can clash or can only reduce their distance. It depends on the ratio between the subspan length to sub-conductor distance l_s/a_s and sub-conductor distance to sub-conductor diameter a_s/d_s as discussed in section 4 of [Ref 1]. The parameter j according to equation (*49) in [Ref 1, Ref 2, Ref 3] indicates clashing or not clashing. Figure 3.5 to Figure 3.11 shows the tensile forces for different subspan characteristics

$$(3.1) \quad \lambda = \frac{l_s/a_s}{a_s/d_s} \sin \frac{\pi}{n}$$

If there is a close bundling which means that the bundle has a large ratio l_s/a_s , obtained by a very

² In the following, the numbers of test cases presented in Volume two of [Ref 1] are marked by *; test cases presented in Volume two of this brochure are not marked.

small sub-conductor separation a_s/d_s , the pinch is generally very limited and its duration is also very short. The oscillograms in Figure 3.5 to Figure 3.8 show clearly the electromagnetic force (the 50 Hz can be seen, progressively transferred to 100 Hz) with a sudden peak, just at the instance of contact. In the case of very large subspan and very short sub-conductor separation, the pinch is noticeable smaller, Figure 3.5. It is quite obvious that the situation is similar to Figure 3.3, single strain conductor.

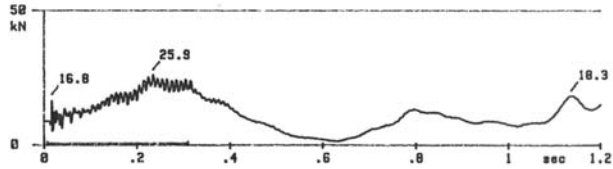


Figure 3.5 Tensile force with bundle pinch in a strain conductor; similar to case *8, twin bundle; very large subspan length, short sub-conductor separation: $l_s/a_s = 400$; $a_s/d_s = 1,9$; $\lambda = 211$

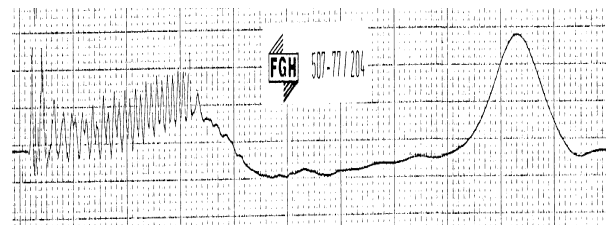


Figure 3.6 Tensile force with bundle pinch in a slack conductor; case 3, Figure 1a; twin bundle; large subspan length, short sub-conductor separation: $l_s/a_s = 79$; $a_s/d_s = 1,9$; $\lambda = 40$

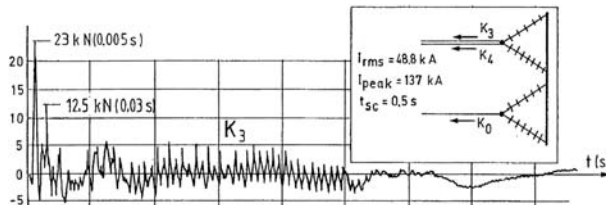


Figure 3.7 Tensile force with bundle pinch in a strain conductor; case *15, Figure 15.2; twin bundle; large subspan length, short sub-conductor separation: $l_s/a_s = 93$; $a_s/d_s = 2,1$; $\lambda = 44$

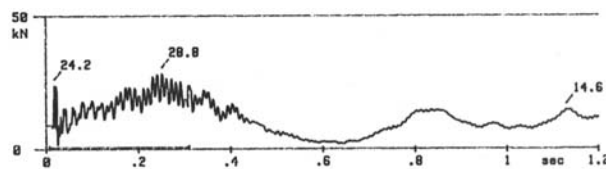


Figure 3.8 Tensile force with bundle pinch in a strain conductor; similar to case *8, twin bundle; large subspan length, short sub-conductor separation: $l_s/a_s = 50$; $a_s/d_s = 1,9$; $\lambda = 26$

In the opposite case, a large sub-conductor separation a_s/d_s , which is so called wide bundling, the contact do not necessary appear and the increase of tension can be rather high and its application rather low. We cannot see any more the electromagnetic force details in Figure 3.9 to Figure 3.11. The electromagnetic force is completely masked by the increase of tension in

the conductor which is due to its movement trying to come into contact. This case is the most dangerous case.

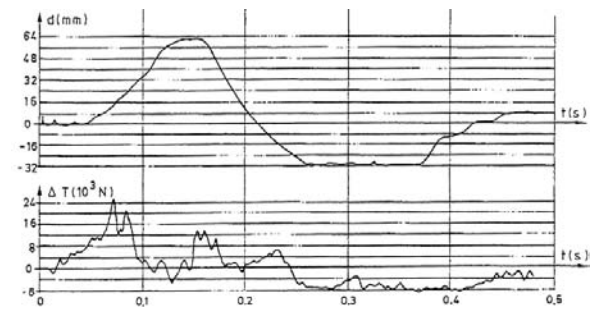


Figure 3.9 Bundle pinch in a strain conductor; triple bundle; case *13, p. 67, Figure 13.3: displacement of the support and pinch effect in the bus; large subspan length, large sub-conductor separation: $l_s/a_s = 67$; $a_s/d_s = 12,4$; $\lambda = 4,7$

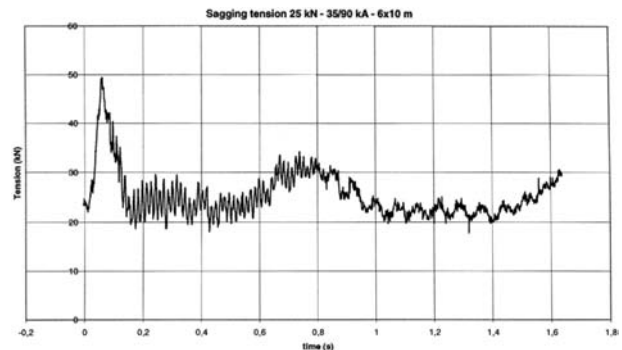


Figure 3.10 Bundle pinch in a strain conductor; case 8 §10.9 of the volume 2, twin bundle; short subspan length, large sub-conductor separation: $l_s/a_s = 21$; $a_s/d_s = 16,5$; $\lambda = 1,3$

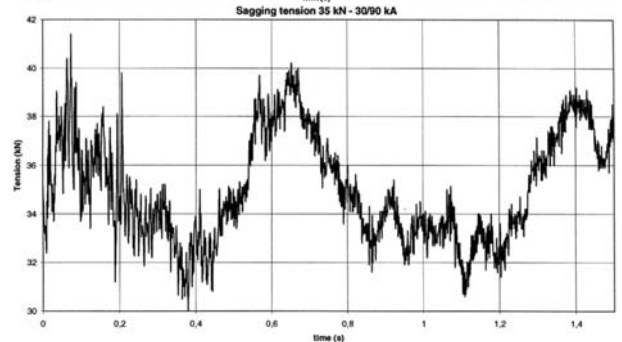
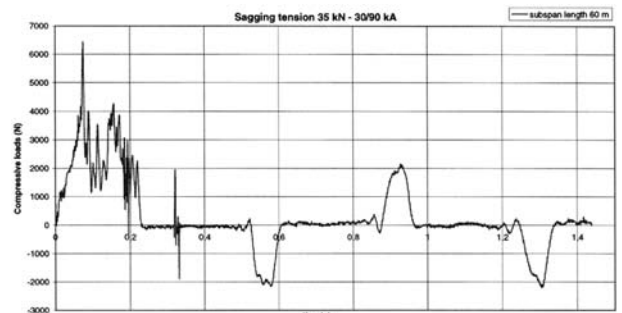


Figure 3.11 Bundle pinch in a strained conductor; case 8 §10.7 of the volume 2, twin bundle; large subspan length, large sub-conductor separation: $l_s/a_s = 131$; $a_s/d_s = 16,5$; $\lambda = 7,9$ The upper oscillogram shows the spacer compression and the lower one the tensile force in the sub-conductor.

In Figure 3.5 to Figure 3.8, the maximum tensile force due to pinch effect is the same magnitude or lower than the tensile force during swing-out of the bus. This indicates that the bundle conductors clash effectively. The ratio λ is greater than about 25 according to equations (*43) and (*44) in [Ref 1, Ref 2, Ref 3] which result from tests e. g. cases 1 and 3. Ratios λ less than 25 should be avoided, Figure 3.9 to Figure 3.11.

In the case shown in Figure 3.11, common for overhead lines, the pinch can depend significantly on the ratios mentioned above. The transient after the short-circuit ends is typical of wave propagation along the subspan. This phenomenon can be observed on the accompanying video.

Depending on the geometry, similar short-circuit have very different design loads. A structure will not behave in a similar way if the load shape is going from Figure 3.1 to Figure 3.11, even if the maximum instantaneous peak would be similar in all cases.

3.2.2. Application of advanced method on high voltage busbar system

Figure 3.12 shows the complete test arrangement consisting of two mechanically coupled spans which is modeled using Finite Element Method (FE).

The lattice type steel towers and cross arms are welded constructions of T and L cross-sections. The mid portal has more stiffness, as it is movable.

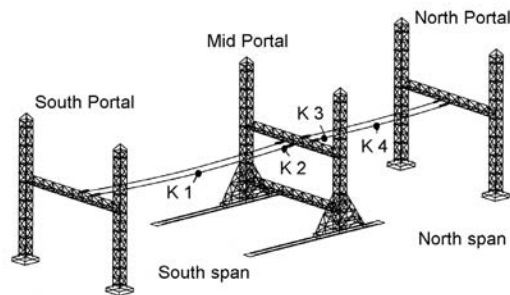


Figure 3.12 FE modelling of the busbar system with force measuring points K1, K2, K3, K4.

To stabilize this type of construction, the towers need larger bottom part. Towers are 18m high, portals 18m wide, cross arms are at ca.10m height and the spans are 37.35m (South) and 27.40m (North). Phase distance of the conductors 1 x AC SR 537/53 is 1.84m.

The suspensions consist of 8-element chains of glass or cap- and-pin insulators.

The components of the studied busbar system represent an assembly. For the FE model, see Figure 3.12, this assembly is transformed into a

finite number of such finite element types that are best suited for modelling the structural parts in question. The discrete elements of the system are connected by nodes.

For modelling the substation, element types from the element library of the FE-programm ABAQUS [Ref 33] were used [Ref 40].

The aim of any modelling is to achieve a quality of the FE model so the deviations between calculation using the model and the behaviour of the real arrangement become negligible. To test and verify the adequacy of the FE model of the portal structures the following comparative FE calculations were performed [Ref 49].

Bending stiffness of the component towers and crossarms, as well as of the complete portals is one important parameter to characterise the mechanical properties. The respective FE calculated characteristic must be in conformity with those of the real arrangement. The 7 step unidirectional test cycles of two identical static loads applied at the conductor suspension points had shown a practically linear characteristic without hysteresis, so that stiffness can be expressed in terms of a spring constant [Ref 34]. Field tests performed by the members of the WG 121.2 of the German Electrotechnical Commission DKE on a variety of portals have come to the same result.

The respective calculations therefore need only one check for one convenient value of the loads and under exact validity of Hook's law.

The calculated and the measured spring constants are graphically compared in Figure 3.13. The achieved conformity for South/North portals of lesser stiffness is excellent and it is very good for the mid portal.

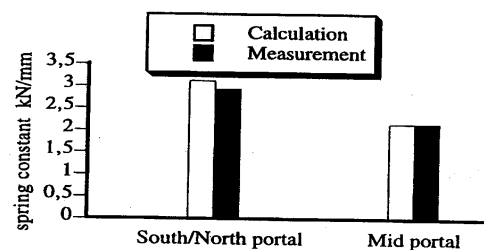


Figure 3.13 Comparison of calculated and measured spring constants

For the dynamic studies on the model, the first, the second, and the third eigenfrequencies should be the same as those of the real arrangement. From measurement only the first modes of the crossarms and of the towers are known. While the calculation of higher modes is easy, measurement is extremely complicated for large mechanical structures and may be, if at all, only available for components. The conformity of the first modes is a very strong criteria for good modelling.

Only the first eigenfrequencies can be compared in Figure 3.14, which shows an excellent conformity between the calculated and the measured values. The very good conformity of the calculated spring constants and first eigenfrequencies with the measured values proves the validity of the FE model used for the simulation of the portals.

Hence, all static and dynamic analyses can be performed on this model.

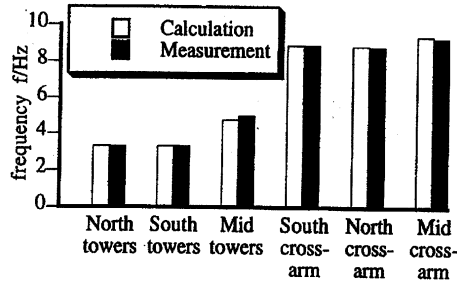


Figure 3.14 Comparison of calculated and measured 1st eigenfrequencies

Experience has shown that, although the short-circuit movements of stranded conductors seem to be chaotic, the relevant effects of symmetric arrangements and excitation are in fact also symmetrical. The measuring points could, therefore, be arranged to a half of the plane of symmetry as shown in Figure 3.15 on crossarm, tower and bottom end of tower, i.e. interface to foundation.

In order to be able to validate and compare the measured, respectively calculated mechanical stresses at the different points of the structure as illustrated in Figure 3.15, the Equivalent Static Load ESL and the ESL-factors are introduced. Since the short-circuit forces F_{pi} , F_t and F_f contain the static pre-load the ESL-factor is to be defined as the quotient of the Equivalent Static Load divided by the short-circuit load including the static pre-load.

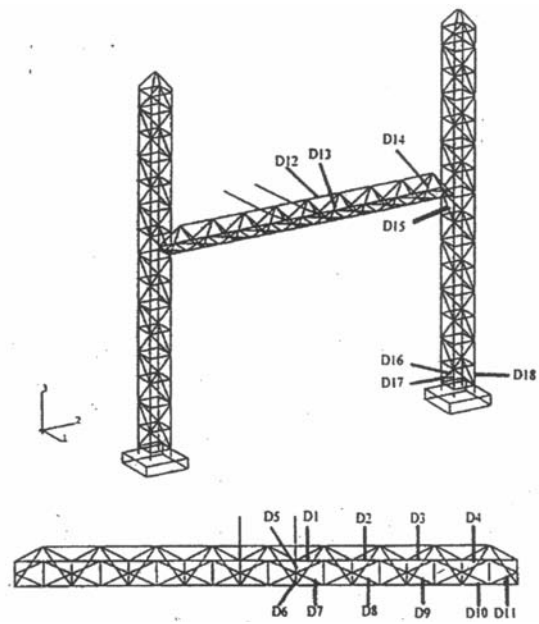


Figure 3.15 Strain gauge measuring points in the South portal

Since it is possible to separate the static pre-load and the dynamic part of F_{pi} , F_b , F_f , one can, also define another type of ESL related to the dynamic portion alone. Since the static pre-load is a particularly important parameter for the magnitude of F_{pi} , this other definition is more suited and practical for the dynamic portion of the swing-out and the conductor-fall maximum. In the present context the index d -for dynamic -is employed in ESLd and ESLd Factor.

The evaluation of the present tests does not explicitly distinguish between swing-out and conductor-fall ESL, the relevant short-circuit test maxima being swing-out (Index t), and the conductor drop- ping tests delivering ESLf anyway. Because of the single conductors there is no pinch effect, i.e. no F_{pi} .

Figure 3.16 and Figure 3.17 display the comparison of the measured and calculated relative static strain for the South/North portals and the Mid portal.

Generally the comparison shows a very good agreement between calculated and measured values with the exception of one diagonal in the bottom girder of the crossarm, for which particular anomaly a reason is being looked for .

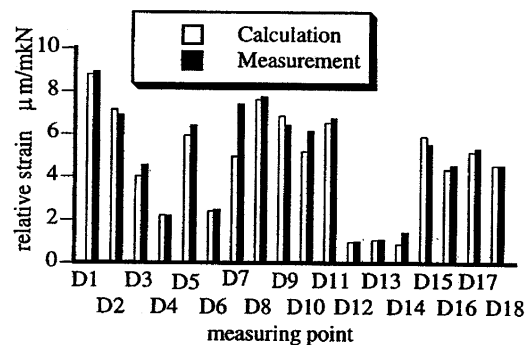


Figure 3.16 Comparison calculated and measured relative static strain South portal

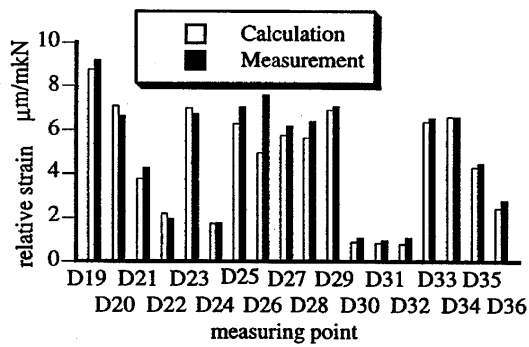


Figure 3.17 Comparison calculated and measured relative static strain Mid portal

As shown in Figure 3.12 force transducers K1 to K4 allow to measure the static and the dynamic forces in the conductor span and onto the mid portal. Material strain is measured at the same strain gauge measuring points as for the static tests.

The calculation was performed for the first 4s of the conductor fall process. As an example for the very good agreement between calculation and test results, Figure 3.18 and Figure 3.19 compare the calculated and measured oscillograms, together with the respective maximum values of the tension forces K2, K3 and the selected material strain at D 17 for the case A, i.e. without counterweights.

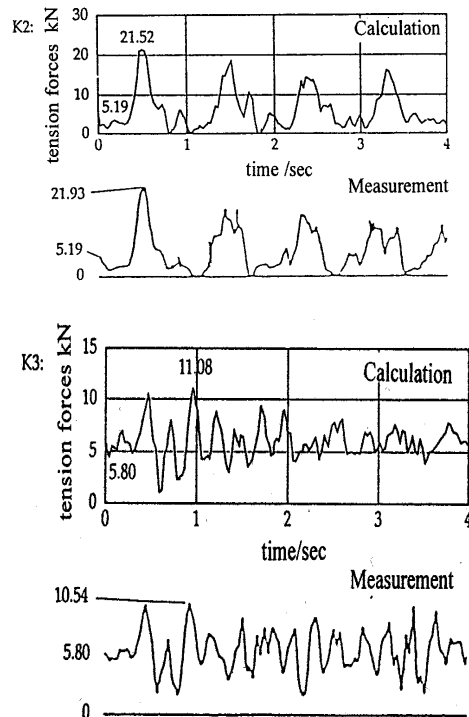


Figure 3.18 Calculated and measured oscillograms for measuring points K1 to K4, Case A .

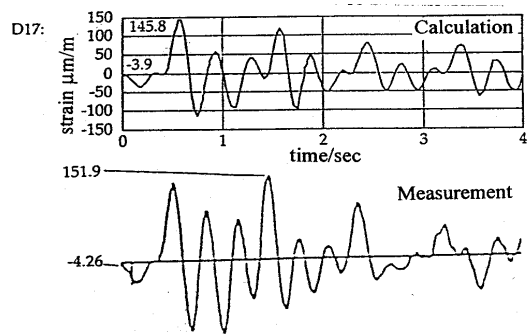


Figure 3.19 Calculated and measured oscillograms for measuring point D17

From the comparison of the calculated and measured oscillograms and maximum values of forces and material strains, as well as of the ESL-factors, it is possible to speak of a very good agreement between calculation and measurement [Ref 49].

3.3. THE DROPPER BEHAVIOUR

3.3.1. Introduction

Droppers are suspended conductors between the main bus bars or switch-bays and apparatus, insulator support or bushing. These are the typical situations B and E in Figure 1.1. The dropper stress is generally very low in initial conditions, i.e. less than 1 N/mm^2 , but can be stretched during short-circuit mechanical effects. Either due to main bus or switch-bay cable oscillations (in such a case there is no need to have any current in it) or simply due to electrodynamic forces if the short-circuit current is going through it or in combination of both.

In addition to stretch, droppers are also submitted to tensile force during swing-out, drop force and pinch effect; (in the case of bundle configuration only). Due to the very unlevelled structure and very low tension in it, dropper behaviour is quite different from the main bus and corresponding effects cannot be evaluated by actual IEC/EN 60865-1.

Droppers, generally more than one per span, and very sensibly influences the main bus mechanical behaviour limiting by, for example, the falling down effects. Their position in the bus, moreover to practical electrical aspects for design, can be chosen to limit the short-circuit effects in the main bus. But the consequence on the dropper and corresponding loads applied at the bottom of the dropper on apparatus must be carefully evaluated.

Figure 3.20 details all kind of dropper effects used in open-air substations and classifies six different configurations.

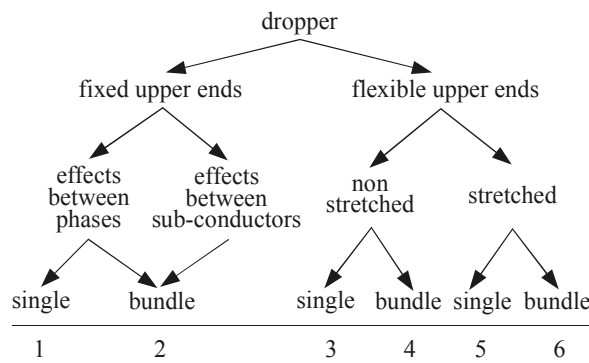


Figure 3.20 Case study for dropper configuration

With configurations 1 and 2 the current is always flowing through the droppers. Configurations 3 to 5 occur when short-circuit current is going through the droppers. When there is no current in the dropper, the dangerous situation is limited to configurations 5 and 6 with stretched droppers.

In this chapter all these configurations will be evaluated either by simplified, if possible, or advanced computation method, which can be used in all configurations. Experimental confrontations with advanced methods are given in section 3.3.3, with

simplified method according to IEC/EN 60865-1 in annex 8.3.

The final result will be to obtain the forces F_i and F_f in the bus during swing-out and fall of the bus and its maximum horizontal displacement as well as the load F_{ds} in the lower clamp of the dropper and its corresponding ESL.

3.3.2. Typical oscillograms

a) Droppers with fixed upper ends (configurations 1 and 2)

A dropper can have a fixed upper end as connection E in Figure 1.1. When connection B is fastened near the insulator string, the upper end will move slightly due to the movement of the span and can be treated as (nearly) fixed. Both correspond to configurations 1 and 2 in Figure 3.20.

In configurations *17 for single conductors and *18 for bundled conductors, oscillograms for droppers with fixed upper ends are given. Figure 3.21 shows an example.

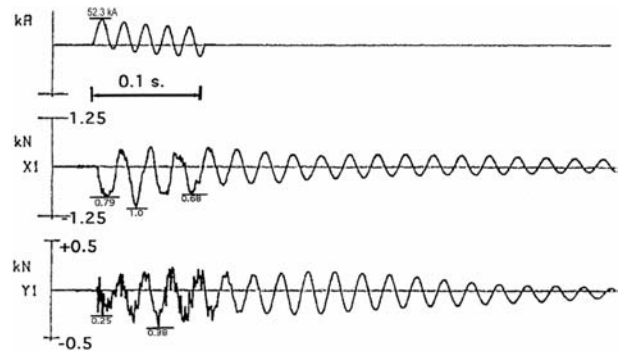


Figure 3.21 Oscillograms of horizontal components x and y of the load applied to supporting insulator at the bottom side. Case *17, p. 79, Figure 17.2

The droppers have no stretching because the two end points are more or less fixed. Generally the electrodynamic load can be directly seen on the force. If the dropper length permits large movement, same behaviour as a main bus can be seen, swing out and falling down can occur, but the force value is much lower due to initial very limited value. Some local effects i.e. right angle at the top can induce some peaks just after short-circuit inception.

The test configuration can considerably affect the results. Especially for voltage level around 123 kV; that is because basic frequency of apparatus are close to 50 or 60 Hz. This is true for test configurations *17 and *18.

Bending stiffness of the conductors usually ignored has also significant influence on the loads applied at the fixation on the insulator at the bottom. The clamp on the top of insulator support was very rigid so that general

movement of the dropper (swing out and falling down) were much more a swing with limited falling down.

We must consider different maxima, the maximum of which will be F_{ds} . Simplified methods are given in paragraph 3.3.4.

b) Droppers with flexible upper ends (configurations 3 to 6)

Droppers in or near the middle of the span as case B in Figure 1.1 have flexible upper ends. The short-circuit current can flow through the whole span and the dropper is without current, current path B in Figure 3.22, or through half the span and then through the dropper, current path C. With path B the dropper behaviour is only affected by the movement of the main bus, whereas with path C additional loads due to the electromagnetic forces between the droppers arise and due to pinch effect in bundled conductors. Current path A is the reference arrangement without dropper.

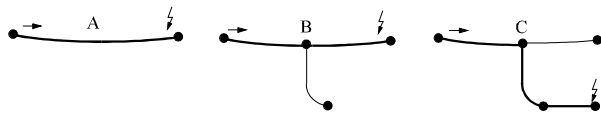


Figure 3.22 Current paths
A without dropper
B, C with dropper

Tests with droppers in midspan are described in test cases *6, *7, 4 and 5 and also in [Ref 39].

The first point to develop is to determine if the dropper will be stretched or not. Advanced method is used to study the structure behaviour. Simplified method can be used to evaluate the horizontal movement of the bus-bars and then to calculate the maximum distance from the attachment points (bus and support) and compare it to the dropper length as derived in section 3.3.4a). If dropper length is unknown you will always assume a stretch.

Configuration 3: non stretched single conductor. This case has not to be considered for design if the current path is B, see Figure 3.23; other loading will be more important (wind speed). With current path C, a significant force at the lower end of the dropper has to be taken into consideration, Figure 3.24 due to the forces induced in the droppers by the currents in the phases. In the main bus, maximum horizontal displacement and tensile forces caused by swing-out and fall of span are similar to those known from spans without droppers, but lower values with current path C than with current path B, see Figure 3.34.

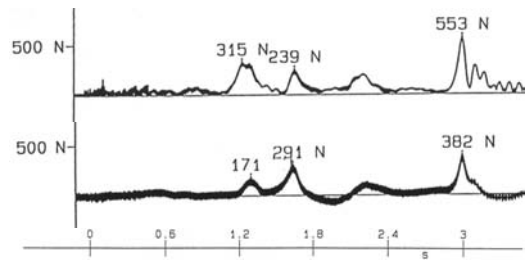


Figure 3.23 Droppers not stretched, current path B: horizontal and vertical forces at the top of the insulator; case 5, of the volume 2 Figure 7.1

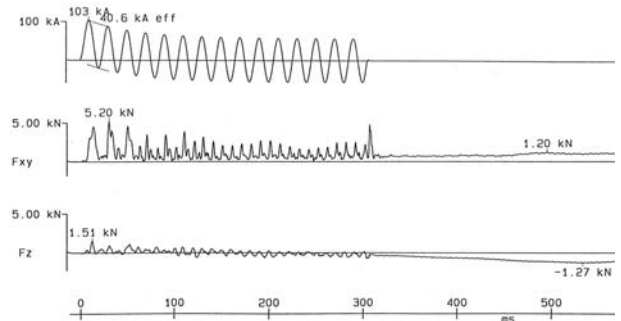


Figure 3.24 Droppers not stretched, current path C: horizontal and vertical forces at the top of the insulator; case 5, of the volume 2 Figure 7.2

Configuration 4: non stretched bundle conductor. With current path B this case needs no consideration in design. With current path C, the pinch effect is in addition to the effects between phases in case 3. The pinch effect can be evaluated following IEC/EN 60865-1 and then transferred to filter for ESL, see paragraph 6.3. The main bus behaviour is the same as in configuration 3.

It should be noticed, that a non stretched dropper also has an influence on the movement of the main bus which is shown in Figure 3.34.

Configuration 5: stretched single conductor. This is an important configuration observed in data reference tests (tests *6, *7, 4 and 5 and [Ref 39]). Some typical dropper stretch are studied in annex 8.1. Applied load on structures can overpass 20 kN. The load is a typical impulse load, maxima occur during the stretching of the dropper, due to the movement of the main busbar. The impulse come back with a frequency connected to the main busbar swing frequency. Impulse duration is about 0,1 s and depends on the dropper length. The swing-out of the busbar is hindered, the swing-out tensile force is nearly the same as that without dropper, but the appearance of a fall of span depends on the dropper length, see Figure 3.35. In addition with current path C, the forces at the lower ends of the droppers are to be minded.

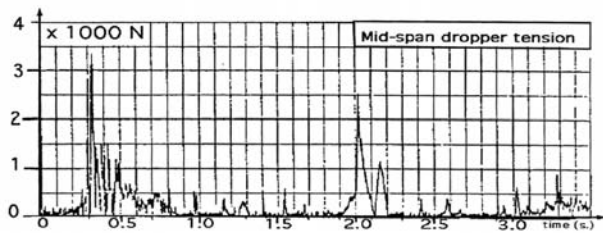


Figure 3.25 Dropper stretch, current path B: force at the top of the insulator (two times); case *6, Figure 6.9

Configuration 6: stretched bundle conductor. With current path B, this case is identical to configuration 5. With current path C, an addition to configuration 5 a force will be obtained by bundle pinch.

3.3.3. Advanced computation results

Advanced method for the simulation of rigid and flexible bus-bars is nowadays easy to handle and very precise, even for very complex cases, like dropper stretch and bundle pinch. Nowadays, commercially available finite element programs such as ADINA [Ref 36], ASTER [Ref 37], SAMCEF [Ref 38] are capable of calculating the electromagnetic forces due to the short-circuit currents.

a) Creation of the finite element model

There are two different ways following the aim of the simulation. Either you design a substation or you would like to compare tests and simulation on a known structure. Refurbishment or uprating can be considered as design, but some more data are sometimes available and will help to refine the approach.

There are no problem concerning busbars itself: known conductor (means mass, cross section, material, diameter) of known sags in given conditions, insulator chain known in their detailed geometry (mass and length being the most important). They can be easily discretised into small conductor (say half a meter long e. g.) elements, neglecting bending stiffness. The bending stiffness has small effect in most of the cases, including bundle behaviour during pinch effect. In case of bundle conductors, very small finite element (say less than half sub-conductor separation) are to be used near spacers. The droppers must of course be included in the model and corresponding reference position must be evaluated taking into account mounting procedure (e. g. sagging tension is defined in absence of droppers, which are connected afterwards), then the structure is evaluated in the initial conditions before short-circuit. It is not necessary obvious which conditions is more critical because of nonlinear behaviour of the structure and the loads. Different assumption have to be made for design. Of course larger sags will give less clearances, but maximum loads on structures can be induced by other initial conditions, the use of simplified method (qualitatively valid) help to find out worst sagging conditions.

The main problem concern supporting structures, which are generally unknown (in the details) at design stage. Mainly the stiffness effect can induce considerable reduction of the resulting loads applied on it. It means that in case of test configurations, detailed data of the structures must be measured and known, like at least anchoring point stiffness and first eigen-frequencies. The finite element model of the structure must utilize those data. But in case of design, neglecting the effect of structure stiffness is too conservative. It is suggested to use classical order of magnitude for corresponding structures, based on the data given in Tables 1.2 and 1.3 of [Ref 1].

b) Comparison of calculation and experimental results

Some examined configurations are shown in the following figures. The accordance of measurement and calculation of all cases is remarkable and shows the validity of this calculation method. The results of Figure 3.26, Figure 3.27, Figure 3.31, Figure 3.32, and Figure 3.33 were simulated with SAMCEF [Ref 38], the results of Figure 3.28 and Figure 3.29 with ABAQUS [Ref 39].

In the first example of a dropper with fixed upper end, it is quite interesting to compare in Figure 3.26 the two simulated curves of case *17, p. 79, Figure 17.3, which shows strong dynamic effects of the support (the two curves are far from being identical) whose basic frequency was close to 30 Hz. The simulation gives access to the bending moment in the support, Figure 3.27, from which design load can be deduced. X1 curve of the Figure 3.21 can be straight fully compared to the left curve.

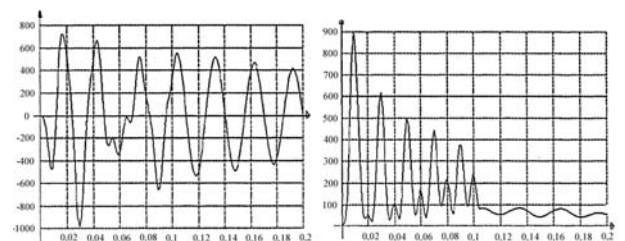


Figure 3.26 Simulation of the horizontal component of the force at the top of insulator support (on the left) and force in the dropper near the clamp (on the right); case *17, Figure 17.3

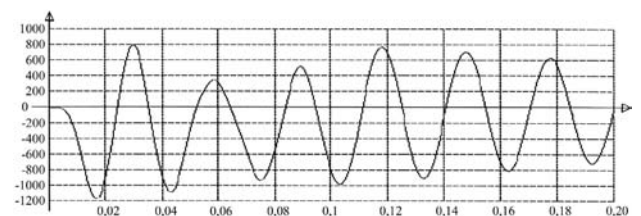


Figure 3.27 Bending moment at the bottom of insulator support; case *17, test 74, $I_{rms} = 20,2$ kA

The ESL which is the design load can be evaluated using maxima of the bending moment and dividing it by the length of the insulator of 1,5 m:

$$(3.2) \quad ESL = 1200 \text{ N.m}/1,5 \text{ m} = 800 \text{ N}$$

This value has to be compared with the minimum cantilever breaking load of the insulator. The corresponding ESL factor becomes: $900 \text{ N}/800 \text{ N} = 1,13$, compared to maximum force in the dropper.

The next example in Figure 3.28 shows the forces in a long span of 102 m. The data and the measured oscillogram can be found in case *10, Figure 10.9, p. 53.

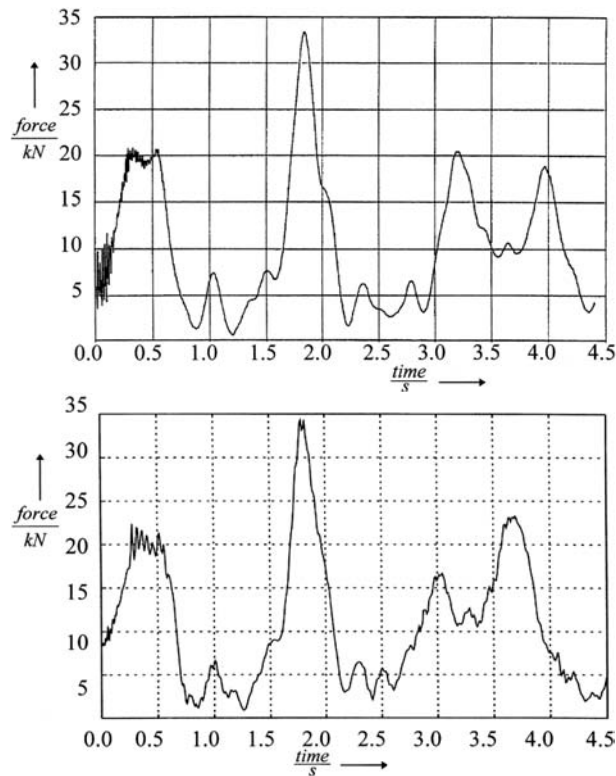


Figure 3.28 Measured and calculated tensile force at the transition between insulator chain and traverse; case *10, Figure 10.9

In the next example, three different current paths A, B and C in Figure 3.22, using sets of three different short-circuit currents, 20 kA, 28,3 kA and 40 kA were measured and calculated for case 4. For each combination of configuration and short-circuit current two measurements at the transition between insulator chain and traverse were conducted. This results in four measurements per combination are registered for current paths A, B and C. Figure 3.29 shows the time histories of the forces and Figure 3.30 compares the maxima of the swing-out force F_t and the drop force F_f for different short-circuit currents.

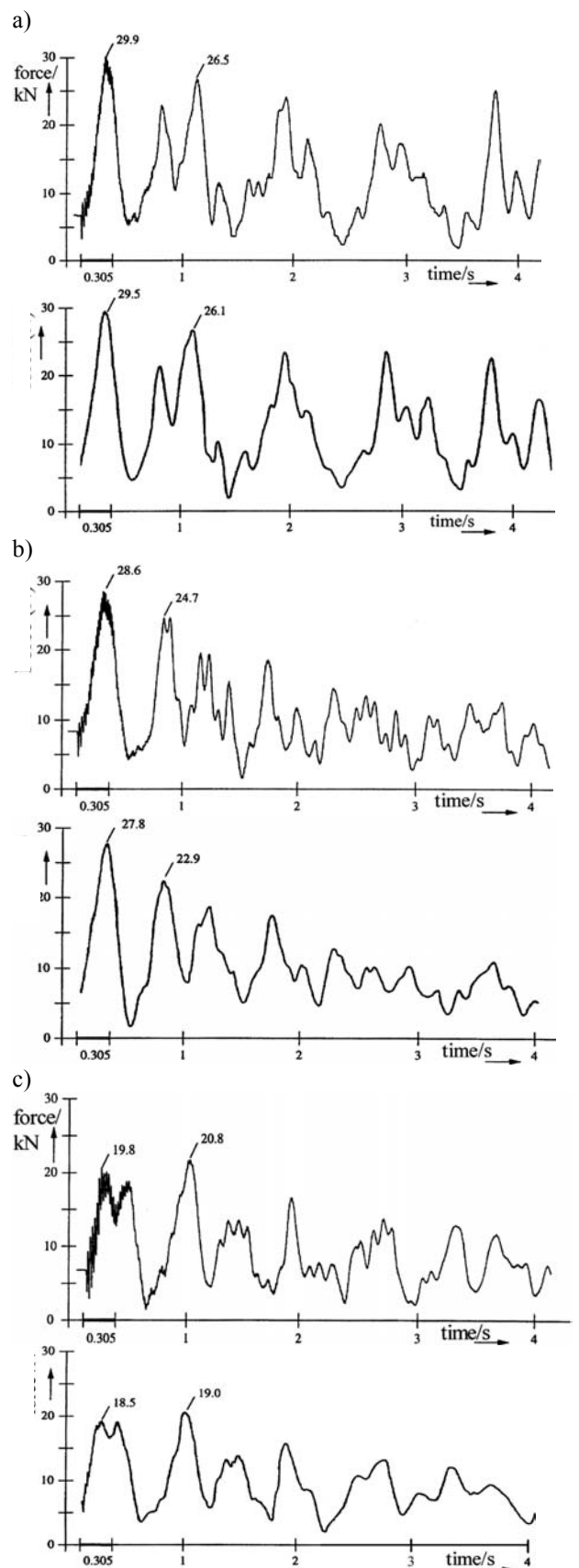


Figure 3.29 Measured and calculated tensile forces (kN) at the transition between insulator chain and traverse (east side), $I_k = 28,3 \text{ kA}$, $t_k = 300 \text{ ms}$

- a) current path A
- b) current path B
- c) current path C

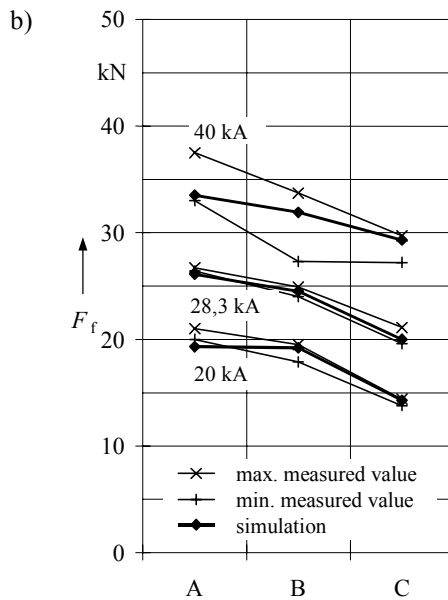
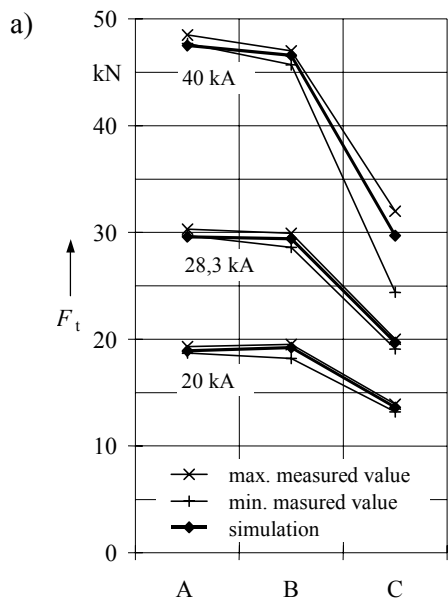


Figure 3.30 Comparison between measured and calculated forces for current paths A, B, C and different short-circuit currents, $t_k = 0,3$ s
 a) Short-circuit tensile force F_t
 b) Drop force F_r

In an other example taken from case *6, the tensile forces in the bus and the moments in the pillars of the tower are shown in Figure 3.31 and Figure 3.32.

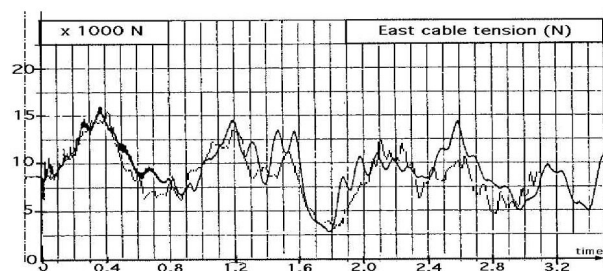


Figure 3.31 Measured and calculated tensile forces at the transition between insulator chain and cross-arm; case *4, Figure 4.6

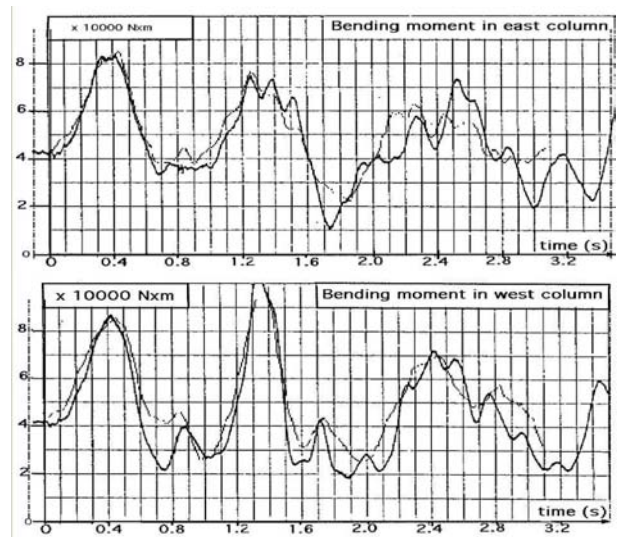


Figure 3.32 Bending moments in the east and west column of north pillar; case *4, Figures 4.8 and 4.9

In the last example, there is a dropper in midspan which is fully stretched during swing-out of the bus, see case *6. Comparison of measured and calculated dropper tension using advanced method is shown in Figure 3.33.

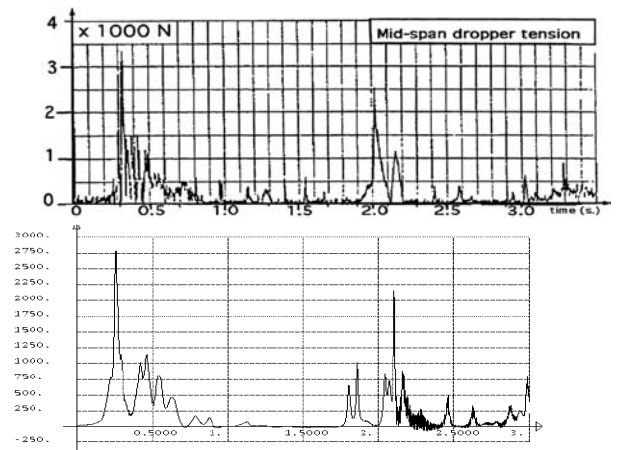


Figure 3.33 Measured and calculated dropper tension, with two dropper stretch; case *6, Figure 6.9.

3.3.4. Simplified methods

As shown in Section 3.3.2, the droppers can cause forces on the apparatus or insulators at their lower end and the clamps at their upper end. Span droppers can have an influence on the movement and the forces in the main conductor buses. Therefore it is necessary to evaluate simplified methods for the calculation of the forces and the horizontal displacements of the main conductors and the forces at the lower ends of the droppers.

a) Effects on main conductors

If the droppers are fixed at the end of the main conductors or at the towers (cases A and B in Figure 1.1) the main conductor effects can be calculated by the simplified method presented in IEC 60865-1 [Ref 2] and

EN 60865-1 [Ref 3] with the assumption to neglect the droppers.

In the case of mid-span droppers, a simplified method is derived based on many tests done by e.g. RTE [Ref 39] and FGH (cases 4 and 5 in Volume two) [Ref 40, Ref 41, Ref 42, Ref 43].

The different geometrical and electrical parameters of the test arrangements give a good overall view of the physical effects. Figure 3.22 shows the current paths: The short-circuit currents are flowing over the complete span (path B), or over half the span and the droppers (path C). Reference is path A, a spans without droppers.

Figure 3.34 and Figure 3.35 show the movements and the corresponding forces in the main conductors. To derive a simplified method, the following values are also drawn in³:

- b_{c0} measured static sag
- b_c equivalent static conductor sag at midspan, according to equation [(22)]
- b_{ct} equivalent dynamic conductor sag at midspan, $b_{ct} = C_F C_D b_c$ according to equation [(41)]
- δ_k swing-out angle at the end of the short-circuit current flow, according to equation [(4.8)]
- δ_l direction of the resulting force on the main conductor, according to equation [(21)]
- δ_m maximum swing-out angle for the span neglecting the influence of the dropper, according to equation [(31)]

To evaluate these values, an equivalent span is regarded which corresponds to the actual span without dropper but having the actual static tensile force F_{st} ; in the following called "*span without dropper*".

There is also a circle given with the centre point in the lower fixing of the dropper and the radius l_{dmax} . l_{dmax} is the projection of the dropper length on the vertical axis which neglects bending stiffness and elasticity. This circle gives a good approximation of the movement upwards of the main-conductor. The intersection point with the circle b_{ct} gives the actual maximum swing out angle δ_{max} of the main conductor which follows from the geometry:

$$(3.3) \quad \cos \delta_{max} = \frac{[H - (b_{c0} - b_c)]^2 + b_{ct}^2 - l_{dmax}^2}{2 b_{ct} [H - (b_{c0} - b_c)]}$$

H is the (vertical) distance between the lower fixing of the dropper and the anchoring points of the main conductor at the tower.

³ In the following, the equation numbers in square brackets with * refer to [Ref 2, Ref 3] and section 4.8 of [Ref 1]; without * to [Ref 1]

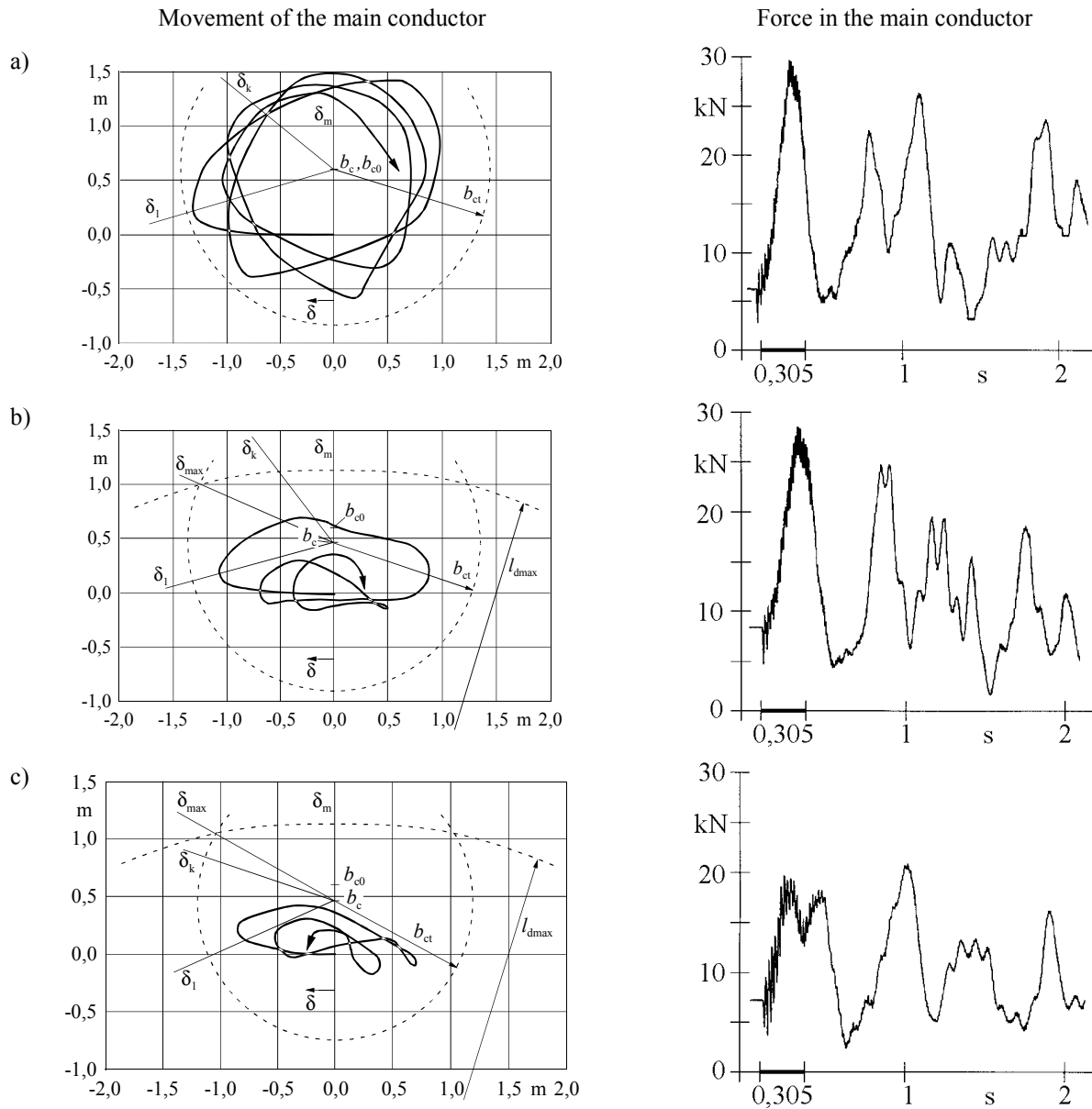


Figure 3.34 Movement of the main conductor and forces in the main conductor; case 4 [Ref 43, Ref 44]

$I_k = 28,3 \text{ kA}$; $t_k = 0,3 \text{ s}$

a) without dropper: current path A

b) with dropper: current path B; dropper length 6,045m

c) with dropper: current path C; dropper length 6,045m

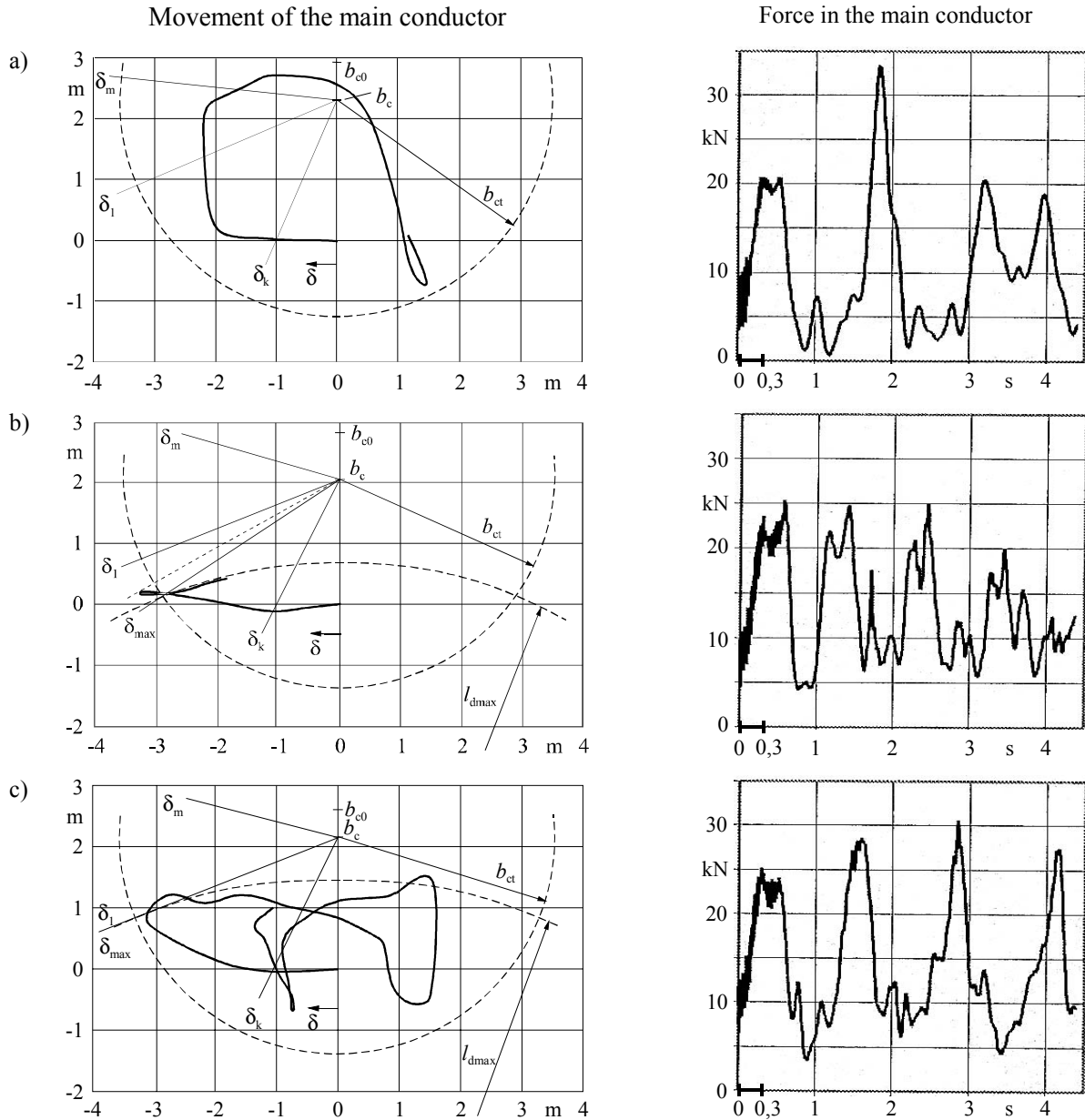


Figure 3.35 Movement of the main conductor and forces in the main conductor [Ref 39]

$I_k = 30 \text{ kA}$; $t_k = 0,3 \text{ s}$

- a) without dropper : current path A
- b) and c) with dropper: current path B; dropper lengths 8,1 m and 9,1 m

To estimate δ_{\max} according to equation (3.3) it is necessary to calculate the dynamic sag b_{ct} of the span without dropper. This needs the knowledge of the short-circuit tensile force F_t without dropper. Therefore the calculation is done with equations [(*)20] - [(*)34] and equations [(*)36] - [(*)39] and it becomes $b_{ct} = C_F C_D b_c$.

The swing-out angle at which the short-circuit tensile force F_t occurs in a span with dropper depends on the actual maximum swing-out angle δ_{\max} . If $\delta_{\max} > \delta_1$, the swingout of the span is not influenced by the dropper during $T_{res}/4$; F_t is reached unless the dropper stretches and the calculation is equal to a span without dropper. In the other case if $\delta_{\max} < \delta_1$, the swingout is influenced by the dropper during $T_{res}/4$ and F_t has its maximum at

δ_k for $\delta_{\max} > \delta_k$ otherwise at δ_{\max} for $\delta_{\max} < \delta_k$. Therefore it has to be distinguished between the following cases when calculating the load parameter φ :

- $\delta_{\max} \geq \delta_1$:
The load parameter φ is obtained as for a span without dropper according to equation [(*)32]

$$(3.4) \quad \varphi = \begin{cases} 3\left(\sqrt{1+r^2}-1\right) & \text{for } T_{k1} \geq T_{res}/4 \\ 3(r \sin \delta_k + \cos \delta_k - 1) & \text{for } T_{k1} < T_{res}/4 \end{cases}$$

- $\delta_{\max} < \delta_1$:
The load parameter φ is obtained as follows:

(3.5)

$$\varphi = \begin{cases} 3(r \sin \delta_{\max} + \cos \delta_{\max} - 1) & \text{for } \delta_k \geq \delta_{\max} \\ 3(r \sin \delta_k + \cos \delta_k - 1) & \text{for } \delta_k < \delta_{\max} \end{cases}$$

In Figure 3.35 b), the dropper is stretched and blocks the movement of the main conductor, the span is swinging nearly horizontal and no drop force occurs; the maxima in the time history of the forces following the first maxima are less or equal.

Due to the increase in dropper length the actual maximum swing-out angle also increases and several fall down follow, Figure 3.35 c); the second one is decisive, because the speed is nearly zero at the lowest point and in the main conductor the mechanical energy is converted to elastical energy. From tests follow that a fall of span can be expected for $\delta_{\max} \geq 60^\circ$. In an arrangement without dropper, a fall of span can only occur if the span has enough energy that the maximum swing-out angle δ_m is greater than 70° , as shown in Figure 4.2 of [Ref 1]. This leads to the assumption that the drop force F_f shall be calculated if the following condition is fulfilled :

$$(3.6) \quad \delta_{\max} \geq 60^\circ \text{ and } \delta_m \geq 70^\circ$$

where δ_k is to be calculated without dropper with equation [(29)] and δ_{\max} with equation (3.3).

At the end of the short-circuit current flow, the electromagnetic energy is converted to potential, kinetic and elastic energy of the swinging system. When the dropper is stretched, a part of the mechanical energy of the main conductor is converted to elastic energy of the dropper and back due to the energy conservation law, the energy in the system is always constant. During and at the end of the fall, the dropper is not stretched and the mechanical energy in the highest point of the main conductor movement is converted to elastic energy during the fall down which gives the drop force F_f . The effect is the same as described in Section 4.2 of [Ref 1] for the span having no droppers. This shows, that the drop force F_f of a span with dropper can be calculated in the same way as for a span without dropper according to equation [(35)].

The maximum horizontal displacement b_h of the span depends also on the actual maximum swing-out angle on δ_{\max} . If $\delta_{\max} \geq \delta_m$ the dropper length has no influence and b_h has the same value as for a span without dropper, also in the case $\delta_{\max} < \delta_m$ when $\delta_m \geq \delta_1$. For $\delta_{\max} < \delta_m$, δ_1 the horizontal displacement is limited by the dropper. Therefore the maximum horizontal displacement b_h can be determined with the two cases:

– $\delta_{\max} \geq \delta_m$:

the horizontal displacement is obtained as for a span without dropper according to equation [(41)]

$$(3.7) \quad b_h = \begin{cases} C_F C_D b_c \sin \delta_1 & \text{for } \delta_m \geq \delta_1 \\ C_F C_D b_c \sin \delta_m & \text{for } \delta_m < \delta_1 \end{cases}$$

– $\delta_{\max} < \delta_m$:

the horizontal displacement becomes:

$$(3.8) \quad b_h = \begin{cases} C_F C_D b_c \sin \delta_1 & \text{for } \delta_{\max} \geq \delta_1 \\ C_F C_D b_c \sin \delta_{\max} & \text{for } \delta_{\max} < \delta_1 \end{cases}$$

where C_F , C_D , δ_1 and δ_m are to be calculated for the span without dropper according to equations [(21)], [(31)], [(38)] and [(39)] and δ_{\max} with equation (3.3).

If the short-circuit current flows through the complete length of the main conductor, the electromagnetic force per unit length is calculated with equation [(19)] in the case of a three-phase system:

$$(3.9) \quad F' = \frac{\mu_0}{2\pi} 0,75 \frac{(I_{k3}'')^2 l_c}{a l}$$

On the other side, if the current flows through half the span and then through the dropper it is assumed, that the span without dropper acts the equivalent electromagnetic force:

$$(3.10) \quad F' = \frac{\mu_0}{2\pi} 0,75 \frac{(I_{k3}'')^2 l_c / 2 + l_d / 2}{a l}$$

where l_c is the main conductor length, l_d the dropper length and l the span length. In single-phase systems, $0,75(I_{k3}'')^2$ is to be replaced by $(I_{k2}'')^2$.

This extension of the simplified method stated in IEC 60865-1 is compared with many tests. The best agreement could be achieved under the assumption that the mass of the droppers is disregarded for the short-circuit stress. That means the calculation is to be done *without droppers*. The results are given in the annex 8.3 and show sufficient accuracy of the method.

For the calculation of the static tensile force F_{st} and the static sag, the mass of the dropper cannot be disregarded. Because the dropper has a bending stiffness, one part of its gravitational force acts on the lower point and the other part including the clamp on the main conductor. Therefore it is recommended to add an additional mass in the span equal to the clamp mass plus half the mass of the dropper.

b) Forces apparatus and insulators

Forces on apparatus and insulators are caused by the electromagnetic forces between the droppers (cases 1, 3, 5 in Figure 3.20) and the pinch effect between the sub-conductors in the dropper (cases 2, 4, 6), and in addition the stretch due to the movement of the busbar (cases 5, 6). First, the droppers with fixed upper ends are analysed which give the forces in cases 1. The pinch effect in cases 2, 4, 6 can be estimated according to the standard.

Droppers with fixed upper ends

During or after the end of a short circuit, a horizontal span oscillates or rotates as shown in section 4 of [Ref 1]. The trajectories of the individual conductor elements are similar and the whole span can be described as a pendulum. In contrast to this, the movement of the individual dropper elements differ very much and the pendulum model is not possible in this case. Besides this the forces in the dropper clamps are not equal.

Based on tests performed by FGH in 1990, see cases 17 and 18 in Volume 2 of [Ref 1], a simplified formula is derived in [Ref 41] which gives the bending force on the fixing point at the lower end of the dropper. In the following, the derivation is summarised.

The results of the tests show the influence of the parameters on the bending force at the lower end of the dropper:

- The maximum force increases with the square of the short-circuit current.
- The conductor mass is of less influence.
- The short-circuit duration has no influence.
- Short times to maximum displacement lead to higher forces; the times depend on the short-circuit currents.
- The maximum displacement does not depend on the short-circuit current and the short-circuit duration but on the geometry. This follows from the fact that the maximum displacement is reached for all short-circuit currents durations later than 100 ms.

Short times to maximum displacement mean higher velocities during the movement and by this higher kinetic energy in contrast to longer times. Therefore the induced kinetic energy is a measure for the bending force.

Figure 3.36 shows the dropper in its static position and at the moment of maximum displacement. With the given quantities and the assumption that the shape of the dropper at maximum displacement can be described by a parabola it follows for the curve of the displaced dropper:

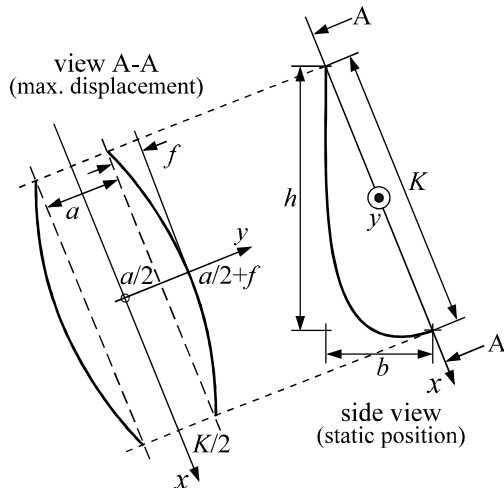


Figure 3.36 Dropper in static position (right side) and at the moment of maximum displacement (left side)

$$(3.11) \quad y(x) = -\frac{f}{(K/2)^2} x^2 + \left(\frac{a}{2} + f\right)$$

with:

- f maximum displacement
- a distance between the droppers
- K distance between the fixing points,
 $K^2 = h^2 + b^2$
- h height of the dropper
- b width of the dropper

From equation (3.11), the dropper length l_d can be estimated:

$$(3.12) \quad \frac{l_d}{K} = \frac{1}{8} \frac{K}{f} \left[\sqrt{1 + 16 \left(\frac{f}{K}\right)^2} + \ln \left(4 \frac{f}{K} + \sqrt{1 + 16 \left(\frac{f}{K}\right)^2} \right) \right]$$

and an approach can be made for the sag f in the range of $1 \leq l_d/K \leq 2$ using the method of least squares:

$$(3.13) \quad \frac{f}{K} = \left[0,60 \sqrt{\frac{l_d}{K} - 1} + 0,44 \left(\frac{l_d}{K} - 1\right) - 0,32 \ln \frac{l_d}{K} \right] \frac{K}{l_d}$$

At the right end, the correction factor K/l_d fits the parabola model with the measured values.

At the beginning of the short circuit, the force on a differential conductor element is given by:

$$(3.14) \quad m' \ddot{y} = \frac{\mu_0 (I_k'')^2}{2\pi a}$$

with the conductor mass m' per unit length and the initial symmetrical short-circuit current (r.m.s.) I_k'' .

Assuming a constant acceleration until this element reaches its maximum displacement at the time t_a , f becomes:

$$(3.15) \quad f = \frac{1}{2} \ddot{y} t_a^2$$

and out of this with equation (3.14):

$$(3.16) \quad t_a = \sqrt{\frac{2f}{\frac{1}{m'} \frac{\mu_0 (I_k'')^2}{2\pi a}}}$$

When a conductor element with the length dx obtains the final velocity v at the place $y(x)$ and the time t_a , the differential kinetic energy becomes:

$$(3.17) \quad dW_{kin} = \frac{1}{2} v^2 m' dx$$

This energy is absorbed by the conductor when it runs into a circular trajectory with the centre in the connection line of the fastening points in Figure 3.36.

With a constant acceleration, the final velocity v follows from:

$$(3.18) \quad y(x) - \frac{a}{2} = \frac{1}{2} \ddot{y} t_a^2 = \frac{1}{2} \frac{v}{t_a} t_a^2$$

$$(3.19) \quad v = 2 \frac{y(x) - \frac{a}{2}}{t_a}$$

The centrifugal force acting on a conductor element is

$$(3.20) \quad dF = \frac{m' dx v^2}{y(x) - a/2} = \frac{m' dx}{y(x) - a/2} \left[2 \frac{y(x) - \frac{a}{2}}{t_a} \right]^2$$

$$= \frac{m'}{t_a} 4 \left[y(x) - \frac{a}{2} \right] dx$$

The integration along half the conductor gives a first approach of the bending force at the insulator:

$$(3.21) \quad F_v = \int_0^{\frac{K}{2}} dF = 4 \frac{m'}{t_a} \int_0^{\frac{K}{2}} \left[y(x) - \frac{a}{2} \right] dx = 4 \frac{K \mu_0 (I_k'')^2}{6 \cdot 2\pi \cdot a}$$

The forces calculated with equation (3.21) are too low compared with the measured ones. The reason may be the simplifications done in the model of the dropper. It is empirically found that F_v is to be corrected by the factors l_d/K and $2,5 l_d/b$ and the actual bending force on the insulator becomes :

$$(3.22) \quad F_d = F_v 2,5 \frac{l_d}{b} \frac{l_d}{K} = 4 \frac{K \mu_0 (I_k'')^2}{6 \cdot 2\pi \cdot a} 2,5 \frac{l_d}{b} \frac{l_d}{K}$$

$$= \frac{5}{3} l_d \frac{\mu_0 (I_k'')^2}{2\pi \cdot a} \frac{l_d}{b}$$

with a validity range of $1,4 \leq l_d/b \leq 3,3$.

In equation (3.22), F_d only depends on the geometry and the short-circuit current but not the conductor mass and the short-circuit duration, as it follows from the tests.

The calculation of F_d according to equation (3.22) is compared with the tests [Ref 41]. Most of the values lie within a range of $\pm 25\%$, some are slightly more than 25% on the safe side. This result allows the application of the simplified method given above.

From this the ESL follows according to Paragraph 3.5.2 and with this the design load.

Droppers with flexible upper ends

The upper ends of droppers in the middle of the span or near to it move with the main conductor in the bus. If

the droppers are not stretched, there will be no significant bending force on the apparatus or insulators at the lower end caused by the movement of the busbar. If the droppers are stretched, a high loading can occur. Until now a simplified method for the calculation of this force is not available. Therefore it is recommended to make the droppers longer to avoid stretching. If this is not possible, advanced methods should be used.

The droppers with current (current path C in Figure 3.22) swing out due to the electromagnetic forces between the droppers. The maximum force at the lower end takes place during swing-out of the busbar. A good estimation of the loading at the apparatus and insulators can be determined assuming fixed upper ends of the droppers and using the simplified method stated above.

3.4. THE BUNDLE PINCH

3.4.1. Introduction

This phenomena has been well described for the first time by Manuzio in 1967 [Ref 53] and briefly repeated here :

From initial rest position, subconductors move towards each other, remaining more or less parallel in most part of the subspan, except close to the spacer. After first impact (in the centre of subspan) there is a quick propagation of the wave through the spacer end of the subspan.

There is a struggle between electromagnetic force which increase on the moving part (the distance is decreasing) and would like to force contact between subconductors, and tension increase in the subconductor which react against the electromagnetic force. There is a maximum pinch when the wave propagation stops towards the spacer and must come back to the centre of the span, this is followed by oscillations (back to the spacer, then to the subspan centre, etc.) because electromagnetic force is still on, these oscillations are damped slightly so that first peak is the maximum peak. If short circuit is long enough, the pinch oscillations tends to a permanent force, considerably lower than peak value (typically 2 times less).

During this phenomenon, spacer is strongly compressed. The compression is related to maximum pinch force in the conductor and angle between the spacer and the subconductor.

Despite the fact that bending stiffness locally change the curvature of the conductors, the deformation energy in bending remain small compared to tensile deformation energy, so that simple or advanced method can neglect bending stiffness in their approach. Only structural damping can be related to bending, which could have influence on pinch oscillations but certainly not on the peak value, which is a design value for the spacer.

Manuzio developed a simplified method for pinch effect in bundle conductors limited to overhead line applications [Ref 53].

Manuzio neglected some important aspects (for substations structures) which are summarised here :

- She neglected supporting structure and insulators effects
- She neglected short-circuit current asymmetry
- She focused on spacer compression and neglected the pinch effect itself. She even assumed that tension increase was negligible, which is certainly not true, as seen in published data reference book [Ref 101] where some cases showed pinch effect larger that 6 times the initial F_{st} .
- She neglected the subspan length effect, which is probably true for overhead lines, but certainly not for substations.

All these aspects have been taken into account in the IEC 60865 for evaluating pinch force F_{pi} . However IEC 60865 gives no recommendation for spacer compression.

The question is : "Do we have to take into account the pinch effect in the design, and how?" (actual recommendation is to use F_{pi} as a design static load).

If there is no doubt that pinch effect must be included in spacer design, the pinch effect is a high frequency dynamic loading. So that inertial behaviour of anchoring structures could be such that pinch effect would have limited impact on design.

It is an obvious fact that pinch loading is certainly not the same as swing and falling down loading, which are basically quasi-static load.

This problem will be investigated in this chapter.

Then we will be ready and have the tools to examine the actual design load, looking on the response of anchoring structures (next chapters).

3.4.2. Advanced computation results

Calculation of the behaviour of triple droppers caused by the effect of a two-phase short-circuit (Pinch forces at the terminals of the disconnector and movement of the conductors).

The calculation was performed on the configuration shown in Figure 3.37. In this case the dropper bundle comprises of three conductors Type "Greely" (469.6 mm^2) spaced at 460 mm, and the short-circuit current applied for the calculation was 40 kA for a period of 1 sec. The phase distance was 9 m.

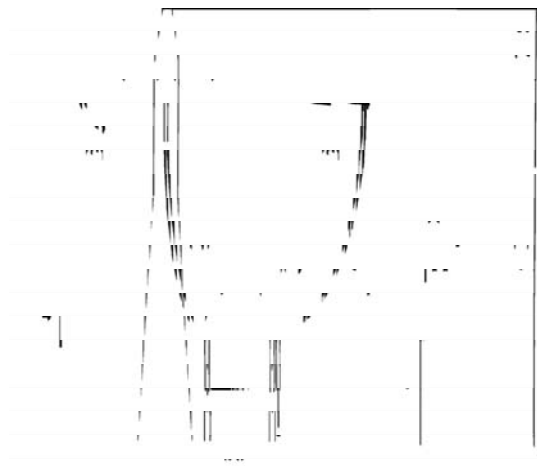


Figure 3.37 A part of 500kV Switchgear under study with triple subconductor. DS: Disconnector, S: Spacer.

In the configuration shown in the Figure 3.37, two droppers are connected to the HV terminals on both sides of a single disconnect switch.

Using a special computer model (load program) which calculates the electromagnetic forces, the Finite Element Program ABAQUS [Ref 33] is used for calculation of the short-circuit effects on the structure.

The conductors in the bundle are accelerated from their static position at $t = 0$ and clash after only a few milliseconds Figure 3.38 and Figure 3.39 (60-80msec) In the close position, the bundle moves laterally until the short-circuit current is interrupted at $t = 1$ sec. From this point onwards the conductors remain in motion as a result of their inertia and the effect of their mass up to the end of the calculation. The changes in the total force, acting on the HV terminals with time are shown in Figure 3.40. It can be seen that the maximum force is achieved when the conductors pinch. Further, as the time increases the force decreases.

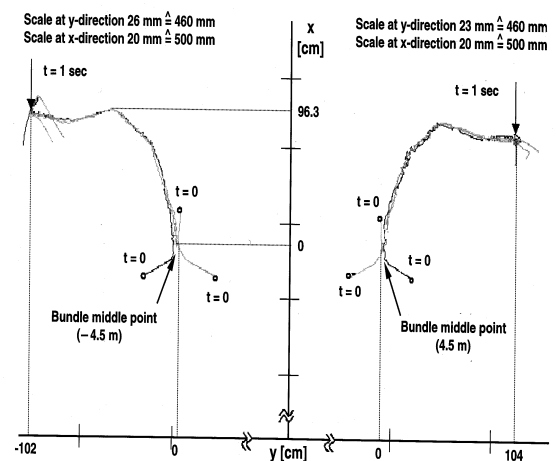


Figure 3.38 Movement plan view at the center of the right dropper (Figure 3.37) at the height approximately 7.5m above the HV terminals(plan views).

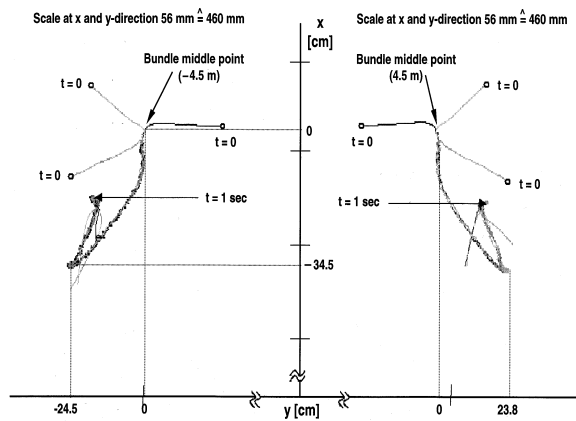


Figure 3.39 Movement plan view at the center of the left dropper (Figure 3.37) at the height approximately 7.5 m above the HV terminals.

The diagrams in the Figure 3.38 and Figure 3.39 shows the movement of the center point of the dropper bundle at height approximately 7.5 m above the HV terminals for all three conductors on clashing and the lateral movement of the pinched conductors, and the separate movement of the individual conductors for a very short time after interruption the short-circuit current.

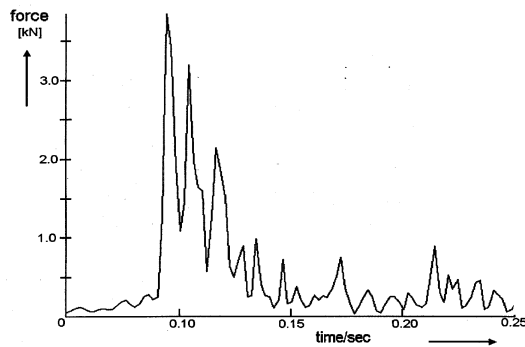


Figure 3.40 Short-circuit force against time curve for the loads on the disconnector right hand HV terminal.

The maximum loads on the HV terminal of the disconnector achieved during the short-circuit have been calculated as:

Right dropper 3.7 kN

Left dropper 3.0 kN

3.4.3. Dynamic behaviour of close and various degrees of wide bundling

Unlike the close bundling of flexible busbars, which is not associated with major short-circuit contraction effects, substantial peak forces due to the contraction of subconductors occur at the dead end and on the spacers in the case of wide bundles. Their magnitude and their eventual static equivalent effect (ESL = equivalent static load) on support structures and foundations depend, apart from a number of additional parameters of configuration and state, as well as of the electrical short-circuit data, on the spacing between sub-conductors, their number and configuration, the stranded conductor

itself, and the number and the design of the spacers (rigid, partially or multiply elastic).

Close bundling of multiple conductors, with a spacing between subconductors approximately equivalent to conductor diameter, minimizes the direct and indirect effects of contraction. Up to 400kV this technique is absolutely viable for substations and has become largely standard for more recent German installations. This does not hold true, however, of older plants with wide bundles, whose reserve potential now needs to be investigated, nor of stranded conductor arrangements abroad, where wide bundle spacing as in overhead lines has been and is the usual technique also in the case below 400kV. Close bundling is, of course, no longer feasible with stranded conductors for higher system voltages.

This section concerns the case A (Figure 1.1) plus B – long-span horizontal buses connected by insulator chains to portal structures – where the bus conductors are twin bundles. The dropper B is connected at midspan and does not carry current.

The sub-conductor centre line distance is varied from 60 to 400 mm in four individual values.

The following parameters were varied:

- the number of spacers n_{AH}
- the sub-conductor centre-line distance a_T
- the short-circuit current duration T_K .

The usual practical solution for a close bundle conductor in Germany is $a_T \approx 2 \times$ conductor diameter.

In the case of wide bundling, a_T is very much larger.

Figure 3.41 shows the studied arrangement.

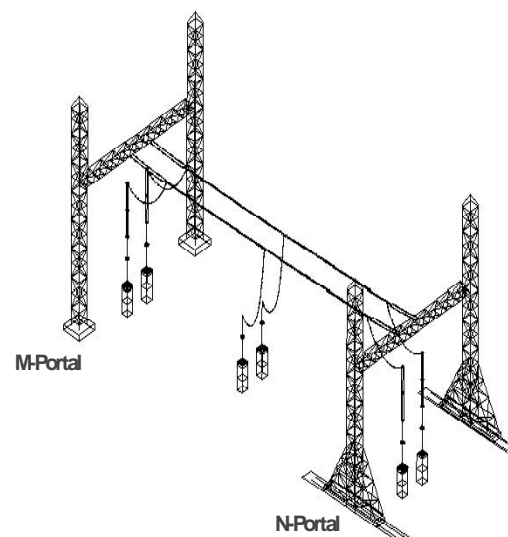


Figure 3.41 The studied arrangement fully discretized

The structure is discretized in a full-detail FE model, using the appropriate beam elements for the framework of the portals and adjusting the model to achieve first the proper stiffness and then eigenfrequency values.

From prior tests the stiffness values are known to be $S_N = 1.086 \text{ kN/mm}$, $S_M = 1.223 \text{ kN/mm}$ ($S_{res} = 0.575 \text{ kN/mm}$).

The relevant first eigenfrequencies excited at the mounted mid crossarm, i.e. next to the suspension points, are 9 Hz for the N-portal crossarm and 9.5 Hz for the M-portal crossarm, while the complete portals have fundamental frequencies of 3 Hz and 4.3 Hz, respectively. It should be noted that the M-portal stiffer than the N-portal.

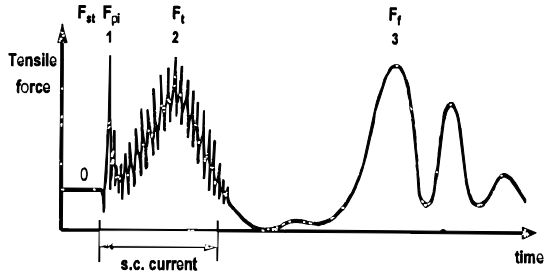


Figure 3.42 Main conductor tensile forces, schematic oscillograph

- 0- Static load F_{st}
- 1- Contraction maximum F_{pi}
- 2- Swing-out maximum F_t
- 3- Fall-of-span Maximum F_f

The results of the calculations performed on the structure model of Figure 3.41 are given in the following [Ref 46].

Figure 3.43 and Figure 3.44 give an example of the reactions of the support structure upon the short-circuit of $100 \text{ kA} - 40 \text{ kA}_{rms} - 0.3 \text{ s}$ on the 400 mm bundle phase conductors with 1 spacer. The comparison of a) against b) shows clearly the relative reduction of the fast events – the contraction and the 50 and 100 Hz phenomena during short circuit. – on the way from the dead-end fixing point at the crossarm to the bottom end of the tower (i.e. foundation).

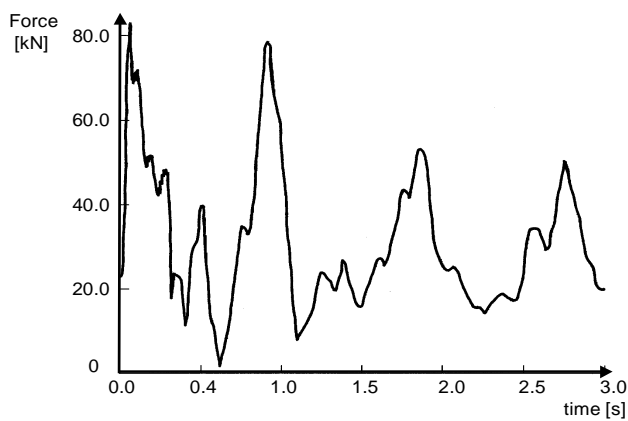


Figure 3.43 Exemplary oscillographs of stresses at dead end

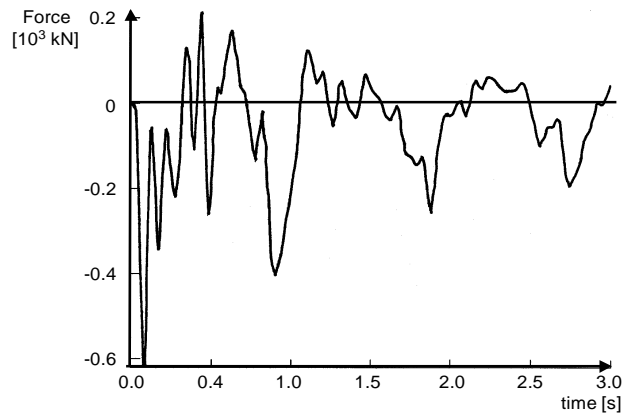


Figure 3.44 Exemplary oscillographs of stresses at foundation

Figure 3.45 and Figure 3.46 exemplarily show the calculated displacements of a bundle conductor for the same arrangement and short-circuit data as above except $t_K=0.1 \text{ s}$ at the spacer location and at $1/4$ span.

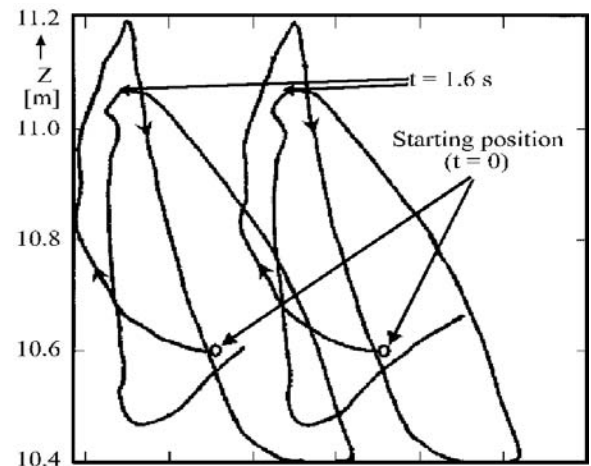


Figure 3.45 Bundle conductor displacement at midspan (position of spacer)

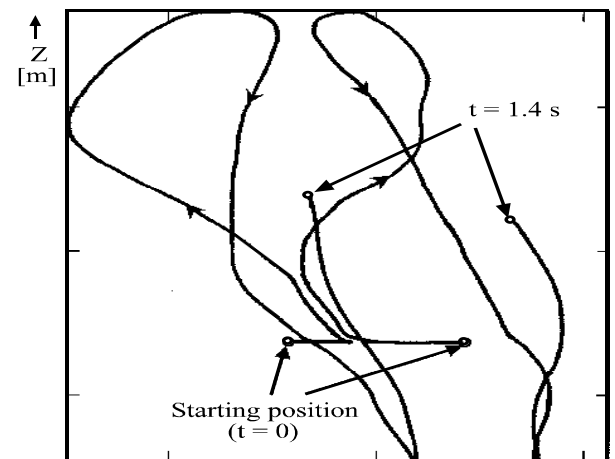


Figure 3.46 Bundle conductor displacement at $1/4$ span (in a location without spacer)

The first sequence of figures - Figure 3.47 a, b and c - gives a collection of the calculation results for the respective tension forces at the dead end in terms of the recorded maxima F_{pi} , F_t and F_f for the variants taken

into account in the calculation. One must consider that the value of $t_K = 0.1$ s is of a rather theoretical nature.

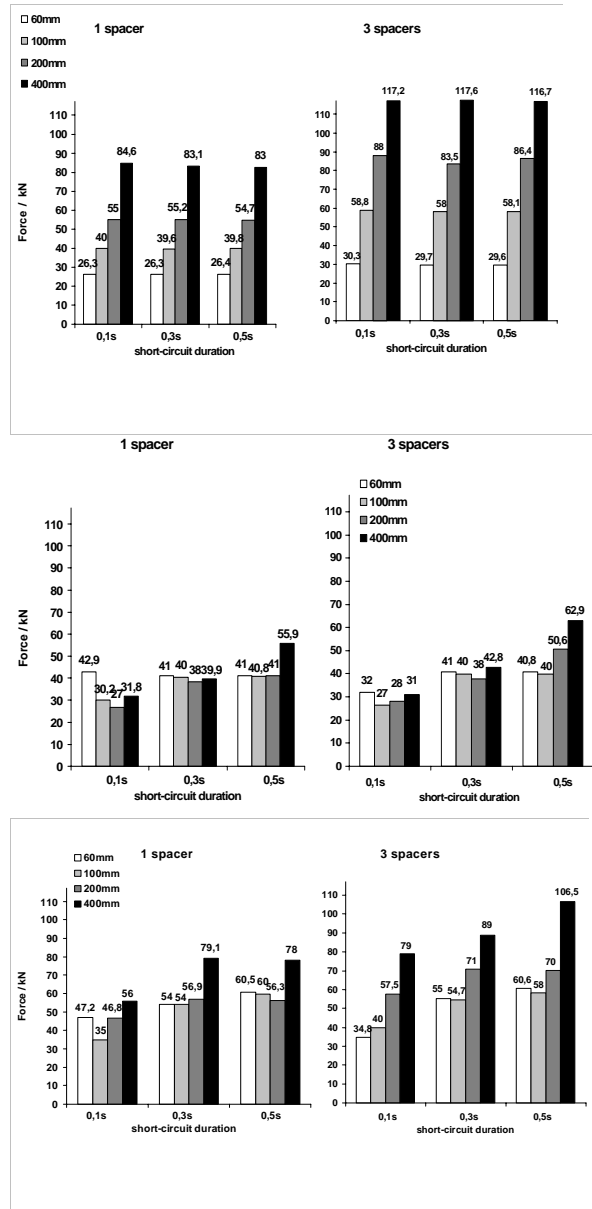


Figure 3.47 a, b, c Calculation results
a) Contraction maxima F_{pi}
b) Swing-out maxima F_t
c) Fall-of-span maxima F_f

The contraction effect rises with the number of spacers and the sub-conductor distance to become the relevant short-circuit tension force at the suspension points for three spacers at $a_T = 400$ mm. The dependency of the second and third maxima on the number of spacers must be attributed to the reduction of sag (i.e. effective conductor length available for the contraction) by the contraction with increasing sub-conductor distance a_T and number of spacers n_{AH} during the short-circuit. Also the existence of the droppers may lead to a reduction of the kinetic possibilities of the span during the swingout and the fall-of-span phases, in particular.

In comparison to the above the same sequence is used for the reactions at the foot of the towers and at the transition to the foundation in Figure 3.48 a, b and c. The *static* relation between the exciting tension force

and the considered reaction force at the tower foot is $1/6.2$.

Of course the respective values of Figure 3.49 for equal conditions must remain independent of the short-circuit duration. The number of spacers and the sub-conductor distance have severe effect on the reactions. The fall of span is generally the more important against swing-out. For up to 100 mm sub-conductor spacing a_T , the reaction to contraction is negligible against all other maximum. Yet, if the calculation and, in particular, the chosen damping is right, the contraction plays the dominant role among the other maximums at $a_T = 200$ mm and above. With one spacer and $a_T = 200$ mm, the ESL factor for contraction is slightly less than 1, while for 400 mm it is 1.2. For a larger number of spacers the factors are even higher.

Finally, the maximum spacer compression was considered. Figure 3.48 gives the results of that calculation. Spacer compression has lately come into renewed interest through [Ref 54].

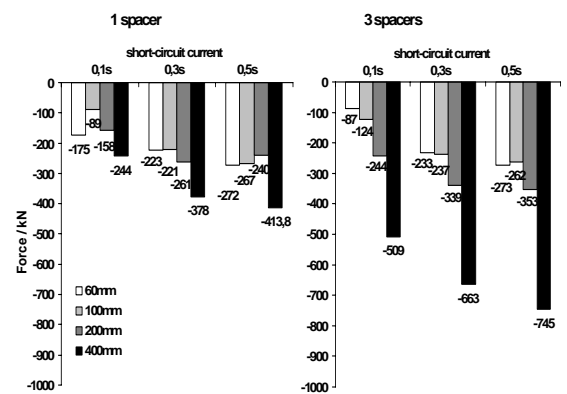
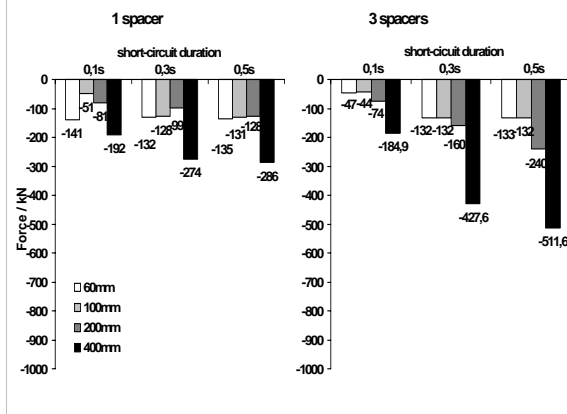
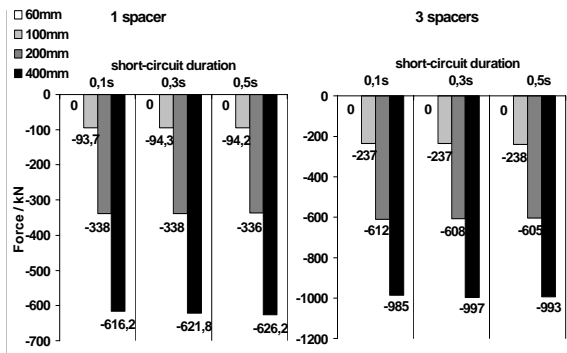


Figure 3.48 Reaction at transition tower / foundation
 a) due to contraction
 b) due to conductor swing-out
 c) due to fall of span

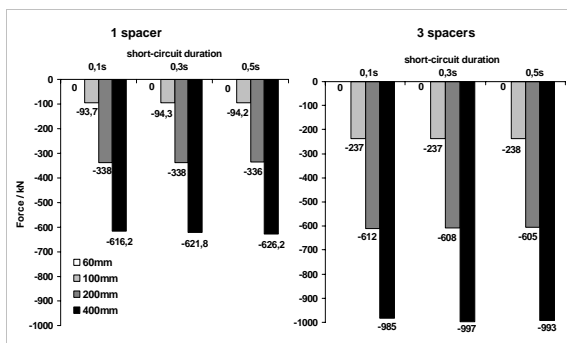


Figure 3.49 Maximum spacer compression

3.5. LOAD ON PORTALS, APPARATUS TERMINALS AND EQUIVALENT STATIC LOAD

3.5.1. Introduction

These loads may be summarized as follows:

- 1) F_t , F_f typical low frequency, quasi-steady loads, see chapter 3.5.4 for ESL
- 2) F_{pi} loads due to pinch effect, typical impulse load. See chapter 3.5.3 For ESL
- 3) F_{ds} loads due to dropper stretch, typical impulse load. See chapter 3.5.2 for ESL

Typical apparatus have a range of frequencies mainly dependent of voltage level, following the table given in [Table 1.1 in the introduction]

As a global overview, let's keep in mind that :

- typical insulator support may have very wide range of their first eigenfrequency and may cover all the range between 4 and 60 Hz. Lower voltage corresponds to higher frequency.
- typical portal structure have very low eigenfrequencies, in the range 1 to 6 Hz. Voltage correlation is very low.
- typical apparatus (isolator, circuit breaker, measuring transformer, surge arrester) have very low eigenfrequencies due to their high mass located on the top of it. Range 1 to 6 Hz. The higher the voltage, the lower the frequency.

Design load on these structures have to be deduced from instantaneous top load applied by the cable connections (F_t , F_f , F_{pi} and F_{ds}). The difference between these loads and design loads is given by ESL factor given in this chapter. ESL factor depends on the structural dynamics as explained in appendix 1.

Such ESL factor is only of interest if using simplified method to evaluate F_t , F_f and F_{pi} for example to calculate the design load for a supporting structure at the lower end of a dropper or if the forces F_t , F_f and F_{pi} on the main conductors of a horizontal strain bus connected to portals (case A in Figure 1.1) are estimated according to IEC60 865. In contrast, IEC 60865 gives the ESL for the design of a slack bus connection (case C in Figure 1.1), see Annex 8.3.1 and Part I in volume 2.

The design load can obviously be evaluated directly by advanced method. But such evaluation can be cumbersome, need software, and give only accurate results if you are using accurate data's.

In the suggested simplified method using ESL factor, some conservative approach has been taken in the synthetic curves given in this chapter.

It is recommended not to add any safety factor over the calculated values.

3.5.2. Maximum instantaneous load and equivalent static load for dropper stretch

The definition of ESL factor is explained in annex 8.1.

There are two different curves to be used for design and concerning ESL factor.

The first one in Figure 3.50 concerns the dropper stretch (in span dropper, single conductor or close bundle), this is an envelop curve obtained from many tests results and simulations. The dropper stretch load shape is a typical triangular excitation, the duration of which is depending on its overlength compared to the distance between its two extremities. But because of its upper fixation to cable structure, the duration of the stretch, even if short, is generally in the range 0.05 to 0.2 s.. It means that it is a quasi-static load (ESL factor = 1) for frequencies higher than about 50 Hz , but higher than one in the range 5-30 Hz and lower than one for lower frequencies. This is quantified on Figure 3.50.

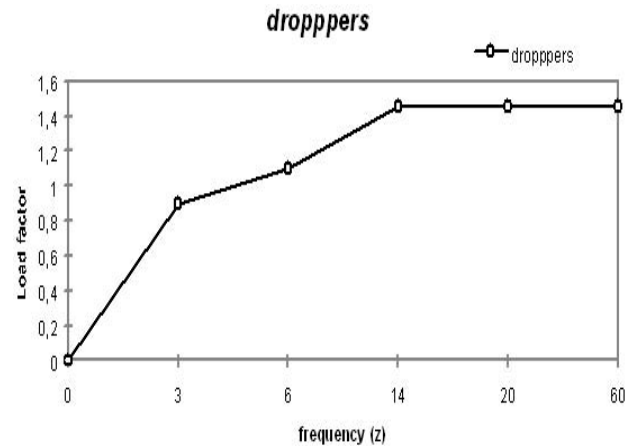


Figure 3.50 ESL factor for typical dropper stretch, envelop curve. Abscissa is the first eigenfrequency of apparatus or bushing or insulator support. The abscissa are not at all distributed linearly.

You just need the maximum stretch force in the cable near the clamp (evaluated by advanced method or simplified method developed in this brochure; no simplified method for in span droppers is given in this brochure). Then following the basic first frequency of your apparatus, you deduce the design load by multiplying the maximum stretch force by the coefficient obtained from the curve. The obtained load must be compared to cantilever breaking load of corresponding apparatus.

3.5.3. Maximum instantaneous load and equivalent static load for bundle pinch.

The second one in Figure 3.51 concerns bundle pinch and is valid for all bundle configuration, this is an envelop curve of many tested cases.

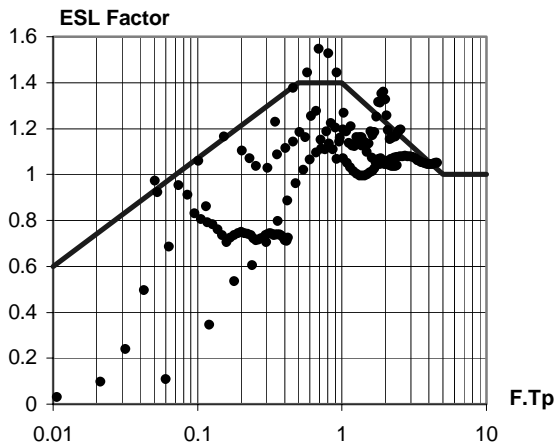


Figure 3.51 Synthetic curve proposed for pinch effect ESL factor. In abscissa, the product : frequency of the supporting structure (Hz) x (contact time evaluated by the simple formula expressed in s)

It is quite interesting that the basic curves (dotted lines) have been correlated using in abscissa the product of the supporting structure fundamental frequency by the time of impact (obviously the ratio between two times : the period of the swinging structure and the time to impact). It obviously points out the biggest interest to work with close bundling, which both decrease F_{pi} and T_{pi} , both effects having a drastic decreasing on the design load.

For example Figure 1.4 in the introduction has a relative pinch effect of 50 kN and an time impact of approximately 20 ms. If the supporting structure has a frequency of approximately 2 Hz, it means $F.T_{pi} = 0.040$ and corresponding ESL of 0.7, thus a design load due to pinch equal to 35 kN + static pull (8.7 kN) = 43 kN which is more or less 75% of instantaneous value of the pinch. (50 + 8.7 = 58.7 kN).

Similarly for Figure 3.7 with close bundling, $F.T_{pi} = 2x 0.005 = 0.010$, thus ESL = 0.6 and design load for pinch is about 10 kN less than the influence of interphase effects.

But the same bundle installed between two insulators support, with the same short-circuit level, would have given very different design loads, especially at low voltage for which the eigenfrequency of the support may be as high as 50 Hz. ESL factor is enlarged to 1.1 instead 0.5, means a doubling of the design load, only due to structural dynamic effects.

3.5.4. Maximum instantaneous load and equivalent static load for Ft, Ff

The problem is very similar to that in the former chapter. But is limited to two different kind of loading : the dynamic effects of swing and drop force (both were assumed quasi-steady loads, then ESL factor was assumed to be equal to 1).

There is one important difference compared to former chapter. The load itself is sensibly influenced by the behaviour of the portals. This is included in the simplified methods developed in IEC 60865 to obtain

F_t , F_f and F_{pi} . So that ESL factor defined here can be correctly used in such case. For advanced method, the supporting structure must be included in the simulation, sometimes with a very simple modelling, so that in such simulations, exact ESL can be obtained directly inside the simulation and we don't need any more to use ESL factor.

Figure 3.52 concerns swing and drop force, this is an envelop curves obtained from many different cases.

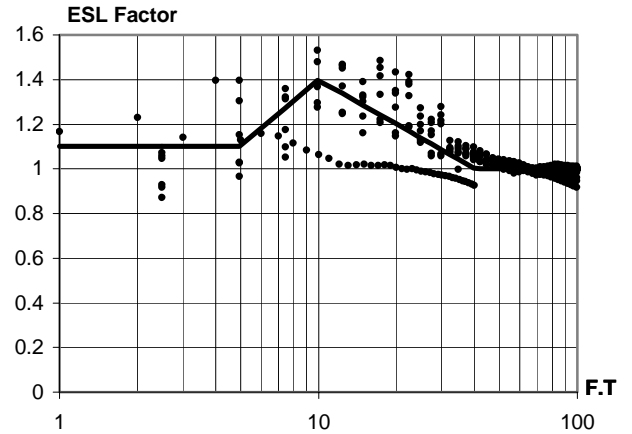


Figure 3.52 ESL factor for tensile load or drop force, to be applied for portal structures. Abscissa is the first eigenfrequency of supporting structure times the swing period (s). This is an envelop curve for bus-bars with sags between 1 and 3 meters.

The Figure 3.52 gives :

- the ESL factor for the maximum of either the tensile load or drop force to be applied for portals.
- Abscissa is F.T
 - F is the first out of plane eigenfrequency of the portal,
 - where T is the swing period of the busbar (s).

The envelop curves are given for damping of the portal structure close to 5% of critical damping.

You just need the maximum swing and drop force in the busbars Then following the basic first frequency of your portal, you deduce the design load by multiplying the maximum force by the coefficient obtained from the curve. The obtained load must be used for the static design of the portals.

But probabilistic aspects of SCC maximum level as well as steel plastic deformation (valid for portal only) may be considered.

3.6. ESL FACTORS FROM NUMERICAL SIMULATIONS.

The following example of application compares a simplified method with advanced method using the structure given in Figure 3.12 (110kV-test arrangement with the two spans).

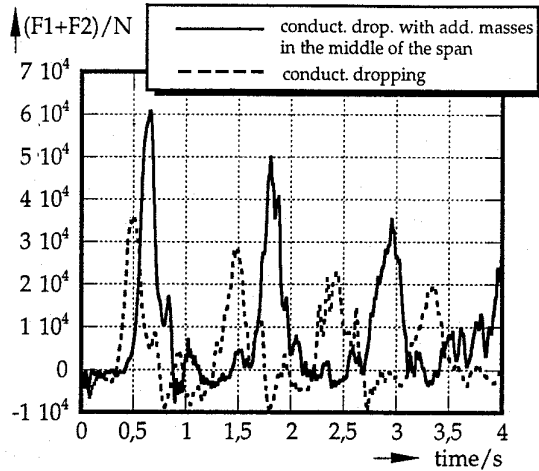


Figure 3.53 Dynamic excitation forces caused by conductor dropping with and without additional weights.

On this 110kV-substation arrangement short circuit tests as well as conductor dropping tests with and without additional weights were done in the South span. The excitation forces for conductor dropping and short circuit are shown in Figure 3.53 and Figure 3.54 [Ref 49].

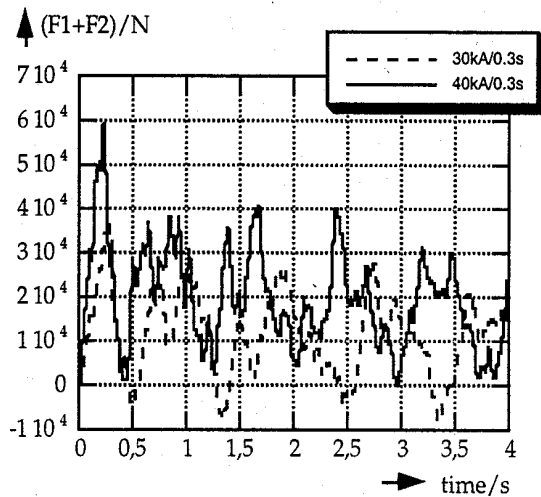


Figure 3.54 Dynamic excitation forces caused by short-circuit (30kA and 40 kA).

excitation	ampl. of total load F1+F2 calculated [kN]	F _{steg} FEM-model detailed [kN]	F _{steg} beam-model simplified [kN]	F _{steg} analy.-num. meth. [kN]	ESL-Factors 1) measured 2) calculated
s-c current 30kA 0.3sec	37.5	46.0	45.5	43.5	1) 1.2 2) 1.4
s-c current 40kA 0.3sec	61.2	79.0	80.0	74.3	1) 1.2 2) 1.3
conduct .drop.	35.4	49.0	52.5	54.8	1) 1.8 2) 1.8
conduct drop. with add. masses in the middle of the span	60.6	79.0	86.0	89.1	1) 1.7 2) 1.6

Table 3.1 Calculated results of the studies on the portal.

In this study an analytical numerical method for the calculation of a static equivalent load (ESL) is presented -Force- and Structure Analysis-. With this static load the design load for the foundations of structures as well as the maximum stresses of structures and equipment, as post-insulators, measuring transformer, can be defined for the dynamic case. Proof of validity of the developed method was led by comparison (ESL-Factors) with measurements on the real structures [Ref 49].

3.7. SPECIAL PROBLEMS

3.7.1. Auto-reclosing

a) Introduction

In order to reduce outage duration, reclosure is very often used to re-energise overhead lines after a tripping due to a fault on the power system. A reclosure cycle will be identified by : $T_k / T_i / T_{k2}$ where T_k is the first short circuit duration, T_i the reclosing interval and T_{k2} the second short circuit duration. For example, on RTE transmission network, the reclosure cycle is 120 ms / 2 to 5 s / 90 ms for 400 kV and 210 ms / 2 to 5 s / 150 ms for 225 kV depending on the protection devices. But fast reclosure is sometimes used to minimize the reclosing interval ($T_i = 300$ ms) on 90, 63 kV customers lines.

When the fault is maintained, the stresses can be larger than before. The calculation of the effects requires the use of finite element techniques and powerful computers. IEC 60865 modelling proposes a simplified method to calculate the tensile force during or after the short-circuit for the simplest arrangements with or without pinch effects. But reclosure is not taken into account.

Span [m]	68	68	34	34
Phase n°	1	2	1	2
Static conductor tension [N]	5740	5370	3579	3390
First short-circuit force [N]	10040	8559	9919	7952
First drop force [N]	12824	13694	9203	9045
Second short-circuit force [N]	11432	9968	10532	6660
Second drop force [N]	21870	22051	8181	9146

Table 3.2 Test results

b) Tests

The case 9 tests in the Cigre brochure concerns two spans of 34 (Figure 3.56) and 68 m (Figure 3.55) using 1 x ASTER (570 mm²) cable per phase made by EDF. The reclosure cycle is 85 ms / 2 s / 95 ms. The difference of the tensile force between two phases (Table 3.2) is due to several causes : static tensile force, portal stiffness (between middle and edge), shift in time. After the second short-circuit, maximum short-circuit force on phase 1 of 68 m span is increased by 13 % (16 % on phase 2) and drop force by 70 % (61 % on phase 2).

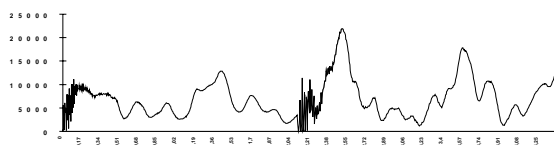


Figure 3.55 Tensile force measurement (N) versus time (s) – phase 68 m – phase 1.

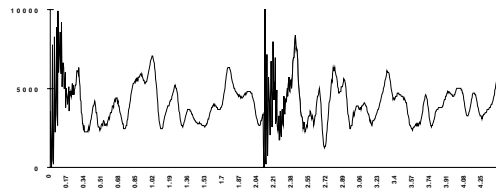


Figure 3.56 Tensile force measurement (N) versus time (s) – span 34 m – phase 1.

c) Extension of the IEC method

Annex 8.4 proposes an extension of the IEC pendulum model for autoreclosing in the simplest cases ($\delta_m < 70^\circ$) without dropping. Several points have been studied relating the second short-circuit to the influence of the first-fault heating. Annex 8.5 gives a synthesis of this proposal and a sample of calculation.

d) Comparisons

These calculations are made in the conditions of EDF tests and give a comparison (Table 3.3) between this extension and tests within several hypotheses.

Span [m]	Maximum tensile force [N]		
	case 9	link 1	link 2
68	22051	22469 (+1,9%)	22276 (+1%)
34	10532	11698 (+11%)	12758 (+21%)

Table 3.3 Influence of linking conditions
Link 1 : $\delta_M = \arccos(\chi)$
Link 2 : δ_M IEC 60865 (*31)

e) Influence of reclosing interval

Reclosure operates on a structure that is already in movement because of the initial fault and depending on whether the second fault occurs within a cable acceleration or deceleration stage (rising to the first gap, drop), the influence of mechanical and geometrical stresses thus differs : either the effect of reclosure is combined with that of the initial fault, amplifying the stress, or its effect opposes the movement of the cables caused by the initial fault and thus reduces forces, contributing to damping their rocking motion.

It will be observed that :

- reclosure can cause larger forces than a simple fault. This is the hypothesis retained in IEC 60865 on rigid conductors.
- a small proportion of faults occurring on reclosure leads to forces exceeding those of the initial fault.
- a reclosing interval will enable the structure to damp out its oscillations before reclosure occurs and thus contributes to reducing the maximum force obtained on reclosure.

Knowledge of the most stressing reclosure instant is of interest for the engineer. The optimum force of drop after reclosure is indeed obtained slightly after the

moment when the distance between the conductors is minimum at mid-span.

The highest magnitude of the force during the second short-circuit is obtained slightly after the moment when the distance between the conductors at mid-span exceeds the distance in normal position. The drop or tensile forces during the short-circuit vary very slightly with the moment of reclosure. Figure 3.57 below indicates, for the 68 m span, the drop force variation versus the reclosing interval (T_i):

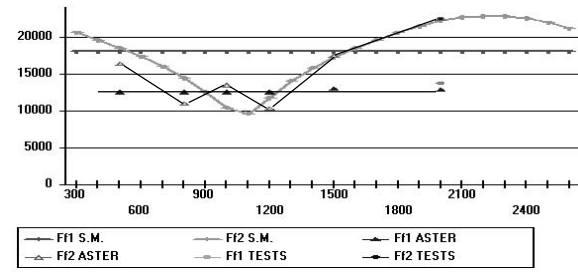


Figure 3.57 Drop force (Newton) versus no supply time (ms).

S.M.= Simplified Method
 ASTER= EDF software
 TESTS=EDF tests
 Ff1= no reclosure
 Ff2=with reclosure

The worst case occurs when the reclosing interval is in the following range :

$$(3.23) \quad T_{kl} + T_i < 0,25 T^\circ$$

and

$$(3.24) \quad 0,75 T^\circ < T_{kl} + T_i < 1,25 T^\circ$$

where :

$$(3.25) \quad T^0 = \frac{2\pi \sqrt{\frac{0,8b_c}{g}}}{1 - \frac{\pi^2}{64} \left(\frac{\delta_M}{90}\right)^2}$$

is the period of the free motion (without current) and δ_M is the maximum swing-out angle in degree.

The maximum of F_{f2} occurs when the reclosing interval is between $0,75 T^\circ$ and T° , and the maximum of F_{f1} occurs when the reclosing interval is between T° and $1,25 T^\circ$.

f). Calculation approach

Without bundle

To calculate the maximum tensile force after an auto-recloser, IEC 60865 standard can be used with a clearance time equal $T_k = T_{k1} + T_{k2}$. If the influence of reclosing interval has to be studied, a simplified method [Ref 100,] can be used in the more simple cases (Annex 8.4 & 8.5).

With bundle

To date pinch effect after auto-reclosing cannot be studied by a simplified method. But after a fast reclosure, pinch effect can have an influence if the pinch effect in IEC 60865 conditions are not satisfied.

3.7.2. Interphase-Spacer

Short circuit power of AIS is a value which is subject to a permanent increase. Unfortunately this leads to an increase of mechanical effects too. Thus investigations have to be carried out to prove that short-circuit withstand is sufficient. Usually this will be done with [Ref 2] which covers short-circuit effects of cable spans up to 60 m. During such calculation it was discovered that, in the case of span lengths with more than about 35 m and short-circuit currents in excess of 20 kA, the usual clearances mainly in the 110kV-level are not sufficient. Given that in overhead-lines interphase-spacers are in common use to avoid wind induced effects, it is obvious they can be used for AIS busbars too.

The subject of the investigation was the 40 m span without droppers as described in case 4 in Vol 2 of this brochure. Test/calculation parameters may be taken from there. The line-to-line initial symmetrical short-circuit current was 28.5 kA and the duration of short-circuit current was 103 ms. The period of investigation chosen was 2 to 3 s. No damping effects were taken into account and the portals were considered by their spring constant.

In a first step calculation was established without interphase spacer. The results of the finite-element calculations are shown in Figs. 1 and 2. Fig. 1

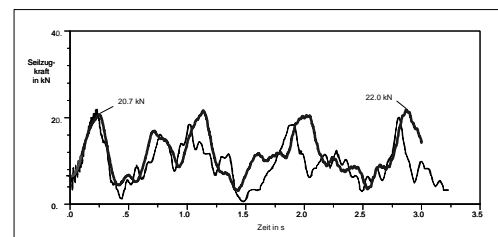


Figure 3.58 Conductor tensile force: comparison between test results and calculation results without interphase-spacer (thin = test; thick = calculation)

shows the movement at the mid-point of the conductor with a maximum deflection of 1.12 m which is in good accordance with test results and calculation of IEC 60865-1 (1.27m). In Fig. 2, where the conductor tensile force is plotted against time, the thin curve shows the test results and the thick curve the calculation results of case 4. The comparison shows good agreement between the time characteristic and the amplitude, which gave

for the maximum outswing and the maximum drop $F_t = 20.7$ kN and $F_f = 22.0$ kN.

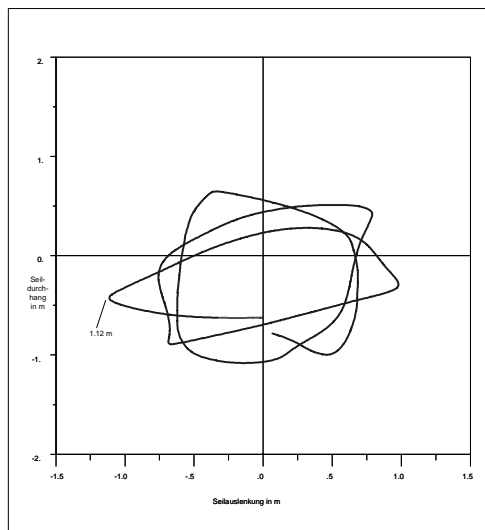


Figure 3.59 Movement of the mid-point of the span in the y/z plane without interphase-spacer

[Ref 79] specifies the minimum values of spacing required in the event of a short-circuit which, in the present case of a 110 kV installation, is 0.55 m. With the dimension verified by the finite element calculations, project design engineers using the formulae of IEC 60865-1 must anticipate a deflection of 1.27 m and, hence, physical contact between the phases, i.e. the danger of a double-circuit fault. A possible solution to this problem can come from IEC 60865-1:

- increase the phase spacing from 2.0 m to 2.75 m
- shorten the span length from 40 m to 23 m (with intermediate portal structures)
- reduce the short-circuit current I_{k2}'' from 28.5 kA to 18.2 kA

All three of the measures mentioned above require substantial modifications, and add substantial cost, to the switchgear installation.

On the other hand, the fitting of interphase-spacers made of a composite material offers a cost-effective and easily implemented solution. A typical preferred type of overhead-line insulator for this application is a long-rod insulator CS60-123/650. The relevant data for the calculations is as follows:

Round rod diameter	36 mm
Round rod length	1300 mm
Modulus of elasticity (bending)	34,000 N/mm ²
Total weight	12.4 kg

When designing the coupling elements between conductor and interphase-spacer the previous approach in the few examples that have actually been installed in switchgear has been based on past experience with

overhead power lines where interphase-spacers have long been a normal feature. Therefore, the following investigations are also intended to clarify whether these coupling elements should be rigid or articulated and be with or without reinforcement spirals.

As a result of installing the interphase-spacer, the span undergoes a change of state which, thanks to the light weight of the composite insulator, is only moderate.

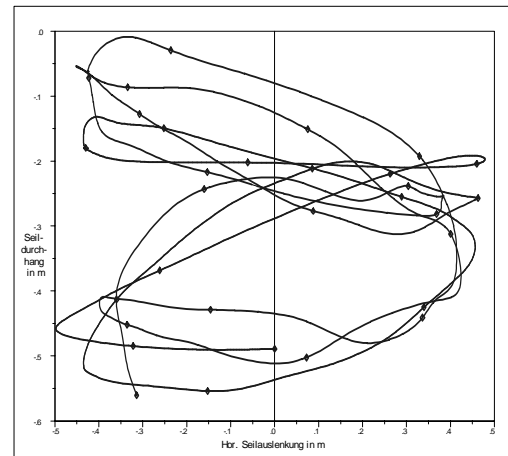


Figure 3.60 Movement of the mid-point of the part-span (1/4) in the y/z plane with interphase-spacer

All other data for the span remains unchanged. The points of maximum horizontal conductor deflection are moved from the mid-point 1/2 to 1/4 (or 3/4). The horizontal motion of the mid-point of the conductor is totally inhibited. As the conductor movement in Figure 3.60 shows, the maximum deflection is now 0.5 m. Thus, interphase-spacers fitted at the mid-point of the span are able to reduce the maximum horizontal deflection by about half. The minimum spacing between the phases is then 1 m, i.e. well within the permitted minimum spacing.

A quick glance at the dynamic behavior of the whole span shows flash taken at times $t_1 = 0.15$ s, $t_2 = 0.4$ s, $t_3 = 0.62$ s, $t_4 = 0.93$ s in Figs. 4a-d.

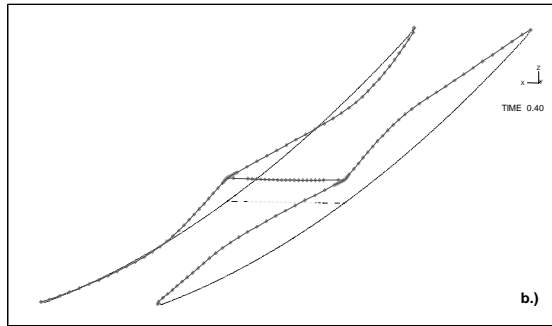
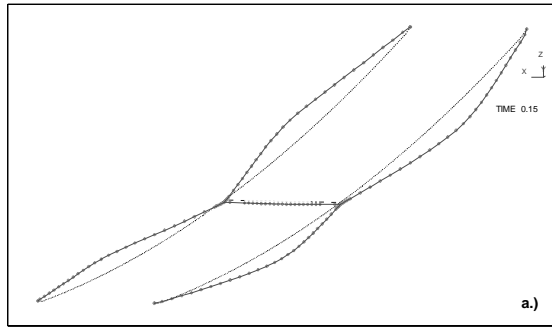


Figure 3.61 Displacement of the span at
a) $t = 0.1$ s; b) $t = 0.4$ s

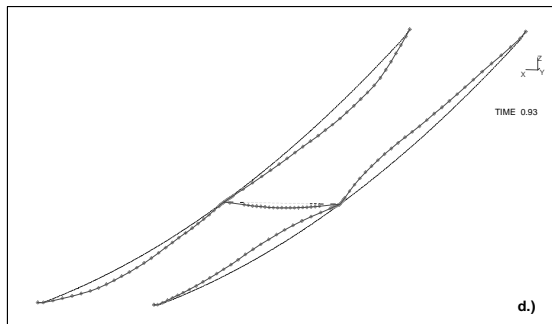
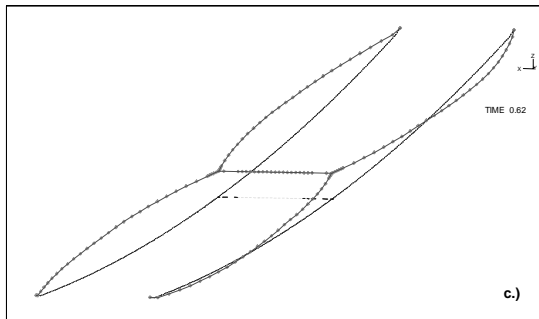


Figure 3.62 Displacement of the span at
c) $t = 0.62$ s; d) $t = 0.93$ s

Whereas, due to the halving of the conductor length, the horizontal motion now has twice the frequency (Figure

3.63b), the period for the unrestrained vertical direction (Figure 3.63c) remains approximately the same as for the calculations without interphase-spacers. From (Figure 3.63d) it can be seen that the horizontally unmoving mid-point of the conductor moves vertically in sympathy at the same frequency. For the tensile force on the conductor in (Figure 3.63a) this means that, due to the fitting of the interphase-spacers, although twice as many tensile maxima F_t occur, the number of drop maxima F_f and their times remain the same. Overall, it can be seen that the value of amplitude $F_t \approx F_f \approx 22$ kN governing the design of the points of suspension has remained largely unchanged. This means that, although fitting a interphase-spacer does not cause higher short-circuit tensile forces, it does not cause substantially lower forces either.

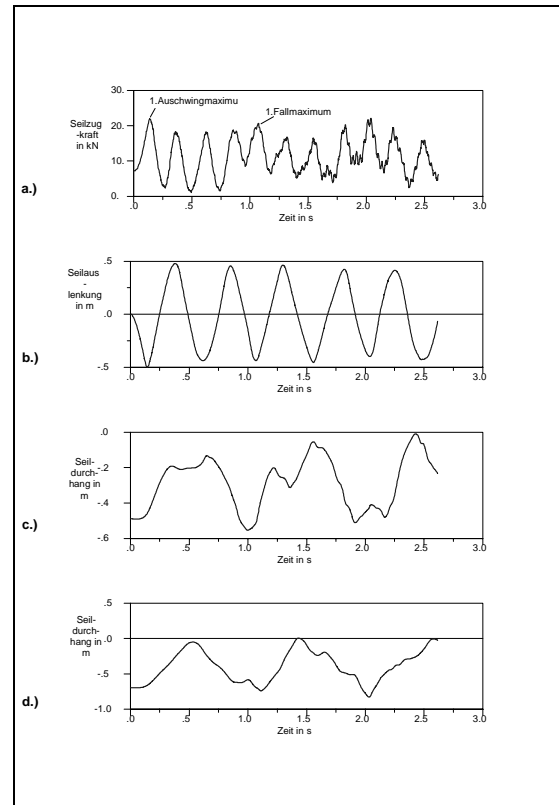


Figure 3.63 Time characteristics of the span with interphase-spacers

- a) conductor tensile force
- b) horizontal motion at 1/4
- c) vertical motion at 1/4
- d) vertical motion at 1/2

Figure 3.64 shows the tensile/compressive stresses caused by the horizontal motion of the conductors in the phase spacer.

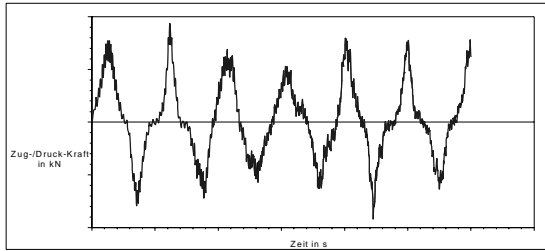


Figure 3.64 Time characteristic of the tensile/compressive force in the interphase-spacer

The frequency of ca. 2 Hz is identical with the one in Figure 3.63b. The values of amplitudes are proportional to the magnitude of the electromagnetic force acting on the phase spacer. The substantially higher frequency harmonics of ca. 40 – 80 Hz arise due to the bracing between conductor and phase spacer. Frequency and amplitude of the harmonics depend on the rigidity of the phase spacer / conductor clamping system. For the case in question, the use of conductor spirals would cause damping of the harmonic amplitudes. However, this effect cannot be said to be universal, i.e. in other arrangements it could just as well result in a gain. Therefore, the use of conductor spirals is not a sensible course of action without prior investigation.

Despite the higher harmonic components, the compressive forces always (even when $I_{k2}'' = 40$ kA) remained below the permitted Euler buckling force (16 kN). Their proportion of the total loading on the round bar is low.

As Figure 3.62d shows, the interphase-spacer cambers vertically downwards when the span drops. The potential energy that builds up during the first 500 ms is converted to energy of deformation (bending) and brings about the first maximum of the reference stress at 0.92 s (Fig. 7).

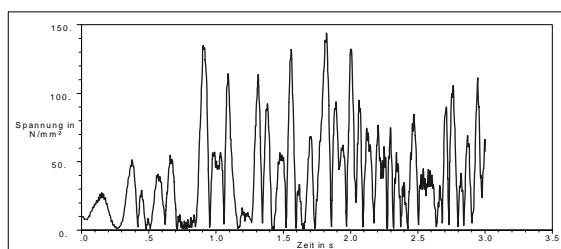


Figure 3.65 Time characteristic of the van Mises stress at the mid-point of the interphase-spacer

The nature of the coupling between conductor and interphase-spacer is irrelevant here. The results with free horizontal or horizontal and vertical rotational motion of the coupling were identical, which was to be expected in view of the low stiffness of the conductor. Therefore, the use of horizontal or even articulated conductor clamps is unnecessary.

In practice, the interphase-spacers are not fitted precisely perpendicular to the conductors. Calculations have been performed in which, for the sake of example, the interphase-spacer has been shifted on one side by 0.2 m along the axis of the conductor. However, the resulting horizontal bending moments only caused a slight increase in the loading on the interphase-spacer. When the interphase-spacer was fitted correctly, such shifts are considerably less than the calculated value so that the stress acting in the horizontal plane is of secondary importance.

Thus, the major load on the interphase-spacer results from the dropping motion.

Summarising the investigation one can say that by fitting a interphase-spacer at the mid-point of the conductor span it is possible to halve the conductor deflection. The static and dynamic conductor tensile forces are little affected in the process.

The coupling between the interphase-spacer and the conductor has no effect on the behavior of the strained conductor or on the mechanical load exerted on the spacer. Couplings with horizontal or articulated joints are unnecessary.

Similarly, the conductor spirals that are widely used in the world of overhead-lines are also unnecessary at the coupling points. Depending on the rigidity of the overall structure, their use can either increase or decrease the tensile/compressive loading on the interphase-spacer.

The compressive loading on the interphase-spacer is of the same order of magnitude as the electromagnetic force $F' \cdot l \cdot (F'$ as defined in equation 15, IEC 60865-1) and, in the case of the alternatives examined, always remained less than the maximum permitted value of buckling load.

The major load on the interphase-spacer results from the bending moments caused by the dropping motion.

The fitting of interphase-spacers at the mid-point of the span enabled the short-circuit strength to be increased from 21 kA to over 46 kA (at $F_i = 38$ kN).

3.7.3. A new simplified method for spacer compression evaluation.

As discussed already in [Ref 54] the well known Manuzio simple formula [Ref 53] neglect some important effects, mainly:

- Tension changes in the subconductor during contact period, so called **pinch effect**. This effect can be quite large, as the pinch can be several times the initial tension (CIGRE brochure 105 [Ref 1]). For example, in our tests presented in this document, the pinch is two times initial value (third case), even higher in [Ref 54]. It is quite clear that the spacer compression, which is directly related to the pinch (both pinch and spacer compression are quasi-simultaneous) is also affected by the pinch.
- **Asymmetry of the short-circuit current**. With increasing short-circuit current, time to contact and to maximum pinch and spacer compression becomes smaller and smaller (lower than 0.1 s in

our cases). It means that the energy input, which is severely increased by the asymmetry of the current (the first peak of the short-circuit current can be more than 2.5 times rms value and the energy is proportional to the square of the current) is totally converted into increase of the tension to create pinch.

- **Subspan length effect.** Manuzio neglected subspan length effect, which was consistent with no pinch, but does not reflect the actual situation as we observed in our tests, even for very large subspan length. In fact, if we imagine that subconductors are moving with fixed end, the subconductor length (in a first rough estimate) will have to increase by about the subconductor spacing (if we imagine that initially parallel subconductors came into contact along all subspan length, except very close to the spacer. It means that, following Hooke's law, the pinch could be estimate by: $\sigma = \epsilon E$ or

$$\frac{F_{pi}}{A} = \frac{a_s}{l_s} E \quad \text{or} \quad F_{pi} = \frac{a_s}{l_s} EA \quad \text{where } a_s \text{ is the}$$

bundle diameter, l_s the subspan length and EA the product of the elasticity modulus times the subconductor cross section. As EA is very large, such rough estimation will produce incredibly high pinch F_{pi} . Such approach clearly point out that subconductor tension cannot remain constant during contact, as Manuzio suggested.

The new simplified method developed must include such parameters. Many ways have been tried. Looking for the simplest one and trying to be as close as possible to known IEC methods, we finally decided to use actual IEC 60865-1 (based on the work developed inside CIGRE and published [Ref 55]) for evaluation of pinch tension in substation structures. We adapted the method to be used also for overhead lines, simply by implementing a constant tower stiffness of 100N/mm for both supports of one span and we focused our goal on the use of the output of IEC60865-1 (the pinch) see also [Ref 1], to evaluate spacer compression using the following method:

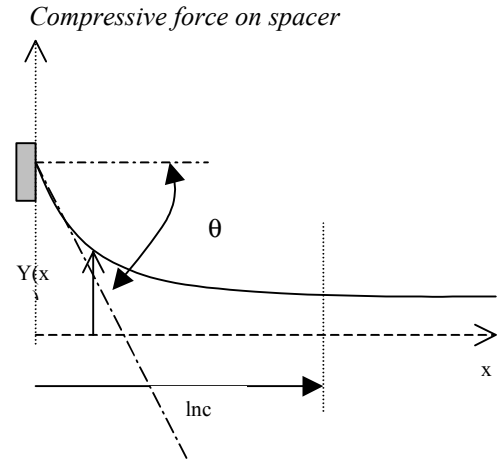


Figure 3.66 Subconductor shape of a twin bundle during a pinch (spacer on the left side)

In Figure 3.66, one subconductor is reproduced near spacer location, at the instant of maximum pinch and maximum spacer compression. The x axis represents the bundle center and the subconductor (straight line) is joining the center of the bundle keeping a certain distance, depending on subconductor diameter. l_{nc} is called the non contact length which is unknown and must be evaluated. Between the spacer location and contact point, the subconductor shape is like a parabola.

The compressive spacer force is the projection of the pinch on the spacer at spacer location (the pinch direction is given by the tangent which has a deviation θ from horizontal). The pinch is the traction in the subconductor, more or less constant along the subconductor. In this simple approach, the bending is completely neglected so that subconductor shape near the spacer can be reproduced as shown in the figure. Half of the spacer compression is given by :

$$F_c = F_{pi} \cdot \sin(\theta)_{x=0}$$

Another way to express it is to use equilibrium equation with electromagnetic load on the non-contact length (here expressed for twin bundle) :

$$F_c = 0,2 \cdot I^2 \cdot \int_0^{l_{nc}} \frac{\cos(\theta(x))}{2y(x)} dx$$

where the short-circuit current I is given in kA and is the so called time average short-circuit current taking into account the asymmetry as defined in CIGRE brochure [Ref 1, equation 4.27, page 49]

where

$$y(x) = \frac{a_s - d}{2} \left(\frac{x}{l_{nc}} \right)^2 - (a_s - d) \cdot \left(\frac{x}{l_{nc}} \right) + \frac{a_s}{2}$$

and

$$\cos(\theta) = \frac{1}{\sqrt{1 + \left(\frac{\partial y}{\partial x} \right)^2}}$$

The numerical resolution of these equations leads to the evaluation of the compressive force and of the minimum length of the sub-conductor, which is still free. The use of such method, combined with evaluation of pinch give access to the following results (Figure 3.67) on 28 known tests (case 8 of volume 2 of this brochure). What is clear is that Manuzio formula is correct for low spacer compression (the first dots are coming from Manuzio tests) but deviate up to 25% for other cases. The new method, described in this paper remains in the range of measurement precision. One dot is clearly out of the range, probably connected to measurement error. The main problem of Manuzio formula is coming from the systematic under-evaluation of spacer compression, which cannot be accepted for spacer design. Most of the validation cases are in the range of overhead line practice (30, 40, 60 and 120 meters), more results would be needed to extend our proposal to substations range, especially if we have no contact between subconductors. Nevertheless, we can point out the good correlation for 10 m subspan length. Of course more complex situations, like asymmetric bundle, very wide bundle, and other range than those used for validations can be evaluated by complex advanced methods, as used in [Ref 54]). But in most practical cases, this method can be used for evaluating

spacer compression, then replacing short-circuit tests by equivalent mechanical test in a classical lab. When designing a spacer or a spacer damper for overhead line, not only the short-circuit level is important, but also the initial value of the tension in the conductors (as well as subconductor spacing, subconductor diameter and subspan length). The same short-circuit on the same structure may have very different effects depending on short-circuit time inception (driving asymmetry of the current).

Important data to be used for IEC evaluation of F_{pi}

The use of this method will need a data in relation with tower stiffness. The proposed method to evaluate spacer compression need a heuristic value of 100 N/mm for each support instead of actual stiffness, used in other part of IEC60865 (see annex 8.3) to evaluate F_{pi} for example.

This relatively low value compared to actual tower data is in relation with a “dynamic stiffness” (which should include the dynamic behaviour of the support and anchoring insulator chain in such a dynamic excitation, more close to an impulse).

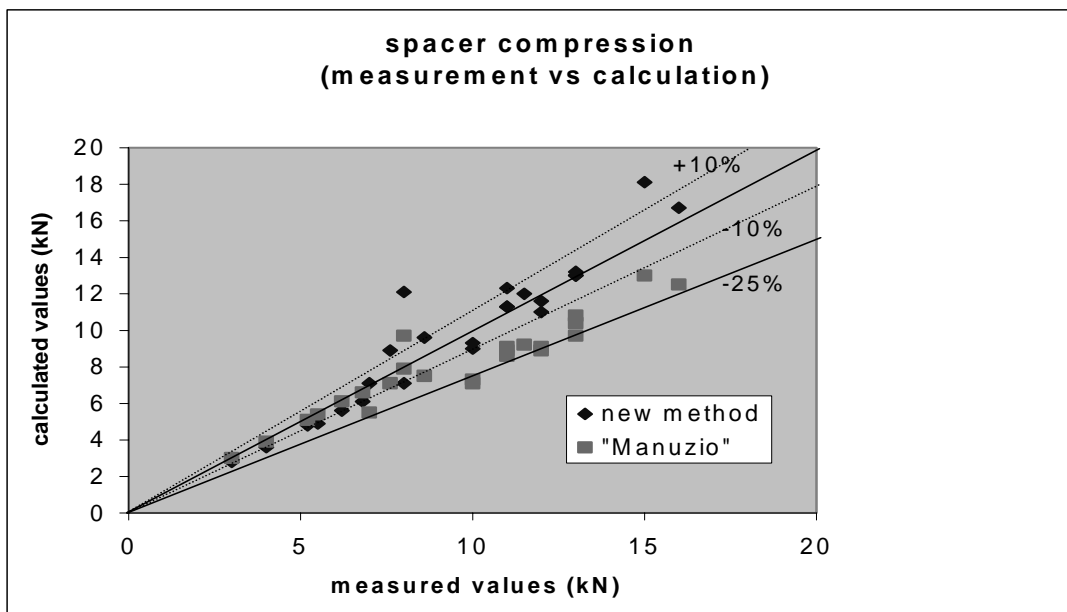


Figure 3.67 Comparison of spacer compression between tests and simplified method

3.7.4. Jumpers

Jumpers are used to connect two strained spans, see configuration D in Figure 1.1 and Figure 3.68a. Because the static tensile force is low, the forces due to the short-circuit currents are not so important but the maximum horizontal displacements are relevant for the short-circuit strength [Ref 56, Ref 57]. Tests show, that the jumpers are fixed in their clamps and the lowest point moves in a circle with centre below the fixing points, Figure 3.68b. The fixation causes a deformation of the swing out plane by which a bending moment acts against the electromagnetic force. It is found empirically [Ref 56] that this moment can be taken into account by an increase of 20 % in the gravitational force to be inserted in the parameter r calculated with equation (3.26) of IEC/EN 60865-1 [Ref 69, Ref 3]:

$$(3.26) \quad r = \frac{F'}{1,2nm'_s g_n}$$

With this assumption displacements are calculated which nearly agree with the measured ones.

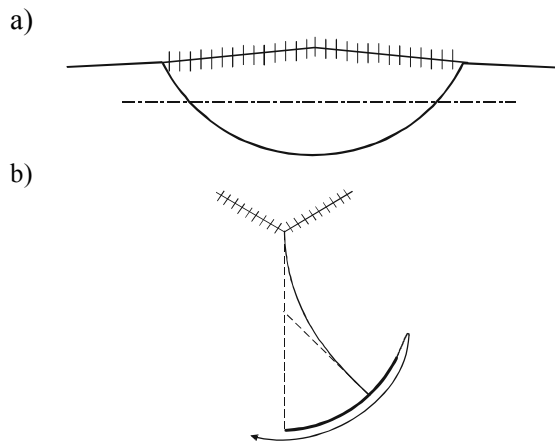


Figure 3.68 Jumper
a) Side view b) Movement

3.7.5. Springs in strained spans

In some substations, springs are built in between towers and insulator strings to limit the change in the sag

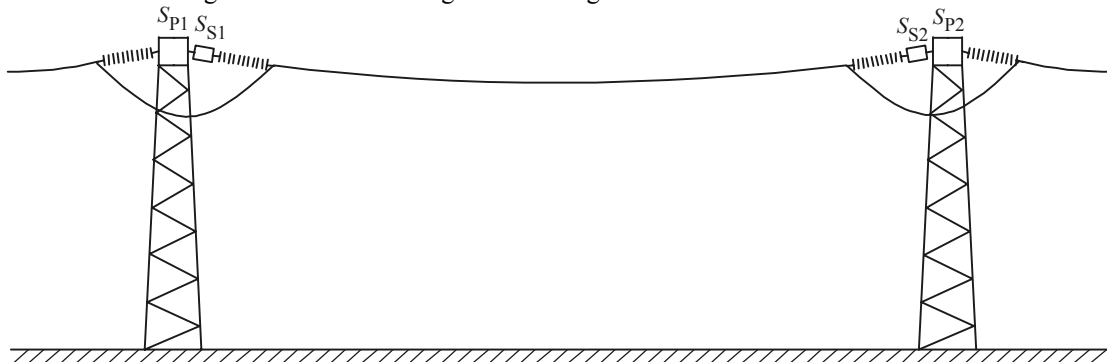


Figure 3.69 Strained span with springs

between minimum winter temperature and maximum operating temperature as shown in Figure 3.69. Therefore the static sag can be calculated by use of resultant spring constant S of both towers and the springs:

$$(3.27) \quad \frac{1}{S} = \frac{1}{S_{P1}} + \frac{1}{S_{P2}} + \frac{1}{S_{S1}} + \frac{1}{S_{S2}}$$

S_{P1}, S_{P2} are the spring constants of the towers and S_{S1}, S_{S2} the spring constants of the springs.

During the short-circuit current flow, the springs reach their end position and the resultant spring constant S suddenly changes to a much higher value:

$$(3.28) \quad \frac{1}{S} = \frac{1}{S_{P1}} + \frac{1}{S_{P2}}$$

This nonlinearity causes additional oscillations in the span which also can lead to tensile forces by which the spring comes back into its range of operation.

In spans with springs, reliable results for the maximum short-circuit forces and displacements cannot be gained by IEC/EN 60865-1, it is necessary to calculate with an advanced method.

IEC/EN 60865-1 can estimate only ranges with lower limits which can be very unsafe and upper limits which can be very safe. The calculation with the resultant spring constant S according to equation (3.27) leads to a lower limit for the forces and an upper limit of the horizontal displacement and S according to equation (3.28) leads to an upper limit for the forces and a lower limit for the displacement. The actual values lie in between.

4. GUIDELINES FOR DESIGN AND UPRATING

4.1. INTRODUCTION

Design guidelines for arrangements, mechanical loads and electrical clearances are provided in [Ref 1] together with detailed recommendation for rigid bus arrangements and for flexible bus (eq: strained and slack connection), droppers and jumpers subjected to mechanical loads due to short-circuit currents. In addition, suggestions for design criteria of support structures can be found there. The object of this chapter is to amend [Ref 1] recommendations due to perceptions presented in chapters 2 and 3. Affected are the design of droppers and the design of support structures – mainly portals – where the implementation of ESL adds new elements. Additional information will be given for limitation of magnitude and duration of short-circuit current and the treatment of foundations. Last but not least recommendations for load cases and safety factors are given (based on an international inquiry) gave a wide range of possibilities, not always meeting an economical solution.

4.2. LIMITATION OF MAGNITUDE AND DURATION OF SHORT-CIRCUIT CURRENT

As mentioned in [Ref 1] many parameters influence magnitude and duration of short-circuit current and subsequently mechanical stress of substation equipment.

Limiting the magnitude of short-circuit current may be achieved by increasing the equivalent impedance of the network. But for this modifications to the network design or operation are necessary which obviously are difficult to perform in existing networks. Nevertheless the use of D.C. links, which separate networks for short-circuit or the choice of uprated voltage level are measures to decrease short-circuit current. Others methods, though expensive, are to increase transformer reactance or to decrease line numbers (increase of the cross section of conductors) which leads to a higher reactive energy consumption but as well to a less degree of network stability. Opening of a ring network could be an efficient alternative since it allows electrical separation of some parts of the network. Frequently adopted for HV networks this method of action is also used for EHV installations even if it decreases network safety.

Another factor which may influence the magnitude and duration of short-circuit current is the performance of the protection system. As an example the mechanical stress of a flexible busbar may be substantially influenced by a reduction of the clearing time. As a matter of fact, diversity and complexity of existing

installations do not allow adoption of a general method. Each case must be studied separately in collaboration with departments having expertise in this domain. A comprehensive analysis is required to check the operational coherence of the systems in order to secure a satisfactory supply quality. But, if measures to decrease mechanical effects are considered improvement of protection systems should be regarded as well.

4.3. FLEXIBLE CONDUCTORS

In [Ref 2] a simplified calculation method for flexible conductors is given. However it is limited and has been verified for the case of horizontal spans only. Whereas in long strained spans the vertical extension is more or less uncommon its a rule in slack connections of different devices. Nevertheless formulas of [Ref 2] may be used for both strained and slack conductor spans up to the point where $\Delta h/l = 1/4$ (l length of the span; Δh vertical extension). If $\Delta h/l$ ratio is greater than $1/4$, the physical model of [Ref 2] cease to be valid and recommendations and formulas of chapter 3.3 have to be used.

On the evidence of eq. 3.13 there, the swing out of droppers doesn't depend furthermore on the magnitude of short-circuit current. Only l/K and K itself are parameters in this equation which points out that dropper geometry and the length of cable are of essential influence. The flexibility of fixing points, if they are definitely fixed, has just as much influence. In the same way as a small change of the arc length in a horizontal span leads to respectable change of its sag, a slight flexibility of the upper fixing point (e.g. at the end of a long span) leads to remarkable increase of the swing out value calculated according eq. 3.13 with corresponding effects to clearance.

Other design criteria for droppers are their length and their position in the span. As described in chapter 3.3 the swing out of the span itself is influenced by this. Consequently the forces on the anchor points of the span vary. Tests at EDF showed that a decrease of 30% of these forces is possible (see Figure 3.34, Figure 3.35). A simplified calculation method is not yet available but advanced methods allow today safe prediction of these phenomena.

Savings in the same order were found in the same test series of EDF through the use of interphase-spacer in long strained spans. This was not confirmed in examinations described in chapter 3.7.2. Thus in these cases as well, advanced calculation is necessary to meet the effects of important parameters e.g. the spring constant of the system.

The combined effect of wind pressure and short-circuit on the dynamic loading is very complex on flexible

structures. Advanced simulations are recommended in such cases.

4.4. SUPPORTING STRUCTURES

One of the recommendations in [Ref 1] is to calculate static loads of supporting structures first and then to proceed with short-circuit effects. Although it is common to consider short-circuit load in two lines only while having in the third line the static load (at three-phase short-circuits F_{pi} is assumed to be at its maximum in two lines at the same time only) short-circuit levels nowadays lead to the situation that short-circuit is the governing load if other severe exceptional loads as extreme wind or earthquake are absent. The new awareness of resonance effects in steel structures which are expressed by ESL-factors up to 1.4 (see chapters 3.5 and 3.5.4) are intensifying this effect. Economical solution may be obtained to this day if calculation models of Eurocode 3 are put opposite precise determination of short-circuit load. Whereas for static (normal) loads a linear material model still is recommended, the (exceptional) short-circuit load may be regarded in a non-linear material model using plastic zones, and the plastic hinge theory as [Ref 2] does for rigid busbars right from the start.

4.5. FOUNDATIONS

Forces which affect structures of AIS are transmitted to the soil by foundations usually designed in accordance with current standards of civil engineering, which solely recommend static calculation methods. As long as those forces are in a vertical direction, sufficient soil withstanding pressure is the only design criterion. Having horizontal forces like short-circuit current forces, and provided that soil conditions are in a normal range, the proof of stability gets to be the most important one. Due to the dynamic character of short-circuit force and the static calculation methods; ESL is the governing factor and not the maximum value of short-circuit current force. This ESL respectively ESL-factor are not checked for foundation until now but contrary to chapter 3.6 where ESL factors are given for steel structures, ESL factors for foundations are assumed to be much smaller than one because foundations are heavy and inert structures. Thus short-circuit current forces are of minor importance for foundation design especially if other horizontal forces as cable pull and wind or earthquake have to be considered. In other words we mean that the dynamic mechanical effects of short-circuit on foundation can be neglected.

4.6. SAFETY FACTORS AND LOAD COMBINATIONS

In a substation external forces apply on the structure and cause internal stresses and forces. The design for mechanical strength requires not only the exact knowledge of the forces and their effects, but also analyses regarding the statistical probability of several events coinciding with regard of the rigidity and ductility characteristics of the elements. Under the aspects of optimum technical and economic efficiency, therefore, it is necessary to lay down requirements which assure the reliability of equipment throughout their whole service life and prevent any danger to life or limb. While taking into account knowledge gained from the building of switchgear it is also possible to refer to existing civil engineering standards for this purpose, such as IEC Publications, European Standards, National Standards, etc. In the following, the safety factors and the load cases are defined and the assumed loads and permitted stresses in substations are described.

According to [Ref 18], an action is defined as

- a force (load) applied to the structure (direct action)
- an imposed deformation (indirect action); e. g. temperature effects or settlements.

These actions are classified

a) by their variation in time:

- permanent actions
- variable actions
- accidental actions

b) by their spatial variation.

The design value F_d of an action is generally defined as

$$(4.1) \quad F_d = \gamma_F F_k$$

where γ_F is the partial safety factor for the action considered, taking into account of, for example, the possibility of unfavourable deviations of the actions, the possibility of inaccurate modelling of actions, uncertainties in the assessment of effects of actions and uncertainties in the assessment of the limit state considered. F_k is the characteristic value of the applying actions. Characteristic values, in general, correspond to a fractile in the assumed statistical distribution. If the necessary basic data is lacking, it is also possible to use deterministic limit values for F_k .

In the same way as the effect, it is also possible to specify a fractile for the materials that will be subject to stress. A partial safety factor γ_M is added to the characteristic value X_k to ensure that any chance deviations in the resistance of the material or the geometrical dimensions are safely taken into account. Characteristic values are specified by relevant

standards and tested under specified conditions, e. g. minimum failing load, routine test load, nominal value.

The design value X_d of a material property is generally defined as

$$(4.2) \quad X_d = \frac{X_k}{\gamma_M}$$

Defining an overall safety factor γ is the product of the partial safety factor γ_F for action and the partial safety factor γ_M for material property:

$$(4.3) \quad \gamma = \gamma_F \gamma_M$$

Thus internal stresses and forces effected by actions shall not be higher than:

$$(4.4) \quad X \leq \frac{X_k}{\gamma}$$

4.6.1. Substations

In the design of a substation due to the classifications of the actions, two general load cases are defined from which it is also possible to specify several more combinations of loads. The first load case takes into account loads that can occur under normal loading conditions only. These are permanent actions and variable actions. The following loads are listed as actions in [Ref 79]:

- Dead weight
- Installation load
- Tensile load
- Ice load
- Wind load

The second load case defines exceptional loads, whereby the load combinations are always all permanent acting together with one accidental load. In AIS the following exceptional loads are to be found :

- Switching forces
- Short-circuit forces
- Removal of a cable run
- Seismic forces

The possibility of several accidental actions working together, or variable actions working together with accidental actions, is precluded because it is unlikely that they will occur at the same time. This is still held to be valid despite the fact that it is easily possible to imagine a wind gust or, say, a seismic event occurring at roughly the same time as a short-circuit. However, simple addition would leave out two important aspects. Firstly, it is mostly dynamic events that are involved for which an ESL has been defined. As can be seen from chapters 3.5 and 3.5.4, an ESL involves the effect of the peak dynamic value. However, the possibility of several peak dynamic values being coincident in time is highly unlikely. The consequence of only specifying

one exceptional load each time is the same as first adding dynamic values together and then determining the ESL afterwards. Another aspect that helps us deal with these combinations is that defining variable loads and exceptional loads involves between 95% and 99% fractiles. Here too it is highly unlikely that adding the loads together before statistical analysis would result in a load of the same magnitude as when adding individual fractiles together.

Table 4.1. Partial safety factors for actions γ_F according to [5.3]

Load case	γ_F
Load case 1 (normal loading)	1.35
Load case 2 (exceptional loading)	1.0

Table 4.2. Partial safety factors for actions γ_M

Material	Safety factor based on	Load case 1 γ_M	Load Case 2 γ_M
steel structures	R _{p0,2}	1.1	1.1
tubular buses	R _{p0,2}	1.1	1.0
wooden poles	failure limits	3.0	
concrete poles	failure limits	1.5	
steel reinforcement or prestressing tendons	failure limits	1.15	
foundations	failure limits	1.1	
support insulators	minimum failing load	1.85	
longrod insulators	minimum failing load routine test load	2.3 1.85	1.0
cap and pin insulators	minimum failing load routine test load	2.3 1.38	
<u>insulator and conductor accessories from</u>			
- forged steel	minimum failing load	2.25	1.0
- cast steel or aluminium	routine test load	3.0	1.0

Partial safety factors for both normal and exceptional loads are given in Table 1 and Table 2. Table 3 gives reference to EUROCODES (EC) because the most important ones are given there too.

4.7. CLEARANCES

In agreement with CENELEC HD 63751 : 1999 [Ref 102], the minimum air clearance in the air, when the

conductors move under the influence of SCC forces can be fixed in amount of 50% of normal clearance.

Table 4.3. Partial safety factors for materials γ_M

Material	γ_M	Reference to
steel	1.1	EC 3
concrete	1.5	EC 2
steel reinforcement or prestressing tendons	1.15	EC 2
wood	3.0	EC 5
foundations	1.1	EC 7

5. PROBABILISTIC APPROACH TO SHORT-CIRCUIT EFFECTS

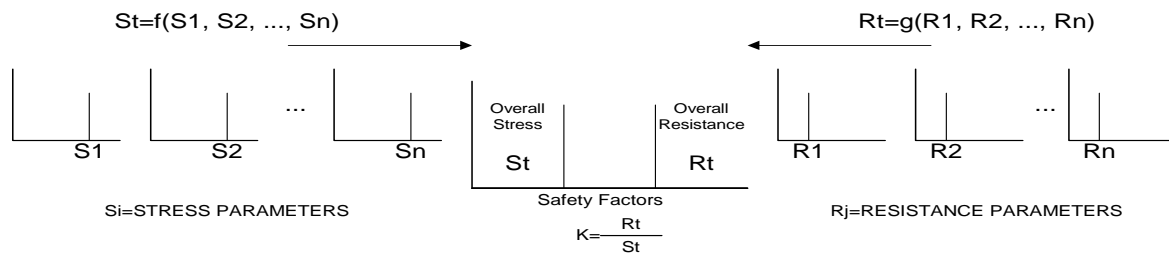
TECHNIQUES FOR DETERMINING THE MECHANICAL WITHSTAND OF STRUCTURES OR COMPONENTS

5.1. THE VARIOUS POSSIBLE APPROACHES

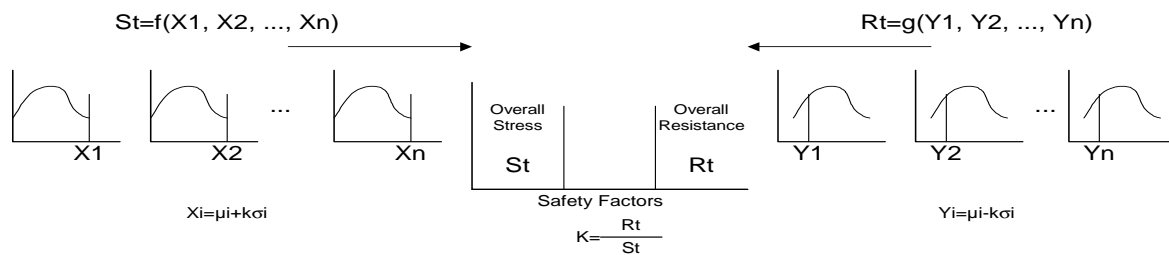
Probabilistic sizing techniques have been developed during the last decades for the analysis of energy transmission structures. A number of probabilistic methods are available. The most important are shown in Figure 5.1, as well as the deterministic design.

The inspiration for this section is drawn from analyses by the former ONTARIO HYDRO and ELECTRICITE DE FRANCE-R&D.

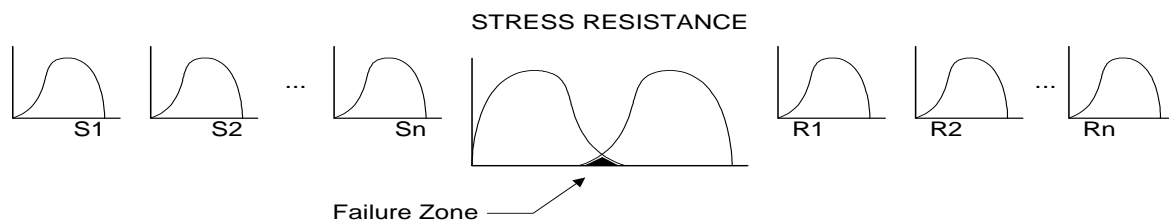
1/ DETERMINISTIC METHOD



2/ SECOND MOMENT METHOD



3/ PROBABILITY METHOD



4/ OPTIMIZATION

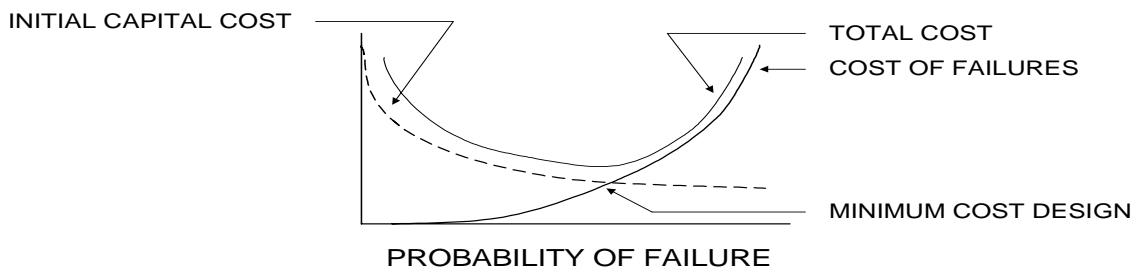


Figure 5.1

5.1.1. *Deterministic Methods*

In deterministic methods, structural design is carried out according to the logical approach given below:

- I. Replace the always complex reality of structures with modelling, which can be approached by calculation,
- II. Define the various actions affecting the structure, as well as their mode of representation, which is merely a diagrammatic simplification of physical reality,
- III. Use a computer model representative of the structure's behavior, insofar as the computer model is the mathematical tool making the transition possible from knowledge of the actions to the determination of overall stress S_t , symbolized by an elementary stress function

$$(5.1) \quad S_t = f(S_1, \dots, S_n)$$

- IV. Check that the margin, characterizing the "degree of safety", between the state of loads and the strength criteria under consideration is sufficient. The overall resistance is calculated on the basis of a composition g of the various criteria.

The degree of safety is represented by a safety factor:

$$(5.2) \quad k = \frac{\text{resistance}}{\text{stress}}$$

The distinction between the representation of reality and the model fitted to computing requirements involves a whole web of simplifications, approximations, hypotheses and uncertainties, which are deterministic in essence and may, for lack of a carefully reasoned choice, distort certain conclusions.

5.1.2. *First Level Probabilistic Method*

In the first level of probabilistic design, illustrated in Figure 5.1, the same computer models (for f and g) are used, but the value of one or several parameters is fixed on the basis of statistical data.

The classic example of this type of design is the choice of maximum annual wind velocity on the basis of a recurrence time obtained from meteorological statistics. As in the deterministic methods, the stresses must be ascertained as lower than the strengths by a set safety factor.

5.1.3. *Second Level Probabilistic Method*

These methods consist in evaluating the risk of failure as a probability, so that the designer can choose from among several degrees of safety, depending on different failure probability values. The computer models on which the design process is based are the same as those used in the deterministic method, i.e. functions f and g . However, the statistical distribution of the parameters serves as the reference in establishing a distribution of stresses and resistances corresponding to the applied loads and the strength of structures. Then, instead of comparing the two distributions in terms of a safety factor, a convolution is operated to calculate a probability of failure of a structure or a failure recurrence time T , expressed in annual frequency.

The hatched area in Figure 5.2 defines the theoretical risk of failure (R), corresponding to the function:

$$(5.3) \quad R = \int_0^{\infty} G(L) f_0(L) dL$$

where: $G(L)$ is the Cumulative Distribution Function (C.D.F.) of the strength of the supports or components in the same batch

and: $f_0(L)$ is the Probability Distribution Function (P.D.F.) of the applied loads.

The theoretical risk of failure may be calculated as a function of the relative position of curves $G(L)$ and $f_0(L)$.

The position of curve $G(L)$ may also be defined as the guaranteed statistical strength L_s and that of curve $f_0(L)$ as the overload probability L_T or as the recurrence time T .

The risk of failure may also be denoted as a function of the ratio:

$$(5.4) \quad \Gamma = \frac{L_s}{L_T}$$

or as a function of the reliability index [Ref 80] (CORNELL, ROSENBLUETH-ESTEVA, HASOFER-LIND, DITLEVSEN).

For a given load recurrence time, the risk of failure decreases as Γ increases.



Figure 5.2 Assessment of the risk of failure of a support under random loads.

IEC 60826 applicable to overhead transmission lines proposes an approach of this type. Specifically, it defines safety classes on the basis of the assumed load recurrence time: 50, 150 and 500 years.

Naturally, probabilistic distributions will only be applied to parameters having a significant variation range and adequately supported statistical data.

The other parameters are then represented by their deterministic values, which are conservative in nature.

5.1.4. Optimization

The full probabilistic level consists of optimizing the design of structures by varying all of the parameters. The selection decision can then be based on a comparison of investment costs and failure costs.

Probabilistic methods avoid the multiplication of safety factors or successive consideration of the most penalizing cases, problems often encountered with deterministic methods.

5.2. SECOND LEVEL PROBABILISTIC METHOD

5.2.1. Stress and strength relationship for supporting insulators

5.2.1.1 Static and dynamic break-load

In many cases post insulators are mounted in disconnectors. The permissible (tensile-) load for the disconnector depends on the minimum breaking load of the post insulator. Post insulators can be stressed by static and/or dynamic loads. In the normal case it is a bending stress. Usually, ceramic materials are inflexible and differences between static and dynamic strength are not known [Ref 94]. Experimental [Ref 95] and theoretical [Ref 96] investigations of 110 kV post insulators under short-circuit loading have not shown any significant differences between static and dynamic porcelain strength. For that reason it is possible to convert the maximum stress at a specific point of the porcelain in the case of a short-circuit (i.e. measured as strain ϵ_{dyn} on the surface of the insulator core over the lowest shed) to an equivalent static load F_{max} which generates the same stress at the same point. This load can be compared with the minimum breaking load.

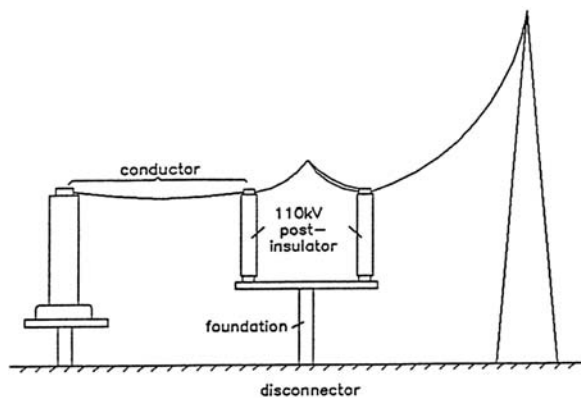


Figure 5.3 Current-conducting-equipment with conductor, post insulator and foundation (scheme)

5.2.1.2 One point distribution of strength

From a statistical point of view, the minimum breaking load fixed by the manufacturer could be considered as a one point distribution of the mechanical strength of post-insulators.

This would mean that each post insulator withstands a load lower than the minimum breaking load. If the load is higher than the minimum breaking load all post insulators would be damaged. This approach does not correspond with reality. The strength of post

insulators is distributed statistically as a result of the fact that the strength of a ceramic body is statistically distributed, due to differences in the structure inside the ceramic body [Ref 97]. In most cases the real bending strengths of post-insulators are higher than the minimum breaking load. But it is possible that some post insulators are damaged by loads lower than the minimum breaking load. Exact knowledge of the strength distribution function is necessary (especially for little quantils of strength) for determination of mechanical reliability of a post-insulator.

5.2.1.3 Strength distribution function of 110 kV post insulators

111 ruptures of post insulators with a minimum breaking load of 8kN were evaluated for determination of the strength distribution function of brand-new post insulators. The statistical evaluation of these test results showed three break value ranges (Figure 5.4) :

1. ruptures due to loads up to 10 kN
2. ruptures due to loads between 10 kN and 20 kN
3. ruptures due to loads greater than 20 kN which can be approximated by a double exponential distribution.

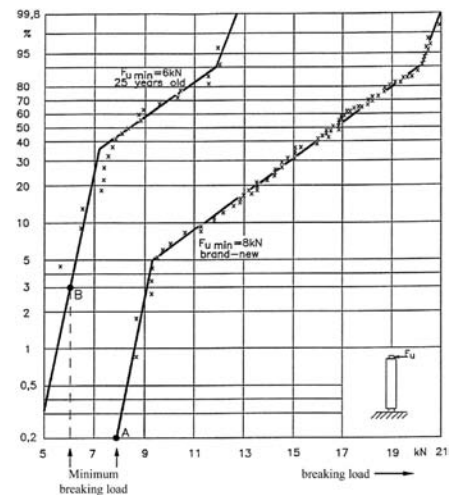


Figure 5.4 Distribution-function of mechanical strength of 110-kV-post insulators with different minimum breaking load $F_{u \min}$ and age (courtesy ABB, Pr. Böhme)

The same procedure is valid for 25-year-old post insulators with a minimum breaking load of 6 kN. To determine the distribution function of this type, 21 post insulators were tested to failure. The theoretical distribution function is also a double exponential distribution with the following break value ranges :

1. ruptures due to loads up to 7,5 kN
2. ruptures due to loads between 7,5kN and 11 kN
3. ruptures due to loads greater than 11 kN.

Only the lowest break values are important for determination of the reliability. It is interpreted as a quasi-incomplete sample test [Ref 98]. As a result it is the minimum breaking load of the brand-new post insulator with a minimum breaking load of 8 kN on the 0,2-%-quantil (Figure 5.4, point A). For the 25-year-old post insulators the minimum breaking load (6 kN) is on the 3-%-quantil (Figure 5.4, point B).

5.2.1.4 Reliability of 110 kV post insulators depending on mechanical stress and strength (example)

5.2.1.4.1. Design practice

The mechanical reliability of a 110 kV post insulator results from the comparison of stress and strength. If the stress is greater than the strength the insulator will be damaged.

For substation design the highest possible short-circuit current at the end of the substation life-time has to be considered. This loading multiplied by a safety factor (i.e. [Ref 56] recommends a maximum load not higher than 70 % of the minimum breaking load) is the criterion for selection of the insulators. This means that the manufacturer-guaranteed strength F_{umin} is higher than the maximum stress which will be achieved in the future. For design, both reliability influencing factors (stress and strength) are considered as one point distributed. It is assumed that the highest possible current appears in each short-circuit and that each post insulator cannot be damaged by loads lower than the minimum breaking load. This procedure is well tested in practice. If the mechanical reliability of a device must be determined exactly (i.e. for short-circuit current level uprating in a substation) the method of consideration must be changed.

5.2.1.4.2. Reliability calculation for a 110 kV post insulator

The reliability Z of a device results from the failure probability p_f :

$$(5.5) \quad Z = 1 - p_f$$

The probability of a mechanical failure depends on the stress density function p_B and on the strength distribution function V_S . If the stress density function and the strength distribution function are known the failure probability can be calculated by solving the Duhamel integral :

$$(5.6) \quad p_f = \int_{F_{\text{min}}}^{F_{\text{max}}} p_B(F) \cdot V_S(F) \cdot dF$$

For the given example (disconnecter equipped with 110 kV post insulator) the stress density function results from the load probability and the mechanical-dynamical behaviour of the system "conductor-support» due to short-circuit current loading [Ref 57]. For this example the relationship determined by experiments is known between

- short-circuit current loading and stress-maximum
- static load and stress

Therefore it is possible to convert the load due to a certain short-circuit current loading to a static load at the top of the post insulator which produces the same stress. The stress density function results then (with the conversion) from the calculated density function of the short-circuit current.

For the given example the strength distribution function was derived from the part-collectives with the lowest break loads. Fault probabilities of $p_f = 5,3 \cdot 10^{-13}$ for the brand-new post insulator with a minimum breaking load of 8 kN and of $p_f = 4 \cdot 10^{-9}$ for the 25-year-old post-insulators with a minimum breaking load of 6 kN result by solving the integral (5.6) for the example.

5.2.1.4.3. Stress and strength influences on probability

Provided that the course of curves of stress and strength are constant the probability depends on stress and strength as follows :

1. If the stress F_{max} increases about 10 % of the value of the minimum breaking load the fault probability will rise tenfold.
2. If the strength F_{umin} of a post insulator is 10 % lower than the minimum breaking load (i.e. $F_{\text{umin}} = 7,2$ kN instead 8 kN) under the same load, the fault probability will also rise tenfold.

That means that the same percentage increase of stress or decrease of strength leads to the same decrease of probability. For the given example (disconnecter equipped with 110 kV post insulators) there is good co-ordination between stress and strength concerning the influence of fault probability: the gradient of fault probability is determined equally by both because the stress-increasing gradients and the strength-decreasing gradients are the same.

For practical cases it can be expected that the loading and the stress increase during the life-time of a device. But the strength normally decreases. In such a

case, the reduction of reliability results from the combination of stress-increasing and strength-decreasing effects. In the example, the stress of a post insulator with a minimum breaking load of 8 kN increased from 5,6 kN to 6,4 kN. At the same time the strength decreased from 8 kN to 7,2 kN. As a result of increasing stress and decreasing strength the failure probability rose by two decades.

If the relative changes of stress and strength are unequal, the probability will be taken as follows :

- For a given permissible failure probability one can find parameter combinations F_{max}/F_{min} which do not exceed the given probability limit.
- If an equivalent static load F_{max} is assumed, it will be possible to determine minimum strength of post insulators with which an assumed limit of failure probability will be observed.

5.2.1.5 Summary

In the described example of mechanical reliability of 110 kV post insulators, it was shown that if the stress density function and the strength distribution function are known, the reliability can be calculated. If the percentage increase of stress and the percentage decrease of strength as the same, the influences on the reliability will be equal. A good co-ordination of effects of increasing stress and decreasing strength of the reliability results in the example considered. For other devices as well, it should be assumed that the reliability is influenced by increasing stress and decreasing strength.

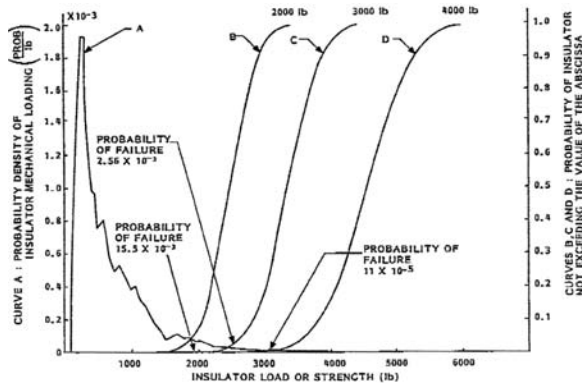


Figure 5.5 Load / strength distributions for rigid bus example

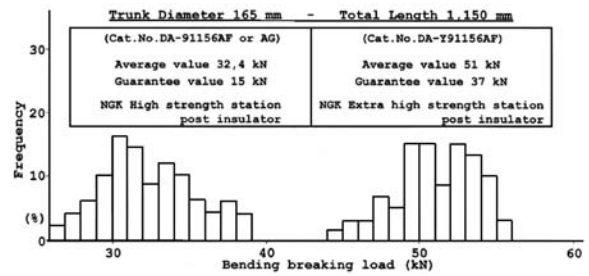


Figure 5.6 Bending breaking load

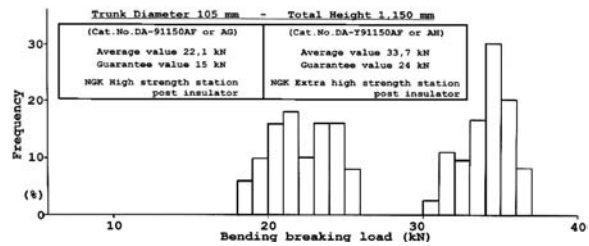


Figure 5.7 Bending breaking load

5.2.1.6 Example of savings using probabilistic approach in renovation ... (Ford, Sahazizian)

Type of short-circuit	Nominal voltage			
	110 kV	220 kV	400 kV	500 kV
1-ph + e	70 %	85 %	90 %	92 %
2-ph	10 %	6 %	3 %	2 %
2-ph + e	15 %	5 %	4 %	3 %
3-ph	5 %	4 %	3 %	3 %
Σ	100 %	100 %	100 %	100 %

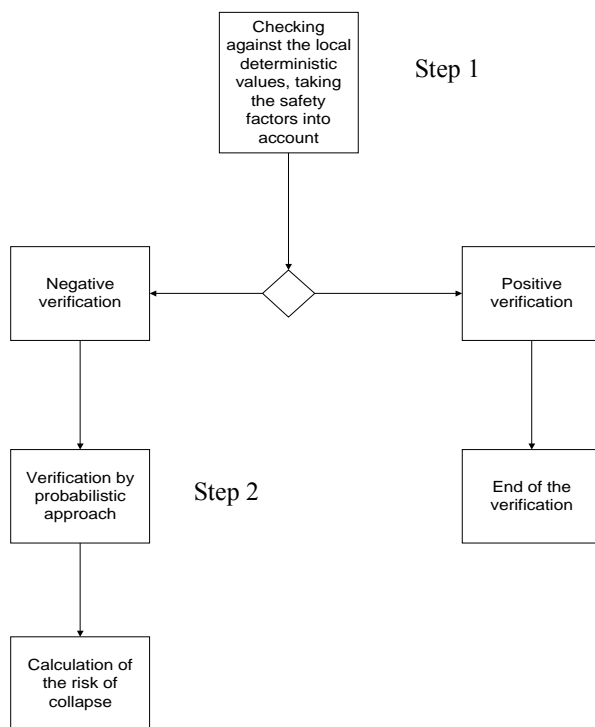
Table 5.1 Various types of short-circuits (contributions) Courtesy M. Daszczyzak, University of Mining and Metallurgy, Cracow, Poland.

5.2.2. A global Approach

For analyzing existing structures, RTE proposes a two-step approach:

Step 1: Check using the local deterministic values of the short-circuit current, the time constant and the clearance time, taking the safety factors into account.

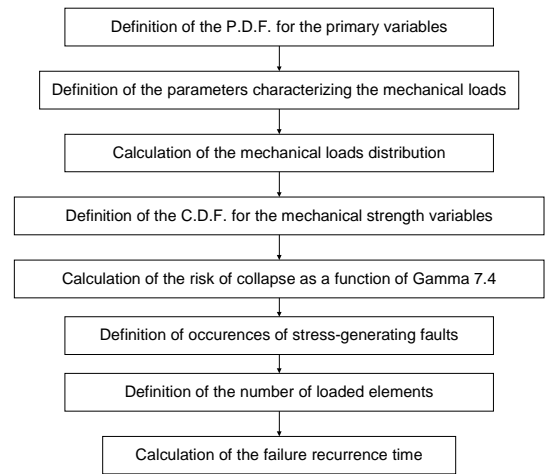
Step 2: Check using the probabilistic values of the short-circuit current intensity, the voltage phases having caused the fault, and possibly the wind velocity concomitant with the occurrence of the fault and the direction of the wind (in this case, the prevailing wind may be taken as perpendicular to the busbars).



This type of approach has been developed below for rigid busbar only.

5.2.3. A Calculation Method

Given the choice of possible approaches, it is best to take into account either the design situation which, if well chosen, corresponds to a penalizing situation, or a more detailed method, described in 5.2.3.1.4. This section is not intended to define that situation specifically for each company and according to local particularities, but rather to outline the main steps in an approach that may be broken down as follows:



5.2.3.1 PRIMARY VARIABLES

The mechanical loads in a substation due to short circuits depend on:

- the high-voltage and low-voltage structural design,
- the amplitude of the fault currents and their distribution over the busbars,
- the instant of occurrence of faults,
- the time constant of the networks,
- the clearance times,
- but also, in the event of a reclosure, the isolating time and the parameters of the possible second short circuit,
- the variation in concomitant parameters such as temperature, wind, ice, etc.

Many of the above are random parameters.

Given the random nature of these parameters, the conservative approach is to consider the maximum number of stresses under the worst conditions and assume no limits or choices. Hence, this approach may result in expensive over-sizing associated with low probabilities of occurrence.

We propose to define the broad outline of a probabilistic approach drawing on existing approaches (Ontario Hydro, IEC 60826 on overhead lines [Ref 93]).

By classifying the penalizing situations according to their probability of occurrence, we can approach the ultimate stress loading frequencies and set a rule of choice in order to determine:

- either the assumptions to be made, depending on the climatic, electrical and structural (HV, LV) stresses,

In that respect, the combined load (Wind + Short Circuit) offers an alternative to the arbitrary choice of a higher safety factor for the isolated electrodynamic assumption.

- or the conditions for rebuilding or reinforcing an existing substation. The analyses in progress focus on this aspect, and more specifically the largest rigid structures, when the primary busbars are concerned.

Here, we propose to define the main features of a probabilistic approach on the basis of an existing approach.

5.2.3.1.1. Short-Circuit Currents

The amplitude of the fault current depends on the type of fault, the number of generating sets in service, the network layout (number of transformers or lines connected at a given instant), and the location of the faults (substation, lines).

In seeking the maximum electrodynamic loads on rigid busbars, the most significant faults are polyphase.

a) An **initial approach** to the variability of fault current amplitudes is shown in the Figure 5.8 below. The various distribution functions concerning the intensity of three-phase short-circuit currents are plotted on the following graph:

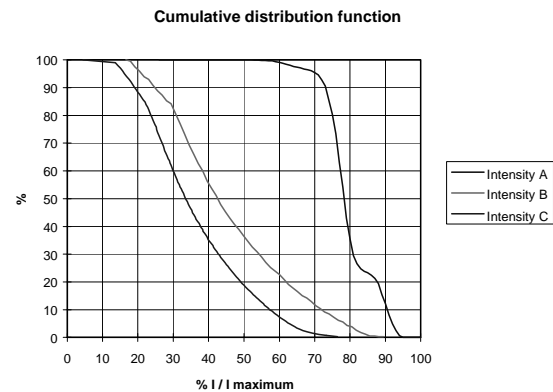


Figure 5.8 the different distribution functions for the intensity of short-circuit currents.

Intensity A: C.D.F. of the short-circuit current in a substation due to variation over the year. The variation over the year in the amplitude of the short-circuit current (Intensity A) is noticeable in the networks where the main generating units are located, but may be reduced in certain networks, when transformers supply the power. In this case, it may be more practical to take a fixed value of the current.

Intensity B: C.D.F. of the short-circuit current passing through a substation for a short circuit located on the connected lines, calculated at the instant of maximum short-circuit power for that substation,

At a constant short-circuit power, the impedance of the lines reduces the amplitude of the fault current as a function of the latter's distance.

Intensity C: the combination of curves A and B thus concerns the variation in the fault current passing through a substation as a function of the location of the fault and the time of year.

b) A **second approach**, which is very useful and practical, concerns **constant short-circuit intensity** analysis.

The system manager often considers the peak withstand current of a substation. In the event of a predictable overload, the manager will need to take steps to operate the substation as several electric nodes (7.2.3.2.2.7.) or to upgrade the station to increase short circuit capability. In such situations, the language of probabilities is highly useful in evaluating a mechanical risk of failure for the different substation layouts. In particular when nodes are interconnected in order to transfer a load from one node to another, the risks of network weakening due

to multinode operation can be compared with risk of another drawback, mechanical failure.

5.2.3.1.2. Instant of Occurrence of Faults

The instants of occurrence of faults (Figure 5.9 and Figure 5.10) were analyzed on the basis of 129 recordings made on RTE's 400-kV network using five digital fault recorders over a period lasting from 1981 to 1984.

Phase to earth fault

The angle φ is defined by the phase angle difference between the rising voltage zero and the instant of occurrence of the fault.

$$(5.7) \quad U = U_0 \sqrt{2} \sin(\omega t + \varphi)$$

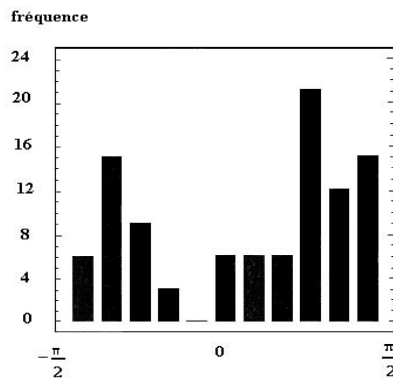


Figure 5.9 Histogram of angle φ distribution for a phase to earth fault. Frequency in %

We note that the events are not equally likely. There is a preference for positive alternation over negative alternation, which is due to the short circuits produced by lightning and wind and explained by the preferentially negative ionization of air. It also appears that the maximum asymmetry $\varphi=0$ is not the most likely event. In other words, the phase distribution may differ significantly from uniform distribution.

Phase To phase faults

The phase to phase fault incidence angle is defined by the phase angle difference relative to the zero point of the phase-to-phase voltage.

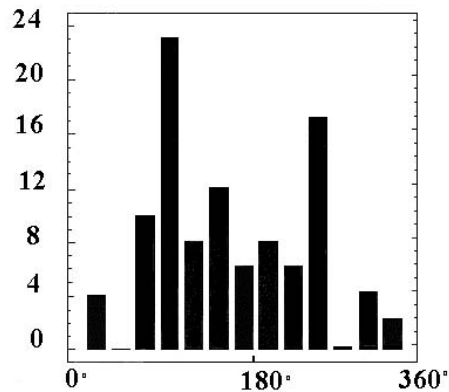


Figure 5.10 Histogram of angle φ occurrence of phase to phase faults. Frequency in %

We note that the frequencies of fault occurrence reach their maximum when φ approaches 90° or 270° , i.e. when the phase-to-phase voltage is maximum, with a preference for positive alternation.

Three-Phase Faults

For these more infrequent faults, establishing statistics with the available data proved impossible.

Proposed choice of an instant of occurrence distribution

Uniform distribution tends to raise the likelihood of maximum asymmetry, thereby increasing the maximum stresses, which is still conservative. Hence, to simplify calculations, we propose a uniform distribution for all faults (Figure 5.18).

5.2.3.1.3. Time Constant

The time constant τ of the network varies depending on the type of fault (single, two or three-phase) and its location. Frequently, the highest time constants arise from the transformer inputs, whereas the lines have lower time constants. For a given substation, the result is a drop in the time constant as the distance between the fault and the substation increases. The usual choice of a standard value of 45 ms does not always cover the values encountered in networks. In other words, this parameter must be chosen with care.

5.2.3.1.4. Clearance Time

The clearance time may vary from one line to another for the same protection threshold, depending on the element on which the load is applied, the possibility of failure of a component such as the circuit breaker or the protection system. The Figure 5.11 shows the variation in clearance time for an extra high voltage line busbar connection in the RTE network.

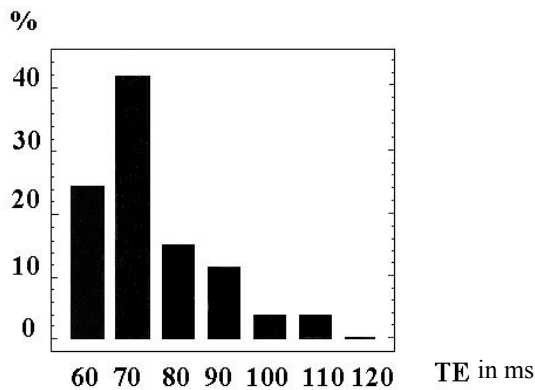


Figure 5.11 Histogram of distribution of the clearance time (TE) for phase to earth faults

This parameter has a crucial influence on the amplitude of the mechanical loads. It is also worth pointing out that the longest clearance times occur with resistive faults, with the result that their amplitudes are lower. These clearance times will depend on the coordination of network protections, the location of the faults and their nature (single or polyphase). For each fault pinpointed, the following sequences may be considered:

normal clearance time: ex $t_k = 120$ ms	normal operating rate: 0.988
--	------------------------------

In the event of a failure, the clearance sequences are often complex and the current inputs are not all cut off simultaneously (see diagram below).

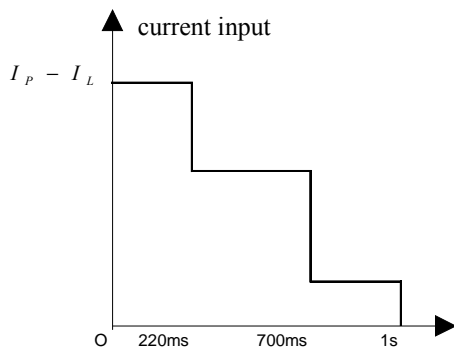


Figure 5.12 Variation of SCC during a fault

This raises the question of how the dynamic response of mechanical systems should be calculated for such clearance sequences. Several remarks are necessary:

- First, regarding the Laplace forces, the effects of which diminish very rapidly due to their quadratic dependence on the amplitude of intensity.
- Beyond a certain duration (between 80 ms and 200 ms), the loads on mechanical structures often

reach their maximum, and this is particularly true for rigid structures like tube busbars. For flexible structures, the response time may be longer.

In light of the above remarks, it is often possible to choose an equivalent mechanical time. Simpler scenarios can then be considered, such as those proposed below:

clearance time in the event of failure of the protection systems: ex $t_k = 220$ ms	rate of failure per year: λ
---	-------------------------------------

λ is the overall failure rate established in accordance with the low voltage devices of a bay. It is established on the basis of the failure rate of the protections composing the unit (e.g., for one protection per year: $\sim 10^{-2}$).

or:

clearance time in the event of failure of the circuit breaker: ex $t_k = 300$ ms	rate of failure per year and per device: $\sim 2 \cdot 10^{-3}$
--	--

5.2.3.1.5. Reclosure

Three parameters characterize a reclosing cycle, $t_{k1} / t_i / t_{k2}$. There are two types of reclosure operation in the networks, the first described as rapid, after a few hundred ms ($t_i > 100$ ms) and the second as slow, after several seconds ($t_i > 2$ s). These reclosures may if the fault recur (~ 1 time out of 10), lead to final trips. A good knowledge of the ranges of variation of these parameters is important in making the choice. If the basis of consideration is a type of substation frequently encountered in the network, a uniform distribution of the isolating time may be taken. The designer may have to choose carefully in order to make an accurate estimation of the distributions of these parameters.

5.2.3.1.6. Other Parameters

If the risk situations are classified by probability of occurrence, an ultimate load frequency approach then becomes possible. In that case, a rule can be set:

- either regarding the assumptions to be taken into account.

In this field, combining the loads (wind + short circuit) may avoid arbitrarily choosing an overly high or ill-suited safety factor based solely on the electrodynamic assumption.

- or as to the maximum capability of the existing substations, acceptable in terms of risk, and thus as to the conditions for rebuilding or reinforcing an existing substation.

5.2.3.1.7. Proposed Approach

The stress-generating faults are non-resistive polyphase faults close to the substation. It is advisable to know the main clearance thresholds involved in this case (zone 1 of the distance protections, for example, or zone 2 or 3 in the event of failure).

5.2.3.2 CHARACTERIZATION OF MECHANICAL LOADS

One method of approaching the calculation of mechanical loads distribution is by mechanical and probabilistic code coupling. We propose here a functional approach to dynamic maximums.

5.2.3.2.1. Rigid Busbars

To study the dynamic response of a system of busbars excited by Laplace force during a short-circuit fault, one of the most common configurations of straight rigid busbars is considered below:

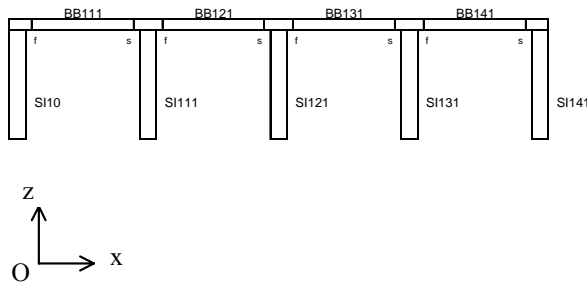


Figure 5.13 Rigid busbar structure

The notations are defined as follows:

- SI: post insulator,
- BB: busbar,
- f or s: clamped (f) or pined (s) connector.

The problem addressed in this section is to determine the functional dependence of usual stresses (force at post insulator top, stresses in the tubes) as a function of the primary variables. Let:

$$(5.8) \quad F = F(I, \varphi, \tau, t_k, V, \theta)$$

This force depends on the short-circuit intensity during the fault, the voltage phase at the instant of occurrence of the fault, the type of fault considered, the time constant, the clearance time and, if a concomitant wind is taken into account, wind velocity V and direction θ applied to the busbars. Such phenomena as ice were not considered in this section. Most of the time, we rely on a function of the form :

$$(5.9) \quad F = F(I, \varphi, V, \theta)$$

The influence of the clearance time is taken into account by discrete selection, the time constant by its maximum value.

5.2.3.2.2. Characterization of the Maximum Amplitude of the Dynamic Response

7.2.3.2.2.1 Expression of the equivalent force at post insulator top

To determine that force, an advanced method such as the Aster-Mekelec software of EDF was used. The values of the moments at the post insulator bottom are calculated in the three spatial directions. Hereafter, we shall consider only moment M_x , along direction Ox , which represents the loading of the Laplace force on the busbars, insofar as M_y , which denotes primarily the action of the post insulator's own weight, and M_z , which accounts for any torsion of the bushings, are generally low.

The equivalent force at the post insulator top (namely, the corresponding force applied to the top of the post insulator that would yield the same bending moment) is given by the following formula:

$$(5.10) \quad F = \frac{\sqrt{M_x^2 + M_y^2}}{h}$$

where: h = height of post insulator, F in newtons, M_x , M_y , in newton-meters.

The dynamic component of the force at the post insulator top, that is, without action of wind and own weight, varies with the square of the short-circuit intensity and depends on the voltage phase at the instant of occurrence of the fault. The maximum of this dynamic component may then be denoted by the relation:

$$(5.11) \quad M_x^{dyn} = \alpha \cdot I^2 .$$

This relation thus gives the influence of the fault current amplitude.

7.2.3.2.2.2 Influence of the Instant of Occurrence φ

The dependence of the maximum mechanical loads as a function of the instant of occurrence φ reveals a periodic dependence of period π . For structures of EHV or HV substations, if φ_0 denotes the maximum

asymmetry, this functional relation may very often be written in the form:

$$(5.12) \quad M_x^{dyn} = \alpha \cdot I^2 \cdot \frac{1 + m \cdot \cos^2(\varphi - \varphi_0)}{1 + m}$$

The coefficient m is denoted as a function of the maximum dynamic components $M_{x\ dyn}^{\max}$ and $M_{x\ dyn}^{\min}$, found at the maximum and minimum asymmetries, φ_0 and $\pi/2 + \varphi_0$ respectively:

$$(5.13) \quad m = \frac{M_{x\ dyn}^{\max} - M_{x\ dyn}^{\min}}{M_{x\ dyn}^{\min}}$$

This coefficient is independent of current amplitude I . It varies slightly between one type of fault and another, as shown in the table below:

Type of fault	m
single-phase	0.783
two-phase	0.800
three-phase on busbar	0.944
three-phase on two busbars	0.831

The calculated phase to phase or phase to earth value provides a good conservative approximation. Formula (5.12) is not applicable to median phases 2 and 5 of the "associated phase" arrangements, see in particular Figure 5.21, Figure 5.24 and Figure 5.26. In such a case, the stresses average out to zero, although the zero value is never reached.

7.2.3.2.2.3. Influence of Time Constant τ

Noting that at the minimum asymmetry, the time constant does not affect the loading, it may be deduced that α' is independent of τ , where:

$$(5.14) \quad \alpha'(t_k) = \frac{\alpha(\tau, t_k)}{1 + m(\tau, t_k)}$$

This leaves a single variable (α or m) for analysis. Interestingly, there is something of an analogy between this factor m and that of IEC 60865 [Ref 2]:

$$m = \frac{\tau}{t_k} \cdot \left[1 - e^{-\frac{2t_k}{\tau}} \right], \text{ deriving from integration of}$$

the square of the DC component of the short-circuit intensity, as well as the differences due to vibration mechanics. Indeed, in the case of a simple oscillator ω , the dynamic response to damped loading

introduces a factor $H \left(H = \frac{\omega^2 \cdot \tau^2}{1 + \omega^2 \cdot \tau^2} \right)$

(transmittance). In practice, it is best to seek a pragmatic dependence in accordance with τ or else opt for a maximized deterministic choice.

7.2.3.2.2.4. Influence of Clearance Time t_k

For rigid structures, we may assume that beyond a certain duration of the short circuit, the maximum response has been reached. In the simplest cases, like the one below, a model of the following type may be used:

- if $t_k \geq t_{peak}$, then α_{MAX}^M is constant

- if $t_k < t_{create}$, then

$$(5.15) \quad \alpha_{MAX}^M = \alpha_{MAX}^M \cdot \left(1 - \cos \left(\frac{\pi t_k}{2 t_{peak}} \right) \right)$$

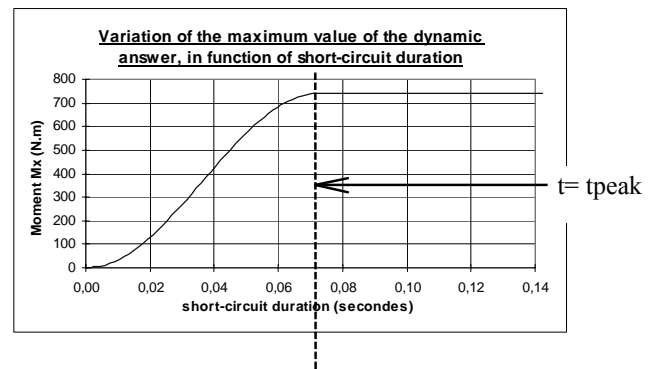


Figure 5.14 Variation of maximum response

In the general case, modal superposition often renders the analysis of clearance time influence complex. An example is given below.

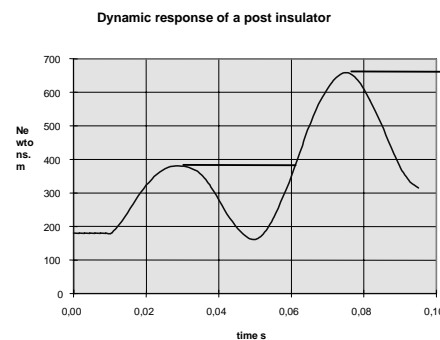


Figure 5.15 Variation of maximum response

The first case (Figure 5.14) corresponded to the dynamic response of a system to a degree of freedom at a constant Laplace force. The second case (Figure 5.15) may be resolved through a purely functional approach or by modal superposition.

7.2.3.2.2.5. Reclosure

When a structure has been set in motion by an initial fault, the possibility of a recurring fault after reclosure may lead to increased mechanical stresses. Between the maximum loads due to the first fault and the maximum loads resulting from the two faults, there may be a build-up factor of as much as 1.8 [Ref 95]. Nevertheless, a fault recurs at reclosure roughly one out of ten times.

One property, superposition, will be particularly useful in studying reclosure.

PROPERTY OF SUPERPOSITION

The displacement of the system is linked to the excitation force by a linear differential operator L and denoted in the following manner:

$$(5.16) \quad L \cdot \vec{U} = \begin{cases} \vec{F}_L(t) & \text{during the short circuit} \\ \vec{0} & \text{outside the short circuit} \end{cases}$$

Following a first fault, for a definite force $F_L(t)$, a fixed short-circuit intensity, voltage phase and circuit time constant, and for a given fault duration, only one physical solution describes the system's displacement over time on the basis of initial break conditions.

$$(5.17) \quad \vec{U}(\vec{M}, 0) = \vec{0} \quad \forall \vec{M}$$

where: \vec{M} : spatial variables.

Following a second fault, the system's response is the superposition of the dynamic responses of the faults over an initial break condition with, however, a time lag t_R corresponding to the reclosure time:

$$(5.18) \quad \vec{U}(\vec{M}, t) = \vec{U}_1(\vec{M}, t) + \vec{U}_2(\vec{M}, t - t_R)$$

where $\vec{U}_1(\vec{M}, t)$ and $\vec{U}_2(\vec{M}, t)$ satisfy (7.16).

Because of this lag property, the search for the maximum following the two short-circuit faults is simplified. In order to superimpose two staggered faults and calculate their optimum, all that is needed is to characterize the dynamic response of a rigid structure to each of them separately. Where the two faults are of the same type, amplitude and duration, this superposition principle is especially useful.

7.2.3.2.2.6. Combined Loads

Each company has to define its own design policy in accordance with the occurrence of extreme loads. We propose here to examine the case of combined short-circuit and wind loads. The action of the wind on the busbars depends on the angle of the wind's direction relative to the tube axis, whereas that relative to the insulating bushings is constant for a given wind velocity, despite its changing orientation. The maximum dynamic response thus varies according to the following formula (5.19):

$$(5.19) F(I, \varphi, V, \theta) = \sqrt{\left(\alpha \cdot I^2 \cdot \frac{1 + m \cdot \cos^2(\varphi - \varphi_0)}{1 + m} + \beta' \cdot V^2 \cdot \cos^2(\theta) + \beta'' \cdot V^2 \cdot \cos(\theta) \right)^2 + (\beta' \cdot V^2 \cdot \sin(\theta) + \gamma)^2}$$

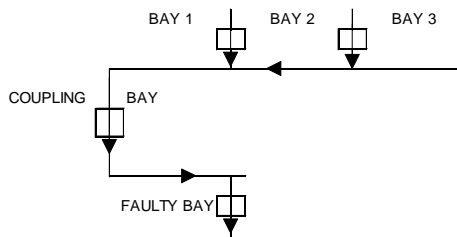
Where: α , β' , β'' , γ and m are coefficients that depend on the geometry of the problem and on the mechanical properties of the components, I is the short-circuit intensity, φ is the short-circuit current phase at the instant of occurrence of the fault, V is the wind velocity, θ gives the direction of the wind relative to the tube (axis Oy in our case), φ_0 is the maximum asymmetry phase, γ corresponds to the deadweight.

Coefficients m , α , β' , β'' and γ are obtained by studying the maximum dynamic variations and the initial, and thus static, component, of the dynamic response; from the perspective of the maximum and then minimum asymmetry, a wind is applied statically perpendicular or parallel to the busbars.

7.2.3.2.2.7. Influence of the Operating Configurations

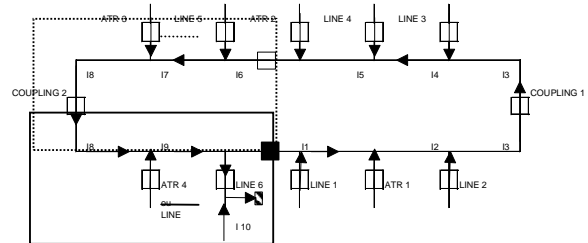
a) Transfer Situation

Furthermore, the risks linked to cases of current parallelism need to be analyzed in the event of two busbar faults (see paragraph. 2.3.2) occurring in a transfer situation (a single line on a section of bars, for which the protections may be shifted to the coupling bay), as outlined in the flow chart below:



b) Transfer Proximity

Of all the possible layouts, those close to the transfer situation of a low input line should be avoided. In the diagram below, based on a 400-kW network, low-input line 6 (low I_{10}) and autotransformer (ATR 4) are connected to the same section of bars. Under such conditions, I_8 and I_9 are at maximum and virtually equal to the substation I_{cc} . The loads may then be very similar to those calculated for the transfer situation.



analysed zone

This situation does not balance the power sources and demand centers, and is therefore extremely rare.

c) Operating Situation

Cases of Ring Structures

In the event of operation with a single electric node, the currents are distributed proportionally to the impedances encountered and thus depend essentially on the length of the circuits. The result is generally a marked reduction in electrodynamic stresses, which account for nearly a quarter of the design loads. In this case, the resistance limits will depend more on the resistance of the transverse busbars or the apparatus.



In the event of two-node operation, when the end coupling(s) delimit(s) the two nodes, the reduction is quite significant, since the factor reducing the electrodynamic stresses is high.

node 1



node 2

Case of U-shaped Structures

Two-node operation comes down to the same case as above. In the case of single electric node operation, the power inputs (lines or transformers) and demand

centers are normally balanced by bar sections, in order to minimize the current flows and risks. Under such conditions, the electrodynamic stresses are very often noticeably reduced compared to the more penalizing layouts. The stresses and operating practices very often narrow down the number of possible scenarios to only a few cases. It then becomes feasible to achieve a good order of magnitude for the electrodynamic stresses likely to occur in such operating situations.

5.2.3.2.3. Flexible Busbars

The dynamic response of the cables often minimizes the quadratic variation of the Laplace force depending on the intensity of the current. Adaptations of simplified methods were developed specifically for bundle cable connections [Ref 90]. This aspect is currently being examined.

5.2.3.3 CALCULATING THE DISTRIBUTION OF MECHANICAL LOADS

On the basis of the elementary distributions of primary variables, we can, for example, associate a bending force $F(I, \varphi, V, \theta)$ with an amplitude probability density $f(I).g(\varphi).h(V, \theta)$. This is the case for the cumulative distribution function (C.D.F.) below, corresponding to the case $I=\text{constant}$ during a three-phase fault in a transfer situation (two busbars).

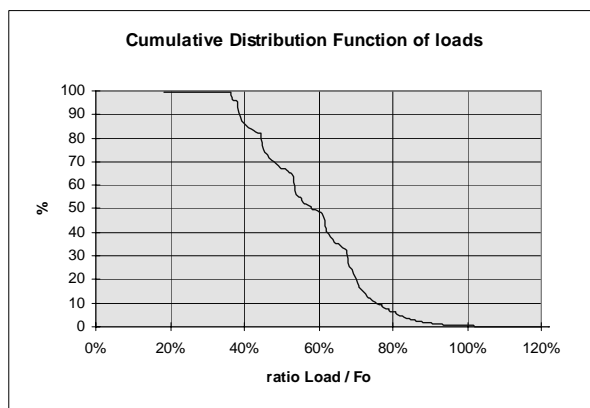


Figure 5.16 $F_0(L)$ overall view of C.D.F.

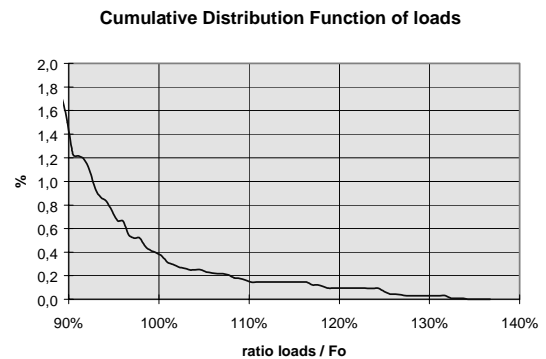


Figure 5.17 $F_0(L)$ extremity of C.D.F

F_0 : design loads

The irregularities of these function are the result of discretization. This type of function can nevertheless be approached using an analytical method.

Case with one random variable

If we consider only the variable φ , the distribution function of stress according to (5.12) takes the following form for a uniform distribution:

$$(5.20) F(C) = \arccos\left(\frac{2(1+m)}{m \cdot \alpha \cdot I^2} \cdot C - 1 - \frac{2}{m}\right) / \pi$$

where the values are defined in the interval $[C_{\min}(I), C_{\max}(I)]$ with $C_{\max}(I) = \alpha I^2$ and $C_{\min}(I) = \alpha I^2 / (1+m)$. Outside this interval, the following extension is adopted: $F(C) = 1$, if $C < C_{\min}(I)$ and $F(C) = 0$, if $C > C_{\max}(I)$.

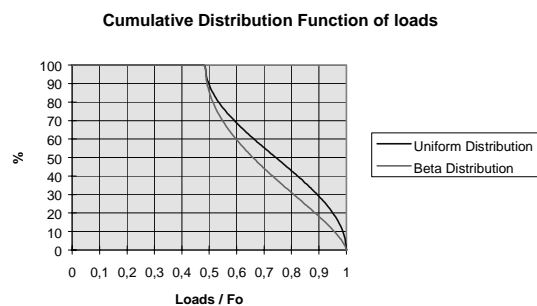


Figure 5.18

For a non-uniform phase distribution, for example a Beta distribution, condensed over the interval $[0, \pi/2]$ established on the basis of the data in Figure 5.9, we can plot the second curve of Figure 5.18 on which the maximum load values are less probable. With a

C.D.F. Φ given by $\Phi_\varphi(\varphi)$, we would obtain the following load distribution:

$$F(C) = \Phi_\varphi \left(\varphi_o + \frac{\arccos\left(\frac{2(1+m)}{m \cdot \alpha \cdot I^2} \cdot C - 1 - \frac{2}{m}\right)}{2} \right)$$

Case with several random variables

If $g(V)$ is the wind distribution, the C.D.F. of loads is given by:

$$\Psi(C, I) = \int_0^\infty g(V) \cdot F(C, V, I) \cdot dV \quad \text{with}$$

$$F(C, V, I) = \frac{\arccos\left(\frac{2(1+m)}{m \cdot \alpha \cdot I^2} \cdot (C - \beta V^2) - 1 - \frac{2}{m}\right)}{\pi}$$

ignoring own weight and assuming that the wind is perpendicular to the tubes.

Similarly, if we know the distribution of the current $h(I)$, we can write:

$$K(C) = \int_0^\infty \int_{I_{min}}^{I_{max}} g(V) \cdot h(I) \cdot F(C, V, I) \cdot dV \cdot dI$$

Combination of various faults

The load distribution function can be calculated by weighting the distributions of the various types of fault as indicated below:

$$F(S) = F_1(S) \cdot pr(\text{phasetoearth}) + F_2(S) \cdot pr(\text{phasetophase}) + F_3(S) \cdot pr(\text{threephase})$$

with $F_1(S)$ corresponding to the fault distribution on a phase to earth fault, $F_2(S)$ a phase to phase fault, $F_3(S)$ a three-phase fault, and with $pr(\text{phasetoearth}) + pr(\text{phasetophase}) + pr(\text{threephase}) = 1$. In this case, the (λ, η) parameters of 5.2.3.8 must be adjusted accordingly.

5.2.3.4 CHARACTERIZATION OF MECHANICAL STRENGTH

The mechanical strength of the various components (post insulator breaking load, yield strength of metallic structures: tube, tower, substructure, etc.) is also a random variable dependent upon the manufacturing characteristics of the various components.

The curve below gives an example of variation in breaking load for a ceramic post insulator:

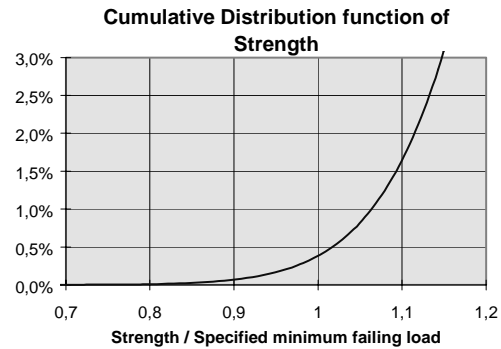


Figure 5.19 Strength distribution function

This figure is based on manufacturer's data established using a Gaussian strength distribution

$$G\left(\frac{L}{F_R}\right) = \int_0^\infty e^{-\frac{1}{2}\left(\frac{L-a}{\sigma}\right)^2} \cdot dL$$

The mean value is in this case between 1.4 and 1.5 F_R^G and the standard deviation σ is around 16% of F_R^G . These data can be obtained from major equipment manufacturers.

5.2.3.5 CALCULATING THE RISK OF FAILURE

The variation of the risk integral as a function of Γ or rather of its reverse F_o / F_R^G is plotted below in semi-logarithmic coordinates:

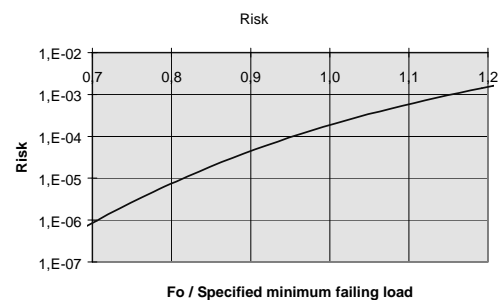


Figure 5.20 Risk integral

We note that a 10% variation in this ratio causes the risk integral to vary by a factor of 3 to 10, depending on the operating point F_o / F_R^G . With the 0.7 safety factor recommended by CIGRE, for combined short-circuit and wind loads represented in 5.2.3.3 (Figure 5.16 and Figure 5.17), the risk integral is here around 10^{-6} for one post insulator.

Remark: The risk integral (5.3) can be estimated as follows.

$$Risk\left(\frac{F_o}{F_R}\right) = \int_0^{\infty} G\left(\frac{L}{F_R}\right) f_0\left(\frac{L}{F_o}\right) dL$$

with, in this case, a Gaussian strength distribution

$$G\left(\frac{L}{F_R}\right) = \int_0^{\infty} e^{-\frac{1}{2}\left(\frac{L-a}{\sigma}\right)^2} .dL .$$

We obtain Figure

5.20 by a contraction of factor k on F_R^G , a , σ in the desired range.

5.2.3.6 STRESS-GENERATING FAULTS

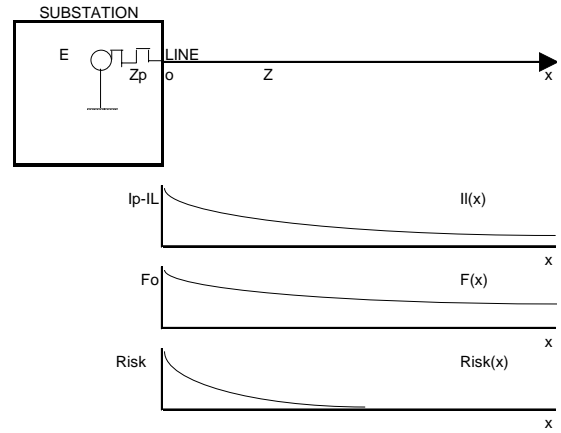
Stress-generating faults are high-amplitude polyphase faults. It is important to weigh the various risk situations such as earths left accidentally in substations or on lines, accidental closures of earthing switches, non-resistive polyphase faults on lines resulting from lightning or other exceptional conditions, climatic or otherwise. It is also important to analyze the risks associated with cases of parallel currents in the event of two busbar faults (see paragraph 2.3.2) occurring in transfer situations (paragraph 7.2.3.2.2.7.). On the basis of this analysis, which must take into account:

- the orders of magnitude of the relative amplitudes of the currents of the various types of fault,
- the operating settings (for example, voltage switching to a busbar section from a line whose current input is necessarily limited),
- operating situations (transfer or normal non-transfer),
- operation of low-voltage automatic controllers, in particular for stress-generating faults (often non-resistive polyphase) or for reclosure cycles,
- high-voltage structures, in particular for two busbar faults.

At this stage, as an example, we will choose the most frequent faults, i.e., line faults, and the most stress-generating faults, i.e., non-resistive polyphase faults. The last point to be defined is the line length to be considered. Two methods can be used:

1. Assuming that a safety factor of 0.7 (load/strength) has been chosen for the post insulator and that the risk of collapse is around 10^{-6} , the risk zone corresponds to the zone for which the fault current transiting through the substation on a line fault leads to a 20% loads variation in the substation. The residual risk is, according to Figure 5.20, around 100 times smaller than that of faults on incoming line towers. It is recommended to take account of line inputs and to pay attention to passive lines or lines with low inputs.

2. The calculation below offers a more accurate method:



Take a line with an input of I_L connected to a substation with a short-circuit current I_p . When the three-phase fault is on the line, the current from the substation is thus $I(x)$, such that $I(0) = I_p - I_L$. This gives the following relations:

$$Z_p = \frac{U_n}{(I_p - I_L)\sqrt{3}}$$

$$I(x) = \frac{U_n}{(Z_p + x.Z)\sqrt{3}}$$

$$F(x) = F(I(x), \varphi, \dots)$$

$$Risk(x) = Risk(F(I(x)) / F_R)$$

If the faults were evenly distributed and equally probable, the line length l_i to be taken into account would be expressed as:

$$l_i = \frac{\int_0^{\infty} Risk(x).dx}{Risk(F_o / F_R)}$$

However, if we assume that the faults occur preferentially at the towers, this relation can be discretized by the following majorant:

$$(5.21) \quad l_i = \frac{\sum_{n=0}^{\infty} Risk(a_n).a_n}{Risk(F_o / F_R)}$$

with $a_0 = 1$ and a_n corresponding to the n th span of the line.

For a substation, the length contributions of each connected line must be added together.

$$(5.22) \quad l_p = \sum_i l_i$$

By treating impedances with complex numbers, this approach is able to take the time constant into account (Paragraph 7.2.3.2.2.3.).

5.2.3.7 STRESSED ELEMENTS

The previous calculations (5.2.3.6) define the risk on the most loaded post insulator or post insulators without specifying their position or number. The loads vary in any switch bay inside the substation. For the outer lateral busbars, maximum loads are generally lower than those affecting inner busbars. As the design fault frequently taken into account is the **three-phase fault on one or two busbars** (Paragraph 2.3.2), the cumulative risk on each post insulator of a single switch bay and the mean equivalent number of post insulators subject to maximum load were calculated. This approach can be schematized as follows:

$$(5.23) \quad \bar{n} = \frac{\sum_{n=1}^6 Risk(F_n / F_R)}{Risk(F_0 / F_R)}$$

The set (Fn) corresponds to the loads on the similar post insulators of the busbars of a single suite (**transverse variation of load**) during maximum asymmetry on the most loaded phase.

This relation implies that the load distribution functions for the various post insulators are the same. In fact, each post insulator should be represented by a specific distribution. An increase is performed, taking the envelope of distribution functions. We will see in the following three sections that the electrodynamic loads have a sum of zero (Paragraph 2.3.1).

For combined hypotheses of short circuit and wind, the wind may or may not act in the same direction as the electrodynamic loads. We will see that the post

insulator number \bar{n} is very often in this case substantially reduced.

The values given in the tables depend upon the operating point chosen in Figure 5.20, and hence on the chosen safety coefficient and on the type of substation structure concerned (associated or separate phases)

5.2.3.7.1. Asymmetrical associated phases layout

For this type of arrangement (Figure 2.23), the stress-generating fault is the **three-phase fault on two busbars**. The diagram below shows the relative variation in amplitudes of dynamic responses when the phase φ is varied on the 6 bars of a switch bay.

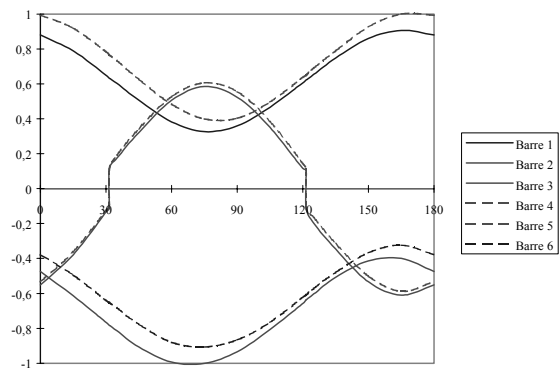


Figure 5.21 Relative variation of the response versus instant of occurrence of fault and busbars

For a three-phase fault on two busbars and for the instant of occurrence leading to maximum asymmetry on the most stressed phase (here central phase n°3), the histograms below show the relative variation of loads on all phases. Phase n° 6 is also at maximum asymmetry, but with 25% lower loads for D=d, and 11% lower loads for D=2d.

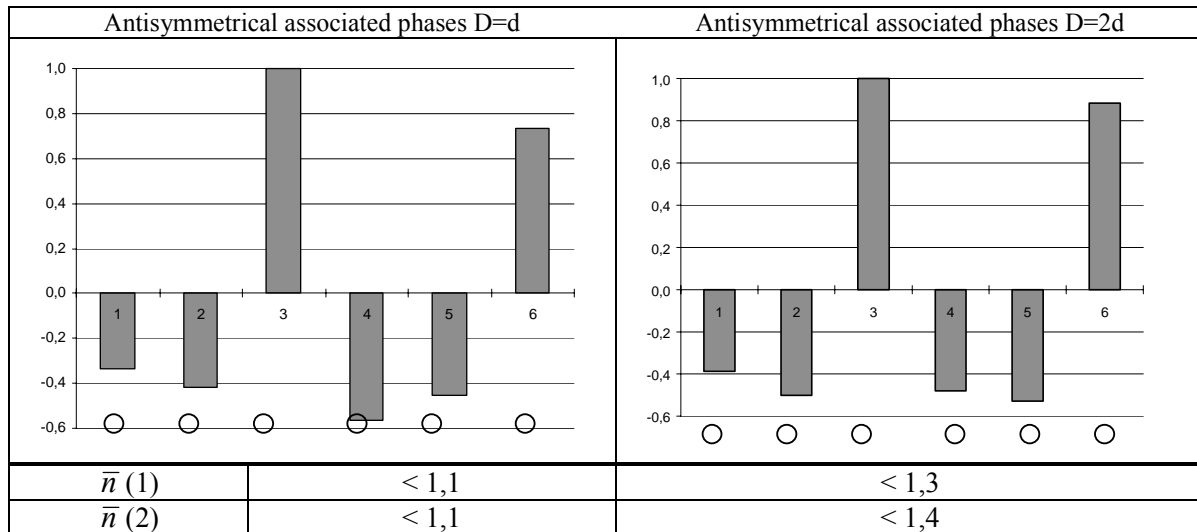


Figure 5.22 Relative variation of response at the maximum asymmetry

- 1) "short circuit" hypotheses
- 2) short circuit and wind combined hypotheses

The wind may act in the same direction as the electrodynamic loads. This is the case for phases 3 and 6 in the above histograms. But for most other phases it acts in the opposing direction. The cumulative risk on the various phases of the two busbars gives a mean equivalent number of loaded post insulators per switch bay of between 1 and 1.4.

5.2.3.7.2. Symmetrical associated phases layout

For this type of structure (Figure 2.25), the stress-generating fault is the **three-phase fault on a single busbar**. However, in view of the proximity of loads for "phase to-phase" or "three-phase faults on the two busbars", the following analysis is necessary. The table below gives the distribution of electrodynamic loads on the various phases and the number of post insulators loaded in each case.

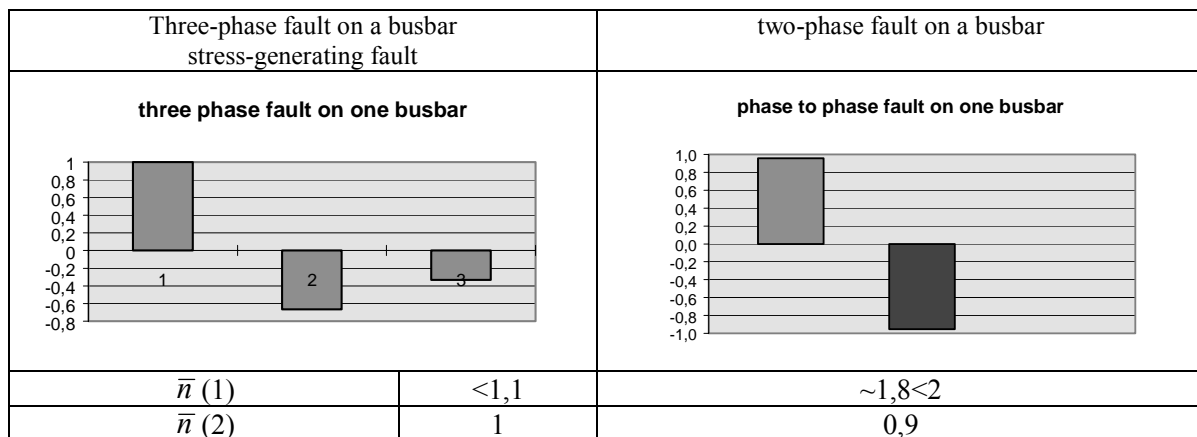


Figure 5.23 Relative variation of response at the maximum asymmetry

- 1) "short circuit" hypotheses
- 2) short circuit and wind combined hypotheses

Though the amplitude of loads depends on d, the distribution of loads in % is independent of d. In the

case of *combined hypotheses*, the wind again reduces the loads on phases 2 and 3. The risk integrals are, in

these cases, very low compared to that of phase 1, loaded at maximum asymmetry in a wind acting positively with respect to the short-circuit loads. For the phase to phase fault, the post insulators are not excited to a maximum level, the risk is reduced by 10% (0.9 equivalent "loaded post insulator"). For the *short circuit hypotheses*, there are almost two loaded post insulators.

Three-phase fault on two busbars

The diagram below shows the relative variation in the amplitudes of dynamic responses when the phase φ is varied on the 6 bars of a switch bay.

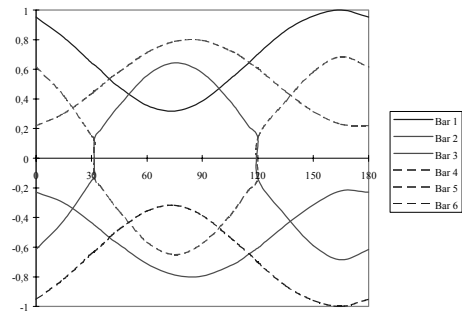


Figure 5.24 Relative variation of the response versus instant of occurrence of fault and busbars

The ratio d/D is only relevant for faults concerning two busbars. On the histograms below we note that the amplitude of loads is smaller compared to the three-phase fault on a single busbar (reference 1).

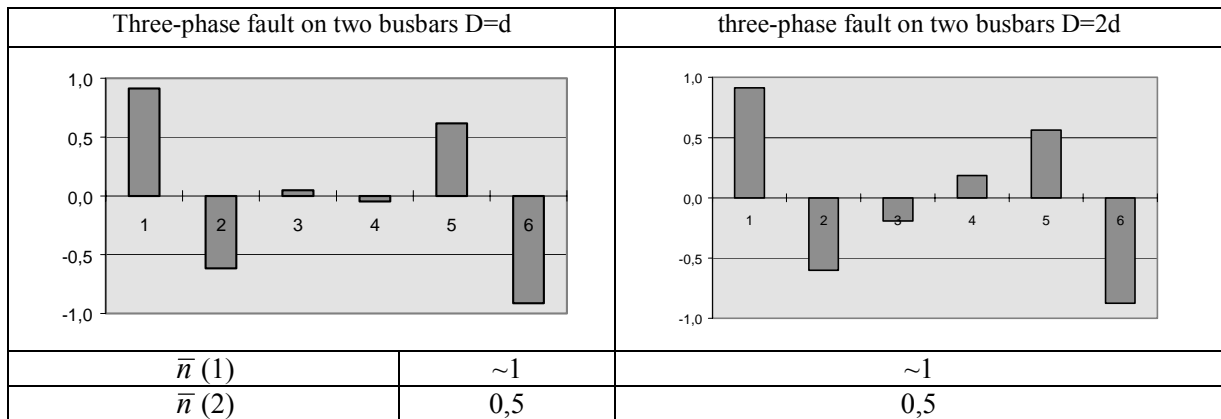


Figure 5.25 Relative variation of response at the maximum asymmetry

- 1) "short circuit" hypotheses
- 2) short circuit and wind combined hypotheses

In terms of loaded elements, the faults on two busbars are substantially less stress-generating. The main contribution is due to the outer post insulators 1 and 6. The ratio d/D has only a minor influence.

5.2.3.7.3. "Separate phases" layout

For this type of arrangement (Figure 2.21), the stress-generating fault is the **three-phase fault on two busbars**. The diagram below shows the relative variation in amplitudes of dynamic responses when the phase φ is varied on the 6 bars of a switch bay.

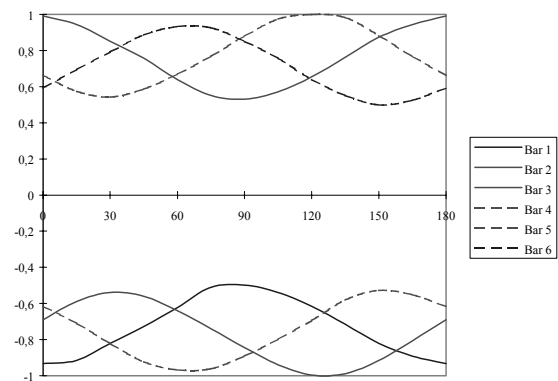


Figure 5.26 Relative variation of the response versus instant of occurrence of fault and busbars

The histograms below for the instant of occurrence leading to maximum asymmetry on the most loaded phase (here central phases n°3 and 4), the histograms

below show the relative variation of loads on the other phases.

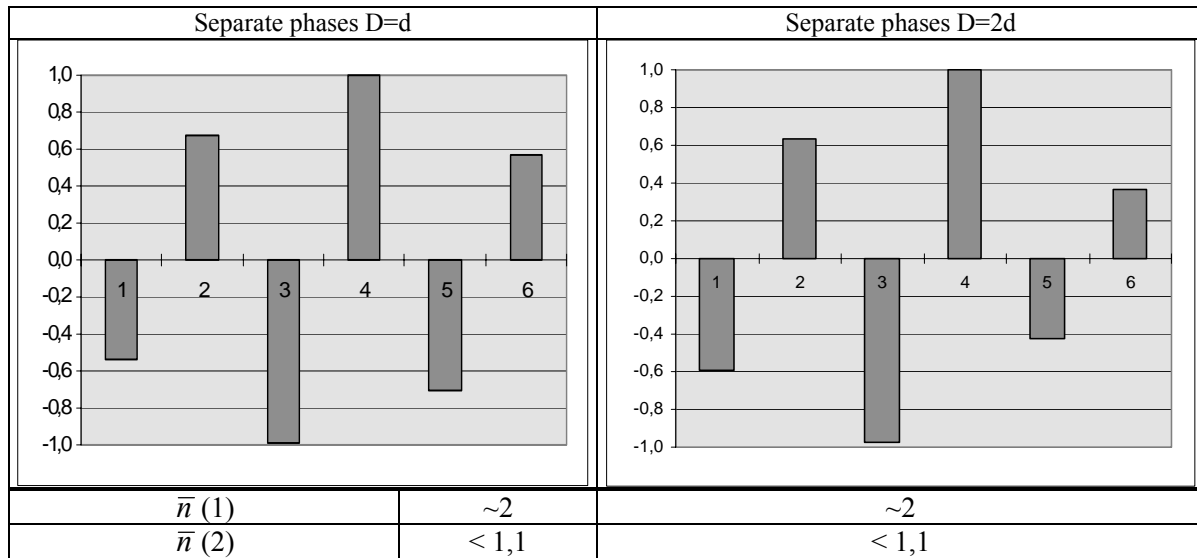


Figure 5.27 Relative variation of response at the maximum asymmetry

- 1) "short circuit" hypotheses
- 2) short circuit and wind combined hypotheses

The wind may act in the same direction as the electrodynamic loads. This is the case for phases 2, 4 and 6 in the above histograms. But for the other phases it acts in the opposing direction. With respect to the number of loaded elements, the cumulated risks on the various phases of the two busbars gives a mean number \bar{n} per suite of loaded post insulators of less than 1.1 in the case of *combined loads* and of approximately 2 in the case of a *simple electrodynamic hypothesis*.

5.2.3.7.4. Structures with a single busbar

For certain substations with only one busbar or for cross connections comprised of rigid bars, the analyses made in 5.2.3.7.2 for the fault on a single busbar can be reused.

5.2.3.7.5. Influence of connectors

Another factor reduces the number of post insulators concerned, i.e., the distribution of loads between post insulators according to the type of connector. The types of connector must frequently installed are:

- successions of clamped - clamped and pinned - pinned connectors. In this case, half the post insulators ($n=2$) are loaded ($\rho=0.5$).
- successions of clamped - clamped then sliding, - sliding then pinned - pinned connectors. In this case, two-thirds of the post insulators ($n=3$) are loaded ($\rho=0.67$).
- clamped - pinned fittings which distribute loads uniformly, which means that all post insulators located relatively far from the extremities along the path of maximum currents are loaded ($\rho=1$).

We define ρ as:

$$(5.24) \quad \rho = \frac{1}{n = 2 \text{ ou } 3} \frac{\sum_{n=1}^{n=2 \text{ ou } 3} Risk(F_n / F_R)}{Risk(F_0 / F_R)}$$

The set (F_n) corresponds to the loads on the post insulators of the most loaded busbar (**longitudinal variation of load**), but limited in size to two or three elements defined in paragraphs a) and b).

5.2.3.7.6. Common mode faults

A distinction must be made between a substation and a family of substations. In the case of one substation, there may be common mode faults such as those resulting from component manufacture or assembly.

Example: On a given substation, it is very likely that many of the ceramic post insulators come from the same production batch. This may give rise to statistically above-average or below-average strength.

In short, for the analysis of a family of substations, the advantages of the probabilistic approach are clearly apparent.

5.2.3.7.7. Conclusions

For N sequences on a section of busbars, we thus take $\bar{n} \cdot \rho \cdot N$ post insulators subject to maximum loads.

5.2.3.8. FAILURE RECURRENCE TIME

5.2.3.8.1. Risk at a substation

For line fault

The overall maximum risk at a substation is given by the expression:

$$(5.25) \quad R_p^L = v \cdot \lambda \cdot \eta \cdot l_p \cdot \bar{n} \cdot \rho \cdot N \cdot Risk\left(\frac{F_o}{F_R}\right)$$

with v : normal operating rate of fault elimination (close to 1).

λ : number of faults on overhead lines connected per km and per year,

η : rate of high-amplitude polyphase faults (hence non-resistive),

l_p : cumulative length of the risk zone in km,

\bar{n} : number of loaded post insulators per busbar suite,

ρ : coefficient depending on the type of connector

N : suite number,

Example:

For $\lambda=20 \times 10^{-2}$ per km and per year, $\eta=30\%$, $l=6$ km,

$\bar{n}=1,5$, $\rho=1$, $N=14$ suites, $Risk\left(\frac{F_o}{F_R}\right) = 10^{-5}$, there is

thus a probability of substation failure of around $7.6 \cdot 10^{-5}$, corresponding to a recurrence time of more than 13000 years for a safety factor of 0.7.

For line fault in the event of failure

The previous analysis is also applicable in the event of failure (circuit breakers or protection devices), though the elimination times may be different and the resulting loads increased. It is important to determine the amplitude of loads amplification, in view of the remarks made in section 5.2.3.1.4 on the effect of saturation when the clearance time exceeds the mechanical reaction time. In (5.25), F_o is replaced by F_1 and the failure rate: v : (protection system and/or circuit breaker failure rate) is taken into account.

The increase in risk is often low and the reduction in the failure rate means that this term can be ignored.

For substation fault

The maximum overall risk at a substation is given by

the expression: $R_p^P = \lambda \cdot \eta \cdot \bar{n} \cdot \rho \cdot N \cdot Risk\left(\frac{F_o}{F_R}\right)$ with

λ : annual frequency of faults in the substation,

η : rate of high-amplitude non-resistive polyphase faults (for example, accidental earthing with all available network power).

5.2.3.8.2. Reliability based design

Whatever the nature of the predominant risks, they depend upon the chosen operating point. Indeed, on a line fault, for example, we can write:

$$R_p^L\left(\frac{F_o}{F_R}\right) = \lambda \cdot \eta \cdot l_p\left(\frac{F_o}{F_R}\right) \cdot \bar{n}\left(\frac{F_o}{F_R}\right) \cdot \rho\left(\frac{F_o}{F_R}\right) \cdot N \cdot Risk\left(\frac{F_o}{F_R}\right)$$

The parameters l_p , \bar{n} , ρ are slow functions of $\left(\frac{F_o}{F_R}\right)$,

by comparison with $Risk\left(\frac{F_o}{F_R}\right)$. On the basis of an

imposed choice of risk $R_p^L\left(\frac{F_o}{F_R}\right)$, it is thus possible to

define $\left(\frac{F_o}{F_R}\right)$ and hence the appropriate safety factor.

Conversely, when the risk has been calculated at constant intensity, for a given substation, it is possible to define the short-circuit capability when a safety factor and a failure rate have been fixed.

5.3. CONCLUSIONS

This kind of methods requires some specific data, not easily available in some utilities. Probabilistic methods, based either on simplified or on advanced methods, feature increasingly in the scientific literature. They are very useful in a context where the uprating of existing substations is seen as a means to minimize restructuring costs when budgets are limited. The full advantages of this approach are brought to the fore when combined loads are taken into account in design.

The probabilistic approach makes it possible to weigh risks and enables power companies to rationalize their restructuring choices, notably for the uprating of existing structures.

6. D.C. CONFIGURATIONS

6.1. INTRODUCTION

A reliable power supply of substations and power plants often needs the construction of enlarged d.c. installations in which batteries act as energy storage devices. Installations without batteries are fed through converter and controlled drives. For these systems to be safe, the knowledge of short-circuit strength is required. Therefore it is necessary to study the currents and forces which can occur and to develop simplified methods for design of d.c. configurations.

As shown in Figure 6.1, such d.c. auxiliary systems may include the following equipment as possible sources of short-circuit currents :

- power converters;
- stationary storage batteries;
- smoothing capacitors;
- d.c. motors, e. g. motor-generator sets.

Usually, the connections between the equipment are done by cables or rigid buses.

D.c. auxiliary systems in substations and power plants are designed for ± 24 V as well as for 220 V. Nominal currents may be as high as 2,5 kA. The current capacity of the storage batteries ranges from 200 Ah up to 2000 Ah. The capacity of smoothing device is rather high; it is about 10 mF to 3 F.

Peak values of short-circuit currents caused by power converters, storage batteries, smoothing capacitors and electric motors may be estimated roughly as follows:

- The peak value of the converter current may be 20 times the nominal current, leading to about 50 kA with nominal currents of about 2,5 kA;
- Estimation of the peak value of the battery current may be based upon the capacity; the peak value in amperes is then 20 times the capacity in ampere-hours, e.g. 40 kA for 2000 Ah;
- The peak current of the capacitor fed by a converter may be as high as the peak value of the converter current;
- The peak value of the motor current is about as high as the starting current, which is 4 to 10 times the nominal current.

High peak and steady-state short-circuit currents cause correspondingly high mechanical and thermal stresses, which must be taken into consideration at the design stage. Short-circuit currents and resulting mechanical and thermal effects in three-phase systems may be calculated according to IEC Publication 60909 [Ref 11] and IEC/EN Publication 60865-1 [Ref 2, Ref 3]. These standards are based upon long-term research, those are about mechanical effects published in the CIGRE brochure [Ref 58]; this document has been revised in 1996 [Ref 1]. A standard for the calculation of short-circuit currents in d.c. auxiliary systems has been published in 1997 [Ref 59], it is based upon [Ref 60]. A

standard for the mechanical and thermal effects has been published in 1997 [Ref 61]. In 2000, a Technical Report with an example of the d.c. installation shown in Figure 6.1 was also published [Ref 62].

In section 6.2, different short-circuit current characteristics as measured on a modelling system are presented and a standardized characteristic is introduced [Ref 60, Ref 63]. In section 6.3, the curve of the electromagnetic force, which corresponds to the standardized characteristic, is transformed into a rectangular substitute time function which may be used for determining the mechanical and thermal stress [Ref 64, Ref 65].

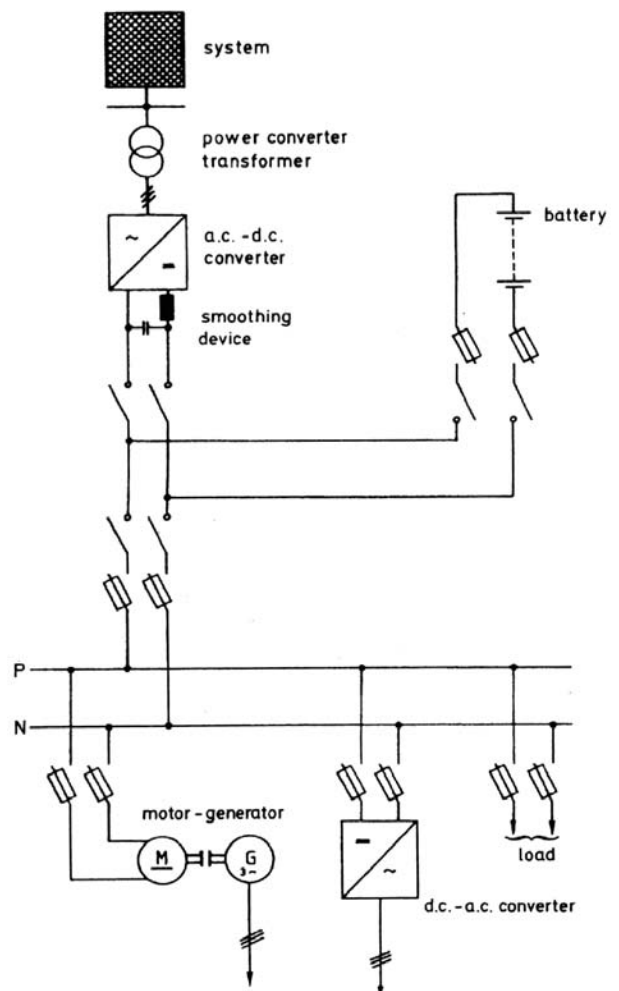


Figure 6.1 Circuit diagram of a d.c. auxiliary system in a substation or a power plant.

6.2. SHORT-CIRCUIT CURRENTS AND ELECTROMAGNETIC FORCES

6.2.1. Short-circuit current characteristics measured

For reasons of operational safety d.c. auxiliary systems are not available for short-circuit experiments. Therefore, a model system for 24 V and 100 A has been designed, cf. Figure 6.2 [Ref 60, Ref 63]. It consists of a

power converter in a three phase bridge connection, which is supplied from the mains through a 380 V/28 V transformer. Smoothing is accomplished by inductor and capacitor. Energy is stored by a storage battery. The with motor-generator converter connected is loaded an ohmic resistance.

Shorting is induced by a thyristor in order to avoid bouncing of the power breaker contacts when the circuit is closed. The short-circuit is switched off by the power breaker.

The short-circuit current characteristics are recorded by a transient recorder, where rapid current variations of up to 60 kA/ms are measured. The data gained are converted and processed on a computer.

Figure 6.3 shows short-circuit current characteristics of the power converter. Curve “a” does not include a smoothing inductor. The L_G/L_N ratio of the d.c. and three-phase inductances is relatively low; the R_N/X_N ratio of active resistance to three-phase reactance is high. After about 10 ms there appears the steady-state short-circuit current. Curve “b” shows lower L_G/L_N and R_N/X_N ratios; this has been accomplished by introducing a smoothing reactor into the three-phase side: In this case, there appears a marked peak of the short-circuit current, which is considerably higher than the steady-state short-circuit current. With $R_N \rightarrow 0$ and $L_N \rightarrow 0$, it may theoretically reach twice the value of the steady-state short-circuit current. In the case of curve “c”, a relatively high smoothing inductor was introduced into the d.c. side; there is no marked peak of the short-circuit

current. The steady-state short-circuit current appears much later than in curves “a” and “b”. In curve “d”, a rapidly acting control limits the short-circuit current to 100 A. In practice, this control often works relatively slow, so that peak as well as steady-state short-circuit currents may flow.

Figure 6.4 shows short-circuit characteristics of fully charged, stationary batteries. The short-circuit current rises rapidly to peak value and thereafter drops at first at a low, later at a high time constant. The final value of the short-circuit current therefore depends upon the duration of the short circuit. In the case of a battery which has been discharged to minimum admissible cell voltage, there still flows a considerably high short-circuit current of a similar shape having a magnitude up to 30 to 40 per cent of that of the current of the fully charged battery.

Figure 6.5 shows the short-circuit current of smoothing capacitors of different capacities. Short-circuit duration is very short. With high capacities, peak short-circuit currents may reach high values.

The short-circuit current of d.c. motors is shown in Figure 6.6. With large motors, the peak short-circuit current may reach 10 times the rated current, and will appear within 10 to 50 ms. Reduction in magnitude and the decay of the current depend upon the overall moment of inertia as well. Owing to the excitation voltage being constant after the occurrence of the short circuit, separately excited motors show higher short-circuit currents.

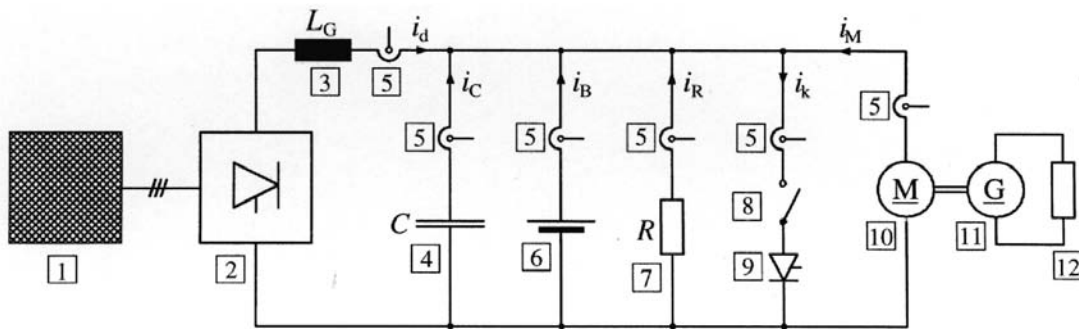


Figure 6.2 Circuit diagram of the modelling system.

- | | | | |
|-------------------------|-------------------------|---------------------|-------------------|
| 1 transformer | 4 smoothing capacitor | 7 ohmic load | 10 d.c. motor |
| 2 three-phase bridge | 5 d.c. transformer | 8 power breaker | 11 d.c. generator |
| 3 smoothing inductivity | 6 lead-acid accumulator | 9 short-circuit SCR | 12 load resistor |

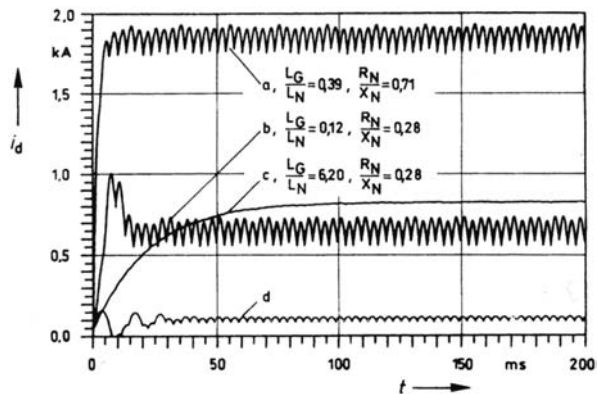


Figure 6.3 Converter short-circuit current.
 a without smoothing inductor
 b with smoothing reactor
 c with smoothing inductor
 d with rapid-acting control, current limited to 100 A

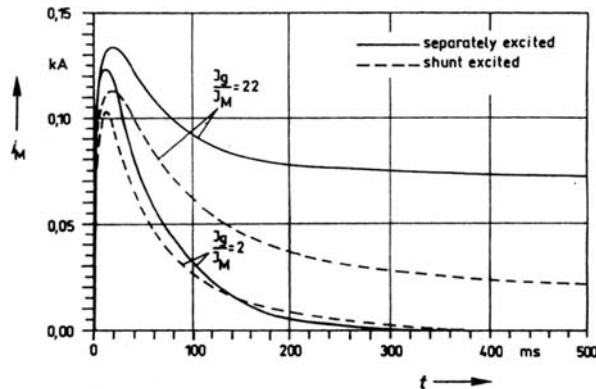


Figure 6.6 Motor short-circuit current. Rated voltage 24 V, rated current 31 A, moment of inertia of the motor J_M , overall moment of inertia J_g .

6.2.2. Standardised characteristics of short-circuit currents and electromagnetic forces

As shown in Figure 6.7, the variety of short-circuit current characteristics in d.c. systems [Ref 60, Ref 63, Ref 66, Ref 67, Ref 68, Ref 69, Ref 70, Ref 71, Ref 72, Ref 73, Ref 74, Ref 75] may be approximated by an exponential rise to the peak short-circuit current i_p and thereafter an exponential drop to the steady-state short-circuit current I_k .

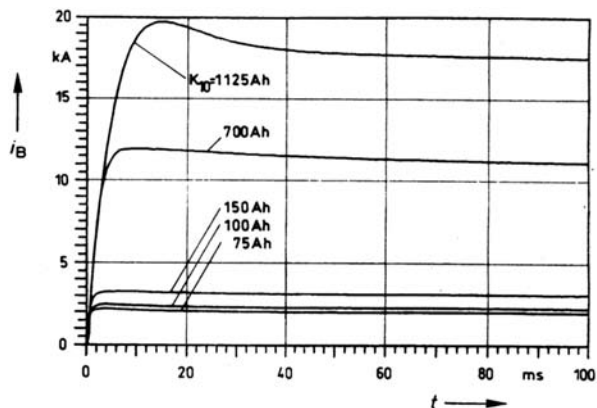


Figure 6.4 Short-circuit current of fully charged lead-acid battery with an open-circuit voltage of 25.2 V. K10 indicates the current capacity for discharge within 10 hours.

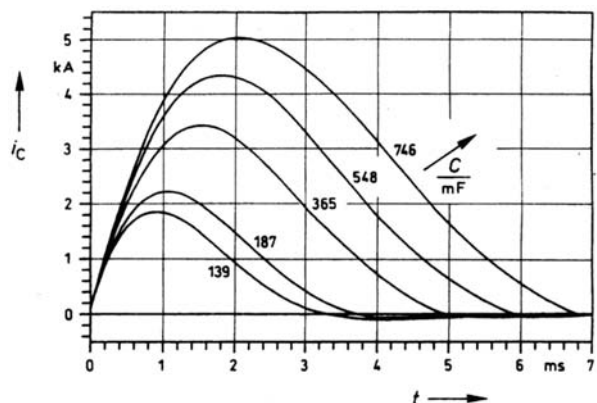


Figure 6.5 Capacitor short-circuit current. Capacitor voltage before short circuit is 24 V.

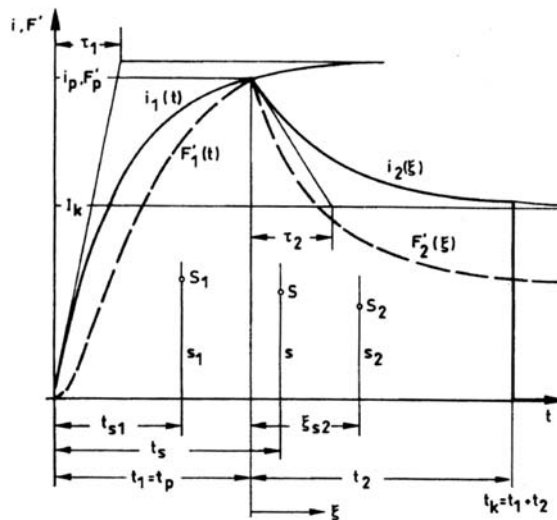


Figure 6.7 Standardised approximation function for the short-circuit characteristic $i(t)$ and for the electromagnetic force per unit length $F'(t)$. Variables t_{s1} , t_{s2} and t_s will be required in section 6.3.2.

The time functions of the currents are

$$(6.1) \quad i_1(t) = i_p \frac{1 - e^{-t/\tau_1}}{1 - e^{-t_1/\tau_1}} \quad \text{for } 0 \leq t \leq t_1 = t_p$$

and

$$(6.2) \quad i_2(\xi) = i_p \left[(1 - \alpha) e^{-\xi/\tau_2} + \alpha \right] \quad \text{for } 0 \leq \xi \leq t_2$$

where

$$(6.3) \quad \alpha = \frac{I_k}{i_p} \quad 0 \leq \alpha \leq 1$$

The parameters of this standardised approximation function are:

- i_p peak short-circuit current
- t_p time to peak short-circuit current, $t_1 = t_p$
- I_k steady-state short-circuit current
- τ_1 rise time constant of current
- τ_2 decay time constant of current
- t_k duration of short circuit, $t_k = t_1 + t_2$

The limit $\alpha = 0$ is valid, when there cannot flow a steady state short-circuit current, e.g. in the case of the capacitor current. The limit $\alpha = 1$, when there is no marked peak short-circuit current $i_p > I_k$.

In addition, Figure 6.7 shows the corresponding curve of the electromagnetic force per unit length, for parallel conductors having a centre to centre distance of a :

$$(6.4) \quad F'(t) = F'_p \frac{(1 - e^{-t/\tau_1})^2}{(1 - e^{-t_1/\tau_1})^2}$$

and

$$(6.5) \quad F'_2(\xi) = F'_p \left[(1 - \alpha) e^{-\xi/\tau_2} + \alpha \right]^2$$

where

$$(6.6) \quad F'_p = \frac{\mu_0 i_p^2}{2\pi a}$$

F'_p is the peak value of the short-circuit force per unit length, and $\mu_0 = 4\pi \cdot 10^{-7}$ H/m is the absolute permeability.

[Ref 59] gives a method for calculating the parameters of the standardised function for the individual short-circuit currents of the power converter, the battery, the capacitor, and the motor. In the case of decoupled individual short-circuit currents, they are added to the overall short-circuit current. In case there are short-circuit currents in coupling branches, they first have to be corrected and then added.

6.3. MECHANICAL AND THERMAL STRESS

6.3.1. Conditions for the equivalent function

The wave form of short-circuit currents and forces may be described by using 6 parameters: i_p , I_k , t_1 , τ_1 , τ_2 , t_2 . Their range of variation is rather wide. In addition, when calculating the dynamic stress, the relevant natural frequency of the system must be considered as well. A variation of one of the parameters will result in a variation in stress. Unlike with three-phase systems [Ref 2, Ref 3], it is not sufficient to define a standardized wave form of the force and provide factors for the calculation of the dynamic stress. In order to develop a simplified method suitable for practical use, it is necessary to reduce the number of parameters required, i.e. to substitute a simple function for the established wave form of the electromagnetic force. This function must be described by no more than 2 parameters, one of time and one of force, and must generate the same maximum instantaneous value of stress as does the original force.

The electromagnetic forces which excite a mechanical system are shock-like non-periodical events of limited duration. The well-known approximation solution [Ref 74, Ref 77] for the maximum value of the dynamic response of a one-mass oscillator exposed to shock-like event of a moderate duration may be used to derive the conditions for establishing the equivalent function. As shown in Figure 6.8 for the substitute rectangular function:

linear momentum

$$(6.7) \quad \int_0^{t_k} F'(t) dt = A = t_R F'_R$$

first moment of area

$$(6.8) \quad \int_{-\zeta_a}^{\zeta_a} F'(\zeta)\zeta \, d\zeta = 0$$

second moment of area

$$(6.9) \quad \int_{-\zeta_a}^{\zeta_a} F'(\zeta)\zeta^2 \, d\zeta = J_s = \frac{1}{12} t_R^3 F'_R$$

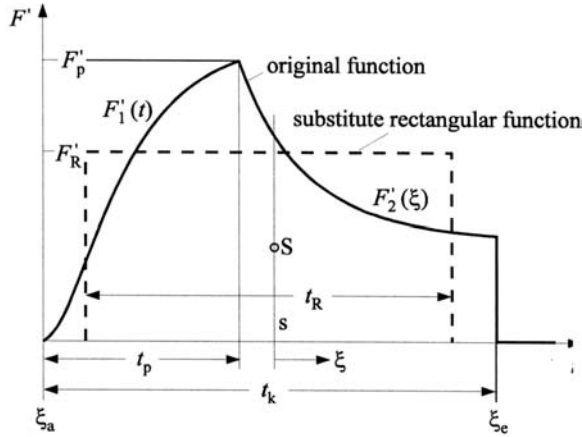


Figure 6.8 Original function $F'(t)$ and substitute function.

It follows from equation (6.7) that $F'(t)$ and the equivalent functions must have the same time area of force A . Equations (6.8) and (6.9) give the first and second moments of the time area of force relative to axis s . According to equation (6.8), the first moment relative to s must disappear, i.e. it must run through the centroid S of the area. Relative to this axis, the equivalent functions must have the same second moment of area J , as the original area.

It follows from equations (6.7) and (6.9) for the substitute rectangular time function:

$$(6.10) \quad t_R = 2\sqrt{3} \sqrt{\frac{J_s}{A}} = 3,464 \sqrt{\frac{J_s}{A}}$$

$$(6.11) \quad F'_R = \frac{\sqrt{3}}{6} \sqrt{\frac{A^3}{J_s}} = 0,2887 \sqrt{\frac{A^3}{J_s}}$$

Generally, any function may be used as an equivalent function, which does not have more than 2 parameters. For the description of the electromagnetic forces due to short-circuit currents broken by fuses, a sine square function according to Figure 6.8 may be used instead of the substitute rectangular function. Here the rectangular function is preferred to other functions, which yields suitable results where the

duration of the exciting force, in this case the duration of the short circuit t_k , does not surpass half the vibration period $0,5 \cdot T_{me}$ of the relevant natural oscillation:

$$(6.12) \quad t_k = t_1 + t_2 \leq 0,5 \cdot T_{me}$$

It has been established [Ref 65] that within the $t_k \leq 0,5 \cdot T_{me}$ range, the equivalent function as developed for the one-mass oscillator may as well be applied with sufficient accuracy to the beam model, which is characteristic for busbars. The analytical method used [Ref 65, Ref 4, Ref 19, Ref 78] is particularly suitable for parametric studies [Ref 8].

For the $t_k \geq 0,5 \cdot T_{me}$ range, however, the results are not on the safe side and may show grave errors. Equation (6.12) seriously limits the applicability of the equivalent functions since for most practical systems, condition (6.12) will not be fulfilled.

In [Ref 65] therefore, modified equivalent functions have been developed, which cover the whole $t_k/(0,5 \cdot T_{me})$ range, yield results on the safe side, and cause minimal errors as compared to the results of the excitation using original equation without approximation. The approach is as follows:

- Where the duration of the short circuit $t_k = t_1 + t_2 \leq 0,5 \cdot T_{me}$, the duration of the short circuit t_k is substituted for the base t_R of the substitute rectangular time function.
- The same is done where the short-circuit current rises uniformly during t_k .
- For $t_k \geq 0,5 \cdot T_{me}$, the ideal short-circuit duration $t'_k < t_k$ is used for the base of the substitute rectangular time function. In this case, $t_k = \max\{0,5 \cdot T_{me}, 1,5 \cdot t_1\}$.

6.3.2. Calculation of the parameters of the equivalent functions

According to equations (6.10) and (6.11), calculation of the equivalent functions requires knowledge of the linear momentum A and the second moment of area J . For this purpose, the position of the centroidal axis s must be known. As shown in Figure 6.7, the linear momenta A_1 for $0 \leq t < t_1$ and A_2 for $0 \leq \xi \leq t_2$, the respective distances of the centroidal axes t_{s1} and ξ_{s2} , and the second moments of area J_{s1} and J_{s2} of the and combined to t_s and J_s by applying known relations of mechanics. In the following, the part results are given in the form of curves, which can be used to determine the parameters of the equivalent function.

- a) Determination of the linear momenta of force
The linear momentum A_1 for the interval $0 \leq t \leq t_1$ is:

$$(6.13) \quad A_1 = m_{\theta 1} t_1 F'_p$$

Correspondingly for the interval $0 \leq \xi \leq t_2$:

$$(6.14) \quad A_2 = m_{\theta 2} t_2 F'_p$$

The conditional equations for $m_{\theta 1}$ and $m_{\theta 2}$ are:

$$(6.15) \quad m_{\theta 1} = \frac{\int_0^{t_1} F'_1(t) dt}{t_1 F'_p} \quad m_{\theta 2} = \frac{\int_0^{t_2} F'_2(\xi) d\xi}{t_2 F'_p}$$

Coefficients $m_{\theta 1}$ and $m_{\theta 2}$ may be taken from Figure 6.9.

- b) Determination of the position of the centroidal axes

The distances t_{s1} for the interval $0 \leq t < t_1$ and ξ_{s2} for $0 \leq \xi \leq t_2$, and t_s for the whole interval $0 \leq t \leq t_1 + t_2$ are shown in Figure 6.7. The distances t_{s1} and ξ_{s2} may be determined by the coefficients m_{s1} and m_{s2} :

$$(6.16) \quad t_{s1} = m_{s1} t_1 \quad t_{s2} = m_{s2} t_2$$

The conditional equations for m_{s1} and m_{s2} are:

$$(6.17) \quad m_{s1} = \frac{\int_0^{t_1} F'_1(t) t dt}{t_1 A_1} \quad m_{s2} = \frac{\int_0^{t_2} F'_2(\xi) \xi d\xi}{t_2 A_2}$$

Coefficients m_{s1} and m_{s2} may be taken from Figure 6.10.

- c) Determination of the second moments of area
The second moments of area J_{s1} relative to axis s_1 for the interval $0 \leq t < t_2$ and J_{s2} relative to axis s_2 for the interval $0 \leq \xi < t_2$ may be determined with the help of the coefficients m_{Js1} and m_{Js2} :

$$(6.18) \quad J_{s1} = m_{Js1} \frac{F'_p t_1^3}{12} \quad J_{s2} = m_{Js2} \frac{F'_p t_2^3}{12}$$

The conditional equations for m_{Js1} and m_{Js2} are:

$$(6.19) \quad m_{Js1} = \frac{\int_0^{t_1} F'_1(t) t^2 dt - A_1 t_{s1}^2}{F'_p \frac{t_1^3}{12}}$$

$$m_{Js2} = \frac{\int_0^{t_2} F'_2(\xi) \xi^2 d\xi - A_2 t_{s2}^2}{F'_p \frac{t_2^3}{12}}$$

Coefficients m_{Js1} and m_{Js2} may be taken from Figure 6.11.

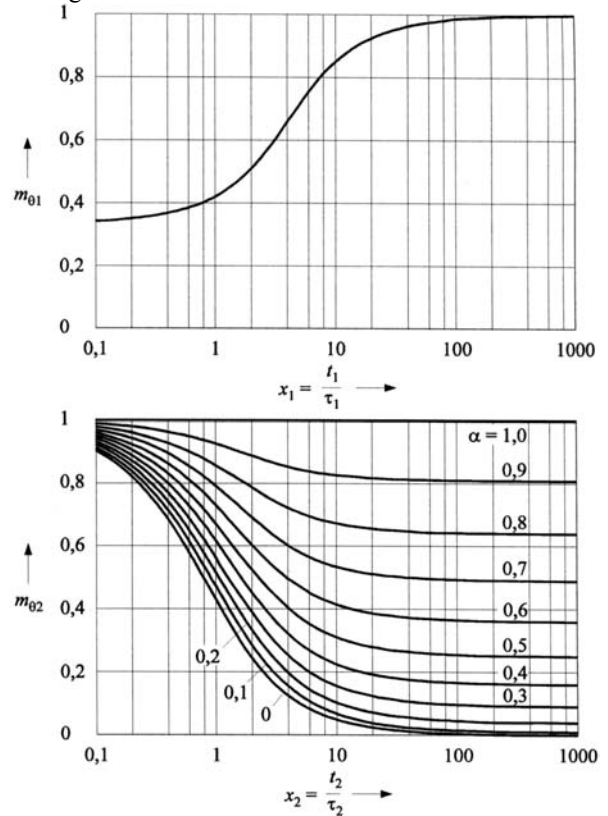


Figure 6.9 Coefficients $m_{\theta 1}$ and $m_{\theta 2}$ for the calculation of the linear moment A_1 and A_2 . The same coefficients may also be used to determine the thermal equivalent short-circuit current I_{th} , see section 6.3.4.

- d) Calculation of the parameters of the equivalent function

Calculation of the parameters of the substitute rectangular time function, t_R and F'_R according to equations (6.10) and (6.11), requires knowledge of the linear momentum A and the second moment of area J_s . They may be determined with the help of the coefficients $m_{\theta 1}$, $m_{\theta 2}$, m_{s1} , m_{s2} , m_{Js1} , m_{Js2} as taken from Figure 6.9, Figure 6.10 and Figure 6.11:

$$(6.20) \quad A = A_1 + A_2 = F'_p (t_1 m_{\theta 1} + t_2 m_{\theta 2})$$

$$\begin{aligned}
J &= J_{s1} + J_{s2} + A_1(t_s + t_{s1})^2 + A_2(t_1 + \xi_{s2} - t_s)^2 \\
&= F'_p \left\{ \frac{t_1^3}{12} m_{Js1} + \frac{t_2^3}{12} m_{Js2} + m_{\theta 1} t_1 (t_s - m_{s1} t_{s1})^2 \right\} \\
&\quad + F'_p \left\{ m_{\theta 2} t_2 (t_1 + m_{s2} t_2 - t_s)^2 \right\}
\end{aligned}$$

where

$$\begin{aligned}
(6.21) \quad t_s &= \frac{t_{s1} A_1 + (t_1 + \xi_{s2}) A_2}{A_1 + A_2} \\
&= \frac{m_{\theta 1} m_{s1} t_1^2 + m_{\theta 2} t_2 (t_1 + m_{s2} t_2)}{m_{\theta 1} t_1 + m_{\theta 2} t_2}
\end{aligned}$$

The analytical equations for the calculation of $m_{\theta 1}$, $m_{\theta 2}$, m_{s1} , m_{s2} , m_{Js1} , and m_{Js2} are given in [Ref 64].

Where the current characteristic may be described solely by an exponentially rising function, so that $t_2 = 0$, the parameters of the substitute rectangular time function are given by:

$$(6.22) \quad t_{R1} = 2\sqrt{3} \sqrt{\frac{J_{s1}}{A_1}} = t_1 \sqrt{\frac{m_{Js1}}{m_{\theta 1}}}$$

$$(6.23) \quad F'_{R1} = \frac{\sqrt{3}}{6} \sqrt{\frac{A_1^3}{J_{s1}}} = F'_p \sqrt{\frac{m_{\theta 1}^3}{m_{s1}}}$$

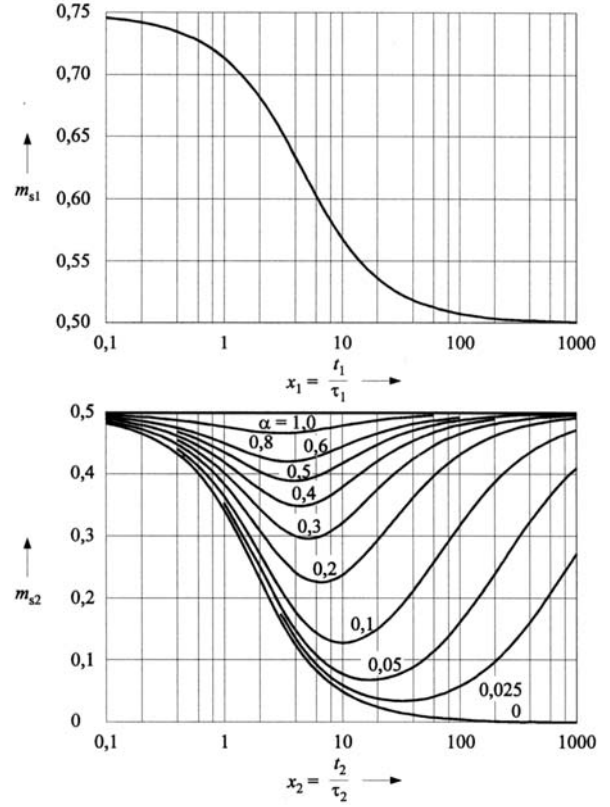


Figure 6.10 Coefficients m_{s1} and m_{s2} for the determination of the position of the centroidal axes s_1 and s_2 in Figure 6.7.

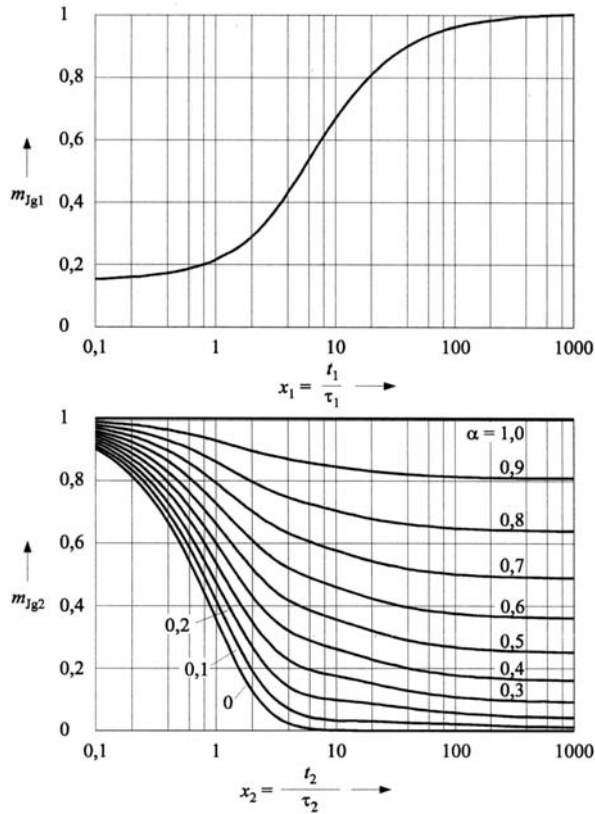


Figure 6.11 Coefficients m_{js1} and m_{js2} for the calculation of the second moments of area relative to axes s_1 and s_2 .

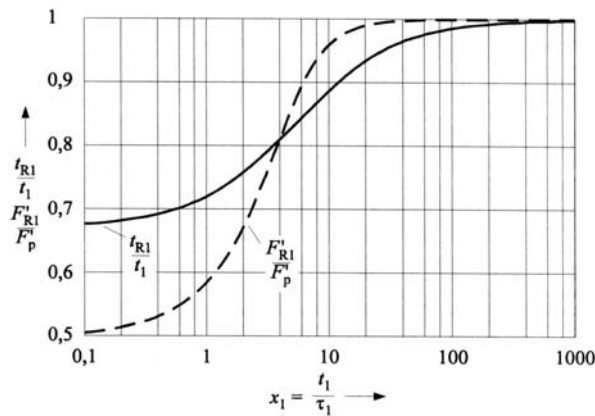


Figure 6.12 Parameters of the rectangular substitute time function for the electromagnetic force as a result of an exponentially rising current.

6.3.3. Mechanical stress

Starting from the rectangular substitute time function, the mechanical fault withstand of rigid conductors may be determined both according to the general method as given in [Ref 2, Ref 3] and according to a number of data derived and stated there. The calculation may proceed as follows:

- a) Calculation of the period of vibration of the relevant natural oscillation $T_{me} = 1/f_c$, according to [Ref 2, Ref 3].
- b) Determination of the parameters of the substitute rectangular time function t_R and F'_R , according to sections 6.3.2 and 6.3.3.
- c) Calculation of the desired quantities with F'_R as static load per unit length:
 - bending forces at the conductor supporting points as a measure of the static insulator stress
 - bending stress inside the conductor at the point of its maximum value as a measure of the busbar stress
 - deflection of the conductor at the point of its maximum, if required
- d) Determination of the coefficients $V_{F,\sigma,\sigma_s,y} = f(t_R/T_{me})$ from Figure 6.13. The figure is the result of calculations according to [Ref 65] where the excitation is rectangular. For this purpose, the conductor is considered a beam with either both ends fixed or both ends supported or one end fixed and one end supported. The curves in Figure 6.13 are given by the envelopes of the maxima, so that the results are on the safe side, irrespective of the boundary conditions fixed or supported.
- e) Determination of the dynamic quantities as the product of the static quantities and the coefficients $V_{F,\sigma,\sigma_s,y}$.

It is as well possible to assess the mechanical stress without determining the parameters of the substitute rectangular time function by assuming that $F'_R = F'_p$ and $t_R = t_k$ (see Figure 6.8). The results will be on the safe side, but may be very inaccurate.

With three-phase arrangements, plastic deformation is allowed as stated in IEC/EN 60865-1 [Ref 2, Ref 3]. Also with d.c. installations, this can be used and is given in IEC 61660-2 [Ref 61]. The explanations and derivations performed in chapters 2.2.1 to 2.2.3 can be applied to d.c. installations, too.

The calculation of the relevant natural frequencies and the section moduli of the main and sub-conductors are described in chapters 2.2.4 and 2.2.5, the superposition of stresses in conductors in chapter 2.2.6

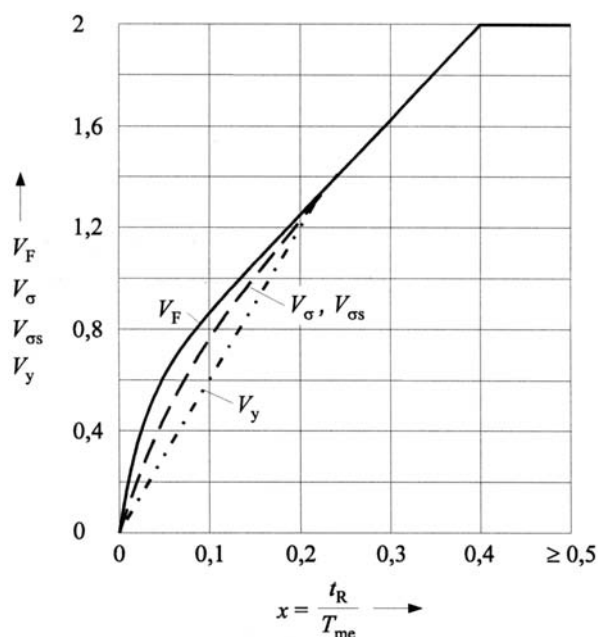


Figure 6.13 Coefficients for determination of dynamic stress and deflection. V_F for insulator stress, $V_σ$ for conductor stress, and V_y for conductor deflection.

6.3.4. Thermal stress

Thermal short-circuit strength may be established according to [Ref 2, Ref 3], where the thermal equivalent short-circuit current I_{th} is known. The quantity I_{th} for d.c. systems may be derived with the help of coefficients $m_{θ1}$ and $m_{θ2}$ as given in section 6.3.2.

$$(6.24) \quad I_{th1} = i_p \sqrt{m_{θ1}} \quad I_{th2} = i_p \sqrt{m_{θ2}}$$

$$(6.25) \quad I_{th} = i_p \sqrt{\frac{m_{θ1}t_1 + m_{θ2}t_2}{t_1 + t_2}}$$

Of course, it is as well possible to assess the thermal stress without determining the parameters of the substitute rectangular time function by assuming that $I_{th} = i_p$. The result will be on the safe side, but may be very inaccurate.

6.4. CONCLUSION

The time curves of short-circuit currents and of electromagnetic short-circuit forces in d.c. auxiliary systems are manifold and include a variety of parameters. For the characteristic time curves of current and of force, a standardized function is

introduced, which needs no more than 6 parameters [Ref 64].

In order to avoid integrating the differential equation of vibration of every system under investigation, a rectangular time function is substituted for the time curve of the standardised electromagnetic force. This rectangular function approximately causes the same maximum instantaneous value of mechanical stress as does the original electromagnetic force, where the short-circuit duration does not surpass half the vibration period of the relevant natural oscillation. After suitable modification, the substitute rectangular time function may be used even where the short-circuit duration surpasses half the vibration period of the natural oscillation.

The parameters of the rectangular function may easily be determined with the help of the coefficients $m_θ$, m_s and m_{js} . The thermal equivalent short-circuit current I_{th} , which is relevant for the thermal stress, may be calculated from $m_θ$ as well.

The calculation of the mechanical stresses and deflections starts from the substitute rectangular time function and proceeds according to the method as standardized in IEC/EN 60865-1 [Ref 2, Ref 3]; the coefficients V_F , $V_σ$ and V_y which are required for d.c. systems are given here.

7. REFERENCES

- Ref 1. IEC TC 73/CIGRÉ SC 23 WG 11: The mechanical effects of short-circuit currents in open air substations (Rigid and flexible bus-bars), Vol. 105, Geneva: IEC, Paris: CIGRÉ, 1996
- Ref 2. IEC 60865-1, Short-circuit currents - Calculation of effects. Part 1: Definitions and calculation method, Geneva: IEC, 1993
- Ref 3. EN 60865-1: Short-circuit currents - Calculation of effects. Part 1: Definitions and calculation method. Brussels: CENELEC, 1993
- Ref 4. Lehmann, W.: Elektrodynamische Beanspruchung paralleler Leiter. ETZ-A 76 (1955), pp 481-488
- Ref 5. VDE 0103/01.61: Leitsätze für die Bemessung von Starkstromanlagen auf mechanische und thermische Kurzschlußfestigkeit. Berlin: VDE, 1961
- Ref 6. IEC 865: Calculation of effects. Geneva: IEC, 1986
- Ref 7. PC-Programm IEC865, Lehrstuhl für Elektrische Energieversorgung, Universität Erlangen-Nürnberg, 1999
- Ref 8. Hosemann, G.; Tsanakas, D.: Dynamic short-circuit stress of busbar structures with stiff conductors. Studies and conclusions for simplified calculation methods. Electra No. 68, 1980, pp 37-64
- Ref 9. Tsanakas, D.: Einfluß der Zeitverläufe der elektromagnetischen Kurzschlußkräfte auf die dynamische Beanspruchung. etzArchiv 4 (1982), pp 365-368
- Ref 10. Tsanakas, D.: Beitrag zur Berechnung der elektromagnetischen Kurzschlußkräfte und der dynamischen Beanspruchung von Schaltanlagen. Thesis D17, Technische Hochschule Darmstadt, 1976
- Ref 11. IEC 60909-0: Short-circuit current calculation in three-phase a. c. systems. Part 0 : Calculation of currents. Geneva: IEC, 2001
- Ref 12. EN 60909-0 : Short-circuit currents in three-phase systems – Part 0 : Calculation of currents. Brussels: CENELEC, 2002
- Ref 13. Dwight, H. B.: Geometric mean distances for rectangular conductors. Transactions AIEE 65 (1946), pp 536-538
- Ref 14. Klar, F.: Die Induktivität gestreckter Leiterschleifen. Wissenschaftliche Zeitschrift der Elektrotechnik der Technischen Universität Dresden 11 (1968), pp 82-100
- Ref 15. Laukner, M.: Berechnung ebener Leiteranordnungen beliebiger Querschnittsform unter Berücksichtigung von Stromverdrängung und Magnetisierung. Thesis Universität Erlangen-Nürnberg, 1998
- Ref 16. Laukner, M.: Transiente Beanspruchung von Leiterschienen unter Berücksichtigung der Stromverdrängung. 40. Internationales Kolloquium der Technischen Hochschule Ilmenau, September 1995, Ilmenau, proceedings pp 315-320
- Ref 17. DIN 18800/11.90: Stahlbauten. Berlin: Beuth, 1990
- Ref 18. EUROCODE 3: Design of steel structures
- Ref 19. Hosemann, G.; Tsanakas, D.: Beitrag zur analytischen Berechnung der dynamischen Kurzschlußbeanspruchung von Schaltanlagen. etz-a 97 (1976), pp 493-498
- Ref 20. Hosemann, G.; Tsanakas, D.: Dynamic stress in substations taking into account the short-circuit currents and electromagnetic forces due to non-simultaneous faults. International Conference on Large High Voltage Electric Systems, Paris, 1978, Report 23-04
- Ref 21. Mavromaras, D.; Sieber, P.: Beitrag zur Ermittlung der bei Kurzschlüssen für Stromleiter zulässigen mechanischen Beanspruchung. ETZ-A 89 (1968), pp 34-38
- Ref 22. Issler, L.; Ruoß, H.; Häfele, P.: Festigkeitslehre - Grundlagen. Berlin: Springer, 1995

- Ref 23. Sieber, P.: Über den Einfluß von Resonanzerscheinungen auf die mechanische Kurzschlußfestigkeit von biegesteifen Stromleitern. AEG-Mitteilungen 49 (1959), pp 322-328
- Ref 24. Tsanakas, D.: Dynamische Kurzschlußbeanspruchung von Hochspannungsschaltanlagen mit biegesteifen Leitern. etz-a 98 (1977), pp 399-403
- Ref 25. Tsanakas, D.: Erhöhung der dynamischen Kurzschlußbeanspruchung von Schaltanlagen infolge erfolgloser Kurzunterbrechung. etz-a (1978), pp 86-88
- Ref 26. Stauch, G.; Böhme, H.: Schwingungsverhalten von Stromleiteranordnungen in Mittelspannungsschaltanlagen bei Kurzschluß - Beeinflussung der Grundfrequenz. ELEKTRIE 37 (1983), pp 651-655
- Ref 27. VDE 0101.6: Messung von Leiter-Eigenfrequenzen mit und ohne Zwischenstücke. Arbeitsbericht Nr. 166, 1960, DKE Frankfurt am Main (unpublished)
- Ref 28. Kocmann, A.: Eigenschwingungen von Sammelschienen bei Berücksichtigung der Abzweigschienen. CEG (Continental-Elektro-Industrie-Gesellschaft) Berichte (1956), pp 180-188
- Ref 29. Dubbel - Taschenbuch für den Maschinenbau. Berlin: Springer, 1990
- Ref 30. HÜTTE. Die Grundlagen der Ingenieurwissenschaften. Mechanik. Berlin: Springer, 1991
- Ref 31. Kießling, G.: Eigenfrequenz zusammengesetzter Sammelschienen mit Zwischenstücken - Frequenzfaktor c nach DIN VDE 0103. etzArchiv 10 (1988), pp 381-387
- Ref 32. VDE 0101.6: Untersuchungen über Trägheits- und Widerstandsmomente von Stromschienen mit 2 Teilleitern. Arbeitsbericht Nr. 24, 1958, DKE Frankfurt am Main (unpublished)
- Ref 33. Hibbit, Karlson & Sorrensen Inc.: ABAQUS theory Manual, Version 5.4, 1994
- Ref 34. Miri A. M.; Stein N.: "Short-Circuit Constraints and Strength of HV Substations Post- Insulators" Proceedings of the 5th International Symposium on Short-Circuit Currents in Power Sytems, Warsaw 1992 pp. 3.3.1- 3.3.6.
- Ref 35. IEC Publication 60865-2: Short-circuit currents - Calculation of effects. Part 2: Examples of calculation. Genève: IEC, 1994.
- Ref 36. ADINA
Adina R&D, Inc
71 Elton Avenus, Watertown,
MA02472,USA
www.adina.com
- Ref 37. ASTER (developed by EDF)
1 avenue du général de Gaulle
92141 CLAMART CEDEX
- Ref 38. SAMCEF (distributed by Samtech, Belgium, developer: University of Liège) Samtech, Parc Scientifique du Sart Tilman, Rue des Chasseurs Ardennais, 8, B 4031 Angleur, BELGIUM. Contact at eric.carnoy@samcef.com
- Ref 39. Declercq, G.: Tests with droppers and interphase spacers. 8th International Symposium on Short-Circuit Currents in Power Systems, Brussels (Belgium), 8-10 October 1998, Proceedings pp. 143-148.
- Ref 40. Stein, N.; Meyer, W.; Miri, A.M.: High voltage substation stranded conductor buses with and without droppers – Tests and calculation of short-circuit constraints and behaviour. 8th International Symposium on Short-Circuit Currents in Power Systems, Brussels (Belgium), 8-10 October 1998, Proceedings pp. 115-121.
- Ref 41. Zeitler, E.: Berechnung der Seilbewegungen und Kräfte bei vorwiegend vertikalen Verbindungen in Schaltanlagen. Thesis University of Erlangen-Nürnberg, 1993.

- Ref 42. Stein, N.; Miri, A.M.; Meyer, W.: 400 kV Substation Stranded Conductor Buses — Tests and Calculations of Short-Circuit Constraints and Behaviour, 7th International Conference on Optimisation of Electrical and Electronic Equipment OPTIM 2000, Brasov (Romania), 11.–12. May 2000; Proceedings pp 251-257
- Ref 43. Stein, N.; Meyer, W.; Miri, A.M.: Tests and Calculation of Short-Circuit Forces and Displacements in High Voltage Substations with Stranded Conductors and Droppers. ETEP 10 (2000) No. 3 , pp 131–138
- Ref 44. Stein, N.; Meyer, W.; Miri, A.M.: High Voltage Substations with Stranded Conductors and Droppers - Tests and Calculations of Short-Circuit Constraints and Behaviour. 9th International Symposium on Short-Circuit Currents in Power Systems, Cracow (Poland), 11.-13. October 2000, Proceedings pp 221-228
- Ref 45. Miri, A.M., Schwab, A.J., Kopatz, M.: *Kurzschlussstroeme und Leiterbewegungen in Hochspannungsschaltanlagen in Seilbauweise*, Elektrizitätswirtschaft 87 (1988), pp. 429-436
- Ref 46. A.M. Miri, N. Stein, Nzoubou W. : Simulation of the dynamic short-circuit behaviour of a substation with stranded conductor buses in bundle configurations with close and various degrees of wide bundling. 9th International Symposium on short-circuit currents in Power Systems, 2000 Cracow Poland
- Ref 47. Schön U.: "Short-Circuit Electrodynamical Load in the Design of High-Voltage substations" Master Thesis, University of Karlsruhe, 1994, unpublished.
- Ref 48. Lilien J. L., Schön U.: "Mechanical loads on substation apparatus -An equivalent static load-" 6th Int. Symposium on short-circuit currents in Polver Systems, 1994.
- Ref 49. G. de Wendt, T. Tietz, A.M. Miri, R. Ahlers, N. Stein: "Dynamic and Static Case Stress Analysis of a HV Substation with Stranded Conductors (Test-Results-Calculation)" 7th Int. Symposium on short-circuit currents in Power Systems, 1996.
- Ref 50. Miri A. M., Stein N.: "Short-Circuit Constraints and Strength of HV Substation Post-Insulators" 5th Int. Symposium on short-circuit currents in Polver Systems, 1992.
- Ref 51. Bathe, Klaus-Jürgen Finite Elemente Methode Springer Verlag, 1990
- Ref 52. Miri, A.M; Kühner, A; Lilien, L; Stein N.; "An Analytical-Numerical Method Based on Static Equivalent Load for the Evaluation of Maximum Dynamic Stress in HV Supporting Structures (Portals)". 7th Int. Symposium on short-circuit currents in Power Systems 1996
- Ref 53. Manuzio C. An investigation of forces on bundle conductor spacers under fault conditions. *IEEE Trans. On PAS, Vol. 86, N°2, 1967, pp166-185*
- Ref 54. J.L. Lilien, E. Hansenne, K.O. Papailiou. J. Kempf. *Spacer Compression for a tripple conductor arrangement*. IEEE Trans. On Power Delivery, **Vol. 15**, N°1, pp 236-241, January 2000.
- Ref 55. J.L. Lilien, K.O. Papailiou. *Calculation of Spacer Compression for Bundle Lines under Short-Circuit*. IEEE Trans. On Power Delivery, **Vol 15**, N°2, pp839-845, April 2000.
- Ref 56. Kießling, G.: Das Seilspannfeld als physikalisches Pendel – eine analytische Lösung der Kurzschlußvorgänge. *Archiv für Elektrotechnik* 70 (1987), pp. 273-281.
- Ref 57. Olszowsky, B.: Computation of jumper swings in EHV-substations under short-circuit currents. CIGRE 23-81 (WG02)11-IWD.
- Ref 58. CIGRE SC 23 WG 02: The mechanical effects of short-circuit currents in open-air substations (Rigid and flexible bus-bars). Paris: CIGRÉ, 1987

- Ref 59. IEC 61660-1. Short-circuit currents in d.c. auxiliary installations in power plants and substations – Part 1 : Calculation of short-circuit currents. Geneva : IEC, 1997
- Ref 60. Nietsch, Ch.: Ermittlung des Kurzschlußstromverlaufs in Gleichstromanlagen. Thesis University of Erlangen-Nürnberg, 1991
- Ref 61. IEC 61660-2. Short-circuit currents in d.c. auxiliary installations in power plants and substations – Part 2: Calculation of effects. Geneva: IEC, 1997
- Ref 62. IEC 61660-3. Short-circuit currents in d.c. auxiliary installations in power plants and substations – Part 3: Examples of calculation. Geneva: IEC, 2000
- Ref 63. Kunz, M.: Berechnung der Kurzschlußströme in Gleichstrom- und Steuerspannungsnetzen. Thesis University of Erlangen-Nürnberg, 1999
- Ref 64. Tsanakas, D.: Ersatzzeitfunktionen für die Bestimmung der mechanischen und thermischen Kurzschlußbeanspruchung in Gleichstromanlagen. etz Archiv 10 (1988), pp 355-360
- Ref 65. Tsanakas, D.; Meyer, W.; Safigianni, A.: Dynamische Kurzschlußbeanspruchung in Gleichstromanlagen. Archiv für Elektrotechnik 74 (1991), pp 305-313
- Ref 66. Pfötenhauer, J.: Digitale Berechnung von Kurzschlußströmen in Stromrichteranlagen in Drehstrombrückenschaltung. Elektrie 6 (1968), pp 221-224
- Ref 67. Pfeiler, V.; Steuber, M; Stade, D.: Bestimmung der Strom-Spannungs-Verhältnisse durch ein digitales Rechenprogramm und durch Kurzschlußmessungen. Elektrie 24 (1970), pp 450-454
- Ref 68. Pfeiler, V.; Stade, D.: Ausschaltvorgänge in Stromrichtersystemen. Elektrie 26 (1972), pp 120-121
- Ref 69. Herold, G.; Finke, J.: Berechnung der charakteristischen Kurzschlußstromgrößen der Drehstrombrückenschaltung. Elektrie 36 (1982), pp 5-8
- Ref 70. Weßnigk, K.D.; Grießbach, A.: Programm zur digitalen Berechnung des zeitlichen Kurzschlußstromverlaufs in batteriegespeisten Gleichstromnetzen. Elektrie 43 (1989), pp 379-381
- Ref 71. IEC-Publication 363: Short-circuit current evaluation with special regard to rated short-circuit capacity of circuit-breakers in installations in ships. Geneva: IEC, 1972
- Ref 72. Nietsch, Ch.; Tsanakas, D.: Kurzschlußströme in Gleichstrom-Eigenbedarfsanlagen. Elektrie 46 (1992), pp 18-22
- Ref 73. Tsanakas, D.; Meyer, W.; Nietsch, Ch.: Short-Circuit Currents of Motors in D.C. Auxiliary Installations in Power Plants and Substations. Electromotion '99, Patras, Greece; 8-9 July 1999, Paper D-10, pp 489-496
- Ref 74. Kunz, M.; Herold, G.: Fast Calculation Method for State Space Investigation of Short-Circuit Currents in Rectifier Fed Networks. 8th International Symposium on Short-Circuit Currents in Power Systems, Brussels, Belgium, 8.-10. October 1998, Proceedings pp 43-48
- Ref 75. Kunz, M.; Herold, G.: Short-Circuit Current Calculation in Rectifier Fed DC Auxiliary Substations. 8th International Symposium on Short-Circuit Currents in Power Systems, Brussels, Belgium, 8.-10. October 1998, Proceedings pp 77-82
- Ref 76. Klotter, K.: Technische Schwingungslehre. Erster Band, Teil A: Lineare Schwingungen. Berlin, Heidelberg, New York: Springer, 1978
- Ref 77. Meier-Dörnberg, K.-E.: Abschätzen von Schwingungsausschlägen bei stoßartig verlaufenden Einwirkungen. VDI-Berichte Nr. 113, VDI-Verlag 1967
- Ref 78. Tsanakas, D.; Papadias, B.: Influence of short-circuit duration on dynamic stresses in substations. IEEE Trans. Power App. Syst. 102 (1983), pp 492-501
- Ref 79. DIN VDE 0101 German Version of HD 637 S1 1999: Power Installations exceeding A.C. 1 kV. (soon IEC 50179)

- Ref 80. Fiabilité des structures des installations industrielles, Théorie et applications de la mécanique probabiliste, H.PROCACCIA, P.MORILHAT, Collection de la Direction des Etudes et Recherches d'Electricité de France EYROLLES 1996
- Ref 81. Probability Concepts in Electric Power Systems, G.J.ANDERS, WILEY Interscience.
- Ref 82. Probabilistic design of rigid bus - Feasibility study, M.D.GERMANI ONTARIO HYDRO-27-09-1990 Report 90405.
- Ref 83. "Probabilistic Short-Circuit Uprating of station strain bus system-overview and application", M.D. GERMANI, G.L.FORD, E.G. NEUDORF, M. VAINBERG, M.A. EL-KADY, R.W.D. GANTON IEEE Transactions on Power Delivery, Vol PWRD-1, N° 3 July 1986.
- Ref 84. Contribution of Reliability analyses to the study of the effects of short-circuit, 5th International symposium on short-circuit currents in power system, WARSAW Congress, 8-9 September 1992, M.BULOT, L.DEMOULIN.
- Ref 85. Influence of the wind on the mechanical design of transmission structures against short-circuits, 5th International symposium on short-circuit currents in power system, WARSAW Congress, 8-9 September 1992, M.GAUDRY, Y.MAUGAIN.
- Ref 86. Anwendung der stochastischen Simulation zur Berechnung von Kurzschlußstrombeanspruchungsverteilungen das verbundnetz, R.LEHMANN, KDT, Dresden ; F.BERGER, KDT Berlin, May 1985.
- Ref 87. Entscheidungsprobleme der Elektroenergietechnik, ELEKTRIE Berlin 42 (1988), E.MUSCHIK ; E.PILZ ; F.BERGER ; ZITTAU.
- Ref 88. Probabilistic Methods Applied to Electric Power Systems, Proceeding of the first International Symposium, TORONTO 11-13 July 1986, SAMY G. KRISHNASAMY Ontario Hydro.
- Ref 89. Influence of the reclosure on flexible conductor arrangements-Evaluation of the risk to increase the stresses in comparison with first short-circuit stresses G.DECLERCQ 6-8 septembre 1994 6th International Symposium on short-circuit currents LIEGE (BELGIQUE)
- Ref 90. Probability Distribution of Supporting Structures Stress, Dr M.DASCZYK WARSAW 1996.
- Ref 91. Symposium de Bruxelles sur les courts-circuits, 310-02 Stochastic determination and evaluation concerning loads of short-circuit current in electric energy Transmission installations, G.STEGEMANN, F.BERGER, 310-03 Probabilistic uprating of 230 kV strain bus system at substations with high fault currents, M.VAINBERG, M.D.GERMANI, M.EL-KADY, R.W.D.GANTON.
- Ref 92. Evaluation des configurations des barres de poste, G.J.ANDERS et L.WANG, Ontario Hydro Technologies report n°390 T 953 October 1995, L'Association Canadienne de l'Electricité.
- Ref 93. Charge et résistance des lignes de transport aériennes, CIGRE 22.06 ELECTRA n°129.
- Ref 94. Hecht, A.: Elektrokeamik, Berlin/Heidelbezg/New York, Springer-Verlag 1976
- Ref 95. Stein, N. a.o.: Dynamic behaviour and strength of high- voltage substation post insulators under short-circuit loads, Cigre-session Paris 1985, pp. 23-12
- Ref 96. Miri, A.M., Stein, N.: Kurzschlußbeanspruchung und -festigkeit von Hochspannungstützisolatoren, etz-Archiv, Bci.10(1988) H.3 S.89-96

- Ref 97. Barthelt, H., Weyl, D.: Mechanische Festigkeit von Porzellankörpern und deren Abhängigkeit von deren Abmessungen, ETZ-A Bd. 80(1959) 14, S.445-449
- Ref 98. Hauschild, W.(Mosch, W.: Statistik für Elektrotechniker, VEB Verlag Technik Berlin 1984
- Ref 99. G.Declercq, « Maximum asymmetry with several main rigid busbars », 7th International Symposium on Short-Circuit Currents in power systems, Varsawa 10-10 September 1996
- Ref 100. G. Declercq, «The influence of the reclosure for flexible conductors in substations- A proposal of a simplified method » IWD -CIGRE 23-11- TF - EAP/93.026 -november-1993]
- Ref 101. The Mechanical effects of short-circuit currents in open-air substations (rigid and flexible busbars).(volume 1 and 2). Brochure N° 105, April 1996. CIGRE central Office, Paris
- Ref 102. CENELEC HD 63751; 1999. Power installations exceeding 1 kV a.c.

8. ANNEX

8.1. THE EQUIVALENT STATIC LOAD AND EQUIVALENT STATIC LOAD FACTOR

8.1.1. Definition of ESL (Equivalent Static Load) and ESL factor

The equivalent static load is a static load which can be taken into account for the design of structures which are stressed by dynamic loading. We only consider here concentrated loads (not distributed).

The ESL is a static load with the same application point as the actual load, which would induce in the structure the same maximum force (generally in connection with the bending moment) as the dynamic load.

ESL is not equal to the peak value of the dynamic load because inertial forces (distributed along the structures) exist during dynamic loadings (Figure 8.1).

ESL can be lower, equal or higher than peak dynamic load, depending on the vibration frequencies (so called eigenfrequencies) of the structures to which the load is applied

The dynamic load can be characterised by its PSD (power spectral density) which point out the range of frequencies in which the loading will have some true dynamic effects.

The **ESL factor** is the ratio between ESL and the relative peak instantaneous load (compared to its initial value, if any). The ESL factor can change from location to another in a structure. For example on (Figure 8.1) $ESL = 0$ for two specific location in the

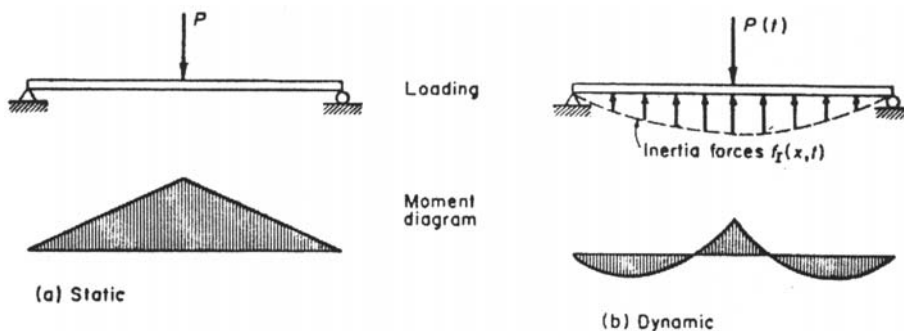


Figure 8.1 taken from "Earthquake response of structures", R.W. Clough, Berkeley, chapter 12. Influence of the dynamic loading compared to static loading. $P(t)$ maximum is equal to P static.

span and changing from 0 to approximately 1 for other positions. It could have been larger than 1 at mid-span if the frequency of load application would have been similar to the first or the third eigenfrequency of the beam. And it could also be smaller than one in case of non resonant effect, in some particular location in the structure. In fact inertial forces can have compensation effect or elimination effect, depending on the modal shape of the structure, which can be very different from the static deformation shape. But these effects are difficult to be predicted and thus can be neglected in a simplified method. A simplified method will then be restricted to particular cases with special loading. In other cases a dynamic simulation is then required.

ESL factor can be estimated by analytical treatment of the load. Its value is determined from the linear theory of the beam based on modal analysis which includes the modal shape of the structure. Due to the typical problems in substations and the necessary simplifications the formula limited to the first eigenmode only are used. Due to this simplification, the structural factor is equal to one, only the load factor has to be evaluated. The ESL factor is given by the following equation :

$$(8.1) \quad ESL_{factor} = \omega_1 \left[\int_0^t f(\tau) e^{-\xi \omega_1 (t-\tau)} \cdot \sin(\omega_1 (t-\tau)) d\tau \right]$$

where ξ is the modal damping, $f(t)$ is the time function of the load, ω (rad/s) is the first eigenfrequency of the structure, t is time duration of the load application.

If the damping is assumed at 3% and if ESL factor is depending on the frequency of the structure ($f = \omega/2\pi$), the ESL factor will only depend of the load shape. For this reason, in chapter 3, we have splitted

the ESL factor synthetic curve in three different type of loading : one curve for the typical interphase effects, one curve for the typical pinch effect and one curve for the dropper stretch. The synthetic aspects have been obtained by the collection of numerous test results and the simulation of these results using advanced calculation method.

Basically:

- ESL is lower than the peak dynamic load if the first eigenfrequency of the structure is lower than the basic frequency of the load (typically, a 4 Hz portal structure cannot be affected by the influence of a 100 Hz dynamic load). **ESL factor <1**
- ESL is equal to the peak dynamic load if the first eigenfrequency of the structure is larger than the basic frequency of the load (typically a 55 Hz insulator support will be affected by a 2 Hz dynamic load as a quasi-static load). **ESL factor =1**
- ESL is larger than the peak dynamic load if we are close to resonance (a frequency of the structure fit with one frequency of the applied dynamic load). In such case structural damping plays a key role. **ESL factor >1**

There are also specific load cases, like impulse loading (one shot in a very short time) and step loading (from zero to maximum load in a very short time, then maintained at maximum value).

For this last a well known dynamic effect give ESL factor equal to 2, for impulse loading ESL will be less than 2.

8.1.2. Concerned structures

Concerned structures are the equipment (transformers, isolators, surge arresters, supporting insulators, bushings, wave trap) and their supporting structures.

8.1.3. Concerned loadings

Concerned dynamic loadings are :

- swing out maximum F_t (**tensile load**)
- falling down maximum F_f
- pinch effect F_{pi}

For all these three first value ESL factor must be applied (to obtain ESL) on (F-Fst), the relative increase of the dynamic load.

- dropper stretch Fds (equipment only)
In this last case the initial value can be neglected, in most of the cases.

For F_b , F_f , F_{pi} , the ESL factor must be applied on the relative increase of the dynamic load, i.e. the static tensile load has to be subtracted first. For Fds the ESL factor can be neglected in most of the cases.

8.1.4. How to use ESL in design together with simplified method of actual IEC 60865

Equipment. In such case, ESL is a static load which is applied at the top of the equipment, perpendicular to it, and can be compared to the maximum specified cantilever load given by the manufacturer. IEC 60865 calculates the ESL and no addition ESL factor is necessary.

Supporting structures (gantries). In such case, ESL consist of several static loads applied at anchoring cable fixation point, perpendicular to the cross-arm, which can be used to design or check the supporting structures. These static loads will be determined from peak dynamic load obtained by the simplified method, corrected by the ESL factor. The initial Fst values have to be added to these ESL to obtain the total response. But, as these structures are generally linear, a superposition of the two cases can be done (one case calculated with Fst, one case calculated with ESL).

8.1.5. Validation of the method : How to evaluate ESL during tests or advanced simulations

This need to analyse where the maximum stress occur in the structure during the dynamic process (generally at the bottom of the structures), then to find out the static load(s) which would have to be applied at the same location as dynamic load(s), in order to obtain similar maximum stress. Such ESL evaluation is rather easy, because we generally deals with linear structures (equipment and supporting structures).

8.1.6. Examples

a) On equipment

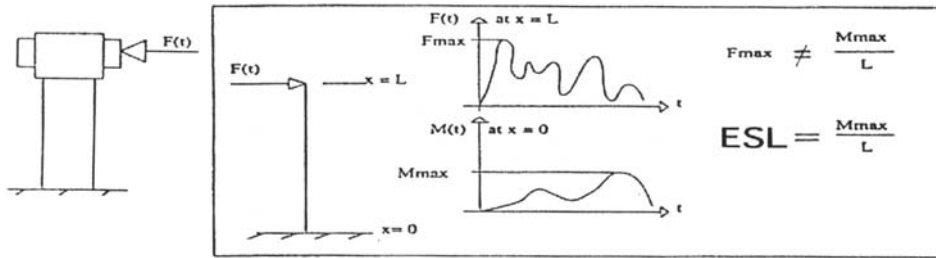


Figure 8.2

What is ESL in this case :

Assume that $F(t)$ is the tension in the cable connecting the equipment to another one or to another flexible connection. $F(t)$ could result from the following effects 1) from pinch effect (if the connection is a bundle), 2) from swing out or falling down loads (horizontal connection between two equipment), 3) from dropper stretch (if the equipment is connected to another level with flexible connection).

In the case shown, effect of $F(t)$ and bending moment at the bottom of the equipment is completely different, it means that the inertial forces have clearly some action. The design value is the maximum bending moment at the bottom. *We could have had the same M_{max} by applying ESL instead of $F(t)$ at the top of the equipments.*

The situation could have been more complex if M_{max} had not occurred at the bottom of the apparatus.

How to apply the simplified method

The problem is to define the cantilever strength needed for such equipment.

- 1) evaluate F_t , F_f and F_{pi} by IEC simplified method
- 2) search first eigenfrequency of the equipment (if not known, use curve given in chapter 1),
- 3) evaluate ESL using synthetic curve given in chapter 3 (one curve for interphase effects, another curve for pinch effect), for example $ESL1 = \max(F_t - F_{st}, F_f - F_{st}) \times ESL \text{ factor (interphase effect)}$ and $ESL2 = (F_{pi} - F_{st}) \times ESL \text{ factor (pinch)}$. Then consider $\max(ESL1, ESL2) = ESL$
- 4) In case of initial static loading (F_{st}), just add F_{st} to ESL and compare total value to cantilever strength of the equipment.

Remark : If you have access to advanced calculation method, you simply evaluate the dynamic response and locate maximum dynamic bending moment in the support, that bending is converted in equivalent top static load, which is compared to the cantilever breaking load. No need of ESL theory in that case.

b) On support structures.

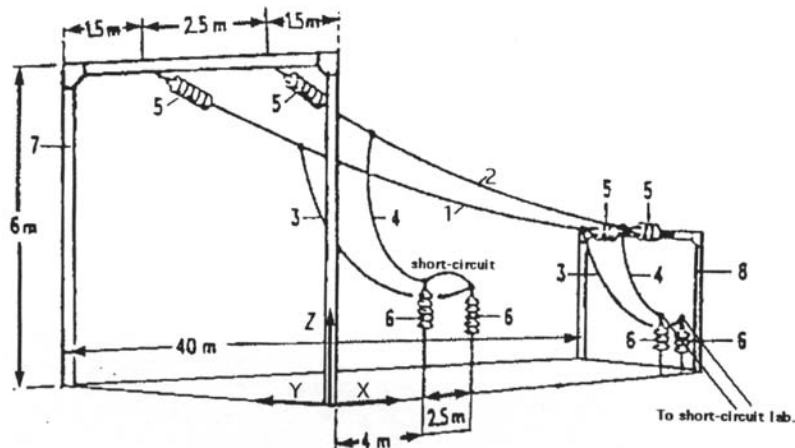


Figure 8.3 Laborelec 150 kV test structure for two-phase fault (Belgium).

We have extracted from CIGRE brochure N°105, second part, the case 5 tested in Belgium, for which we have access to both tension in the cable and

bending moment at the bottom of the support structures.

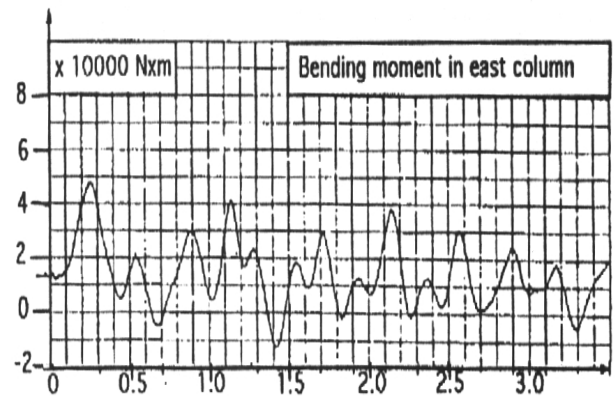
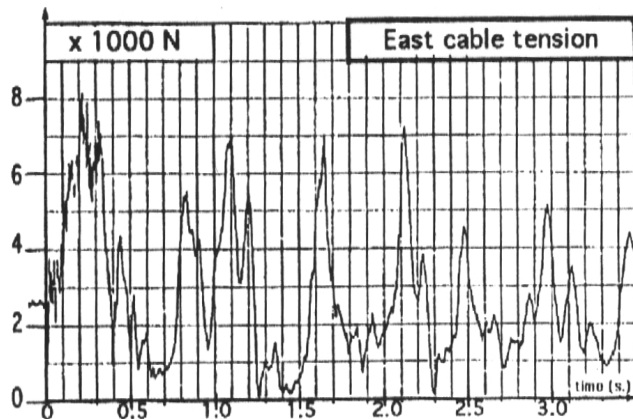


Figure 8.4 East cable tension evolution and bending moment at the bottom of west pole of the gantry

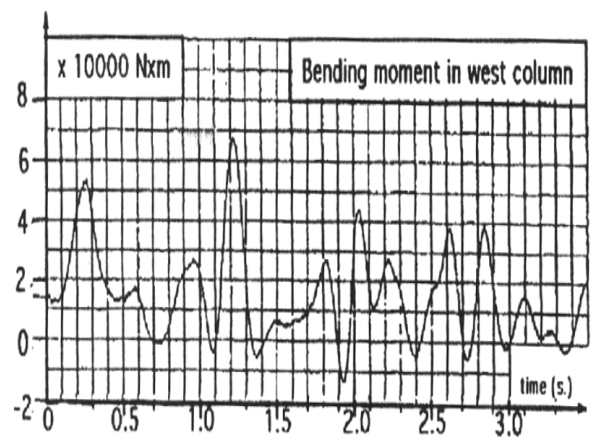
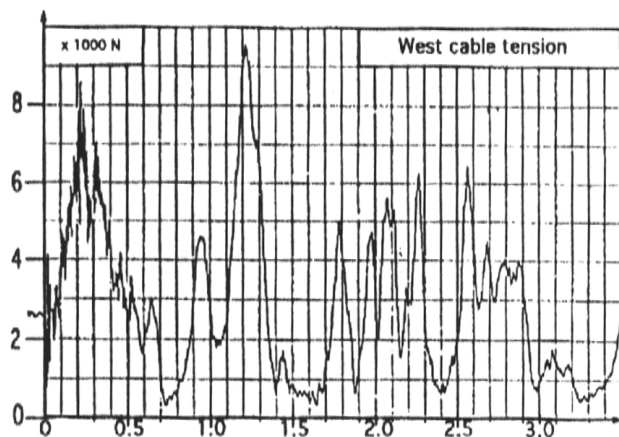


Figure 8.5 West cable tension evolution and bending moment at the bottom of west pole of the gantry

What is ESL in this case

$F(t)$ is the tension of the cable (the two left curves in Figure 8.4 and Figure 8.5). $F(t)$ contains swing out and falling down loads (no pinch because it was a single conductor). $F_{max} = 8000$ N(east) and 9500 N(west). These are measured values. Advanced calculation methods would have given very similar results. IEC simplified method would have given identical results for both phases, more close to west cable values of F_t and F_f values (because dropper influence is less on that phase). Obviously, measured values or advanced calculation values do not need any further analysis, because they give access directly to the design values, which are bending moment in the portal. Nevertheless it is of some interest to evaluate on an actual basis if any dynamic effect occurred. This can be done by the exact evaluation of ESL factor as obtained during real test measurements :

- 1) the maximum peak dynamic load is 8000 (east) + 9500 (west) = 17500 N. (in this simplified method the fact that both load are not occurring simultaneously is neglected).

- 2) as initial static load is $F_{st} = 2560$ N in each phase, the relative increase is $17500 - 2 \times 2560 = 12400$ N
- 3) the ESL determined from the bending moment is $(50000 - 15400) / 6 = 5800$ N (east) and $(70000 - 15400) / 6 = 9100$ N for each phase, this means a global value of 14900 N (6 is in meters and represent the height of the portal)

ESL factor = $14900 / 12400 = 1,2$. This is an exact value determined from test measurement. The dynamic effect corresponds to a 20% increase of the actual stress in the portal. Evaluation of the same ESL factor for different tests on the same structure but with different conductors (case 4 in brochure 105 f.e.) gave a factor in between 0.8 and 1.4 .

How to apply the simplified method

The use of the simplified method in this case would have given the following values :

IEC 60865 evaluation of F_t and F_f is given in Ref 2.

As the eigenfrequency of the portal is around 4 Hz, ESL factor synthetic curve given in chapter 3 is 1.4
 So that the portal design loads obtained by simplified method recommended in this brochure is :
 Load on phase 1 : $\max (F_t, F_{st}) \times 1.4 = \dots$
 Load on phase 2 : idem
 (only two phase for this test)
 and these load can be considered as static load.

8.2. CLAMPED-FREE BEAM DYNAMIC RESPONSE TO A TOP LOAD IDENTICAL TO A SHORT-CIRCUIT FORCE. ESL VALUE, ESL FACTOR FOR DIFFERENT STRUCTURAL DATA OF THE SUPPORT.

This case is different from the former one, as the load application has not the same shape as the load applied to flexible busbars. This case is more close to rigid busbars for which we would like to know how to design supporting structure (insulator support).
 We would like first to emphasise that no synthetic ESL factor curve had been given for this case in this brochure. This case is reserved here just to point out what could be ESL load and ESL factor in a simple case.

8.2.1. The geometry

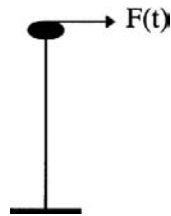


Figure 8.6. A clamped-free beam with uniform mass distribution. Internal damping chosen as 2% of critical on the first eigenmode.

8.2.2. Excitation

Top load time definition

$$(8.2) \quad F(t) = A \left(\sin(2\pi\nu t + \phi) - \sin(\phi) e^{-\frac{t}{\tau}} \right)^2$$

using $\tau = 60 \text{ ms}$
 $\phi = -\pi/2$
 $\nu = 50 \text{ Hz}$
 $A = 1000 \text{ N}$

Observation time of the time response is fixed to about 0.4 s in all cases.

We have treated three different case, only by changing the structural data to change its frequencies. These values are taken from typical supporting insulator data's used in substation from 110 kV to 400 kV. At least one of the three first eigenfrequencies is tuned to be resonant with either 50 Hz or 100 Hz. That is to show the dynamic effects in such structure. As the structure is supposed to be uniform mass distribution, if one frequency is fixed, the other are easily evaluated by classical beam theory.

8.2.3. Examples

a) Case study number one

The 50 Hz is the first eigenfrequency, thus 300 Hz is the second and 850 Hz is the third.

Which has been reproduced using following data : (a typical 110 kV insulator support)

- : height of the support 0,77 m
- bending stiffness of the support : 5,9e5 N/m

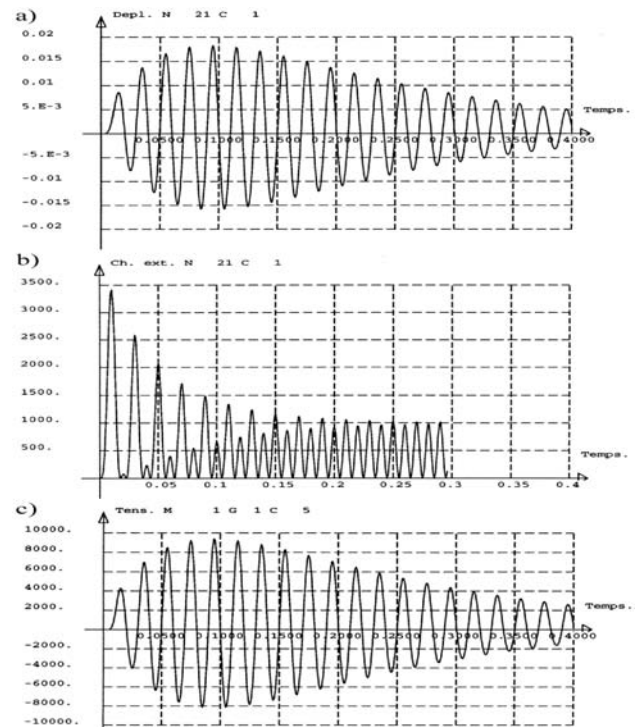


Figure 8.7 Case 1 (first eigenfrequency of 50 Hz). Curve a) is the top displacement of the insulator (m) b) is the applied top load in N and c) is the bottom bending moment (N.m).

- There is a 50 Hz oscillation of the beam during the 50 Hz dominant load application. The Resonance is clearly enhanced.
- The maximum displacement at the top is around 180 mm at around 0,9 s.
- Bending moment is in phase with the top displacement.

ESL factor can easily be determined :

Max bending moment around 9000 N.m means $ESL = 9000/0.77 = 11700$ N.

Max dynamic load value (not at the same time as the max bending) : around 3500 N.

ESL factor = 3.3

b) case number 2.

The second eigenfrequency is at 100 Hz, which give a first one at 16 Hz .

Which has been reproduced using following data : (a typical 245 kV insulator support)

: height of the support 2.3 m,
bending stiffness of the support : $1.8e5$ N/m.

- There is a 16 Hz oscillation of the beam during all the time with very low damping.
- The maximum displacement at the top is around 120 mm at around 0,02 s.
- Bending moment is in phase with the top displacement but has a clear presence of 100 Hz component.

ESL factor can easily been determined :

Max bending moment around 6500 N.m (means $ESL = 6500/2.3 = 2800$ N)

Max dynamic load value (not at the same time as the max bending) : around 3500 N

ESL factor = 0.8

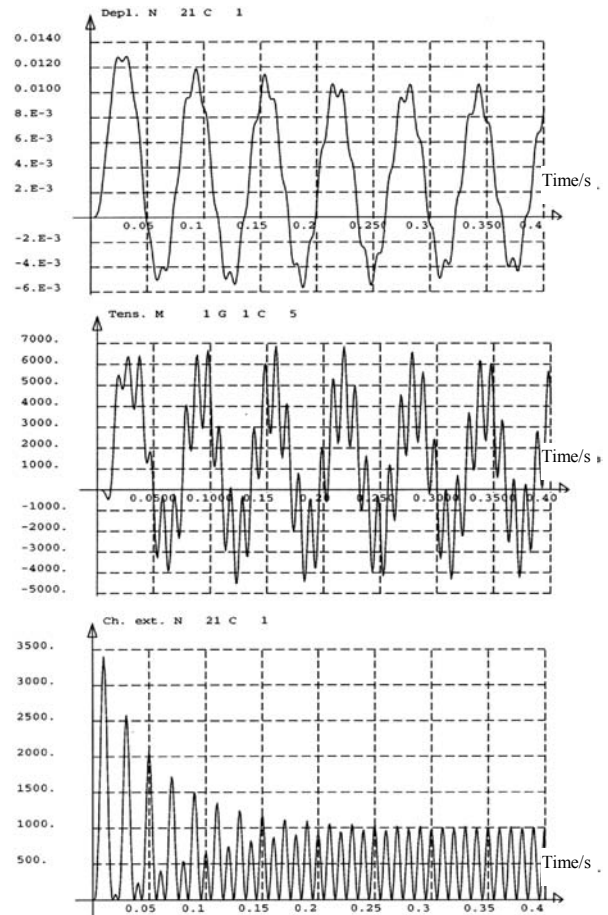


Figure 8.8 Case 2 (second eigenfrequency of 100 Hz). Curve :
a) is the top displacement of the insulator (m)
b) is the bottom bending moment (N.m)
c) is the applied top load in N.

c) case number 3

The third eigenfrequency is at 50 Hz, which give a first one at 4 Hz .

Which has been reproduced using following data : (a typical 400 kV insulator support)

: height of the support 3.8 m
bending stiffness of the support : $0.9e5$ N/m

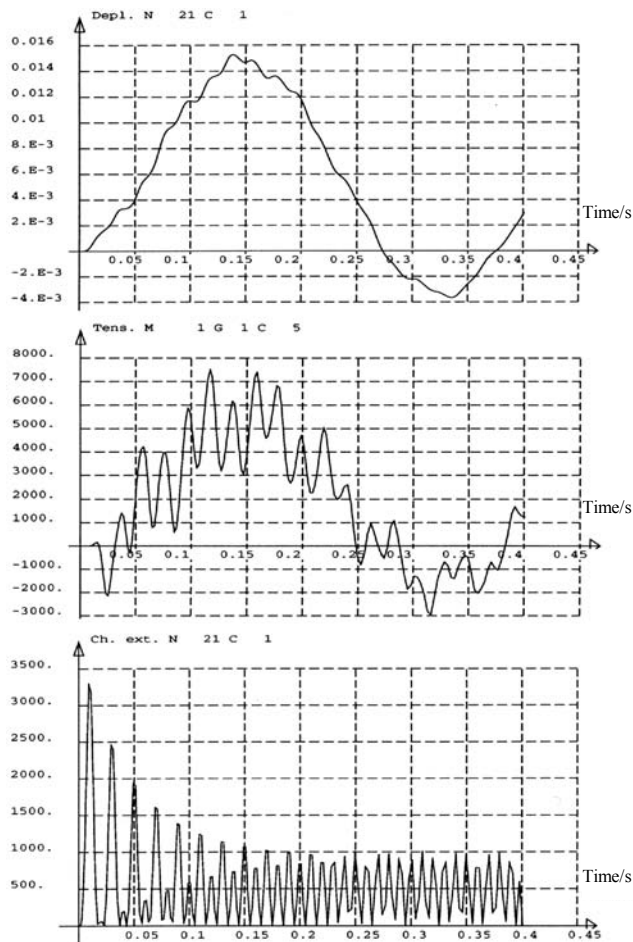


Figure 8.9 Case 3 (third eigenfrequency of 50 Hz). Curve :
a) is the top displacement of the insulator (m)
b) is the bottom bending moment (N.m)
c) is the applied top load in N

- There is a 3 Hz oscillation of the beam.
- The maximum displacement at the top is around 150 mm at around 0,13 s.
- Bending moment is in phase with the top displacement but has a clear presence of 50 Hz component

ESL factor can easily be determined :

Max bending moment around 7500 N.m (means $ESL = 6500/3.8 = 1980 \text{ N}$)

Max dynamic load value (not at the same time as the max bending) : around 3500 N

ESL factor = 0.6

8.3. COMPARISON OF TEST RESULTS AND CALCULATION ACCORDING TO IEC PUBLICATION 60865-1

Because of the very high complexity of the matter, CIGRE SC 23 WG 03, IEC TC 73 and DKE UK 121.2 (VDE 0103) introduced new calculation rules for so far uncovered particular arrangements only under the condition that sufficient evidence from test results was available. In spite of this time and cost consuming, quite a satisfactory number of rigid as well as stranded conductor arrangements have been made accessible to standardised calculation procedure for short-circuit stresses and strength. It is only natural that the more complex the matter gets, the more experimental and analytical efforts are required to cover new areas of calculation.

To understand the effects and the physics caused by the short-circuit currents in substations, a lot of different test cases are given in Volume 2 of [Ref 1] and in Volume 2 of this brochure. In these cases, the test arrangements are described in detail, oscillograms and values of forces and stresses in the conductors and substructures, and the conductor displacements are given.

In IEC Publication 60865-1 [Ref 1] and the European Standard EN 60865-1 [Ref 2] simplified methods are given for the calculation of the short-circuit stresses, forces and strength of substations with rigid and flexible busbars. The physical background and the derivation of these methods are outlined in the sections 3 and 4 of [Ref 1] and section 3 of this brochure.

In the following, the data of the tests with flexible conductors are taken and a calculation according to the standard is carried out. The comparison of the calculation results with the test results is shown in diagrams and is discussed.

For the design of busbars, the maximum short-circuit duration T_k is stated by the protection concept. The actual short-circuit duration t_k is unknown, it can be lower and can lead to higher tensile forces than with T_k . Therefore the maximum values are determined using the standard [Ref 2, Ref 3] which occur within $0 < t_k \leq T_k$ [Ref 1]. In contrast, the short-circuit duration t_k is known when calculating tests and out from this the swing-out angle δ_k at the end of the current flow, see Equation. (4.8) in [Ref 1]. If $t_k \geq T_{res}$, the conductor swings out to its highest position at $\delta_m = 2\delta_1$ and then back. T_{res} is the resulting oscillation period of the span during current flow and $\delta_1 = \text{Arctan } r$ the direction of the maximum radial force F_t . r means the ratio of electromagnetic force and gravitational force on the conductor. If $t_k \leq T_{res}$, $\delta_m = \text{Arccos}(1 - r \sin \delta_k)$ holds; F_t is maximum at δ_1 if $\delta_k \geq \delta_1$, otherwise at δ_k . F_t acts at the end of the drop down from δ_m . For further details see [Ref 1].

When calculating the short-circuit effects of spans with strained conductors, the masses and the influence of the droppers at the ends or near the ends of the spans is neglected, see paragraph 3.3. With droppers in midspan, the calculation is done according to the method given in Paragraph 3.3. When calculating the static tensile force and the sag, the masses of the droppers have to be considered.

The calculation of the pinch force F_{pi} is done as stated in the standard.

In all cases, the static stiffness of the sub-structures measured during the tests are taken into account.

In the following diagrams, the measured values of short-circuit forces and horizontal displacements are given on the horizontal axis (index m) and the calculated ones on the vertical axis (index c). In most cases, the forces are related to the initial static tensile forces. Each sign point represents a result, the number of evaluated tests is given in the legends. The lines are drawn marked by 0 %, +25 % and -25 %, which show the deviation between test and calculation; the signs above the 0 % line, the calculation results in higher values than the test, the signs below the 0 % line, the calculation results in lower values than the test.

This presentation of the comparisons is done in three parts:

- Slack conductors on supporting insulators,
- Strained conductors fastened with insulator strings on towers,
- Tests only for bundle pinch effect.

In the following, the numbers of test cases presented in Volume 2 of [Ref 1] are marked by *, the numbers of test cases presented in Volume 2 of this brochure are not marked. For the details of the tests, reference is made to both volumes.

8.3.1. Slack conductors on supporting insulators

Case 1 (FGH.1972)

In this case, a 110-kV-structure is tested. The stress in the bottom of one insulator is measured and hence an equivalent static force on the top of the insulator is calculated, which gives the same stress in the insulator as the short-circuit force. If the subconductors fulfil either $a_s/d_s \leq 2,0$ and $l_s/a_s \leq 50$ or $a_s/d_s \leq 2,5$ and $l_s/a_s \leq 70$ (so called close bundling), the conductors are considered to clash effectively; then the pinch force F_{pi} does not have to be calculated, the short-circuit tensile force F_t is to be taken, Figure 8.10a. On the other hand, if the conditions are not fulfilled, the maximum of F_t and F_{pi} is decisive, Figure 8.10b. A good agreement is achieved.

Cases 2 and 3 (FGH.1978)

Both cases have the same 200-kV-arrangement, case 2 with single conductors and case 3 with close bundled conductors. Figure 8.11 and Figure 8.12 give the results.

In Figure 8.11a, many results lie within the range $\pm 25\%$. In Figure 8.11a and Figure 8.12a, the marks above $+25\%$ show that the standard calculates values far on the safe side; this is due to the fact that in some cases the span rotates one or several times, see Figure 4.2 of [Ref 1]. The measured second maximum of the force at the bottom of the movement is lower than the force in a span falling down from its highest position. When the kinetic energy is exhausted a fall from the highest position can occur and this is taken into account in the standard. In addition, at the beginning of the fall down the kinetic energy in the conductor is not zero which is considered by the factor 1.2 in Equation (*35) of the standard, see Section 4.2.4 of [Ref 1]. The results under the -25% line are only with low short-circuit forces compared to the static force and also with short-circuit durations less than 0,1 s.

In both cases 2 and 3, the horizontal displacements had only been measured in a few tests and are in good agreement, Figure 8.11b and Figure 8.12b.

8.3.2. Strained conductors

Case *8 (FGH 1985)

The span length is 40 m, in case 8 with a single conductor Al/St 537/53 and with single and bundled conductors Al/St 537/53 and Al/St 1045/55. Figure 8.13a compares the maxima of F_t and F_f , including the tests where the sub-conductors clash effectively. Only in some tests, the sub-conductors do not clash effectively, Figure 8.13b, but in the most cases, the swing out and drop forces are decisive, Figure 8.13c. The horizontal displacement b_h is given in Figure 8.13d. A good agreement is achieved.

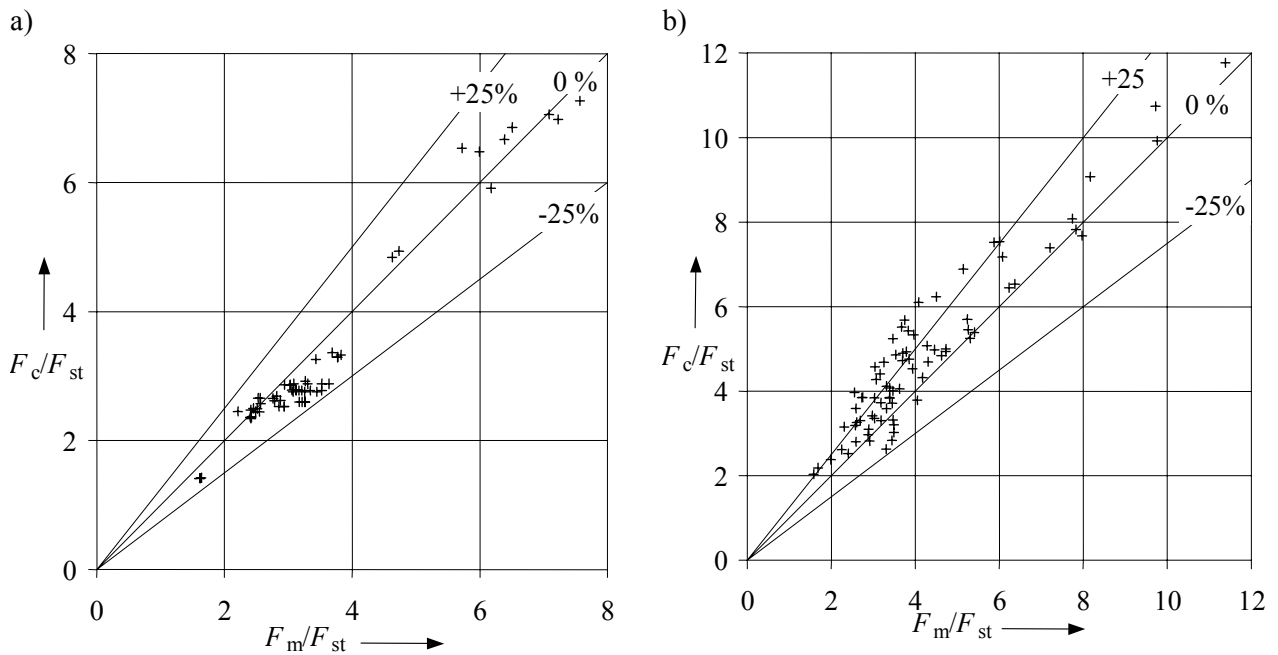


Figure 8.10: Case 1: Short-circuit forces
a) Sub-conductors are clashing effectively (60 tests)
b) Sub-conductors do not clash effectively (78 tests)

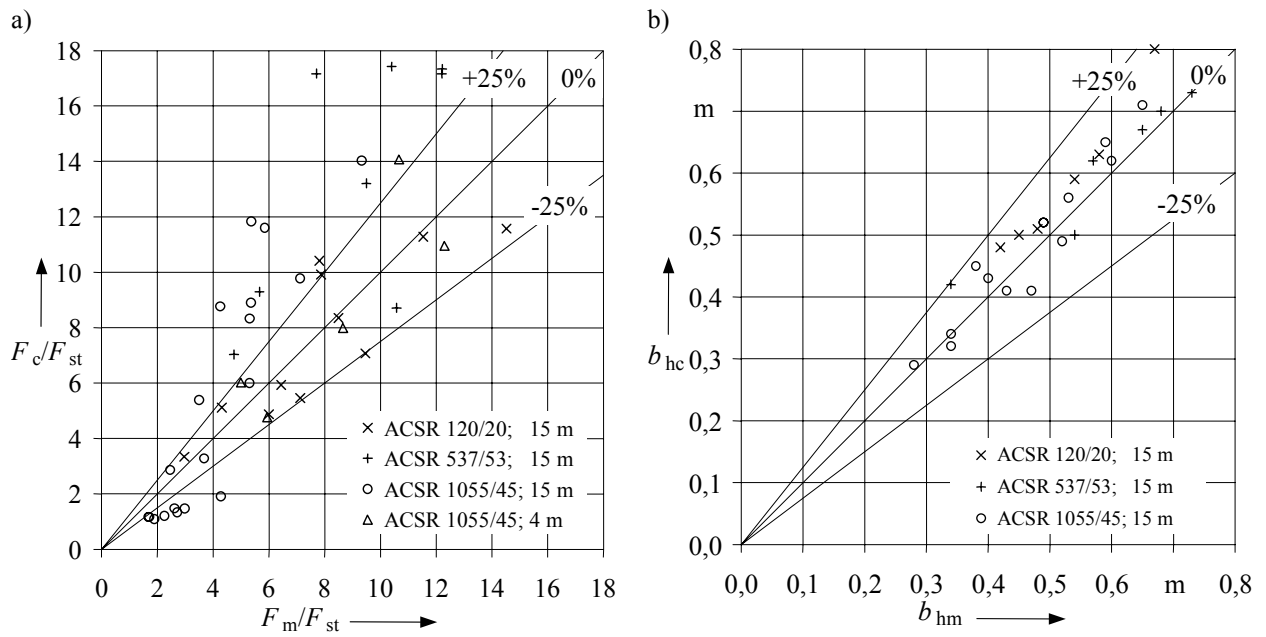


Figure 8.11: Case 2: Single conductor
 a) Short-circuit force: Maximum of F_t and F_f (43 tests)
 b) Horizontal displacement (26 tests)

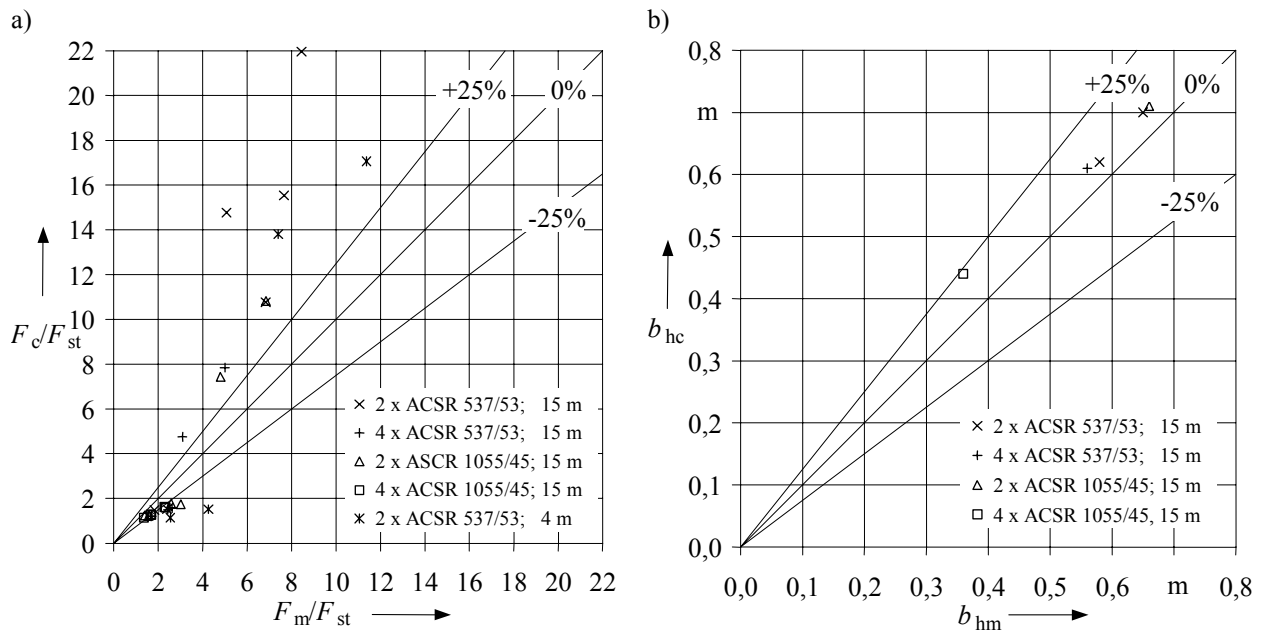


Figure 8.12: Case 3: Bundled conductors
 a) Short-circuit forces: Maximum of F_t and F_f (28 tests)
 b) Horizontal displacements (5 tests)

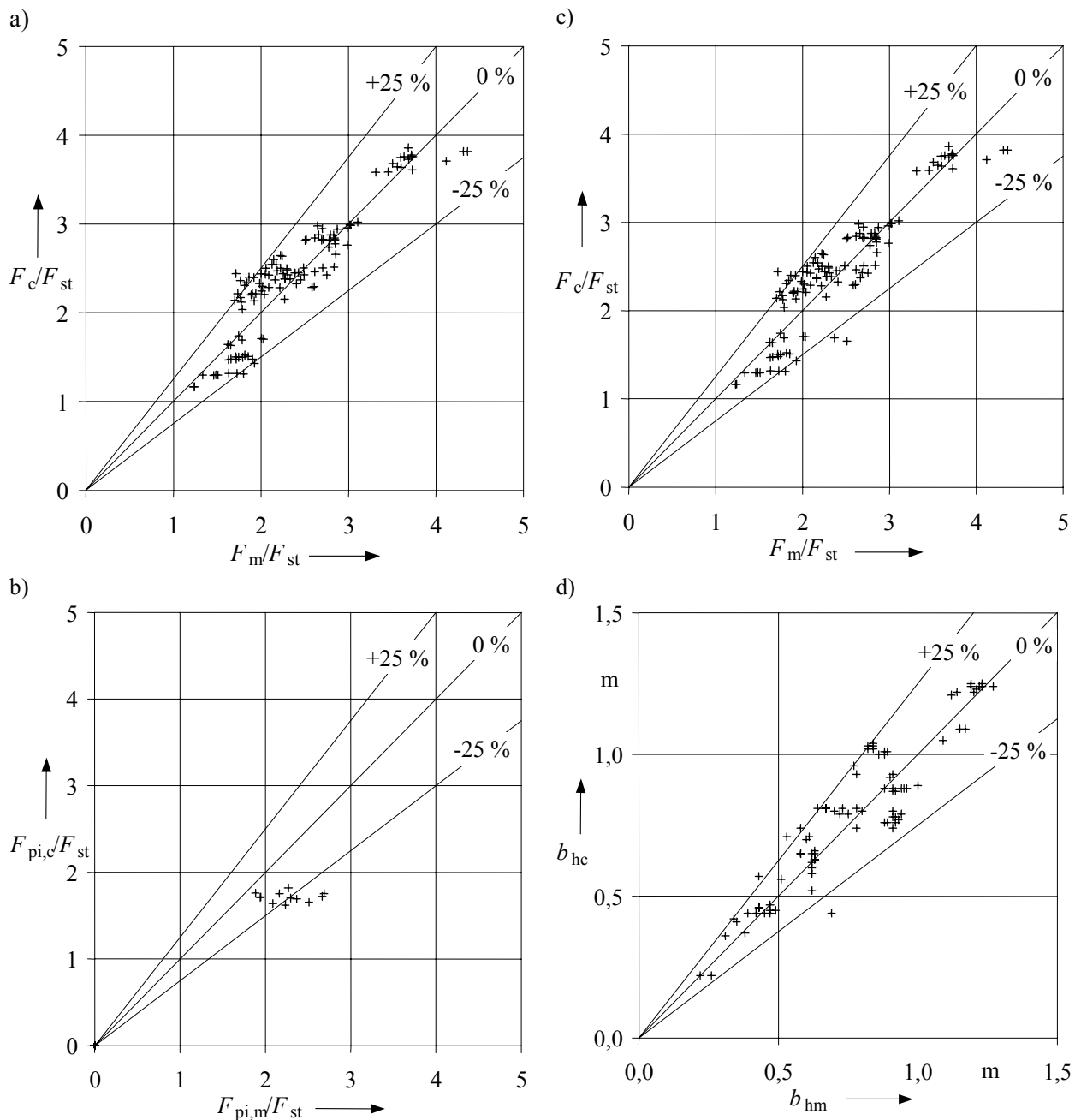


Figure 8.13: Cases *8

- a) Short-circuit forces: Maximum of F_t and F_f (118 tests)
- b) Pinch forces F_{pi} (12 tests)
- c) Short-circuit forces: Maximum of F_t , F_f and F_{pi}
- d) Horizontal displacements b_h (89 tests)

Cases *12 to *14 (ASEA 1976)

A 70-m-span with triple bundles is investigated. Because in case 12 the sub-conductors are in one plane, only F_t is compared in Figure 8.14a, whereas in cases 13 and 14 only the pinch is measured, Figure 8.14b.

Cases *9 to *11 (EDF 1990)

The span lengths are different: 34 m, 68 m and 102 m. Although the standard is restricted to span lengths ≤ 60

m, the method gives also good results for longer spans and permits the extension to spans >60 m.

The points below the -25 % line represent two tests with three-phase automatic reclosing; the standard gives forces which are too low, because this is not included; but using the sum of both short-circuit current durations as actual duration as proposed in paragraph 3.7.1, the calculation results in values with a very good agreement at the 0 %-line.

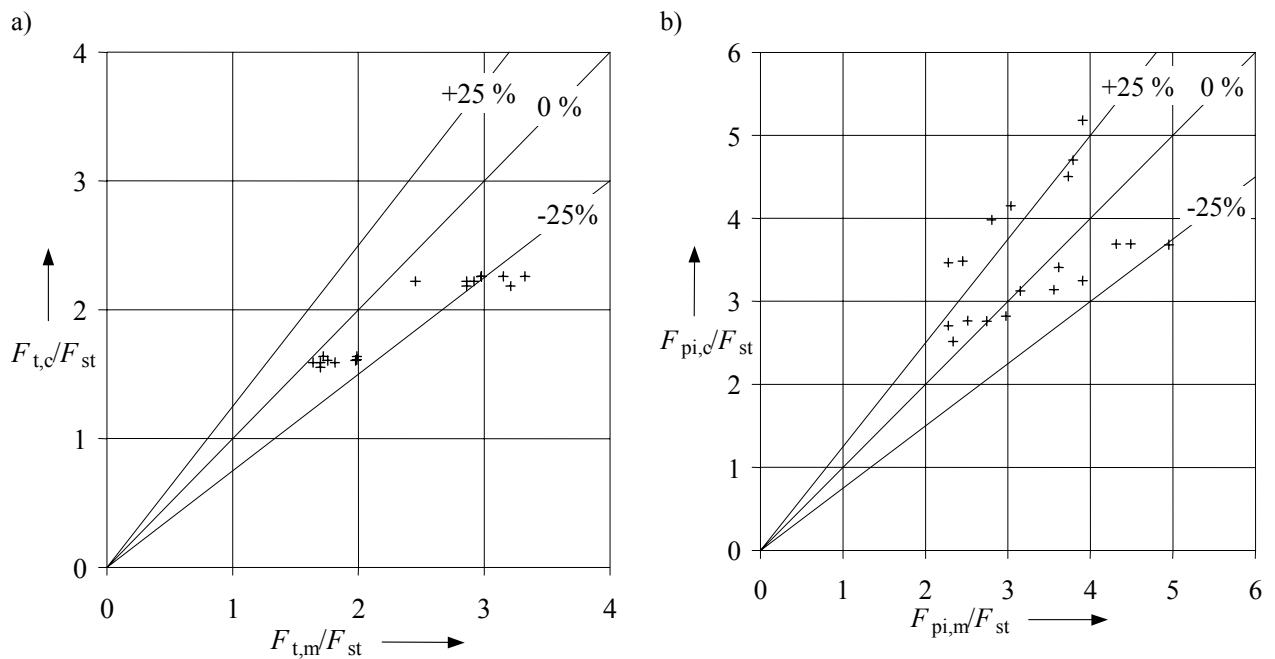


Figure 8.14: Cases *12 to *14
 a) Case *12: Short-circuit tensile force F_t (18 tests)
 b) Cases *13 and *14: Pinch force F_{pi} (19 tests)

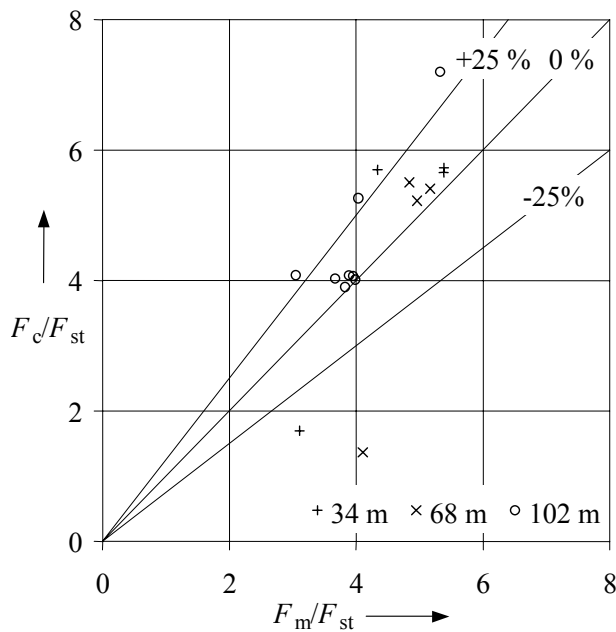


Figure 8.15: Cases *9 to *11: Short-circuit force Maximum of F_t and F_f
 Span lengths: 34 m (4 tests), 68 m (4 tests), 102 m (8 tests)

Cases *4 to *7 (Laborelec 1980).

There are droppers in the distance of 2,5 m and 5 m from the ends of the span, but through 88 % of the bus conductor the short-circuit current flows. The conductor in the west cable is able to swing out free, but the movement of the cable in the east is hindered by the droppers to ascend as high as the west cable. Nevertheless, these droppers are ignored.

In Cases *4 and *6, the conductor is Cu 324 mm², in Cases *5 and *7, it is Cu 105 mm².

In Figure 8.16a and Figure 8.17a, the forces are separately shown for west and east. In Figure 8.17a, the standard calculates higher drop forces because in the tests, the conductors have a considerable kinetic energy at the beginning of the fall.

In three tests, droppers are in midspan. Therefore the calculation is done according to paragraph 3.3. The results are shown in Figure 8.16a and Figure 8.17a.

The horizontal displacements are given in Figure 8.16b and Figure 8.17b without and with droppers in midspan.

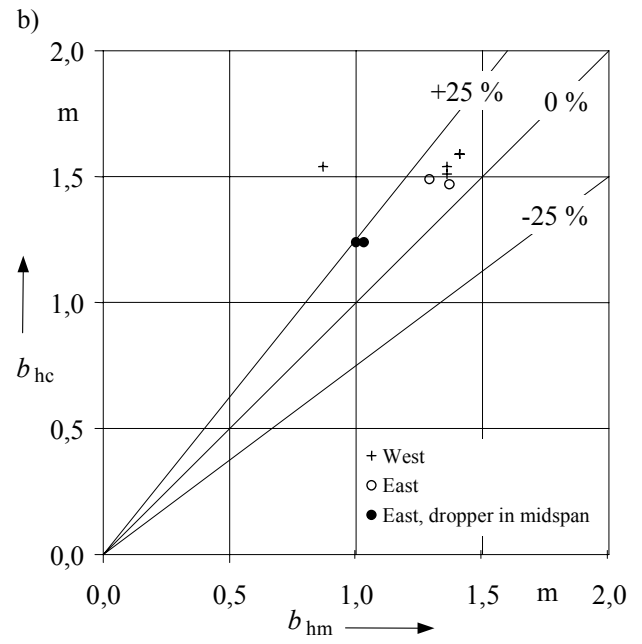
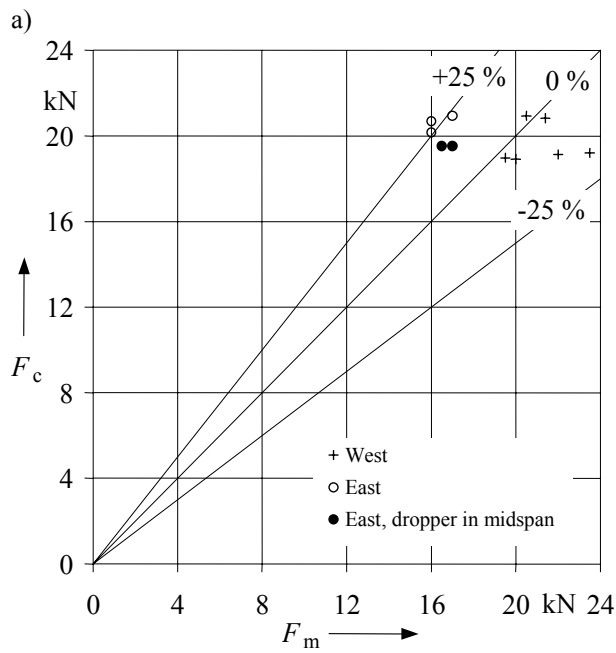


Figure 8.16: Cases *4 and *6: Cu 324 mm²
 a) Short-circuit force (10 tests)
 b) Horizontal displacement b_h (8 tests)

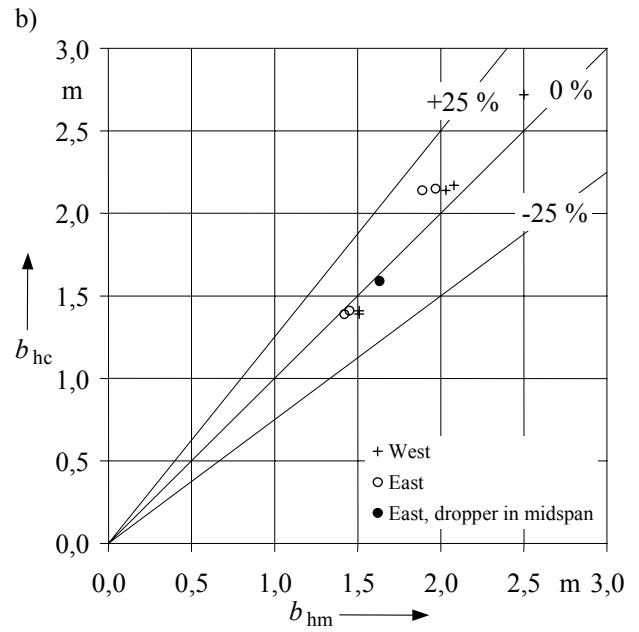
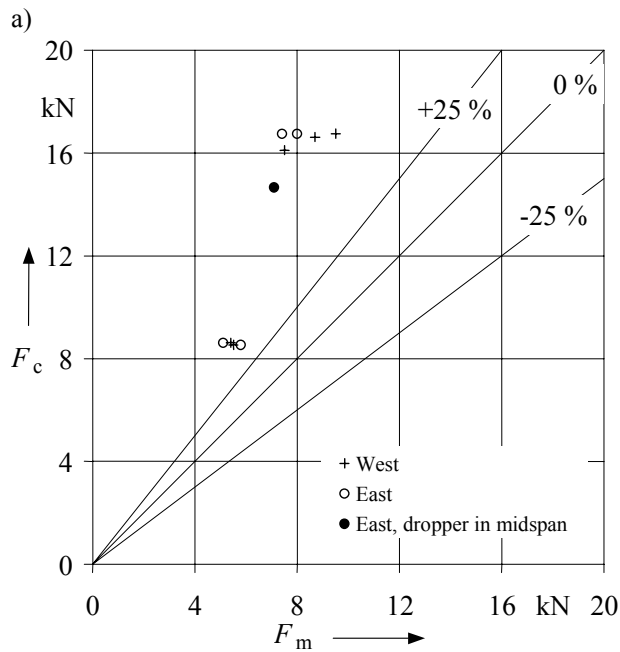


Figure 8.17: Cases *5 and *7: Cu 105 mm² (5 tests)
 a) Short-circuit force
 b) Horizontal displacement b_h

Cases 4 and 5 (FGH 1997)

Both cases have the same 40-m-span with droppers at midspan. Case 4 is a 100-kV- and case 5 a 400-kV-arrangement. The short-circuit current flows either

through the complete span and the droppers are without current (path B) or through half the span and through the droppers (path C). Reference is path A without droppers. The calculation is done using the method described in paragraph 3.3 and Figure 8.18 and Figure 8.19 give the results.

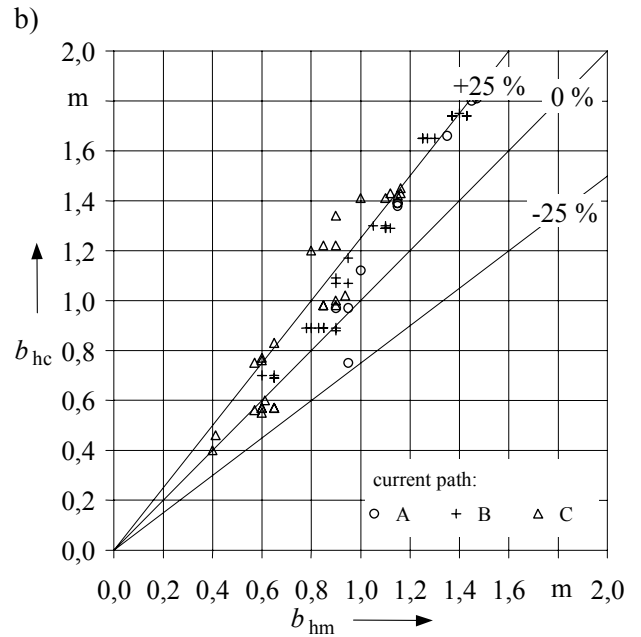
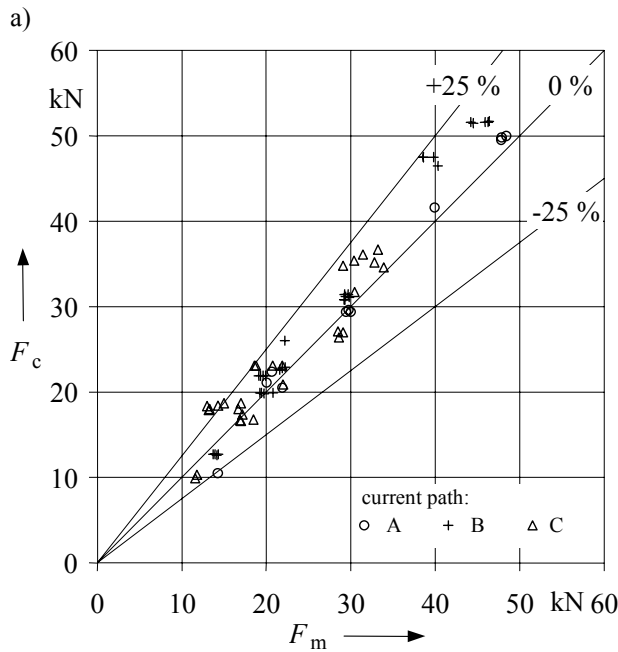


Figure 8.18: Case 4: 100-kV-bus (59 tests)

- a) Maximum of F_i and F_f
- b) Horizontal displacement b_h

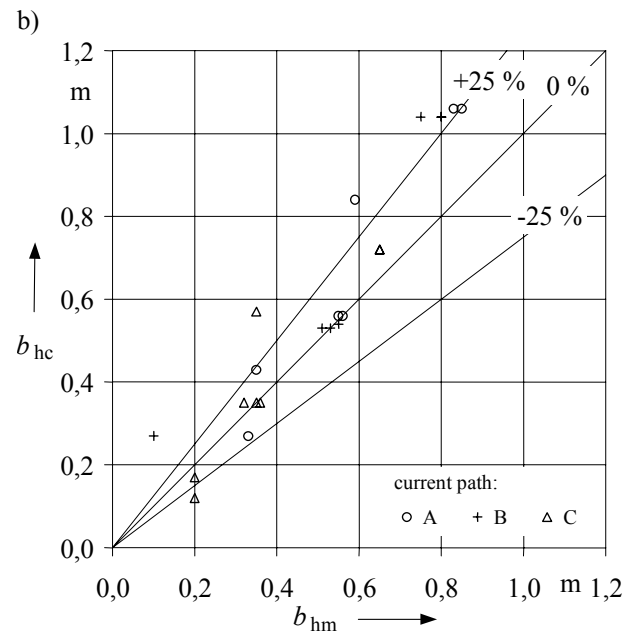
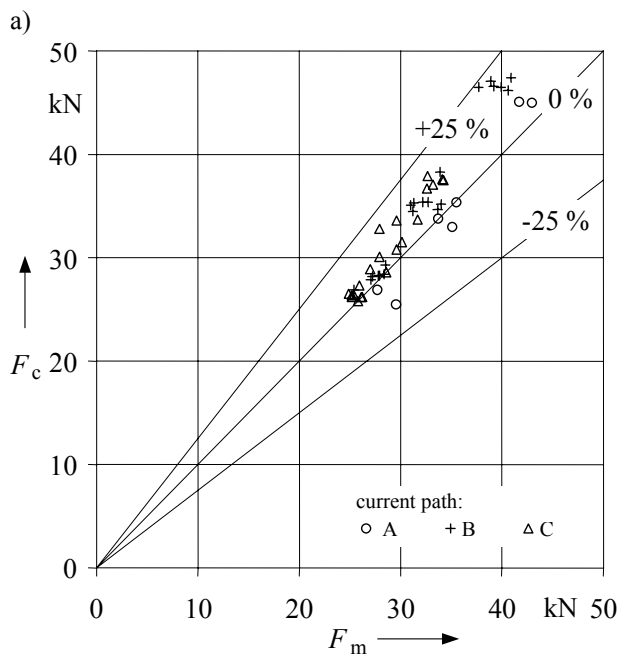
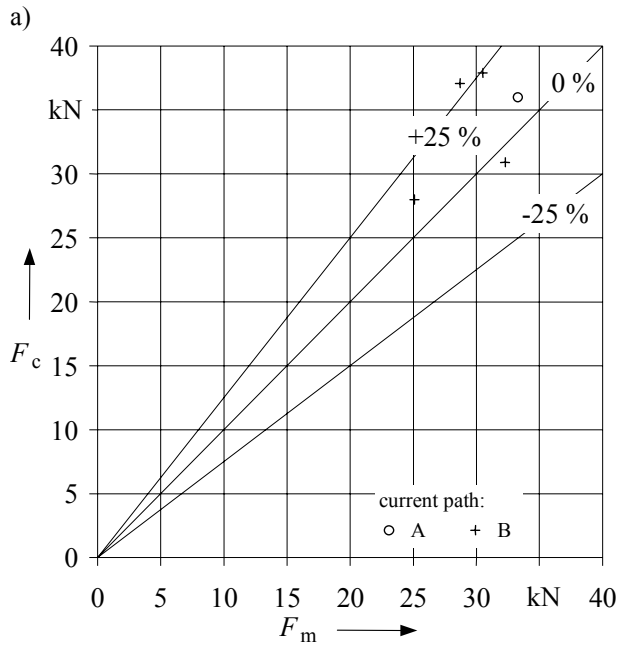


Figure 8.19: Case 5: 400-kV-bus

- a) Maximum of F_i and F_f (49 tests)
- b) Horizontal displacement b_h (20 tests)

Case *11 (EDF 1990)

This is the 102-m-span in Case *11 but with dropper in midspan. The short-circuit current flows through the complete span, path B is with dropper and path A the reference without dropper, see also [Ref 3]. The calculation is also done using the method described in paragraph 3.3. Figure 8.20 gives the results.



8.3.3. Bundle pinch effect

In cases 7 (University of Erlangen-Nürnberg 1985) and *16 (Furukawa 1966), only bundle pinch effect is measured. In case 7, a special test arrangement had been used with short span length and low static tensile forces, whereas in case *16 a 35-m-span with high static tensile force. For these very different test structures, sufficient accuracy is obtained in most tests, Figure 8.21 and Figure 8.22.

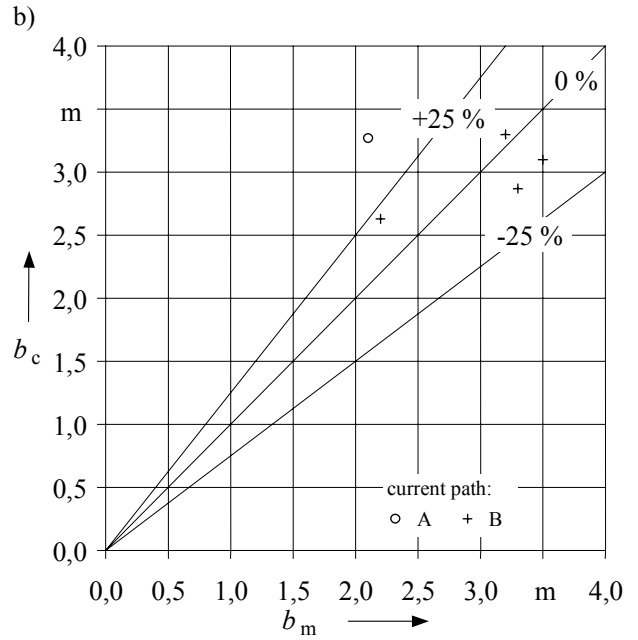


Figure 8.20: Case *11 (5 tests)

- a) Maximum of F_t and F_f
- b) Horizontal displacement b_h

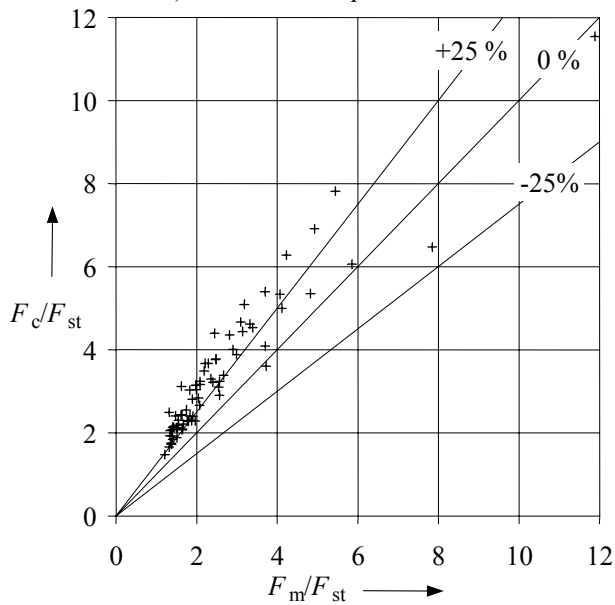


Figure 8.21: Case 7: Pinch force F_{pi} (73 tests)

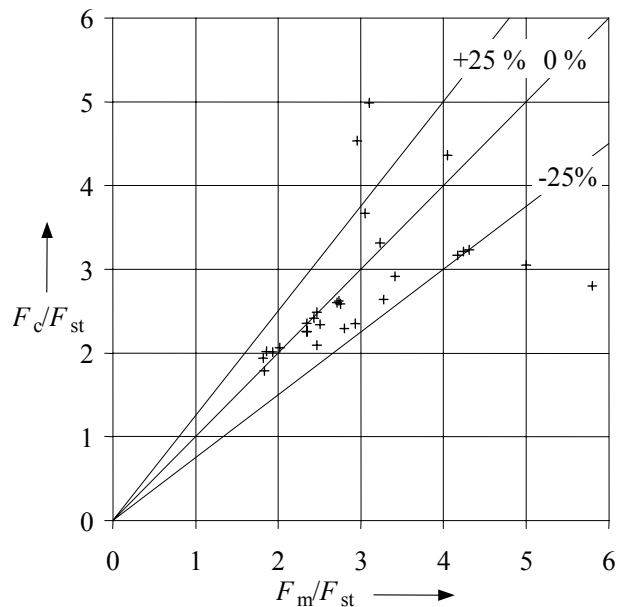


Figure 8.22: Case *16: Pinch force F_{pi} (29 tests)

8.3.4. *Conclusions*

For flexible conductors, the calculations according to the IEC Publication 60865-1 [Ref 2] and the European Standard EN 60865-1 [Ref 3] are compared with tests done in different laboratories. Most results lie in the range of $\pm 25\%$ and show a good agreement with the tests. Higher values evaluated by the standard can be traced back to effects which cannot be taken into account in the method, or that are not measured, whereas the worst case is calculated, or due to safety factors considered. Also, the extension on spans with droppers in midspan in paragraph 3.3 and on three phase automatic reclosing in paragraph 3.7.1 gives good results. Furthermore, the limitation of the method to span lengths ≤ 60 m is no longer necessary.

The confrontation confirms the validity of the simplified method stated in the standard for design purposes in substations.

8.4. INFLUENCE OF THE RECLOSURE

The following annex gives a simplified method without dropping after the first fault. The motion of the equivalent pendulum is on a circle.

After the first short-circuit

Let us examine the most simple case when: $\delta_m \leq \frac{\pi}{2}$

without dropping.

This connection can be done following two methods:

- chapter 4.2 (volume 1 of [Ref 1]) gives the maximum angle after the first short-circuit:

$$\delta_m = \arccos \chi.$$

- the IEC 60865 gives the following formula (*31).

This swing -out angle has been chosen to take into account the "worst case" which is a short-circuit duration less than or equal to the stated short-circuit duration Tkl.

At the end of dead time Tu, the angle of the pendulum is called δ_i . Its values :

$$\delta_i = \delta_m \cos\left(2\pi \frac{Tu}{T^0} + \alpha\right)$$

$$\delta_i = \delta_k \cos\left(2\pi \frac{Tu}{T^0}\right) + \frac{T^0 \cdot \delta'_k}{2\pi} \sin\left(2\pi \frac{Tu}{T^0}\right)$$

where $T^0 = \frac{2\pi \sqrt{\frac{0.8b_c}{g}}}{1 - \frac{\pi^2}{64} \left(\frac{\delta_m}{90}\right)^2}$ is the period of the free

motion (without current) and δ_m is the maximum swing-out angle (4.9 volume 1 of [Ref 1]).

The speed before the reclosure is given by :

$$\delta'_i = -\frac{2\pi}{T^0} \delta_k \cdot \sin\left(2\pi \frac{Tu}{T^0}\right) + \delta'_k \cdot \cos\left(2\pi \frac{Tu}{T^0}\right)$$

Let us consider the time $t_0 = -\frac{T^0 \alpha}{2\pi}$ for

which the δ angle is equal to δ_m . If Tu is higher than to t_0 , the angle δ is effectively equal to δ_m . If not done δ angle and subsequently δ_i is always lower than δ_m .

Linkage to the second short-circuit

During the second short-circuit, the movement is ruled by equation :

$$\frac{T^2}{4\pi^2} \delta'' = r_2 \cos(\delta) - \sin(\delta) = -\sqrt{1+r_2^2} \sin(\delta - \delta_{1,2})$$

in which r_2 is the ratio of LAPLACE force due to the second current I2 to gravitational force per unit length. The first range integral can be expressed by :

$$\frac{T^2}{8\pi^2} [\delta'^2 - \delta_i'^2] = r_2 \cdot \sin \delta + \cos \delta - r_2 \cdot \sin \delta_i - \cos \delta_i$$

leading to the relation :

$$\delta'^2 = \frac{8\pi^2}{T^2} \sqrt{1+r_2^2} [\cos(\delta - \delta_{1,2}) - \cos(\delta_i)]$$

with $\cos(\delta_i) = \frac{\chi_i}{\sqrt{1+r_2^2}}$ and χ_i parameter

defined by $r_2 \cdot \sin \delta_i + \chi_i$.

The period is given by :

$$T_{res2} = \frac{2\pi \sqrt{\frac{0.8b_c}{g}}}{\sqrt[4]{1+r_2^2} \left(1 - \frac{\pi^2}{64} \left(\frac{\delta_2}{90}\right)^2\right)}$$

At first approximation, the movement is given by :

$$\delta = \delta_{1,2} + \delta_2 \sin\left(2\pi \frac{t}{T_{res2}} + \varphi\right) =$$

$$\delta_{1,2} + (\delta_i - \delta_{1,2}) \cos\left(2\pi \frac{t}{T_{res2}}\right) +$$

$$\frac{T_{res2} \delta'_i}{2\pi} \sin\left(2\pi \frac{t}{T_{res2}}\right)$$

At the end of the short-circuit $t=T_{k2}$, the angle is $\delta_{k2} = \delta(T_{k2})$

The radial force during this short-circuit is given by the (4.11 in volume 1 of [Ref 1]) formula type which is transformed as follows :

$$\frac{R'}{G'} = 3 \cos(\delta) + 3 r_2 \sin(\delta) - 2\chi_i$$

Tension during the short-circuit

The mechanical tension given by this relation leads to the study of the following function :

$$y = 3 \cdot \cos \delta + 3 \cdot r_2 \cdot \sin \delta - 2\chi_i$$

since δ^2 is always positive, the following relation is true : $\cos \delta + r_2 \cdot \sin \delta \geq \chi_i$

The consequence is : $y \geq \chi_i$.

The maximum of the tension is reached when $\delta = \delta_{1,2}$. Effectively the derived value is equal to 0 for this value :

$$\frac{dy}{d\delta} = -3 \cdot \sin \delta + 3 \cdot r_2 \cdot \cos \delta = 0$$

$$\text{tg } \delta = r_2 \quad \delta = \delta_{1,2}$$

This maximum has a value :

$$y_M = 3 \cdot \sqrt{1 + r_2^2} - 2\chi_i$$

This maximum is reached for

$$t_1 = \text{Min}_k \left(\frac{T_{\text{res}2}}{2\pi} (k \cdot \pi - \varphi) \right)$$

if $\varphi < 0$ then $k = 0$ else $\varphi > 0$ $k = 1$

The variation of the tension between the starting position $y=1$ and this maximum is equal to :

$$\Delta y_M = y_M - y_0 = 3 \cdot \sqrt{1 + r_2^2} - 1 - 2 \cdot \chi_i \text{ If}$$

$$T_{k2} \geq t_1 \text{ then } \varphi_2 = \Delta y_M \text{ else}$$

$$T_{k2} < t_1 \quad \varphi_2 = \Delta y$$

with

$$\Delta y = 3 \cdot (\cos \delta_{k2} + r_2 \cdot \sin \delta_{k2}) - 2\chi_i - 1$$

The tension at anchoring points during this second short-circuit is given by the equation (*34). For the equation (*33), the influence of the heating due to the first short-circuit can also be analyzed.

Influence of the first-fault heating

In IEC 60865, the heating is not taken into account during the movement. The heating is used to estimate the distance between the two conductors (C_D).

But in case of a reclosure, it is necessary to understand the influence of the first-fault heating :

-in the state change equation for the tensile force during the second short-circuit.

-on the second short-circuit drop force.

The applied force during a short-circuit F_t to anchoring points is given by the relation (*34).

The equation for state changes allows calculation of tensions at anchoring points by the use of the formula of the IEC 60865, described in (*33).

The heating modifies this change state equation as following :

$$\varphi^3 \psi^3 + \varphi^2 (2 + \zeta + \zeta^*) \psi^2 + \varphi (1 + 2\zeta + 2\zeta^*) \psi$$

$$- \zeta (2 + \varphi) \varphi + \zeta^* = 0$$

$$\text{with } \zeta^* = \frac{\alpha \cdot \Delta \theta \cdot E \cdot s}{F_{st}}$$

The drop force can change with the heating . The IEC 60865 does not take into account this influence. It is also neglected here because this heating influence is very low.

Value of angle at the end of the second short-circuit.

$$\delta_{k2} = \delta_{1,2} + (\delta_i - \delta_{1,2}) \cos \left(2\pi \frac{T_{k2}}{T_{\text{res}2}} \right) +$$

$$\frac{T_{\text{res}2} \delta'_i}{2\pi} \sin \left(2\pi \frac{T_{k2}}{T_{\text{res}2}} \right)$$

$$\delta_{k2}'^2 = \frac{8\pi^2}{T^2} [r_2 \cdot \sin \delta_{k2} + \cos \delta_{k2} - \chi_i]$$

Free movement after the short-circuit

The equation (4.4 volume 1 of [Ref 1]) is the rule for the movement. Its first range linked with the above conditions leads to :

$$\delta'^2 = 2\omega^2 [\cos \delta + r_2 \cdot \sin \delta_{k2} - \chi_i]$$

The maximum angle δ_{m2} after the second short-circuit is given by :

$$\begin{aligned} \cos(\delta_{m2}) &= \chi_i - r_2 \cdot \sin \delta_{k2} \\ &= r_2 (\sin \delta_i - \sin \delta_{k2}) + \cos(\delta_m) \end{aligned}$$

Work of LAPLACE forces

Work of LAPLACE forces after the first short - circuit is given by :

$$\begin{aligned} T_{L1} &= Mg 0.8 b_c r \cdot \sin(\delta_k) \\ &= Mg 0.8 b_c (1 - \cos(\delta_m)) \end{aligned}$$

Work of LAPLACE forces after the second short - circuit is expressed by :

$$T_{L2} = Mg0.8b_c r_2 \cdot (\sin(\delta_{k2}) - \sin(\delta_i))$$

The whole work of LAPLACE forces after the second short - circuit is equal to :

$$T_{L1+2} = Mg0.8b_c \left(1 - \cos(\delta_m) + r_2 \cdot (\sin(\delta_{k2}) - \sin(\delta_i)) \right) \text{ which}$$

$$\text{means: } T_{L1+2} = Mg0.8b_c (1 - \cos(\delta_{m2}))$$

The whole work of LAPLACE forces has the same form after the second short-circuit.

Subsequently we can use again the relation (*35) :

$$F_{f2} = 1.2F_{st} \sqrt{1 + 8\zeta \frac{\delta_{m2}}{\pi}}$$

8.5. EXAMPLE OF RECLOSURE CALCULATION

The case 9 EDF tests in the CIGRE brochure 105 concerns two spans of 34 and 68 m using 1 x ASTER (570 mm²) cable per phase. The reclosure cycle is :Tk1=85ms / Tu=2s / Tk2=95 ms.

The short-circuit current pattern are illustrated in Figure 9.1 (volume 2). The main characteristics of short circuit current are the following : two-phase short-circuit current of $I_{k2}=30\text{kA}$, time constant of 81ms, maximum asymmetry.

The test arrangement are illustrated in Figure named « Configuration for case 9 to 11 »-volume 2: distance between conductors: a=4.75 m, linear weight of cables: $m'_s=1.574\text{ kg/m}$, cable Young's modulus: $E=5.4\text{e}10\text{ N/m}^2$, sag at mid span at 45°C: 3% corresponding to $F_{st}=5740\text{ N}$. $l_c/l=96\%$, span $l=68\text{ m}$.

IEC 60865 : THE FIRST FAULT CALCULATION

The main parameters are the following : $F=36.4\text{ N/m}$; $r_1=2.356$; $\delta_1=67^\circ$; $bc=1.55\text{m}$; $T_{res}=1.53\text{s}$; $\delta_k=4.05^\circ$; $\chi=0.834$; $\delta_m=41.9^\circ$; $\varphi=0.49$; $E_s=2.79\text{e}10\text{ N/m}^2$; $N=7.67\text{e}-8\text{ N}^{-1}$; $\zeta=3.165$; $\psi=0.823$; $F_{t1}=8060\text{N}$; $F_{f1}=18083\text{N}$;

RECLOSURE EFFECT CALCULATIONS

Radial speed at the end of the first short-circuit : $\delta'_k=92.1^\circ/\text{s}$

Maximum swing out angle : $\delta_m = \arccos(\chi)=33.5^\circ$

Swinging period : $T^\circ=2.286\text{ s}$

Angle at the end of dead time : $\delta_1 = -20.9^\circ$

Radial speed at the end of dead time : $\delta'_1=69.8^\circ/\text{s}$

LAPLACE force of the second short circuit : $F_2=36.4\text{ N/m}$

Ratio of F2 to gravity : $r_2=2.356$

Angular direction of the force :

$$\delta_{1,2} = \text{artg}(r_2)=67^\circ$$

Quantity for the maximum swing out angle

$$\chi_i = r_2 \cdot \sin \delta_i + \chi = -0.005$$

Angle δ_2 of the second short-circuit :

$$\delta_2 = \arccos\left(\frac{\chi_i}{\sqrt{1+r_2^2}}\right) = 90.1^\circ$$

Resulting period of conductor swinging during the second short-circuit :

$$T_{res2} = 1.71\text{s}$$

Radial speed at the end of the second short-circuit :

$$\delta_{k2} = -9.1^\circ$$

Maximum fist time of the second short-circuit :

$$t_{1,1} = \frac{T_{res2}}{2\pi} \arcsin\left(\frac{\delta_i - \delta_{1,2}}{\delta_2}\right) = 0.367\text{s}$$

Factors φ for tensile force of the second short-circuit : 0.859

Actual young modulus : $2.796\text{e}10\text{N/m}^2$

$$\text{Stiffness norm } N = \frac{1}{E_s} + \frac{1}{S_a} = 7.67\text{e}-8\text{ N}^{-1}$$

Stress factor $\zeta = 3.165$

Factor ψ at the second short-circuit : 0.798

Tensile force during the second short-circuit : Ft2=9676N

Maximum swing-out angle at the second short-circuit

$$\delta_{m2} = \arccos(\chi_i - r_2 \cdot \sin(\delta_{k2})) = 68.5^\circ$$

Drop force at the second short-circuit : Ff2=22469N

IEC 60865 Calculations

If the clearance time is taken equal $T_k = T_{k1} + T_{k2} = 0.175$ s, IEC standard calculations give the following values : **$F_t = 13816\text{N}$, $F_f = 24235\text{N}$**

span 68 m	IEC 865	Appendix 1	tests
F_t N	13816	9676	11432
F_f N	24235	22469	22051

Table 8.2 : Comparisons between tests and calculations

8.6. FLOW CHARTS TO THE STANDARDISED METHOD FOR RIGID BUSBARS

In paragraph 2.2, the formulas are listed and the background is described for the estimation of the short-circuit strength of busbars with rigid conductors according to the standard IEC/EN 60865-1 [Ref 2], [Ref 3]. For better clearness, the flow charts of the procedure are performed in this chapter with and without calculating the relevant frequencies.

The flow charts are divided in several parts to show the foregoing for single main conductors as well as for main conductors consisting of sub-conductors.

In the statements, the equations [...], figures [F...] and tables [T...] of the standard are cited. 'reclosing' means three-phase automatic reclosing.

The statements are to execute in the given order. They are suitable for three-phase systems as well as for single-phase two-line systems; at this F_m is either F_{m3} or F_{m2} .

For the yield point of conductor materials the actual values should be used. If only minimum and maximum values are available, $R_{p0,2}$ is the minimum value and $R'_{p0,2}$ the maximum value.

If there is no three-phase automatic reclosing used in the network,

- with calculation of the conductor frequencies the parts a) to e)
- without calculation of the conductor frequencies the parts a) to d)

are to be passed and the calculation is finished when reaching END 1.

If three-phase automatic reclosing is used in the system, there is a first short-circuit current flow, a dead time and after this a second short-circuit current flow if the reclosing is unsuccessful which has to be taken into account for short-circuit withstand. Determining according to the standard, the conductor stresses and the forces on the support are calculated during the second short-circuit current flow. In this case,

- with calculation of the conductor frequencies the parts a), b), c), f) and g)
- without calculation of the conductor frequencies the parts a), b), e) and f)

are to be passed with neglect of the statements in the dotted boxes. The calculation is finished when reaching END 2.

In paragraph 2.2.3 it is shown that the conductor stresses are greater in the second current flow according to Table 2 of the standard and can be greater according to Figures 4 and 5 of the standard with relevant frequencies. This can cause higher forces on the supports during the first current flow. Therefore it is recommended to follow the complete flow chart including the statements in the dotted boxes which compare the forces at the supports during the first and second current flow:

- if $V_F V_r > 1$ and $V_F > 1$ follows from Figures 4 and 5 of the standard with calculation of the conductor frequencies,
- and always without calculation of the conductor frequencies.

In the flow chart, four flags STOP 1 to STOP 4 are included. When they are reached, the stresses in the conductors is too high and modifications in design are necessary:

STOP 1: The sub-conductors do not withstand. Either the distance between two adjacent spacers is too large or the sub-conductors are too small.

STOP 2: The main conductors do not withstand. Either the distance between two adjacent supports is too large or the main conductors are too small.

STOP 3: The sub-conductors do not withstand in the case of three-phase automatic reclosing. Either the distance between two adjacent spacers is too large or the sub-conductors are too small.

STOP 4: The main conductors do not withstand in the case of three-phase automatic reclosing. Either the distance between two adjacent supports is too large or the main conductors are too small.

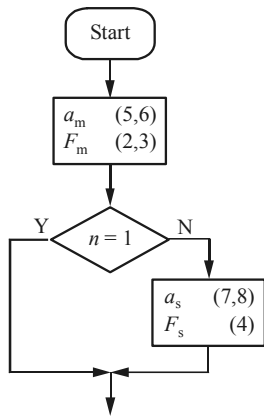
For better design, it is recommended to do the calculation always considering the relevant frequencies of the conductors especially in the case of HV- and UHV-busbars which have low frequencies.

In the following, the flow charts are given for the determination of the short-circuit stresses and forces with and without calculating the relevant conductor frequencies:

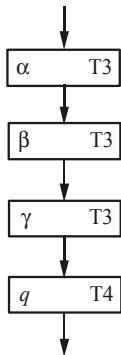
8.6.1.1 *With calculation of the relevant frequencies*

The calculation has to be done in the following steps:

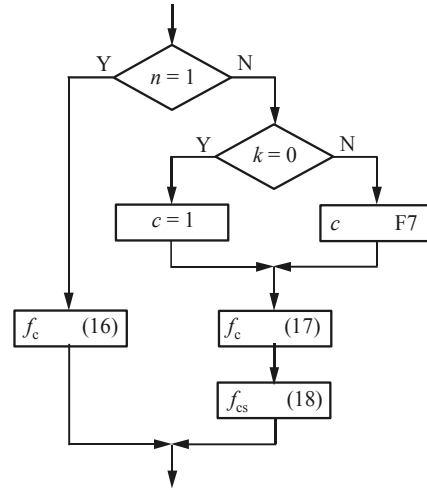
- a) Calculation of the short-circuit current forces between the main conductors and between the sub-conductors:



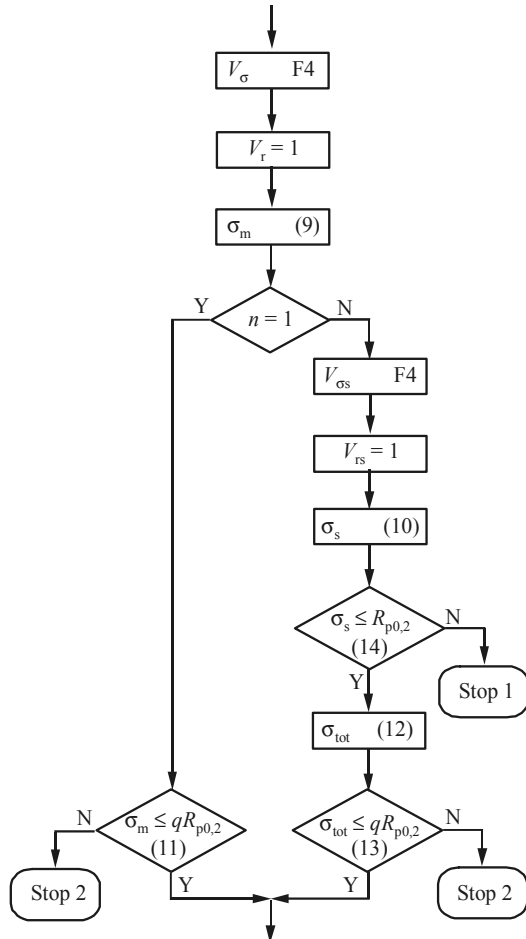
- b) Make available the factors α , β , γ and q :



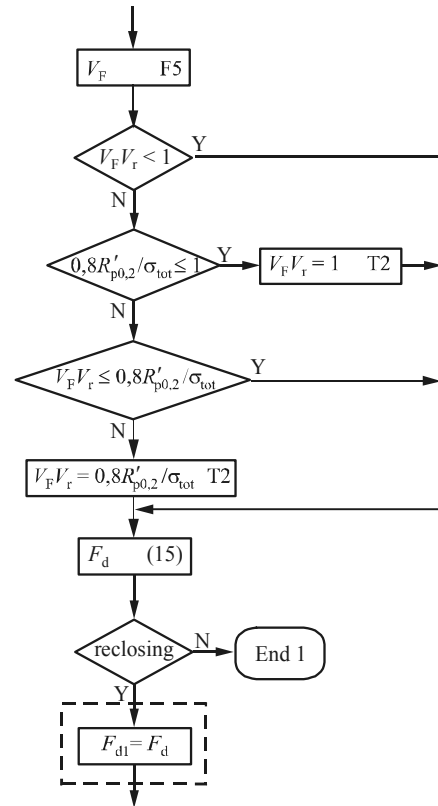
- c) Calculation of the relevant natural frequencies of main conductors and sub-conductors:



d) Calculation of the stresses due to the forces between the main conductors and due to the forces between the sub-conductors; check of the short-circuit withstand of main conductors and sub-conductors:

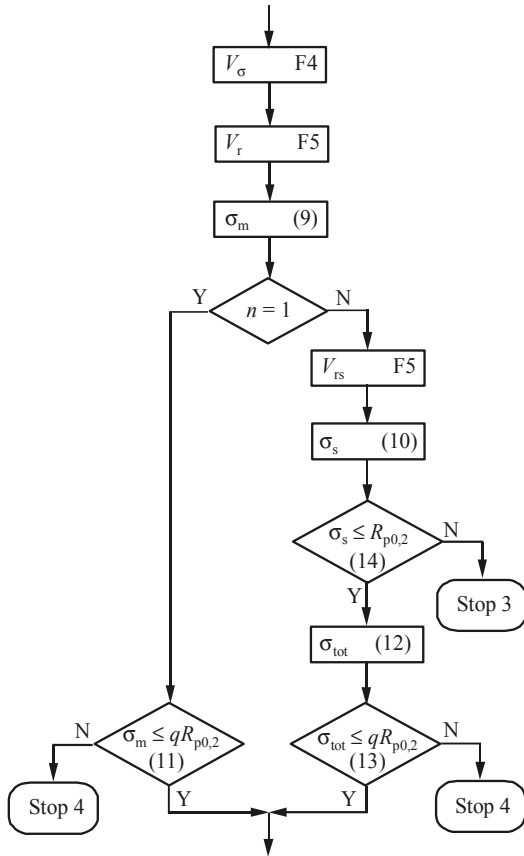


e) Determination of the forces at the supports:

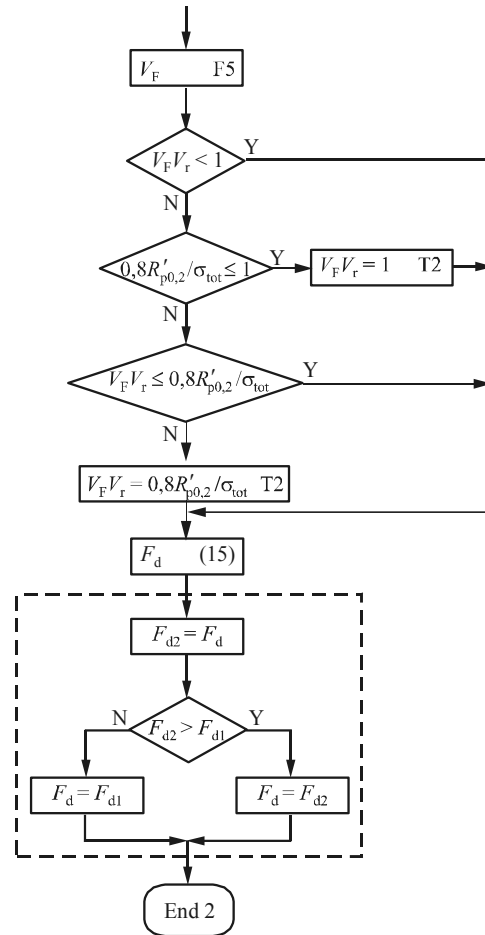


In case of a single conductor, σ_{tot} is to be replaced by σ_m .

f) Calculation of the stresses due to the forces between the main conductors and between the sub-conductors during the second short-circuit current flow; check of the short-circuit withstand of main conductors and sub-conductors:



g) Determination of the forces at the supports during the second short-circuit current flow and estimation of the design load:

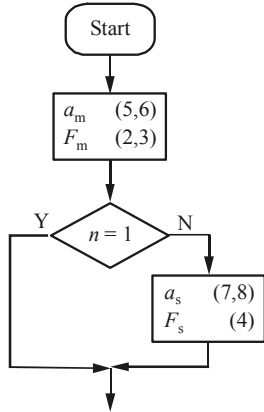


In case of a single conductor, σ_{tot} is to be replaced by σ_m .

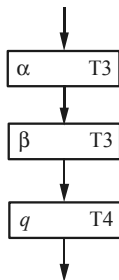
8.6.1.2 *Without calculation of the relevant frequencies.*

Without consideration of the relevant frequencies, the calculation is carried out using the maximum possible values according to Table 2 of the standard.

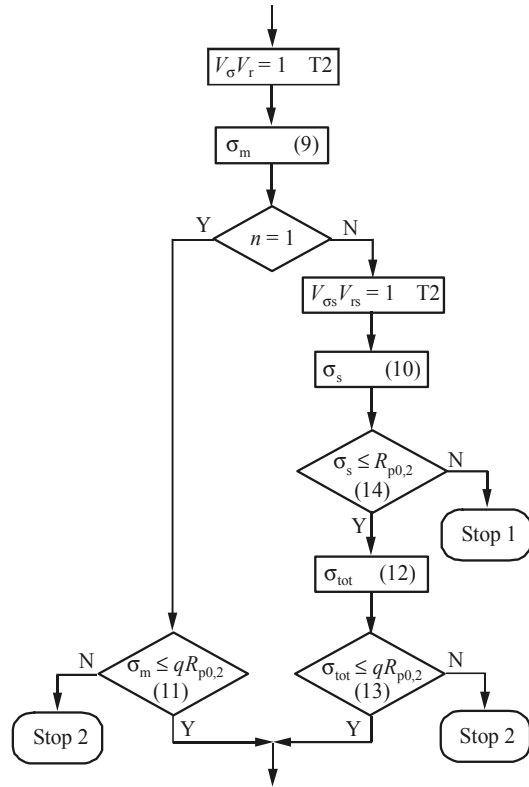
- a) Calculation of the short-circuit current forces between the main conductors and between the sub-conductors:



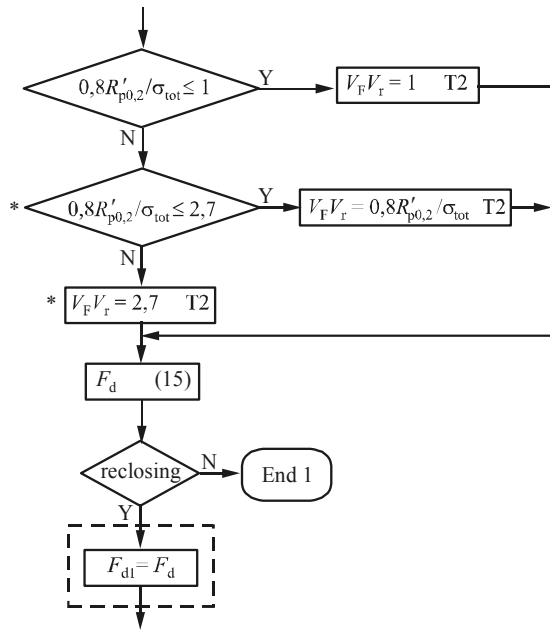
- b) Make available the factors α , β , and q :



- c) Calculation of the stresses due to the forces between the main conductors and due to the forces between the sub-conductors; check of the short-circuit withstand of main conductors and sub-conductors:



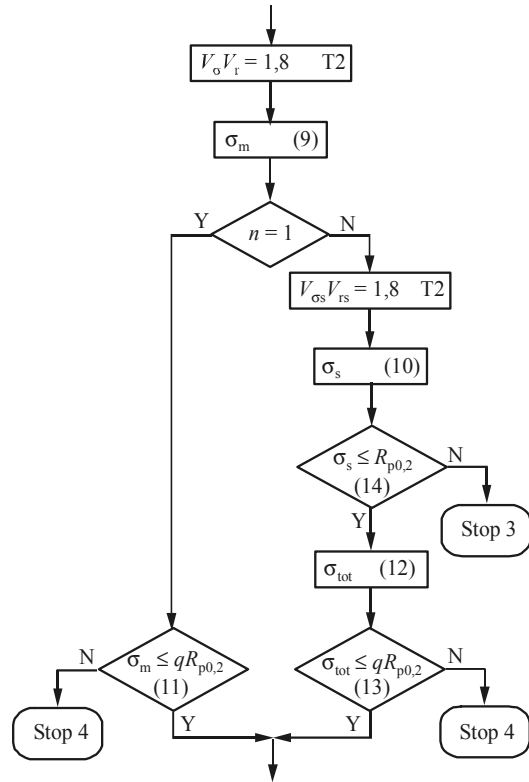
d) Determination of the forces at the supports using Table 2 of the standard:



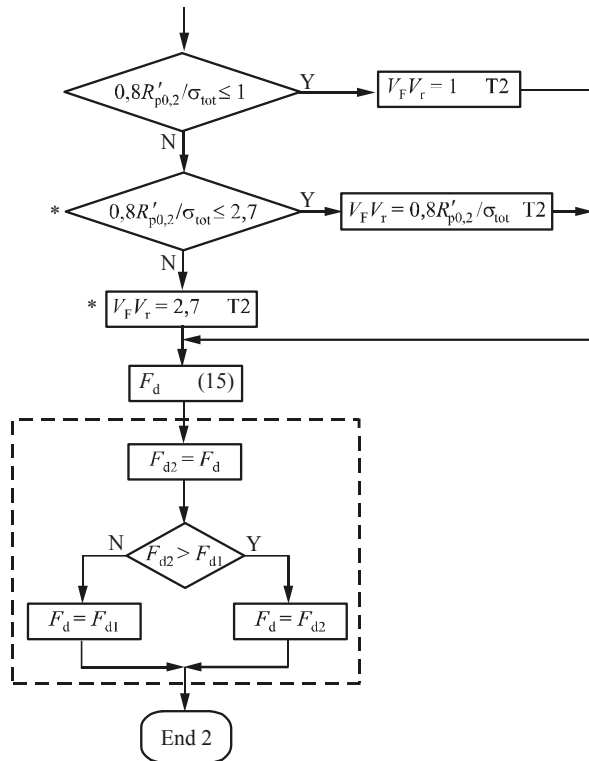
In case of a single conductor, σ_{tot} is to be replaced by σ_m .

* for short-circuit in single-phase systems, 2,7 is to be replaced by 2,0

e) Calculation of the stress due to the forces between the main conductors and between the sub-conductors during second short-circuit current flow; check of the short-circuit withstand of main and sub-conductors:



f) Determination of the forces at the supports during the second short-circuit current flow using Table 2 of the standard and estimation of the design load:



In case of a single conductor, σ_{tot} is to be replaced by σ_m .

* for short-circuit in single-phase systems, 2,7 is to be replaced by 2,0

8.7. ERRATA TO BROCHURE NO 105

In Volume 1 of the Brochure No 105
THE MECHANICAL EFFECTS OF
SHORT-CIRCUIT CURRENTS
IN OPEN AIR SUBSTATIONS
(Rigid and Flexible Bus-Bars)

April 1996

misprints were detected and the reader is asked to correct them as follows:

Section 3.4.1, p 30, right column:

In the para following equation (3.12), replace
and $q = 1,7$

by

$q = 1,7$ and

Section 4.2.5, p 42, right column:

In the para following equation (4.15), replace
(4.13)

by

(4.15)

Section 4.2.6, p 43, right column:

Replace equation number
(4.10)

by

(4.17)

In the next para, replace

with (4.14)

by

above

Section 4.3.2.1, p 46, right column:

In equation (*43), replace

$l_s \leq 50 a_s$

by

$l_s \geq 50 a_s$

In equation (*44), replace

$l_s \leq 70 a_s$

by

$l_s \geq 70 a_s$

Section 4.3.2.2-4.3.2.6, pp 47-52:

Renumber equations

(4.11) to (4.32) respectively

by

(4.18) to (4.39) respectively

[shift by 7].

In accordance, the references in these subsections are to be replaced by the changed numbers

Section 4.3.2.3, p 49, right column:

Replace equation number

(*A.5)

by

(*A.6)

Section 4.5.1, p 55, right column:

Replace equation number

(4.3)

by

(*19)

Section 4.5.1, p 56, left column:

Replace equation number

(4.33)

by

(4.40)

and equation number

(4.34)

by

(4.41)

Section 4.5.1, p 56, right column:

In the first equation, replace equation number

(4.35)

by

(4.42)

In the equation following equation (*25), replace equation number

(4.35)

by

(4.43)

Replace equation number

(4.28)

by

(4.44)

and equation number

(4.36)

by

(4.45)

In the para following equation (4.43), replace
15 and 300

by

0.4 and 8

Section 5.3.1, p 72, right column:

In the last para, replace

1.35 – 1.5

by

1.3 – 1.7

and

[39]

by

[107], see also section 3.4.1

Section 5.3.1, p 73, left column:

In the last para, replace

formula 4.2.6

by

formula (*34) in section 4.2.4,
see also section 4.3.3

Section 5.3.2, p 74, right column:

Delete the para

On the other hand ... calculation methods.

Section 5.3.2, p 75, right column:

In the second para, delete

(section 5.3)

CIGRE Study Committee 23 (Substations)
Working Group 23-03
ESCC Task Force (Effects of short-circuit currents)

**The Mechanical Effects of Short-Circuit Currents
in Open Air Substations
(Rigid and Flexible Bus-Bars)**

Volume 2:

Data Base of Reference Tests

September 2002

TABLE OF CONTENT

PREFACE	3
I . ARRANGEMENTS WITH SINGLE AND BUNDLED SLACK CONDUCTORS	4
CASE 1	5
Tests performed at FGH (Germany) in 1972 cross section: Al 240 mm ² and ACSR 537/53 mm ² twin bundle ($n = 2$) short-circuit current: 20 kA (52 kA peak) and 30 kA (78 kA peak) span length: 15 m, 10 m and 7 m	
CONFIGURATION FOR CASES 2 AND 3	11
Tests performed at FGH (Germany) in 1978 short-circuit current: 10 kA (26 kA peak) to 40 kA (104 kA peak) span length: 15 m and 4 m	
CASE 2	12
cross section: ACSR 120/20 mm ² , ACSR 537/53 mm ² and ACSR 1055/45 mm ² , single conductor	
CASE 3	18
cross section: ACSR 537/53 mm ² and ACSR 1055/45 mm ² , two and four sub-conductors	
II . ARRANGEMENTS WITH STRAINED CONDUCTORS AND DROPPERS IN MIDSPAN	27
CONFIGURATION FOR CASES 4 AND 5	28
Tests performed at FGH (Germany) in 1997 cross section: 537/53 mm ² short-circuit: 20 kA (50 kA peak) and 40 kA (100 kA peak) span length: 40 m	
CASE 4	31
CASE 5	42
III . CONDUCTOR PINCH EFFECTS	47
CASE 6	49
Tests performed at Österreichische Elektrizitätswirtschafts-AG (Austria) in 1963 cross section: ACSR 537/53 mm ² twin bundle ($n = 2$) short-circuit current: 4 kA eff to 21,5 kA eff span length: 12 m	
CASE 7	52
Tests performed at Lehrstuhl für Elektrische Energieversorgung (Germany) in 1985 cross section: ACSR 340/30 mm ² and ACSR 605/70 mm ² twin bundle ($n = 2$) short-circuit current: 3,5 kA eff to 11 kA eff span length: 7,6 m	
CASE 8	56
Tests performed at VEIKI Laboratories (Hungary) in 1997 cross section: CONDOR 455, twin bundle ($n = 2$) short-circuit current: 35 kA eff and 48 kA eff span length: 60 m	

PREFACE

Because of the very high complexity of the mechanical effects in substations caused by short-circuit currents, a great number of short-circuit tests have been conducted by many companies. The aim was

- to learn about the physical phenomena,
- to test installation hardware,
- to verify the calculation with Finite-Element or Finite-Differences Programs,
- to develop simplified methods for calculation of forces and stresses.

Test results are the only basis for the evaluation and the use of advanced calculation approaches as well as simplified methods. On the other hand, calculation methods unhide the effects and relations between different causes and define new test directions which need to be carried out. The importance of tests has more weight due to the nonlinear character of the phenomena. Any extrapolation or generalisation of previously obtained results needs further checking.

Evaluation of the structural response due to the short-circuit dynamic loading is one of the aims of studies. Nowadays there is no particular problem in the case of advanced methods but for simplified methods due to the multifrequency character of the systems, the spectrum density techniques are the most suitable for describing loadings, and transfer functions are the most compatible description for the response of the structure. Tests results are the only option to obtain practical data to build up acceptable models of transfer functions for calculation approaches.

In Volume 2 of [1] a data base with reference tests is published. It consists of 18 different cases of arrangements with rigid busbars as well as flexible conductors done in international test laboratories. In this brochure, the presentation of tests is continued. Results of tests with flexible conductors are described in eight cases.

- three cases concerning arrangements with single and bundled slack conductors,
- two cases concerning strain conductors with droppers in midspan
- and three cases where only conductor pinch effects are studied.

Tests have been performed in Forschungsgemeinschaft für Elektrische Anlagen und Stromwirtschaft FGH, Mannheim (Germany), Österreichische Elektrizitätswirtschafts AG, Wien (Austria), Lehrstuhl für Elektrische Energieversorgung, Erlangen (Germany), VEIKI Laboratory, Budapest (Hungary).

All reference cases are divided in three parts:

- bus-bar geometry
- basic data
- results

Reference:

- [1] CIGRE SC 23-11/IEC TC 73: The mechanical effects of short-circuit currents in open air substations (Rigid and flexible bus-bars). Volume 2: Data base of reference tests. Paris: CIGRE, 1996.

PART I

Arrangements with single and bundled slack conductors

1. CASE 1

Tests performed at FGH (Germany) in 1972

cross section: Al 240 mm² and ACSR 537/53 mm² twin bundle ($n = 2$)

short-circuit current: 20 kA (52 kA peak) and 30 kA (78 kA peak)

span length: 15 m, 10 m and 7 m

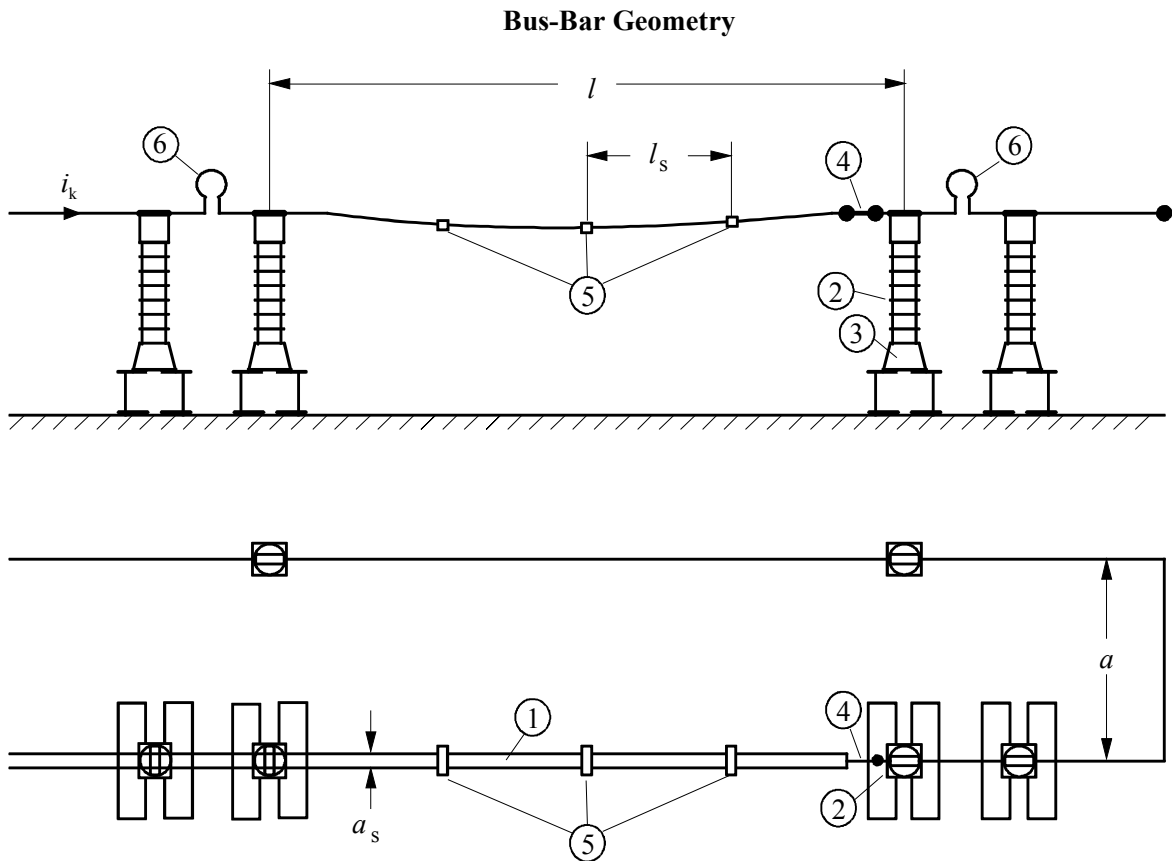


Figure 1.1: Test set-up

- 1 bundle conductor under test
 - 2 post insulator
 - 3 strain gage for measuring the forces at the bottom of the insulator
 - 4 strain gage for measuring the forces on the top of the insulator
 - 5 spacers (in the figure three)
 - 6 flexible connection
-
- l span length
 - l_s centre-line distance between spacers
 - a centre-line distance between main-conductors
 - a_s centre-line distance between sub-conductors
 - k number of spacers

Aim of the tests is to define conditions for a_s/d_s and l_s/a_s where the sub-conductors clash effectively and the pinch force F_{pi} becomes not higher than $1,1 F_t$; F_t is the swing-out maximum of a single conductor with the same cross-section and material properties as both sub-conductors.

Basic data

Conductors:

	cross-section	diameter	mass per unit length	Young's modulus	temperature coefficient
	A	d	m'	E	α_θ
	mm ²	mm	kg/m	N/mm ²	10 ⁻⁶ /K
Al 240	242,5	0,670	20,3	55000	23,0
ACSR 537/53	590	1,937	32	69000	19,8

bundle configuration: twin bundle ($n = 2$)

number of spacers: 0 ... 12

centre-line distance between subconductors: 45 mm ... 100 mm

centre-line distance between main-conductors: $a = 4$ m

eigenfrequency of the supports: 58 Hz

spring coefficient of both supports: $l = 15$ m: 730 N/mm
 $l = 10$ m and 7 m: 630 N/mm

initial static stress: 0,55 ... 3,3 kN/mm²

short-circuit characteristics: $\kappa = 1,85$ ($\tau = 55$ ms)

short-circuit duration: $T_k = 0,6$ s

Results

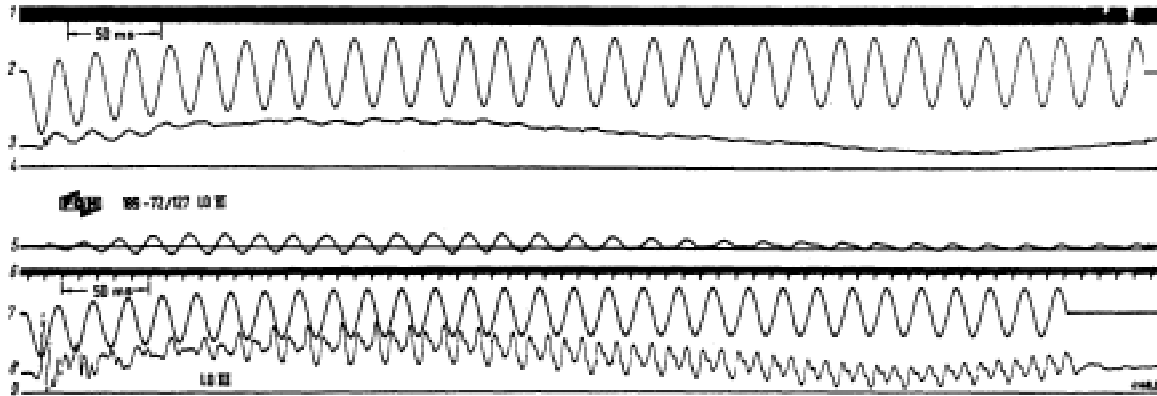


Figure 1.2: Oscillogram of short-circuit test with twin-bundle $l = 15$ m, ACSR 537/53, $a_s = 60$ mm, $k = 3$

- | | |
|------|---|
| 1, 6 | Time traces |
| 2, 7 | Current: $I_k = 30$ kA; $i_p = 78,3$ kA; $t_k = 0,6$ s |
| 3, 5 | Insulator stresses: in direction (3) of conductor 6,45 kN; at right angles (5) to conductor 1,45 kN; initial static tensile force 2,65 kN |
| 8 | Conductor tensile force: 9,5 kN after 0,1 s |
| 4, 9 | Zero line for curve 3 and for curve 8 |

The recordings of the tests were stopped a few milliseconds after the end of the short-circuit current flow, therefore no fall of span is recorded.

At the bottom of the insulator, the strain is measured and an equivalent static load is calculated which acts on the top of the insulator and leads to the same dynamic stresses. This equivalent static load is given in the diagrams below as function of the number of spacers. Parameters are the centre-line distance of the sub-conductors, the short-circuit current and the initial static tensile force.

The tests show, that the tensile force due to pinch effect is not higher than $1,1 F_t$ if one of the conditions

$$a_s/d_s \leq 2,0 \text{ and } l_s/a_s \geq 50$$

or

$$a_s/d_s \leq 2,5 \text{ and } l_s/a_s \geq 70$$

is fulfilled. In this case, the conductors clash effectively and the pinch force F_{pi} can be ignored in contrast to F_t . F_t is the swing-out maximum of an equivalent single conductor. With this, the tensile force at the top of the insulators is not greater than $1,5 F_t$. If the conductors do not clash effectively the forces on the top can be higher; but its impulse length is short.

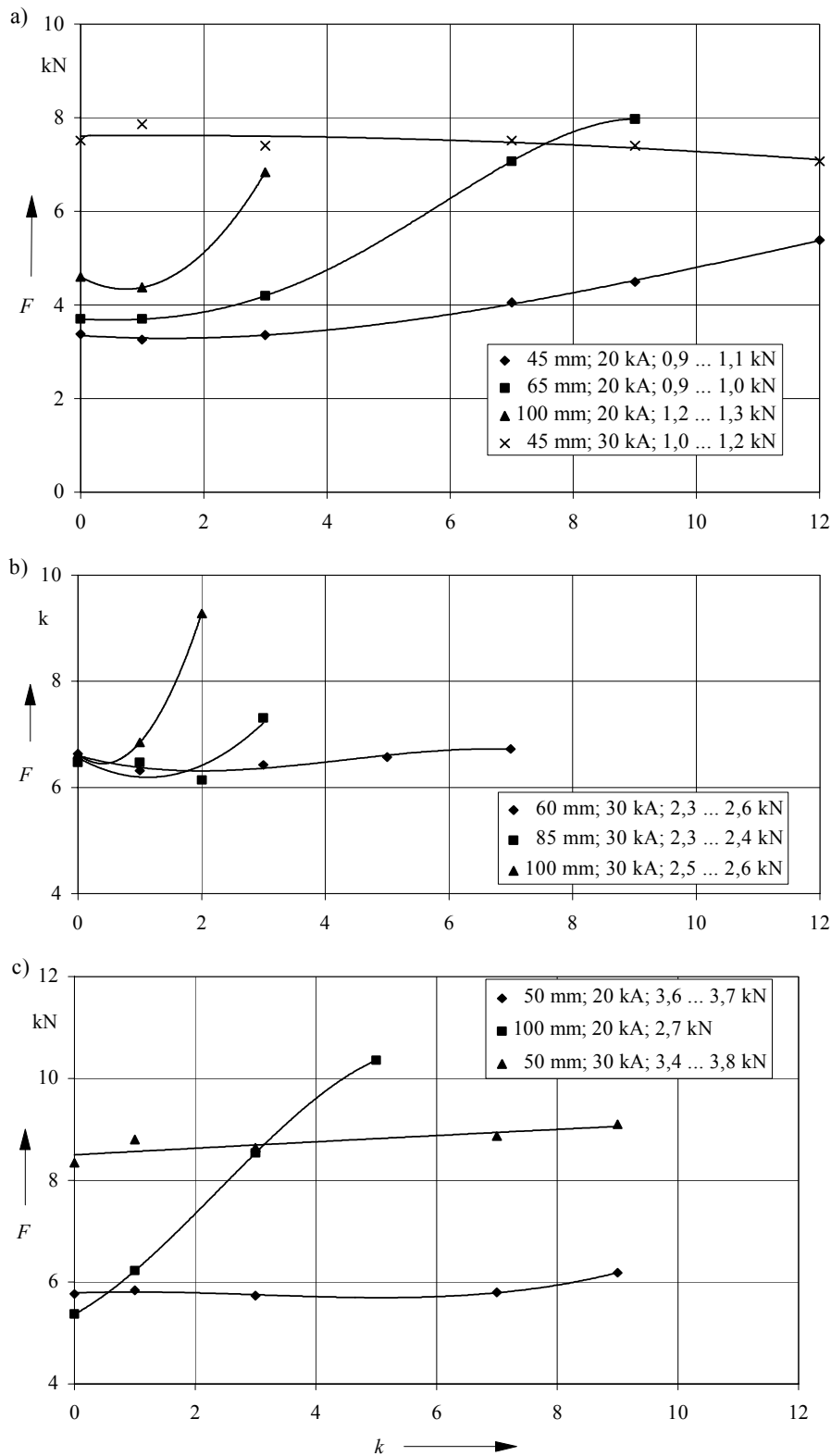


Figure 1.3: Short-circuit tensile force F as a function of number of spacers k with 15-m-span

- a) Al 240
- b) ACSR 537/53, medium static tensile force
- c) ACSR 537/53, high static tensile force

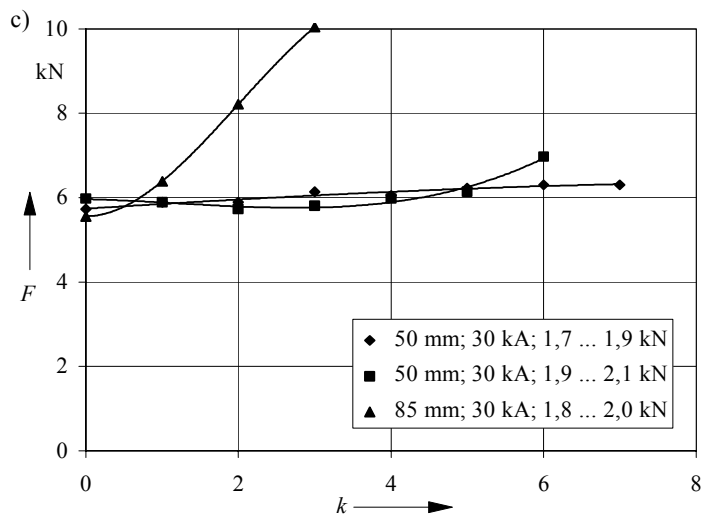
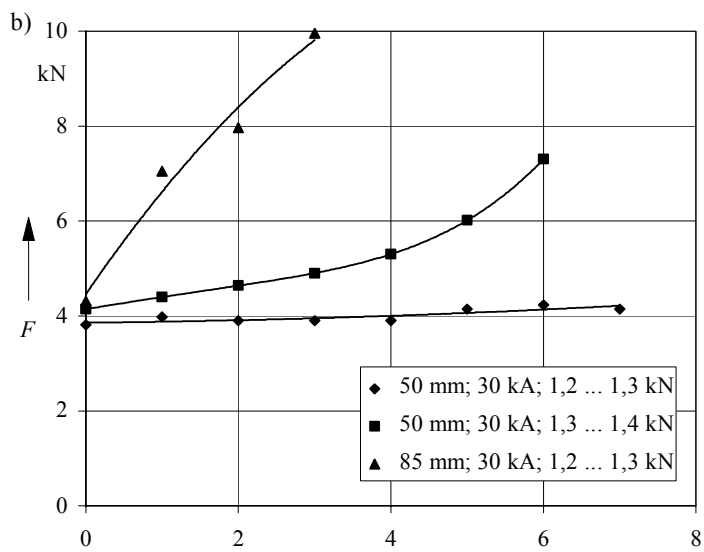
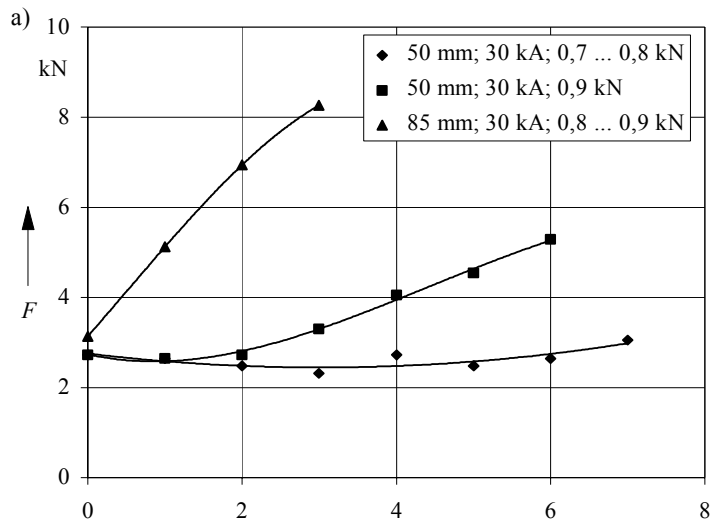


Figure 1.4: Short-circuit tensile force F as a function of number of spacers k with 10-m-span with ACSR 537/53

- a) Low static tensile force
- b) Medium static tensile force
- c) High static tensile force

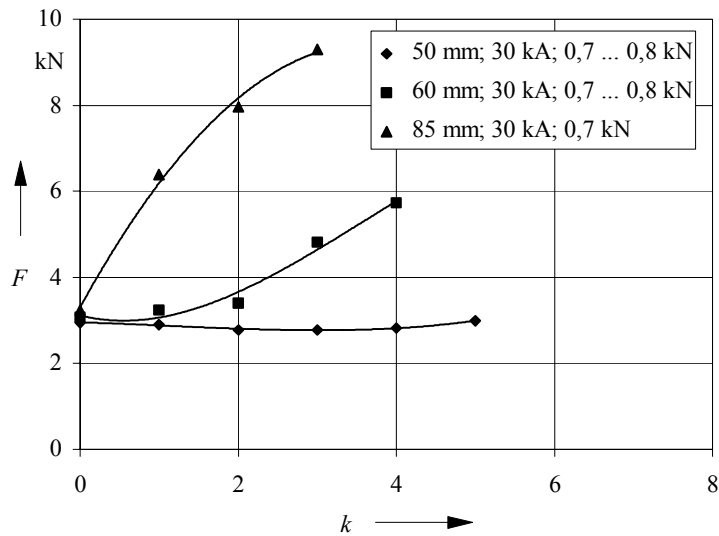


Figure 1.5: Short-circuit tensile force F as a function of number of spacers k with 7-m-span with ACSR 537/53

References:

- [1] Mathejczyk, M.; Stein, N.: Kurzschlußseilzüge enggebündelter Doppelseile in Schaltanlagen. etz-a 97(1976), pp 323-328.
- [2] Hosemann, G.; Mathejczyk, M.; Stein, N.: Short-circuit forces in single and bundled conductors. Cigre 23-77 (WG 02) 2 IWD, April 1977.

2. CONFIGURATION FOR CASES 2 AND 3

Tests performed at FGH (Germany) in 1978
 short-circuit current: 10 kA (26 kA peak) to 40 kA (104 kA peak)
 span length: 15 m and 4 m

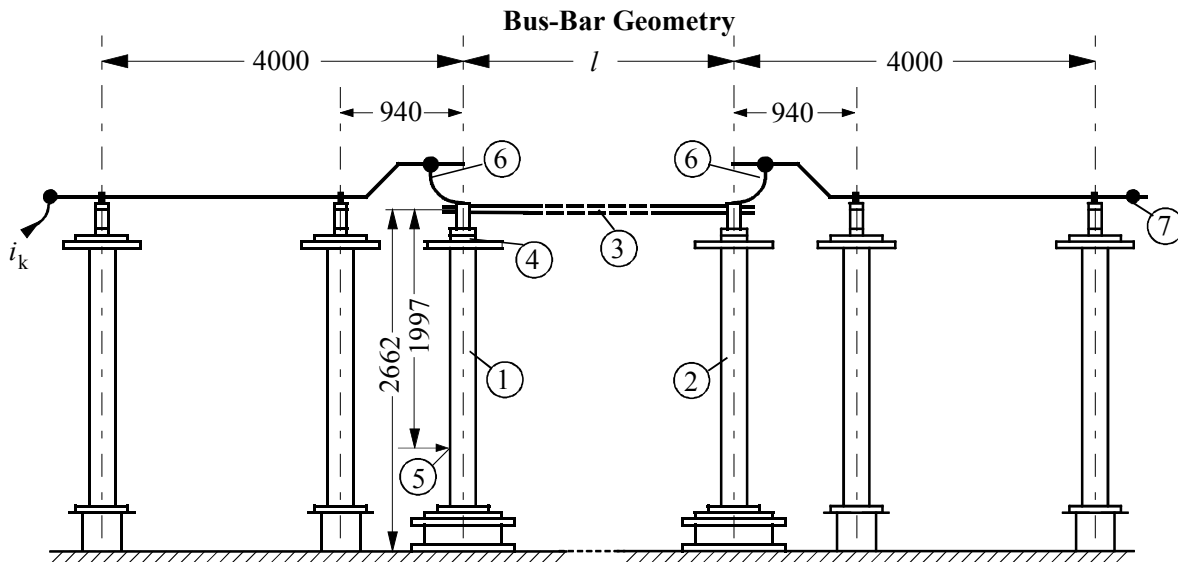


Figure 2.1 Test set up

- 1,2 post insulator
 - 3 conductor under test
 - 4 device for measuring the tensile forces on the top of the insulator
 - 5 strain gage for measuring the forces at the bottom of the insulator
 - 6 flexible connection
 - 7 short-circuit connection
- l span length
 a centre-line distance between main conductors

Basic Data

centre-line distance between main-conductors: $a = 4$ m

characteristics of the supports:

	support 1		support 2	
	eigenfrequency Hz	spring coefficient kN/mm	eigenfrequency Hz	spring coefficient kN/mm
$l = 15$ m	30	2,5	30	2,0
$l = 4$ m	30	2,5	28	1,7

spring coefficients of both supports: $l = 15$ m: 1,11 kN/mm
 $l = 4$ m: 1,01 kN/mm

short-circuit characteristics: $\kappa = 1,84$ ($\tau = 55$ ms)
 short-circuit duration: $T_k = 0,3$ s

Reference:

- [1] Stein, N.; Herrmann, B.: Kurzschlußseilzüge in Schaltanlagen. Elektrizitätswirtschaft 78 (1979), 179-186.

3. CASE 2

cross section: ACSR 120/20 mm², ACSR 537/53 mm² and ACSR 1055/45 mm², single conductor

Basic data

Conductors:

	cross-section	diameter	mass per unit length	Young's modulus	temperature coefficient
	A	d	m'	E	α_θ
	mm ²	mm	kg/m	N/mm ²	10 ⁻⁶ /K
ACSR 120/20	141,4	20,3	0,670	77000	18,9
ACSR 537/53	590,0	32,0	1,937	69000	19,8
ACSR 1055/45	1100,9	43,18	3,290	60000	18,1

initial static stress in the conductor:

$l = 15$ m	ACSR 120/20:	1,4 ... 5,7 N/mm ²
	ACSR 537/53:	1,7 ... 2,5 N/mm ²
	ACSR 1055/45:	1,4 ... 4,4 N/mm ²
$l = 4$ m	ACSR 1055/45:	0,1 ... 0,9 N/mm ²

short-circuit characteristics: $\kappa = 1,84$ ($\tau = 55$ ms)

short-circuit duration: $T_k = 0,3$ s

Results

During the movement of the conductor, several maxima of the short-circuit force can be observed as shown in figure 2. The first maximum occurs during or at the end of the short-circuit current flow when the conductor swings out from its initial static position. The other maxima are some hundred milliseconds after the end of the short circuit when the conductor rotates or at the end of the fall down.

At the bottom of the insulator, the strain is measured and an equivalent static load is calculated for the maxima which acts on the top of the insulator. This equivalent static load is given in the Figure 3.2 to Figure 3.5 as function of the ratio :

$$r = \frac{F'}{G'} = \frac{\mu_0 I_k^2}{2\pi a m' g_n}$$

Parameter is the initial static tensile force F_{st} . The first maximum belongs to the swing out, the second to the rotation or fall down.

In Figure 3.6, the short-circuit duration is varied. The equivalent static load as well as the short-circuit tensile force acting on the top of the insulator are shown.

The first maximum of the short-circuit tensile force on the top of the insulator is not greater than 150 % of the equivalent static load. The second maximum of the short-circuit tensile force is between 80 % and 100 %. In the case of the 4-m-span with ACSR 1055/45, the short-circuit tensile force is much greater than the equivalent static force: up to 350 % for the first and up to 250 % for the second maximum.

In a lot of tests, the movement of the conductors is recorded with a high-speed camera. The maximum horizontal displacement is taken from the films and given in the Figure 3.7 to Figure 3.9.

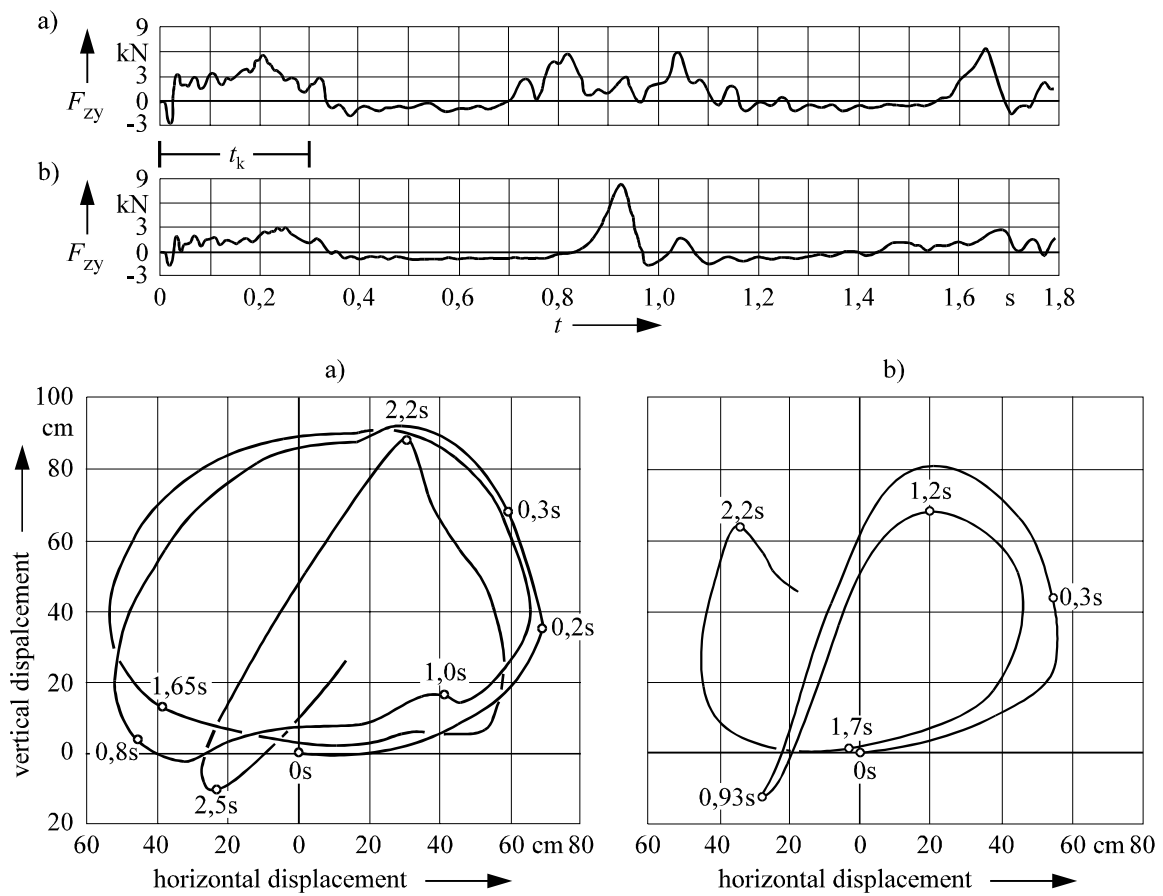


Figure 3.1: Stress at the bottom of support and conductor movement in midspan

Conductor ACSR 537/53; span length 15 m; initial static tensile force 1 kN; static sag 0,53 m

a) Rotation of span: $I_k = 29$ kA

b) Fall of span: $I_k = 22$ kA

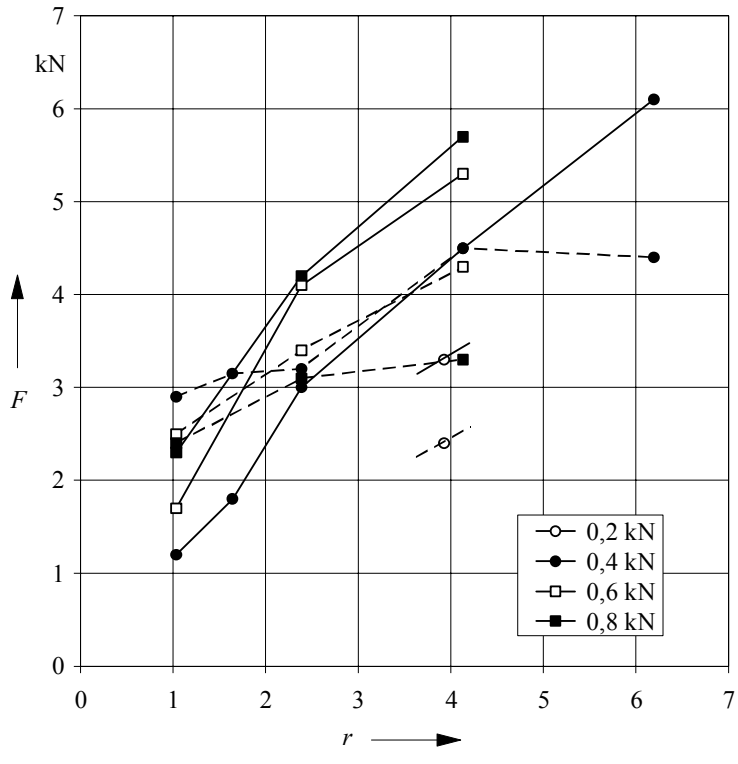


Figure 3.2: Equivalent static load: ACSR 120/20, $l = 15$ m
 ——— 1. Maximum - - - 2. Maximum

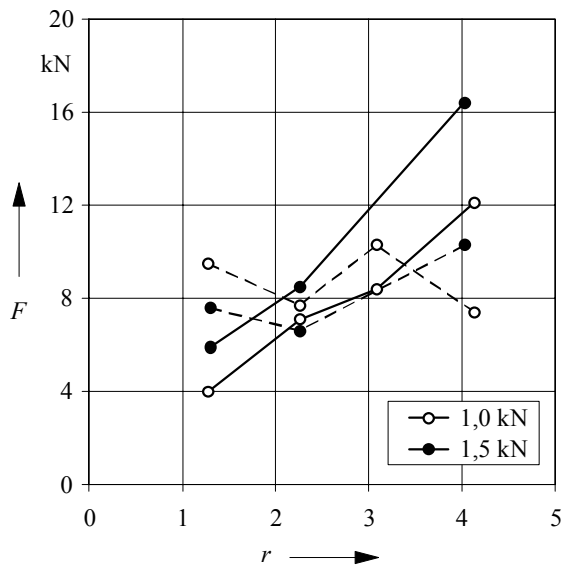


Figure 3.3: Equivalent static load: ACSR 537/53, $l = 15$ m
 ——— 1. Maximum - - - 2. Maximum

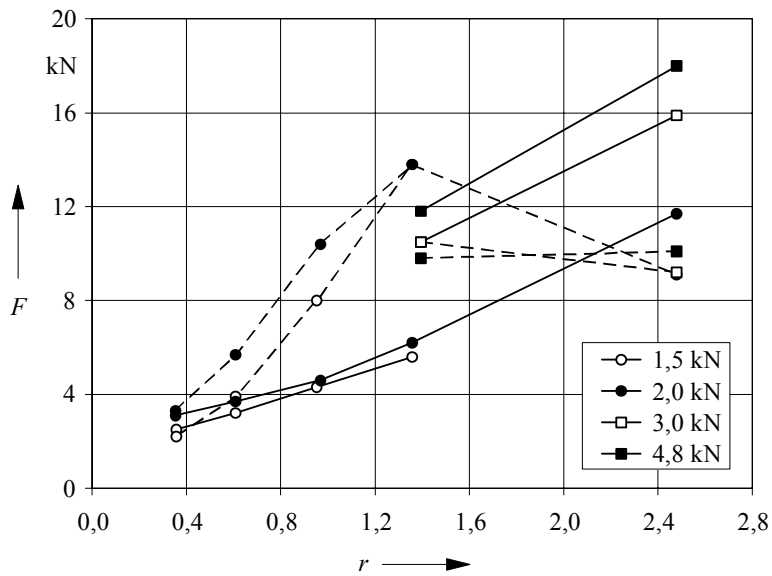


Figure 3.4: Equivalent static load: ACSR 1055/45, $l = 15$ m
 ——— 1. Maximum - - - 2. Maximum

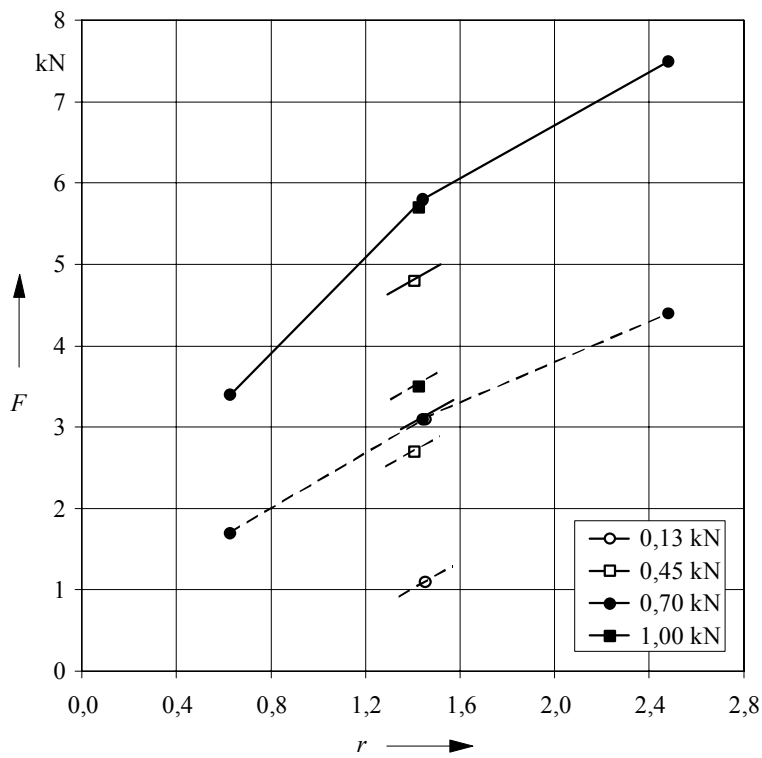


Figure 3.5: Equivalent static load: ACSR 1055/45, $l = 4$ m
 ——— 1. Maximum - - - 2. Maximum

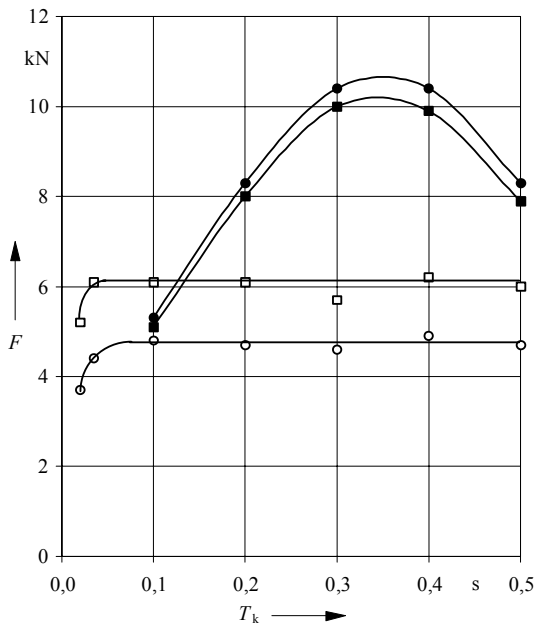


Figure 3.6: Influence of the short-circuit duration: ACSR 1055/45, $l = 15$ m, $F_{st} = 2$ kN, $I_k = 25$ kA

1. Maximum: short-circuit tensile force ○ equivalent static load
 2. Maximum: short-circuit tensile force ● equivalent static load

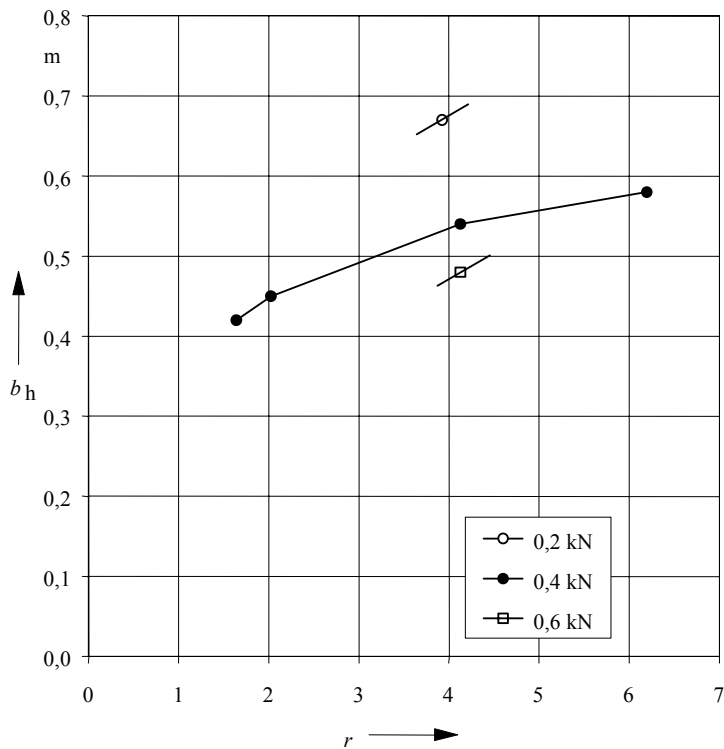


Figure 3.7: Maximum horizontal displacement: ACSR 120/20, $l = 15$ m

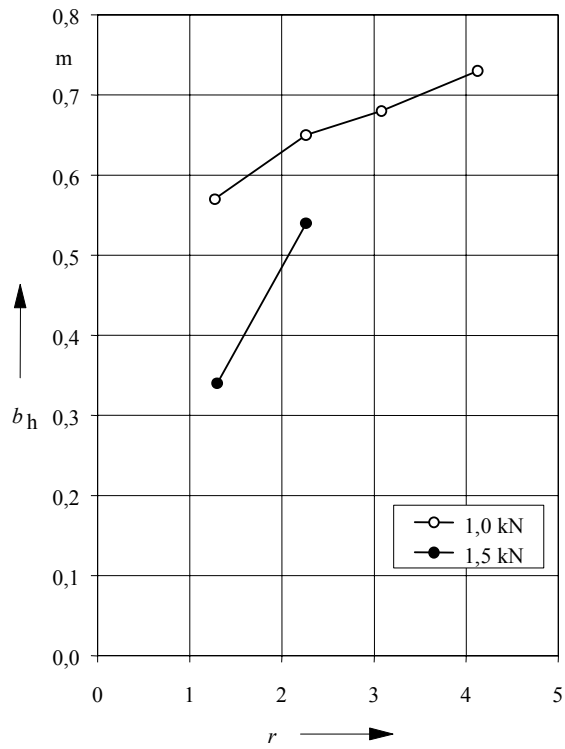


Figure 3.8: Maximum horizontal displacement: ACSR 537/53, $l = 15$ m

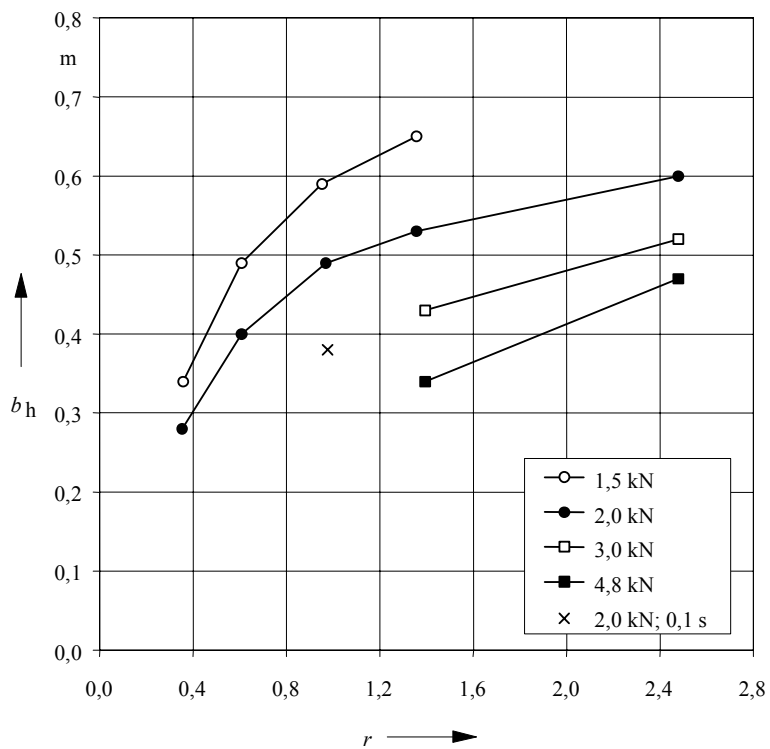


Figure 3.9: Maximum horizontal displacement: ACSR 1055/45, $l = 15$ m

4. CASE 3

cross section: ACSR 537/53 mm² and ACSR 1055/45 mm², two and four sub-conductors

Basic data

Conductors:

	cross-section	diameter	mass per unit length	Young's modulus	temperature coefficient
	A	d	m'	E	α_0
	mm ²	mm	kg/m	N/mm ²	10 ⁻⁶ /K
ACSR 537/53	590,0	32,0	1,937	69000	19,8
ACSR 1055/45	1100,9	43,18	3,290	60000	18,1

bundle configuration: twin ($n = 2$) and quadruple ($n = 4$)

number of spacers: 0 ... 3

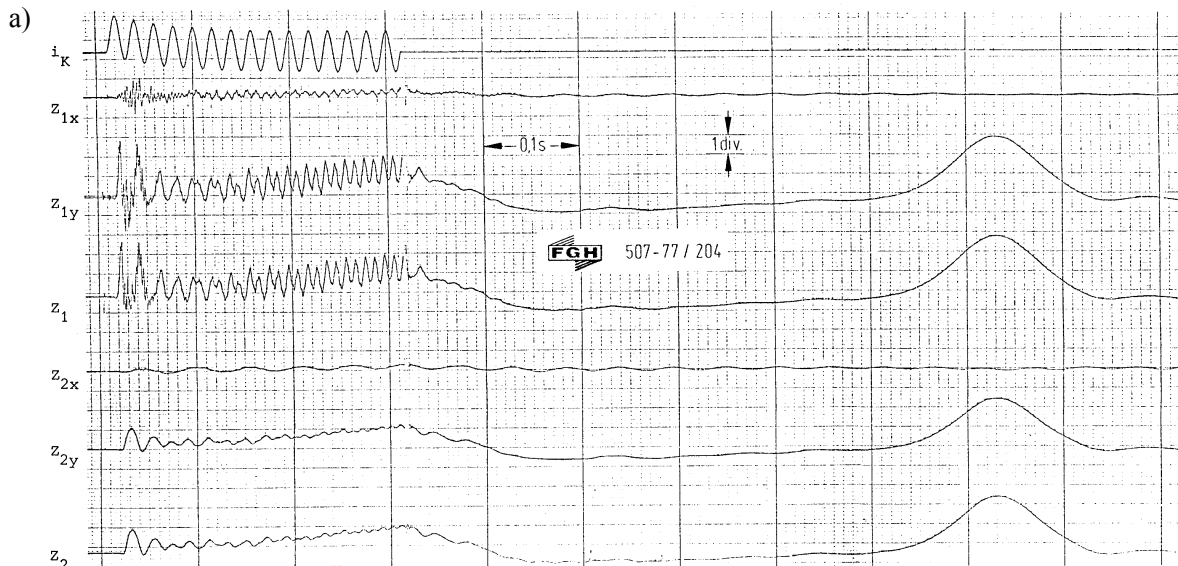
centre-line distance of subconductors: 60 mm and 80 mm

initial static stress in the conductor:

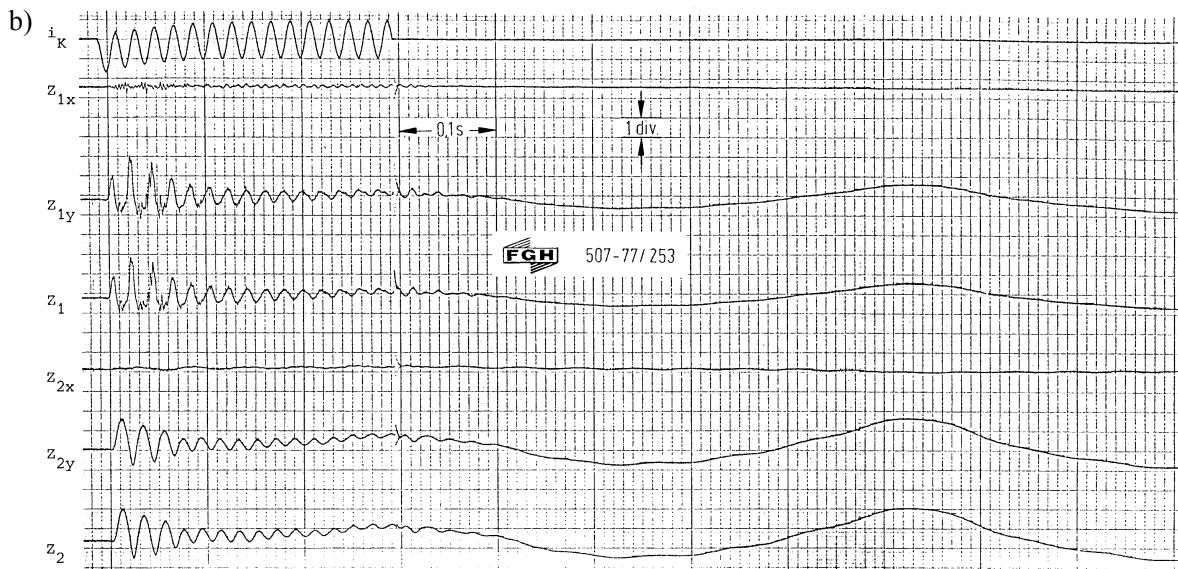
$l = 15$ m	ACSR 537/53	$n = 2$:	1,1 ... 1,7 N/mm ²
		$n = 4$:	1,7 ... 2,5 N/mm ²
	ACSR 1055/45	$n = 2$:	1,4 ... 1,8 N/mm ²
		$n = 4$:	1,3 ... 1,8 N/mm ²
$l = 4$ m	ACSR 537/53	$n = 2$:	0,4 N/mm ²

Results

During the movement of the conductor, several maxima of the short-circuit force can be observed as shown in Figure 4.1. The first maximum occurs a few milliseconds after the initiation of the short-circuit, the second one at the end of the short-circuit current flow when the conductor swings out from its initial static position. The third maximum is some hundred milliseconds after the end of the short circuit when the conductor rotates or at the end of the fall down.



scales: $Z_{1x} = 4,7 \text{ kN/div};$ $Z_{1y} = 4,7 \text{ kN/div};$ $Z_1 = 4,7 \text{ kN/div};$
 $Z_{2x} = 5,7 \text{ kN/div};$ $Z_{2y} = 6,4 \text{ kN/div};$ $Z_2 = 5,7 \text{ kN/div};$



scales: $Z_{1x} = 11,6 \text{ kN/div};$ $Z_{1y} = 11,6 \text{ kN/div};$ $Z_1 = 12,3 \text{ kN/div};$
 $Z_{2x} = 5,7 \text{ kN/div};$ $Z_{2y} = 6,4 \text{ kN/div};$ $Z_2 = 6,1 \text{ kN/div};$

Traces in the oscillograms:

- i_k short-circuit current
- Z_{1x} tensile force in the clamp perpendicular to the span
- Z_{1y} tensile force in the clamp in the direction of the span
- Z_1 tensile force in the clamp
- Z_{2x} force at the bottom of the support perpendicular to the span
- Z_{2y} force at the bottom of the support in the direction of the span
- Z_2 force at the bottom of the support

The static part is suppressed in the oscillograms

Figure 4.1: Oscillogram of the forces and conductor displacements at midspan

$i_p = 104 \text{ kA}, I_k = 40 \text{ kA};$ span length 15 m

a) Conductor 4xACSR 537/53; $k = 3; F_{st} = 4 \text{ kN}$

b) Conductor 4xACSR 1055/45; $k = 3; F_{st} = 8 \text{ kN}$

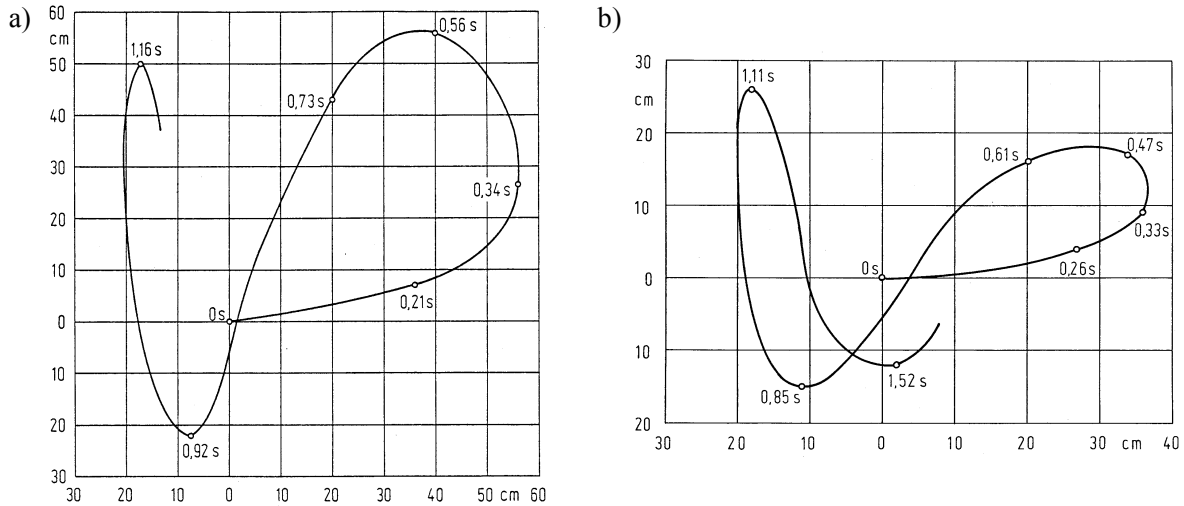


Figure 4.2: Oscillogram of the forces and conductor displacements at midspan (continued)

$i_p = 104 \text{ kA}$, $I_k = 40 \text{ kA}$; span length 15 m

a) Conductor 4×ACSR 537/53; $k = 3$; $F_{st} = 4 \text{ kN}$

b) Conductor 4×ACSR 1055/45; $k = 3$; $F_{st} = 8 \text{ kN}$

The presentation of the results is done in two parts. In the first part, the forces during the movement of the main conductor are shown, i. e. the second and third maxima in the time history, and afterwards the forces due to pinch effect in the bundle, which are given by the first maxima.

4.1. MAIN CONDUCTOR EFFECTS

At the bottom of the insulator, the strain is measured and an equivalent static load is calculated for the maxima which acts on the top of the insulator. This equivalent static load is given in the Figure 4.3 to 4.7 as function of the ratio

$$r = \frac{F'}{G'} = \frac{\mu_0 I_k^2}{2\pi a nm'g_n}$$

Parameters are the bundle configuration, span length and the initial static tensile force F_{st} . The second maximum (continuous lines) belongs to the swing out, the third (dotted lines) to the rotation or fall down. The lines connect the test results for better reading.

Because these maxima are nearly independent of the number of spacers, the results are given for the tests without spacers ($k = 0$).

The tests show that the equivalent static load F_f during rotation or fall of the span (third maximum) is always higher than the load F_t during or at the end of the short-circuit current flow (second maximum), as shown in Figure 4.3 to 4.6, except for the 4-m-span, Figure 4.7.

The second maximum of the short-circuit tensile force in the clamp at the top of the insulator is not greater than

- 1,3 F_t in the case 2×ACSR 537/53, $l = 15 \text{ m}$;
- 1,1 F_t in all other cases with $l = 15 \text{ m}$;
- 1,7 F_t in the case 2×ACSR 537/53, $l = 4 \text{ m}$.

The third maximum of the short-circuit tensile force on the top of the insulator is in the range of

- 0,9 F_f and 1,04 F_f in the case of $l = 15 \text{ m}$;
- 0,95 F_f and 1,2 F_f in the case of $l = 4 \text{ m}$ and I_k up to 30 kA ; but 1,4 F_f for $I_k = 40 \text{ kA}$.

In some tests, the movement of the conductors is recorded with a high-speed camera. The maximum horizontal displacement is taken from the films and given in Figure 4.8.

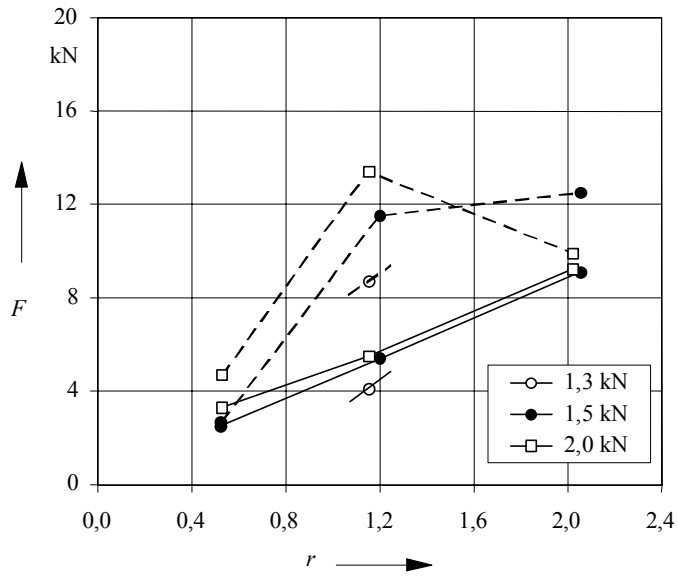


Figure 4.3: Equivalent static load: 2xACSR 537/53, $l = 15$ m

———— 2. Maximum - - - 3. Maximum

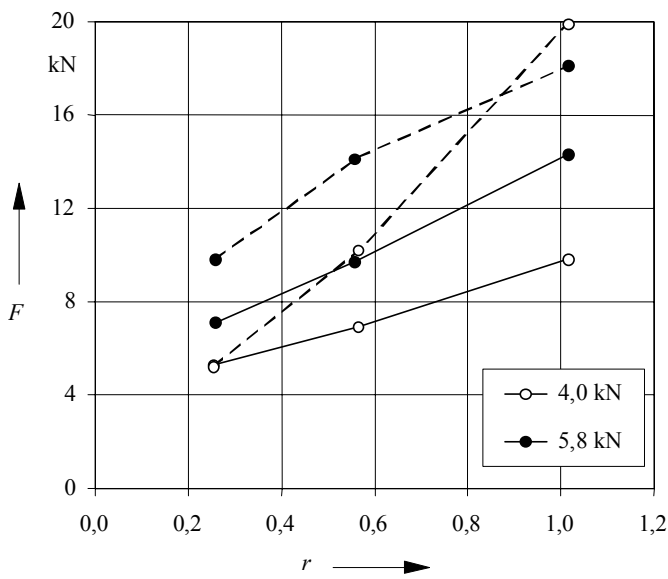


Figure 4.4: Equivalent static load: 4xACSR 537/53, $l = 15$ m

———— 2. Maximum - - - 3. Maximum

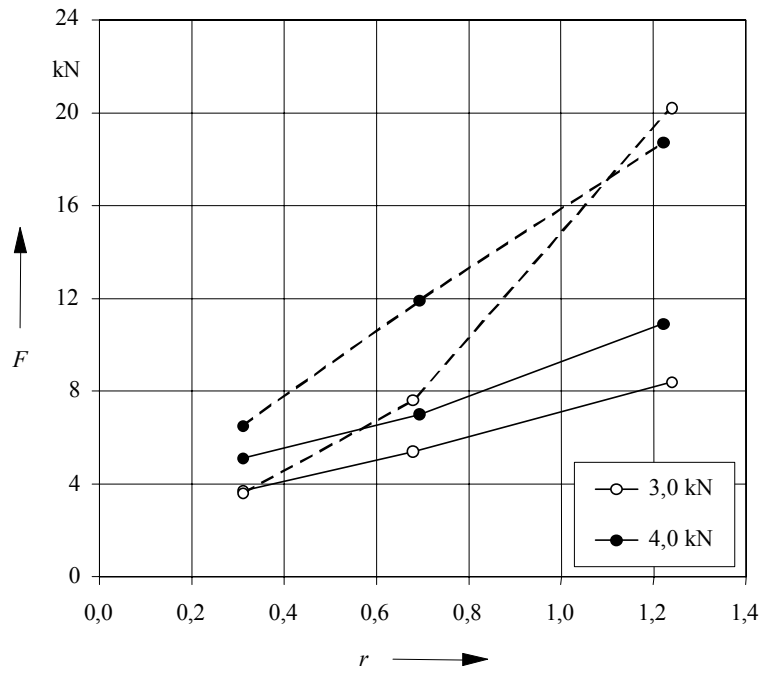


Figure 4.5: Equivalent static load: 2xACSR 1055/45, $l = 15$ m
 ——— 2. Maximum - - - 3. Maximum

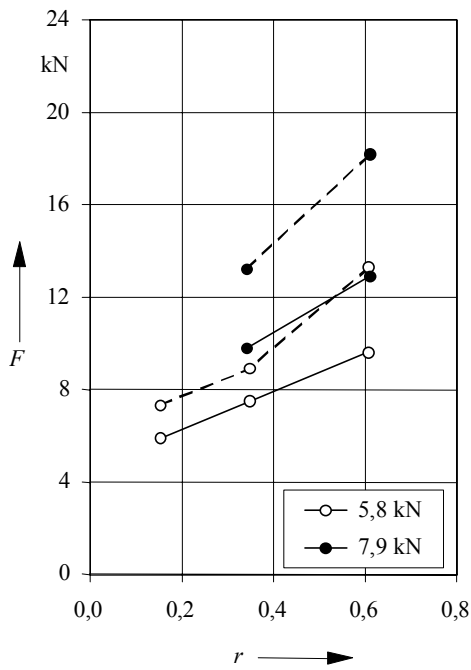


Figure 4.6: Equivalent static load: 4xACSR 1055/45, $l = 15$ m
 ——— 2. Maximum - - - 3. Maximum

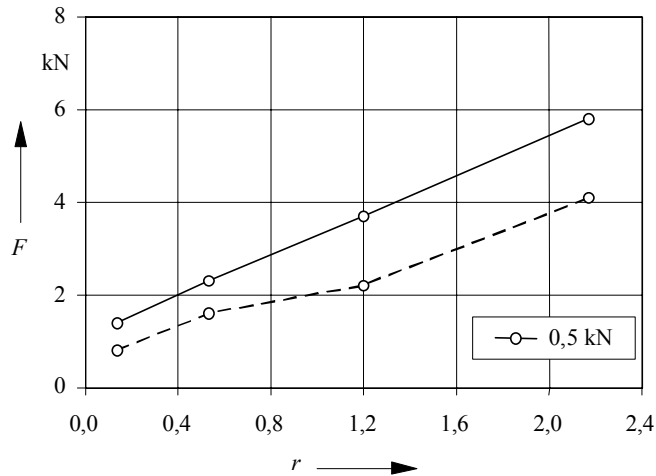


Figure 4.7: Equivalent static load: 2xACSR 1055/45, $l = 4$ m
 ——— 2. Maximum - - - 3. Maximum

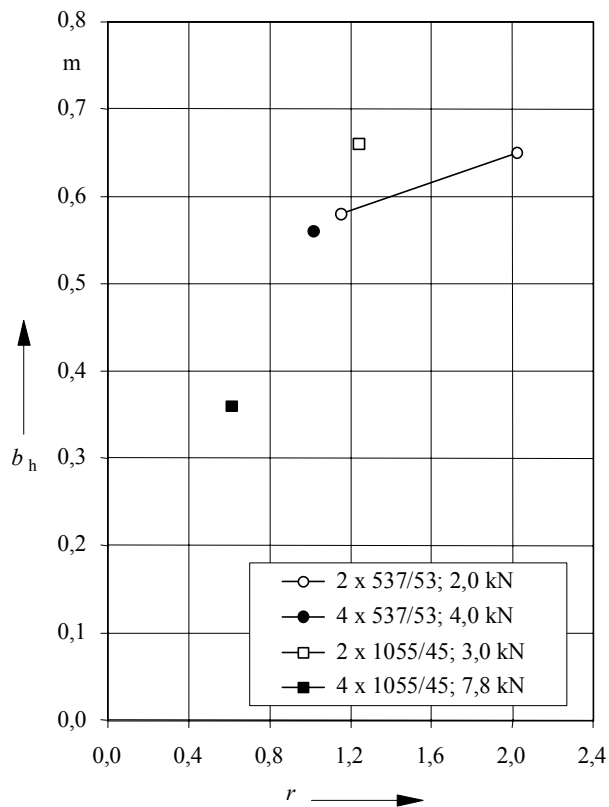


Figure 4.8: Maximum horizontal displacement, $l = 15$ m

4.2. FORCES CAUSED BY PINCH EFFECT IN BUNDLES

The equivalent static loads F_{pi} caused by pinch effects represented by the first maximum in the time scale history are shown in Figure 4.9 to 4.12 as functions of the number of spacers k for the 15-m-span. Parameters are the bundle configuration, the short-circuit current and the static tensile force. The test results are connected by continuous lines for better reading.

Because the equivalent static load F_t during swing out is lower than the load due to rotation or fall of span, the latter one is also given in the figures, connected by dotted lines.

The figures point out:

- The first maximum F_{pi} can exceed the third maximum F_f if $r \leq 0,6$; more spacers promote this.
- If $k = 0$ or 1 and with the highest current $I_k = 40$ kA, F_f is always decisive.
- This is also true for $I_k = 30$ kA. Except $2 \times \text{ACSR } 1055/45$ with low static tensile force and $n = 0$ where F_{pi} and F_f are almost equal.

Due to the 100-Hz-component in the time scale, Figure 4.1, the tensile forces in the clamp at the top of the insulator during the first maximum can be

- up to $3,8 F_{pi}$ with $2 \times \text{ACSR } 537/53$; up to $1,8 F_{pi}$ with $4 \times \text{ACSR } 537/53$;
- up to $2,5 F_{pi}$ with $2 \times \text{ACSR } 1055/45$; up to $2,0 F_{pi}$ with $4 \times \text{ACSR } 1055/45$.

Compared to the equivalent static force caused by the third maximum in the time scale, the tensile forces in the clamp at the top of the insulator during the first maximum can be

- up to $1,6 F_f$ with $2 \times \text{ACSR } 537/53$; up to $1,5 F_f$ with $4 \times \text{ACSR } 537/53$;
- up to $1,3 F_f$ with $2 \times \text{ACSR } 1055/45$; up to $1,9 F_f$ with $4 \times \text{ACSR } 1055/45$

for $I_k = 30$ kA, 40 kA and usually used $n = 1, 2$. As the impulse length of the first maximum is very short, the rating of the clamp should not be based on this.

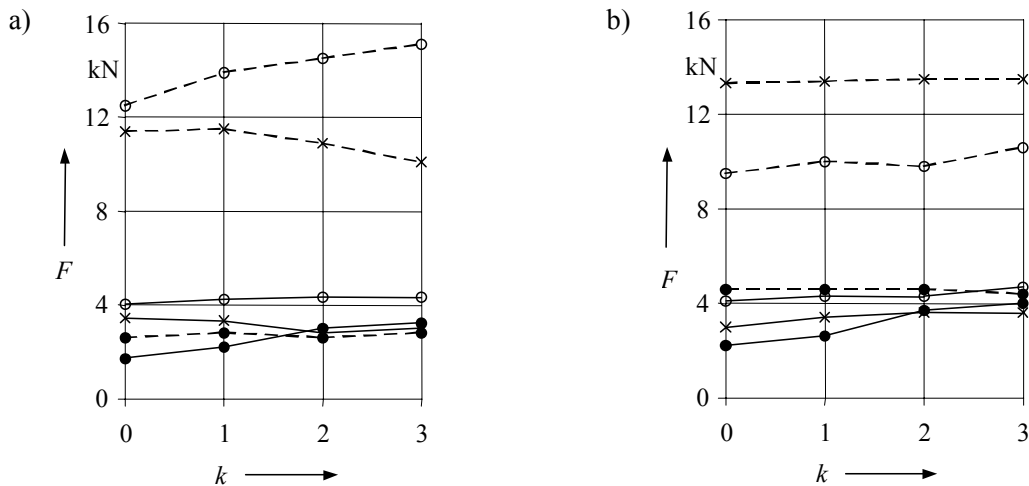


Figure 4.9: Equivalent static load: $2 \times \text{ACSR } 537/53$, $l = 15$ m, $a_s = 60$ mm

a) $F_{st} = 1,5$ kN

b) $F_{st} = 2$ kN

— 1. Maximum

- - - 3. Maximum

● 20 kA

× 30 kA

○ 40 kA

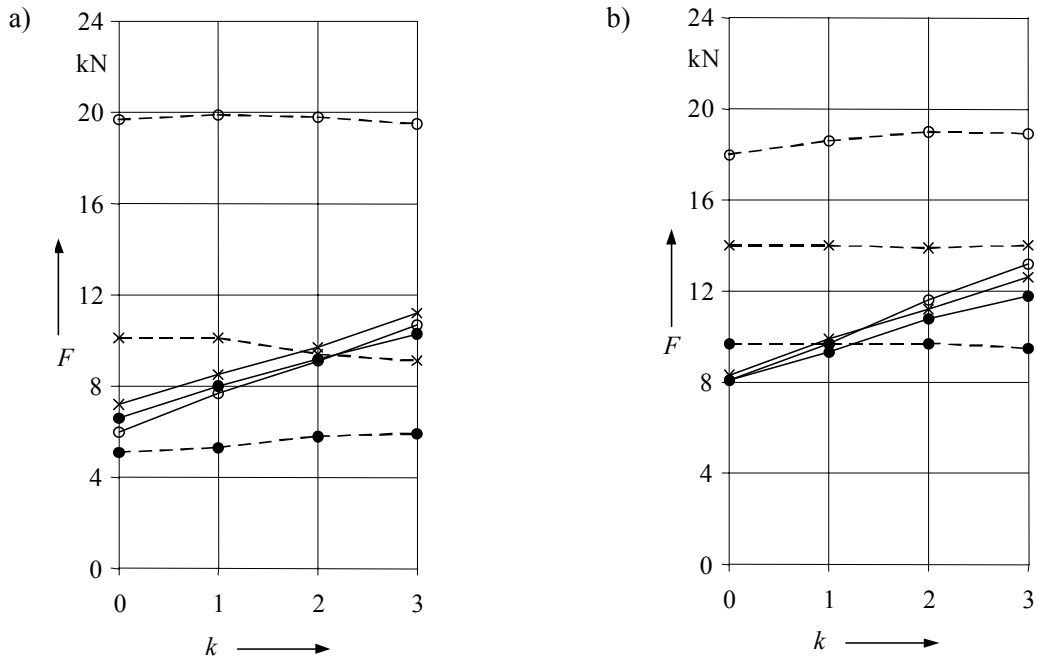


Figure 4.10: Equivalent static load: 4xACSR 537/53, $l = 15$ m, $a_s = 60$ mm

a) $F_{st} = 4$ kN
 ——— 1. Maximum
 ● 20 kA × 30 kA
 ○ 40 kA

b) $F_{st} = 6$ kN
 — — — 3. Maximum
 ○ 40 kA

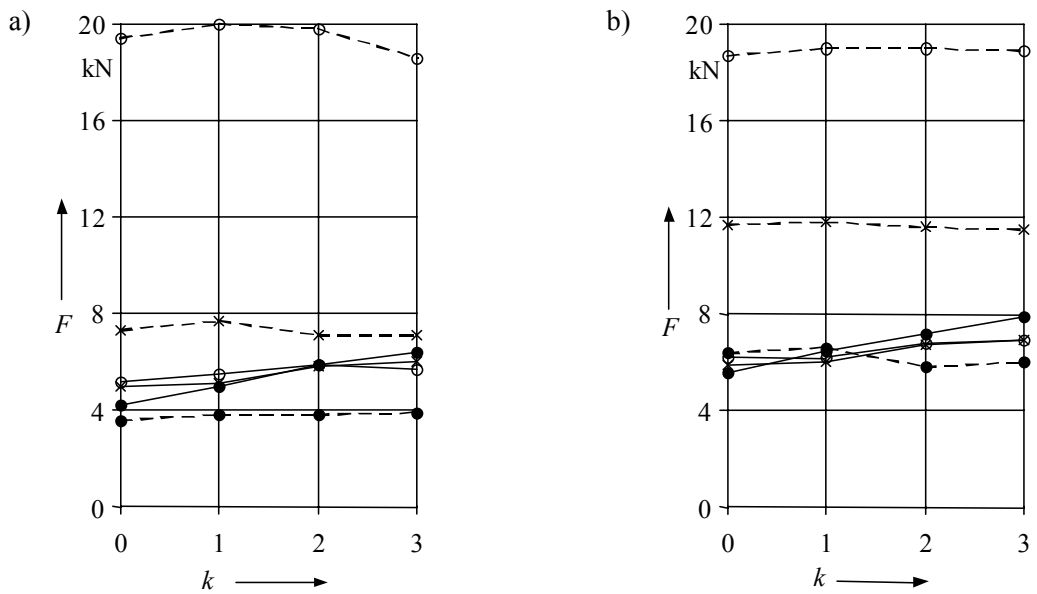


Figure 4.11: Equivalent static load: 2xACSR 1055/45, $l = 15$ m, $a_s = 80$ mm

a) $F_{st} = 3$ kN
 ——— 1. Maximum
 ● 20 kA × 30 kA
 ○ 40 kA

b) $F_{st} = 4$ kN
 — — — 3. Maximum
 ○ 40 kA

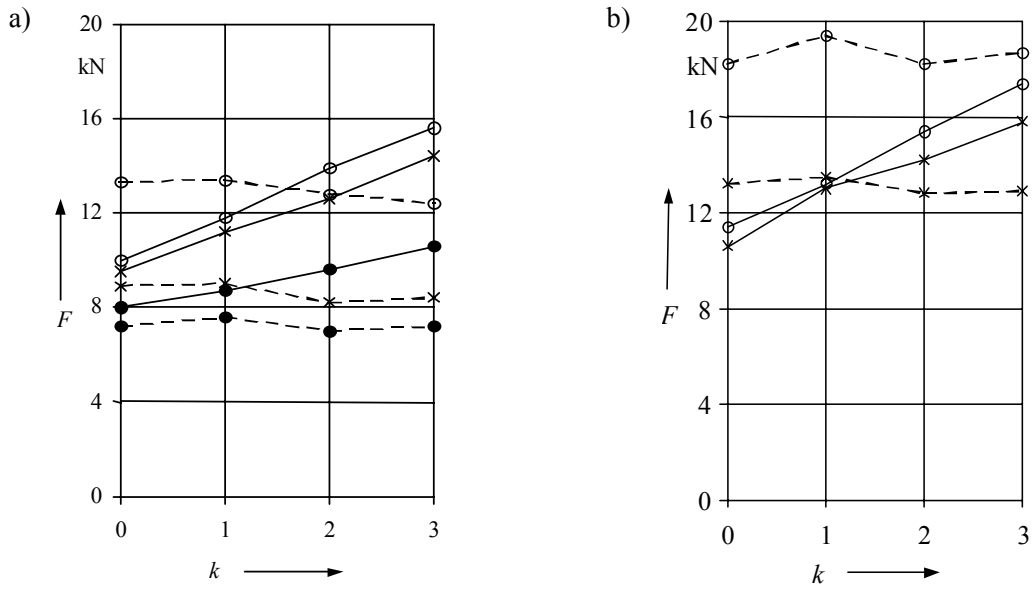


Figure 4.12: Equivalent static load: 4×ACSR 1055/45, $l = 15$ m, $a_s = 80$ mm

a) $F_{st} = 6$ kN

— 1. Maximum

● 20 kA

× 30 kA

b) $F_{st} = 8$ kN

- - - 3. Maximum

○ 40 kA

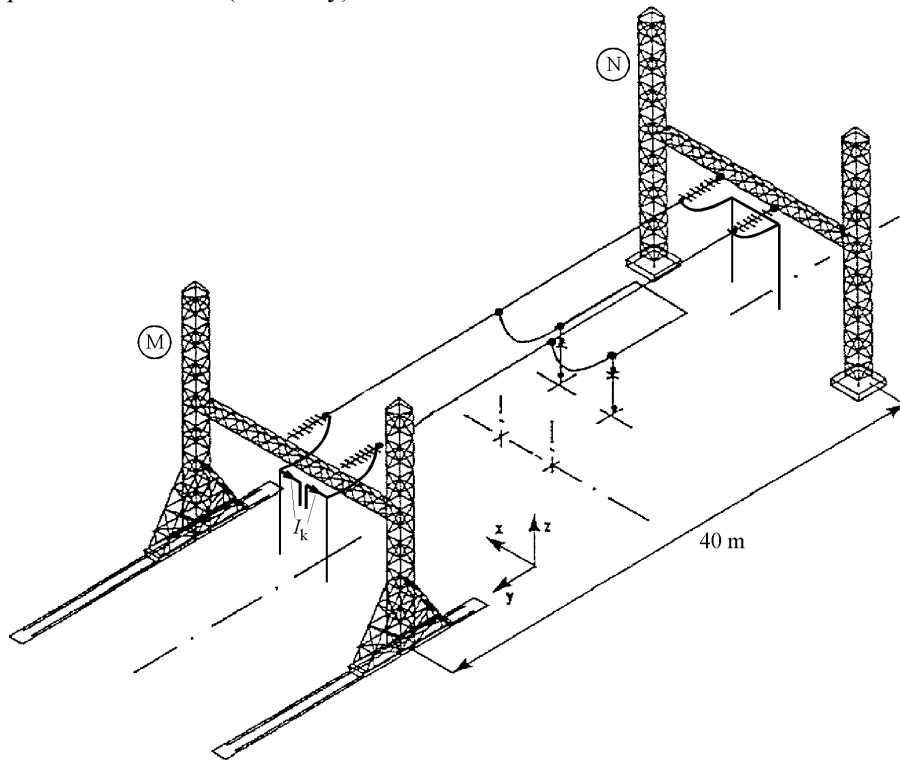
PART II

Arrangements with strained conductors and droppers in midspan

5. CONFIGURATION FOR CASES 4 AND 5

Tests performed at FGH (Germany) in 1997

a)



b)

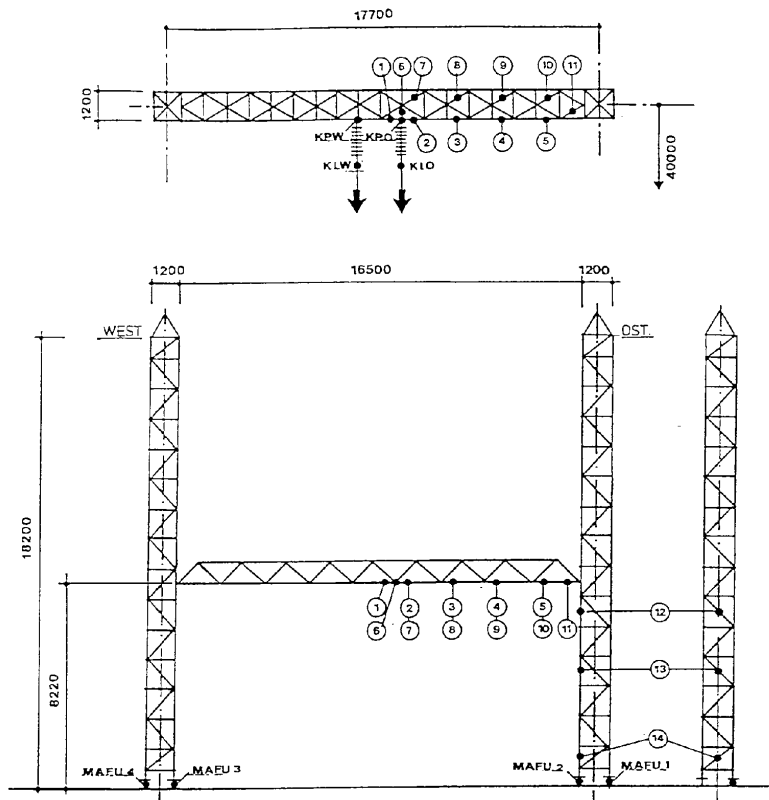


Figure 5.1 Test arrangement

a) Span

b) Portal N: geometric data and measuring points

Basic data

cross section: 537/53 mm²
 short-circuit current: 20 kA (50 kA peak) and 40 kA (100 kA peak)
 span length: 40 m

The test arrangement is shown in Figure 5.1, the essential data, force and strain measuring points of the northern portal are shown in Figure 5.1 b). Its structural/geometrical parameters as well as the short-circuit parameters are in Table 6.1 for case 4 and Table 7.1 for case 5. Three current paths (in the following called cases) are tested:

- case A: span without droppers, reference case
- case B: span with droppers; the short-circuit current flows through the whole span, the droppers are without current
- case C: span with droppers; the short-circuit current flows through half the span and through the droppers to the lower level buses

The support structures, beside their design drawings and construction data, are defined by their essential structural properties stiffness and eigenfrequency measured in separate mechanical tests and listed in the following. The mechanical tests show linear elastic characteristics for the supports given in terms of stiffness values. The first eigenfrequencies are excited at mid crossarm, i.e. next to the suspension.

For each combination of test parameters as collected in Table 6.1 for case 4 and Table 7.1 for case 5 at least two identical tests were performed to show the variance of behaviour and effects. For symmetry reasons this gives at least 4 values for forces from 2 tests. The variance is, as can be seen, astonishingly small.

Conductor:

	cross-section	diameter	mass per unit length	Young's modulus	temperature coefficient
	A	d	m'	E	α_θ
	mm ²	mm	kg/m	N/mm ²	10 ⁻⁶ /K
ACSR 537/53	590	32	1,937	69000	19,8

static sag: $\approx 0,6$ m

short-circuit characteristics: $\kappa \approx 1,77$ ($\tau \approx 55$ ms)

characteristics of the bus supports:

voltage level	case	height of conductor anchoring	spring coefficient support		eigenfrequency			
			M	N	crossarm		complete support	
		m	kN/mm	kN/mm	M	N	M	N
					Hz	Hz	Hz	Hz
100 kV	4	8,22	1,551	1,229	9,0	8,3	4,6	3,5
400 kV	5	11,22	1,223	1,086	9,5	9,0	4,3	3,0

Characteristics of the supporting structure at the lower end of the droppers:

direction →		spring coefficient		eigenfrequency	
		x	y	x	y
		kN/mm	kN/mm	Hz	Hz
steel pillar	left	1,58	1,59	26,1	26,0
	right	1,51	1,50	25,8	26,3
support *)	left	0,38	0,37	13,0	13,0
	right	0,38	0,37	12,8	13,2

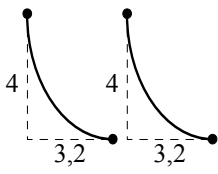
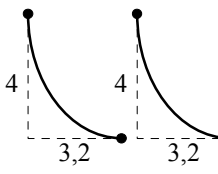
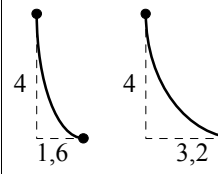
*) complete including measuring device and clamp, total mass of both: 26,7 kg

References:

- [1] Stein, N.; Meyer, W.; Miri, A.M.: High Voltage Substation Stranded Conductor Buses with and without Droppers Tests and Calculation of Short-Circuit Constraints and Behaviour. 8th International Symposium on Short-Circuit Currents in Power Systems, Brussels, Belgium, 8.-10. October 1998, Proceedings pp 115-121
- [2] Stein, N.; Miri, A.M.; Meyer, W.: 400 kV Substation Stranded Conductor Buses —Tests and Calculations of Short-Circuit Constraints and Behaviour, 7th International Conference on Optimization of Electrical and Electronic Equipment OPTIM 2000, Brasov (Romania), 11.-12. May 2000; Proceedings pp 251-257
- [3] Stein, N.; Meyer, W.; Miri, A.M.: Tests and Calculation of Short-Circuit Forces and Displacements in High Voltage Substations with Strained Conductors and Droppers. ETEP 10 (2000) No. 3 , pp 131–138
- [4] Stein, N.; Meyer, W.; Miri, A.M.: High Voltage Substations with Stranded Conductors and Droppers - Tests and Calculations of Short-Circuit Constraints and Behaviour. 9th International Symposium on Short-Circuit Currents in Power Systems, Cracow (Poland), 11.-13. October 2000, Proceedings pp 221-228

6. CASE 4

Table 6.1: Test parameters

test arrangement		1	2	3	4
span		40 m 1 x ACSR 537/53 a = 2 m			
droppers 1 x ACSR 537/53		without			
dropper length / m			6,045	6,045	5,045 / 6,045
current path		A	B	C	B
$\frac{I_k}{kA}$	20	0,1 / 0,3 / 0,5	0,1 / 0,3	0,1 / 0,3	0,1 / 0,3 / 0,5
	28,3	0,1 / 0,2 / 0,3 / 0,5 / 1,0	0,1 / 0,3 / 0,5	0,1 / 0,3	0,1 / 0,3
	40	0,1 / 0,2 / 0,3 / 0,5 / 1,0	0,1 / 0,3 / 0,5	0,1 / 0,3 / 0,5	0,1 / 0,3

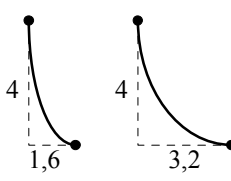
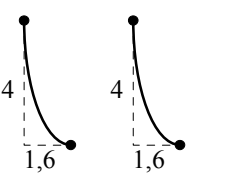
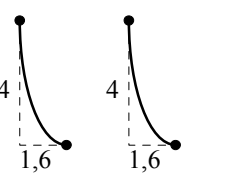
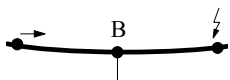
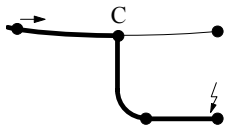
test arrangement		5	6	7	current path:
span		40 m 1 x ACSR 537/53 a = 2 m			
droppers 1 x ACSR 537/53					
dropper length / m		5,045	5,045	5,045	
current path		C	B	C	
$\frac{I_k}{kA}$	20	0,1 / 0,3	0,1 / 0,3 / 0,5	0,1 / 0,3 / 0,5	
	28,3	0,1 / 0,3	0,1 / 0,3 / 0,5	0,1 / 0,3 / 0,5	
	40	0,3 / 0,5 / 1,0	0,1 / 0,3	0,1 / 0,3 / 0,5	

Figure 6.1 & Figure 6.2 show oscillograms of the forces for variants 6 (current path B) and 5 (current path C). For current path variants A, B and C, Figure 6.3 to 6.11 give the measured forces, minimum air clearances and maximum horizontal displacements over the respective values of short-circuit duration. The mean values are connected by straight lines only for better readability.

Results

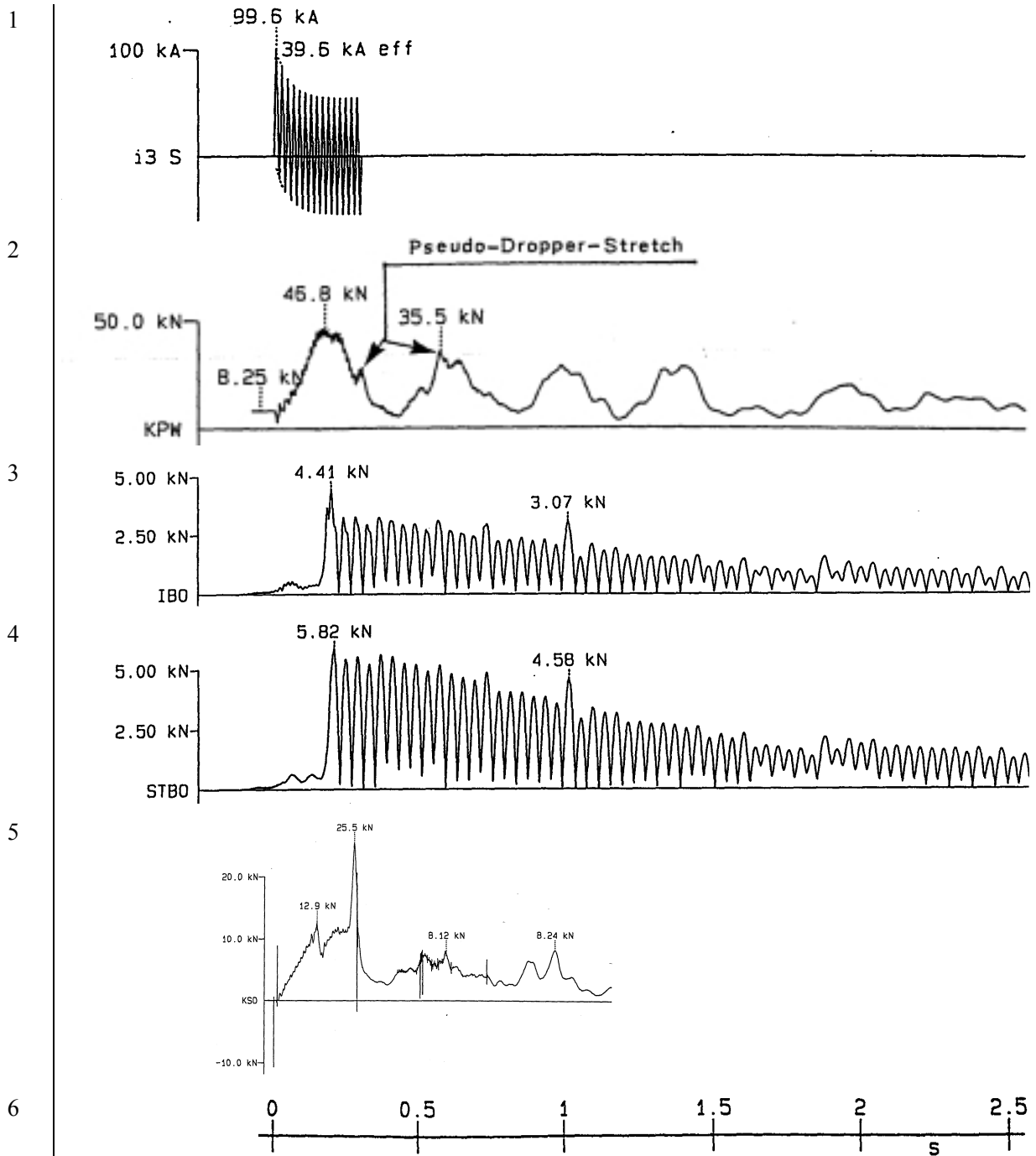


Figure 6.1: Oscillogram of short-circuit test: case B (variant 6); $I_k = 40 \text{ kA}$, $t_k = 0,305 \text{ s}$

Traces:

- 1 short-circuit current
- 2 force at the anchoring point of the main conductor
- 3 force at the bottom of the supporting insulator
- 4 force at the bottom of the steel support structure
- 5 force in the clamp at the upper end of the dropper
- 6 time scale

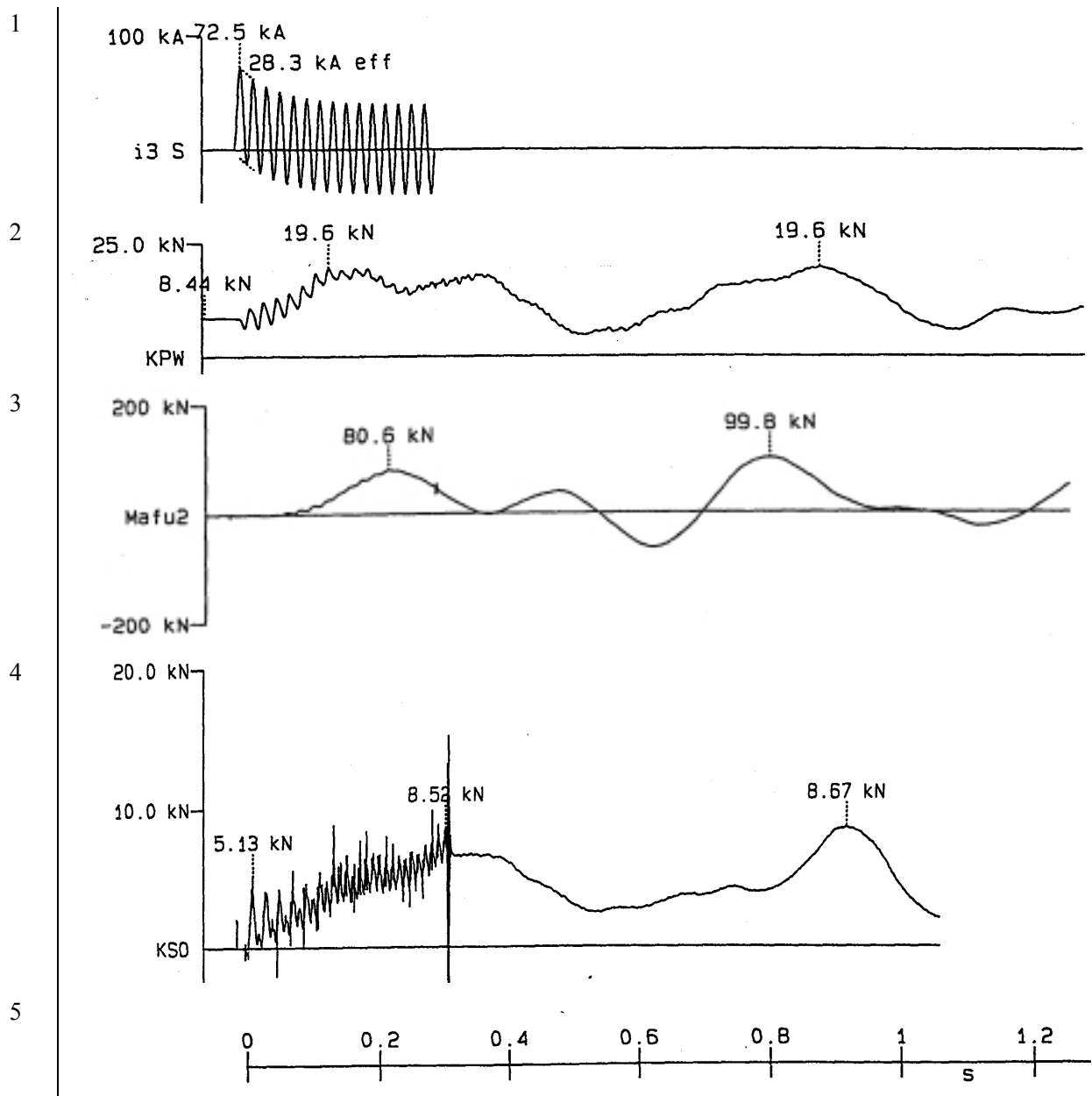


Figure 6.2: Oscillogram of short-circuit test: case C (variant 5); $I_k = 40 \text{ kA}$, $t_k = 0,305 \text{ s}$

Traces:

- 1 short-circuit current
- 2 force at the anchoring point of the main conductor
- 3 force at the bottom of the tower (MAFU2)
- 4 force in the clamp at the upper end of the dropper
- 5 time scale

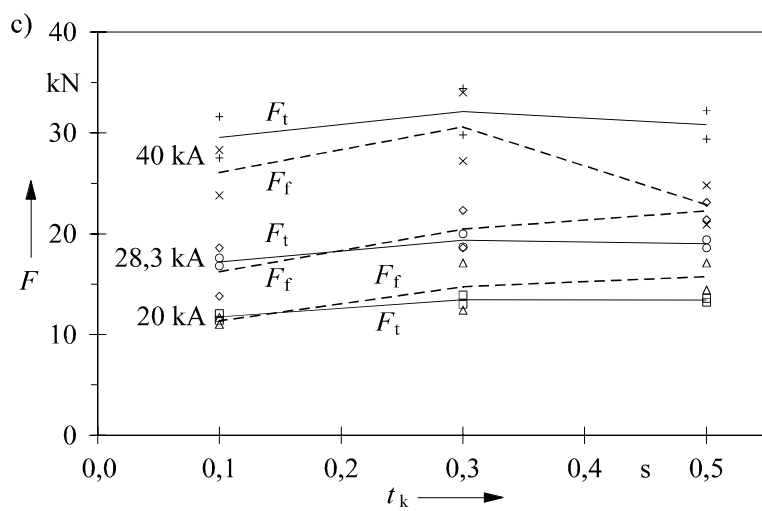
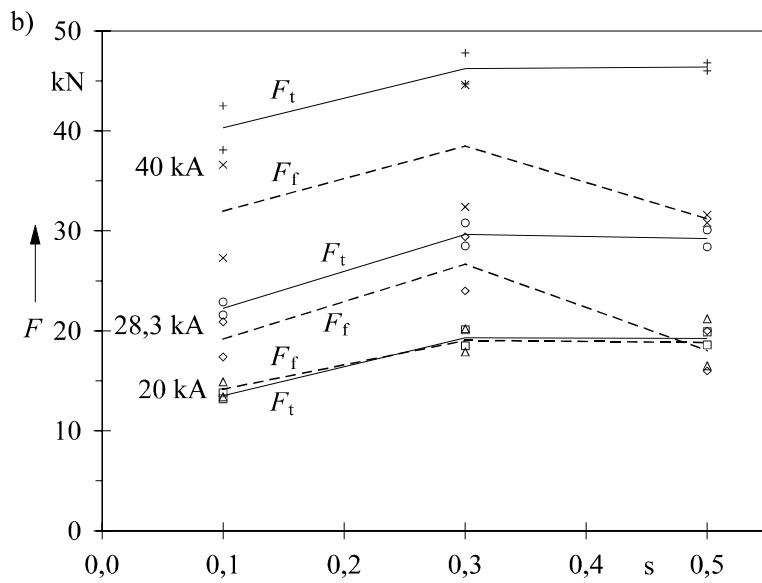
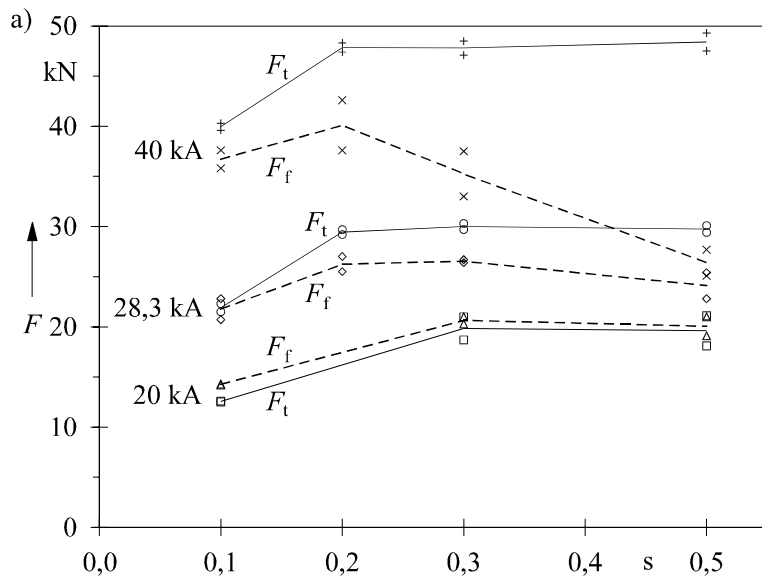


Figure 6.3: Short-circuit tensile force F_t and drop force F_f
 a) Case A b) Case B c) Case C

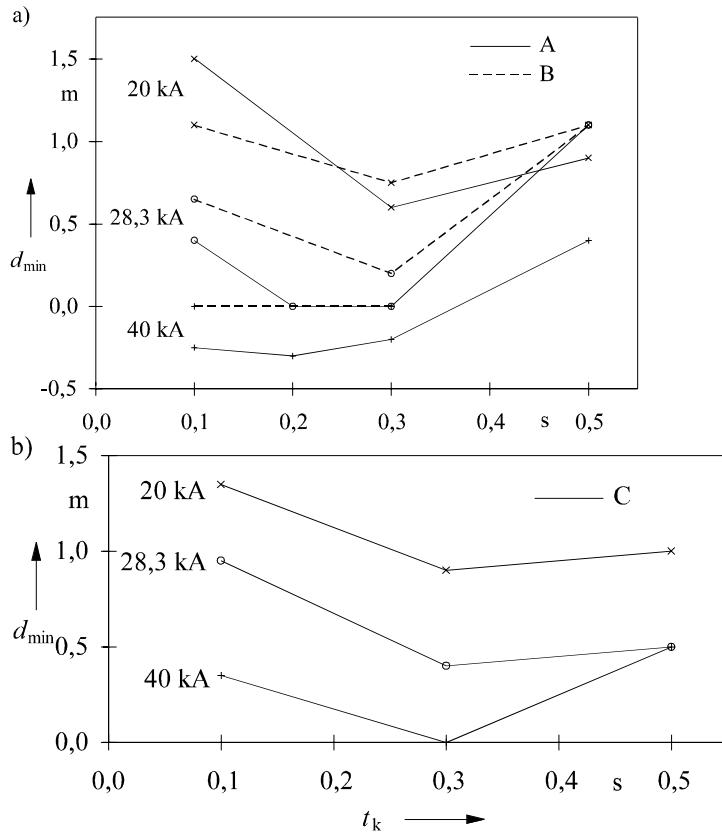


Figure 6.4: Minimum air clearance d_{\min}
 a) Cases A and B b) Case C

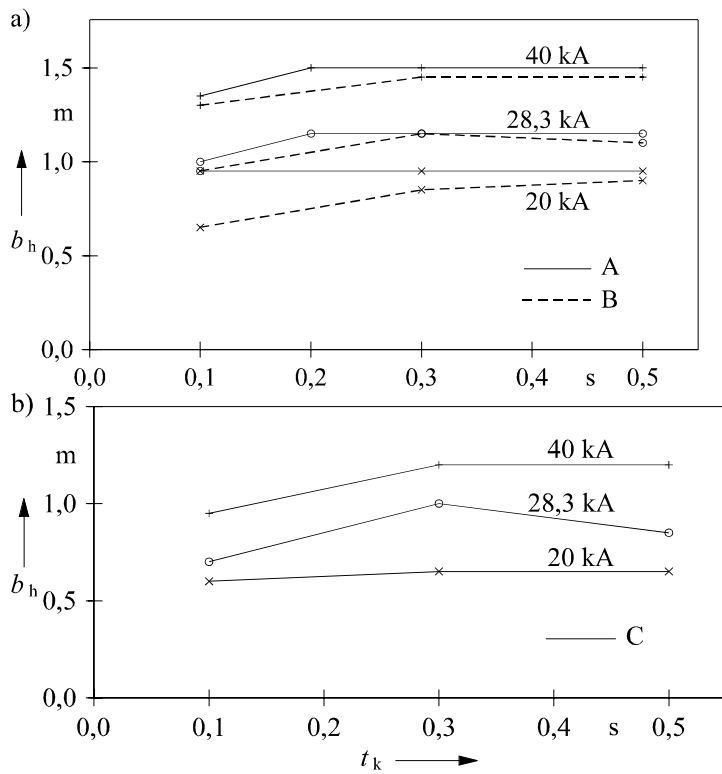


Figure 6.5: Maximum horizontal displacement b_h
 a) Cases A and B b) Case C

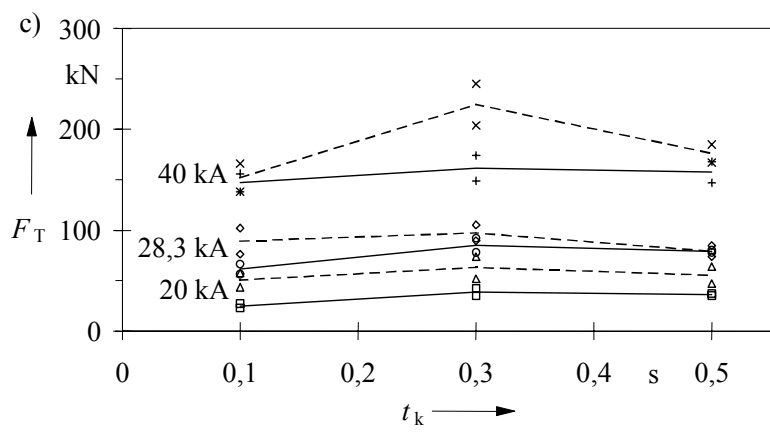
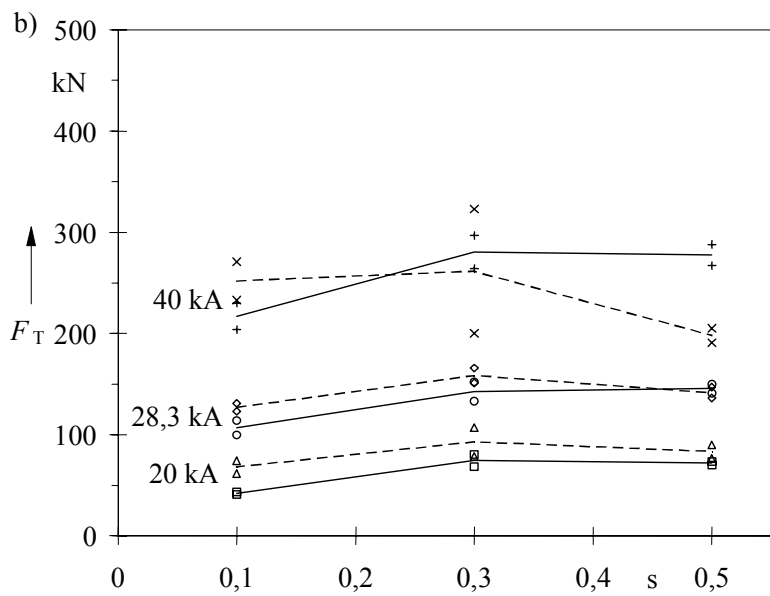
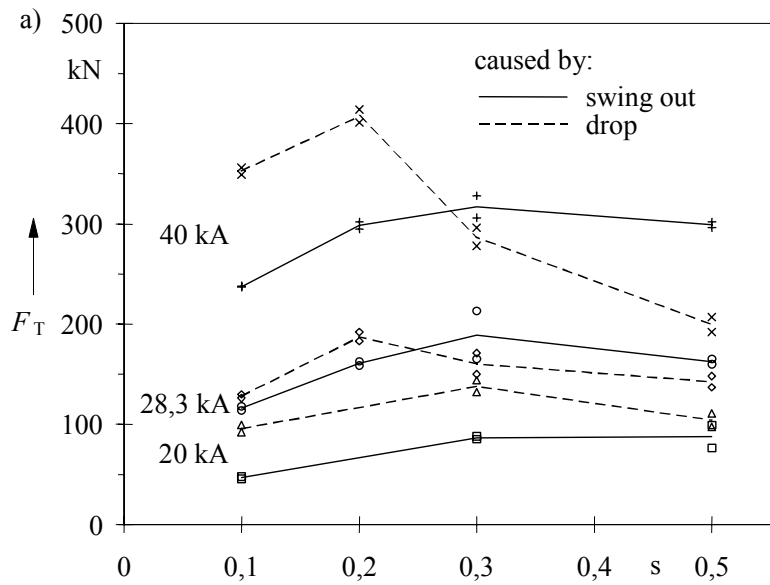


Figure 6.6: Forces F_T at the bottom of the support structure N (MAFU1 and MAFU2)
 a) Case A b) Case B c) Case C

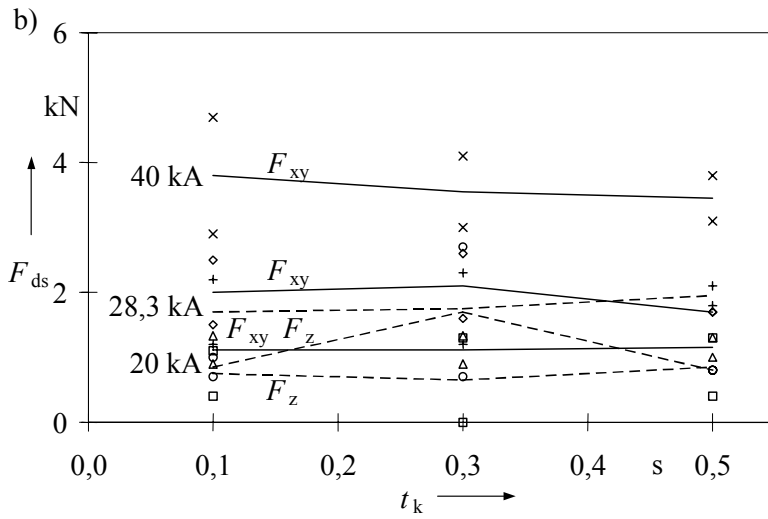
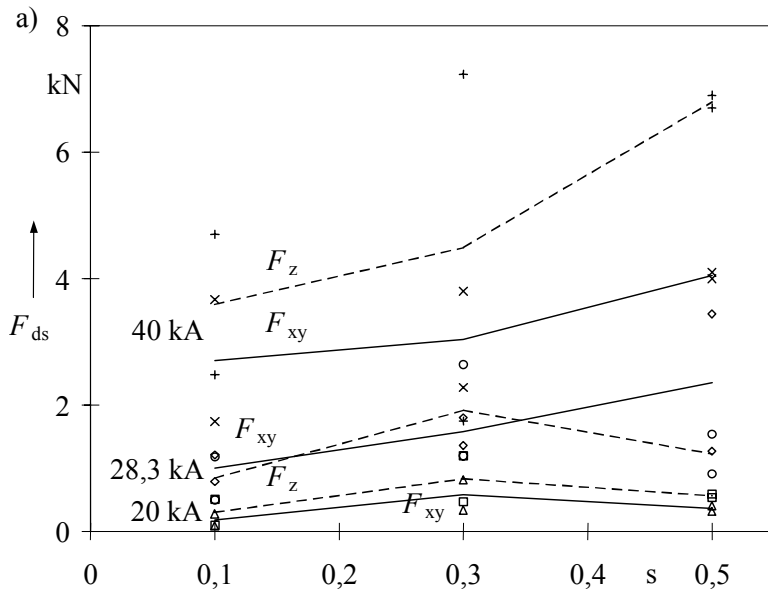


Figure 6.7: Forces F_{ds} at the top of the supporting structure : F_{xy} horizontal, F_z vertical
 a) Case B b) Case C

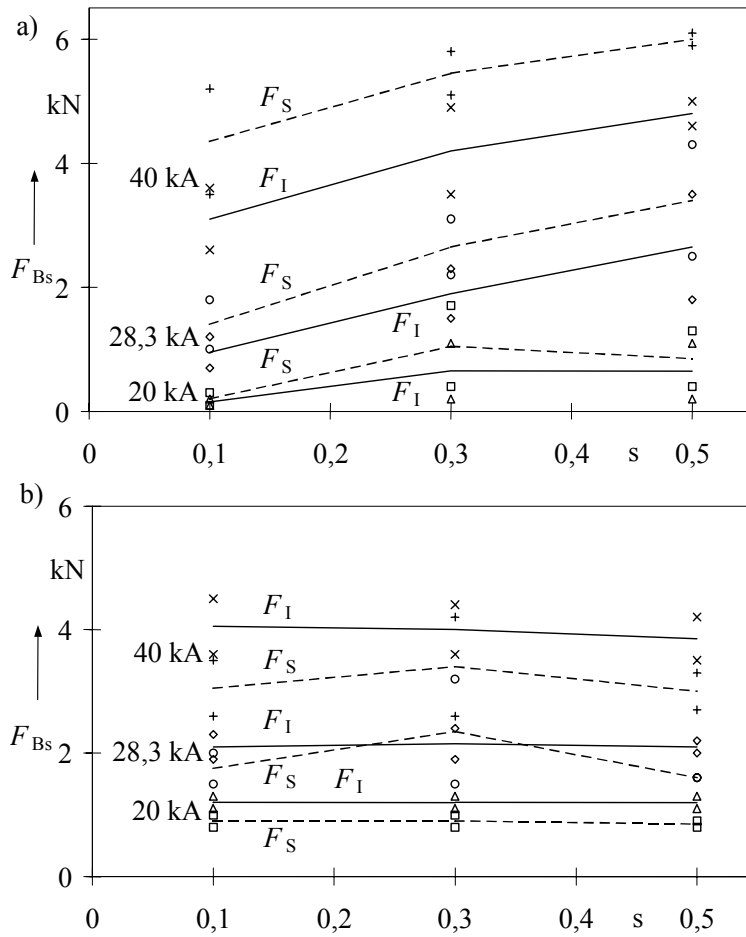


Figure 6.8: Forces F_{Bs} at the bottom of the supporting structure : F_I insulator, F_S steel support structure

a) Case B b) Case C

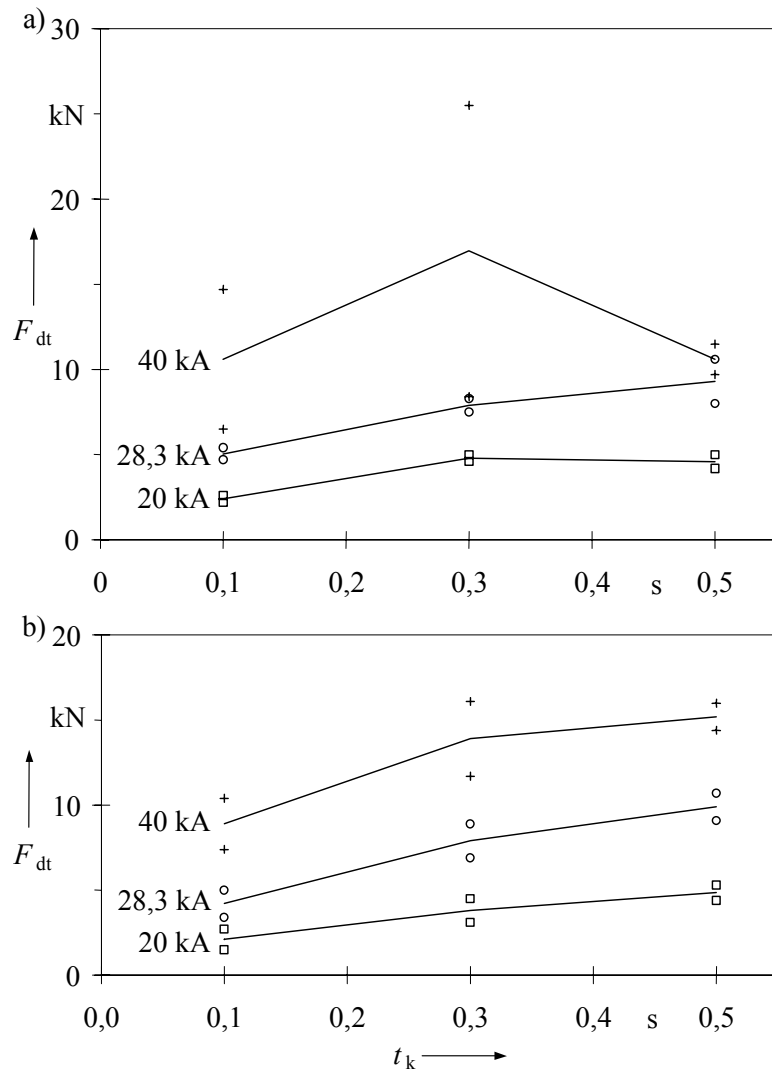


Figure 6.9: Forces F_{dt} in the clamp at the upper end of the dropper
 a) Case B b) Case C

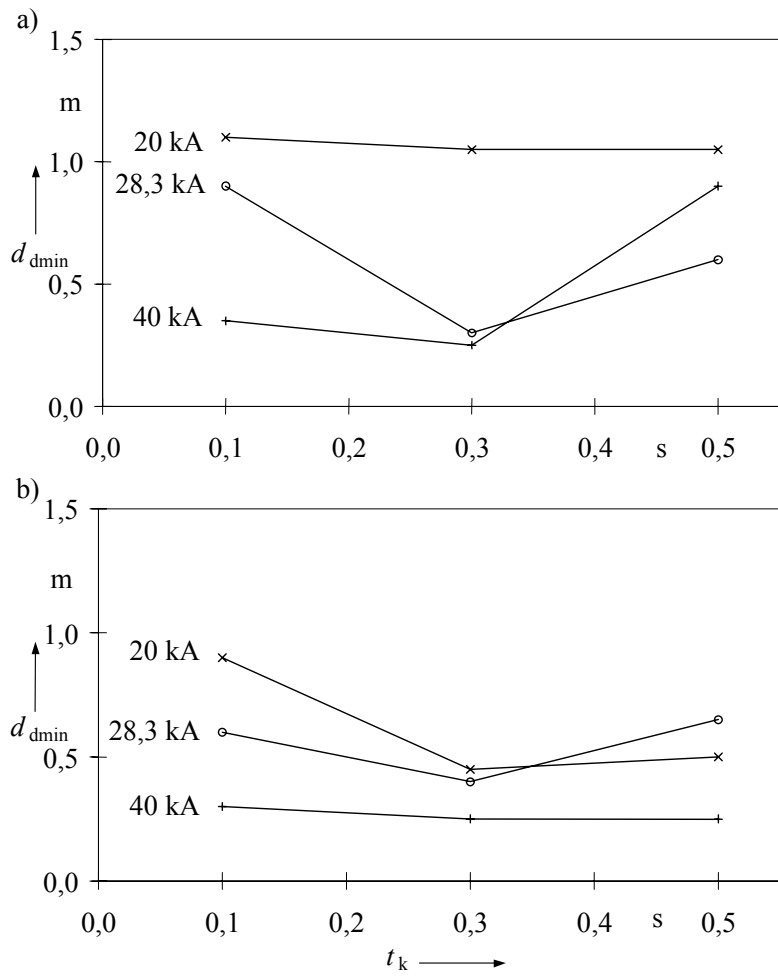


Figure 6.10: Minimum air clearance d_{dmin} of the dropper
 a) Case B b) Case C

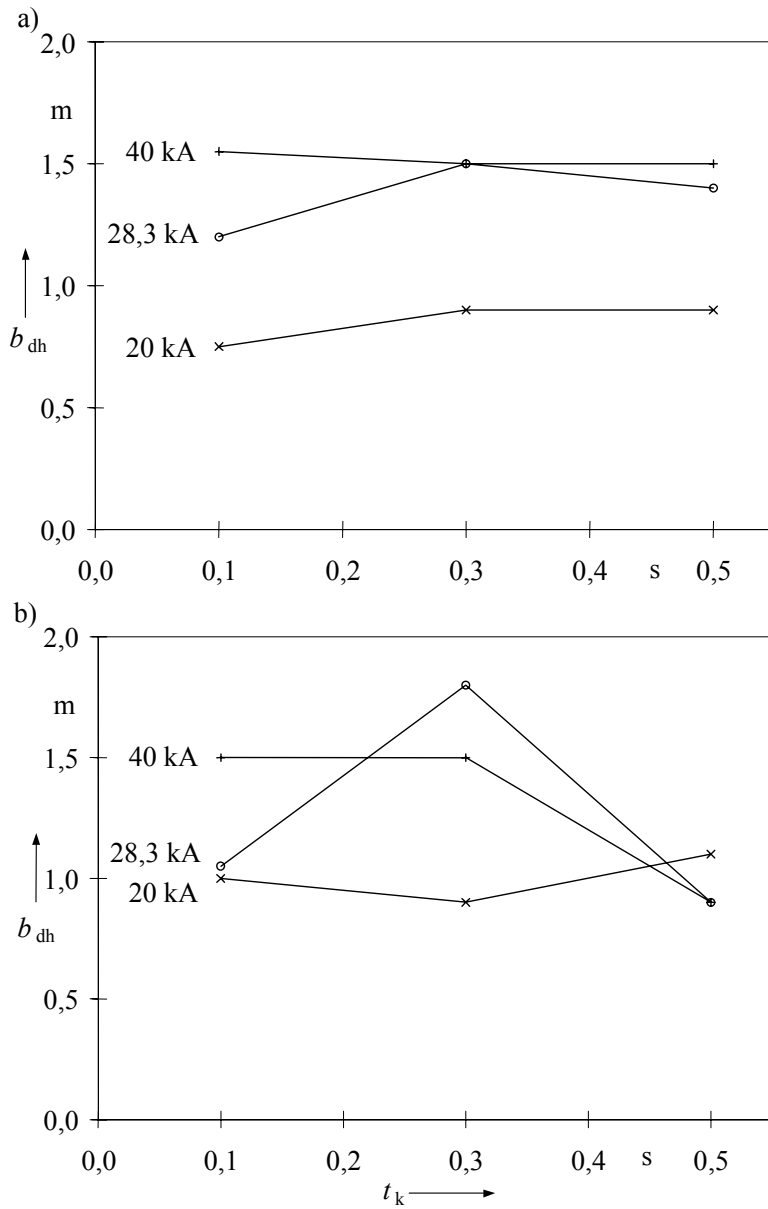
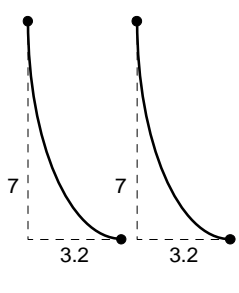
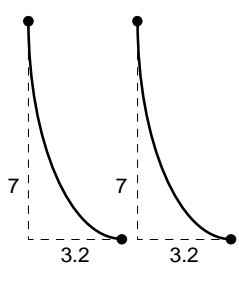


Figure 6.11: Maximum horizontal displacement b_{dh} of the dropper
 a) Case B b) Case C

7. CASE 5

Table 7.1: Test parameters

test arrangement		8	9	10
span		40 m 2 x ACSR 537/53 $a = 3$ m $a_s = 60$ mm		
droppers 1 x ACSR 537/53		without		
dropper length / m			9,145	9,145
current path		A	B	C
$\frac{I_k}{\text{kA}}$	20	0,5	1,0	0,3 / 1,0
	28,3	0,1 / 0,3 / 0,5	0,3 / 0,5 / 1,0	0,3 / 0,5 / 1,0
	40	0,1 / 0,3 / 0,5	0,3 / 0,5 / 1,0	0,1 / 0,3 / 0,5
t_k s				


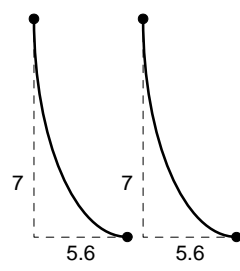
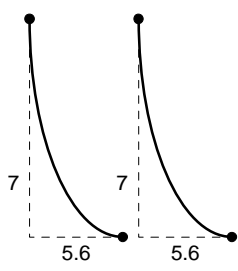
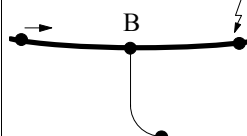
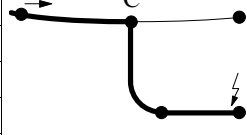
test arrangement		11	12	current path:
span		40 m 2 x ACSR 537/53 $a = 3$ m $a_s = 60$ mm		
droppers 1 x ACSR 537/53				
dropper length / m		10,545	10,545	
current path		B	C	
$\frac{I_k}{\text{kA}}$	20	0,1 / 0,2 / 0,3 / 0,5 / 1,0	0,1 / 0,2 / 0,3 / 0,5 / 1,0	
	28,3	0,1 / 0,2 / 0,3 / 0,5 / 1,0	0,1 / 0,2 / 0,3 / 0,5	
	40	0,1 / 0,2 / 0,3 / 0,5	0,1 / 0,2 / 0,3 / 0,5	
t_k s				

Figure 7.1 & Figure 7.2 show oscillograms of the forces for 9 variants (current path B) and 10 (current path C). For current path variants A, B and C, Figure 7.3 to 7.5 give the measured forces, minimum air clearances and maximum horizontal displacements over the respective values of short-circuit duration. The mean values are connected by straight lines only for better readability.

Results

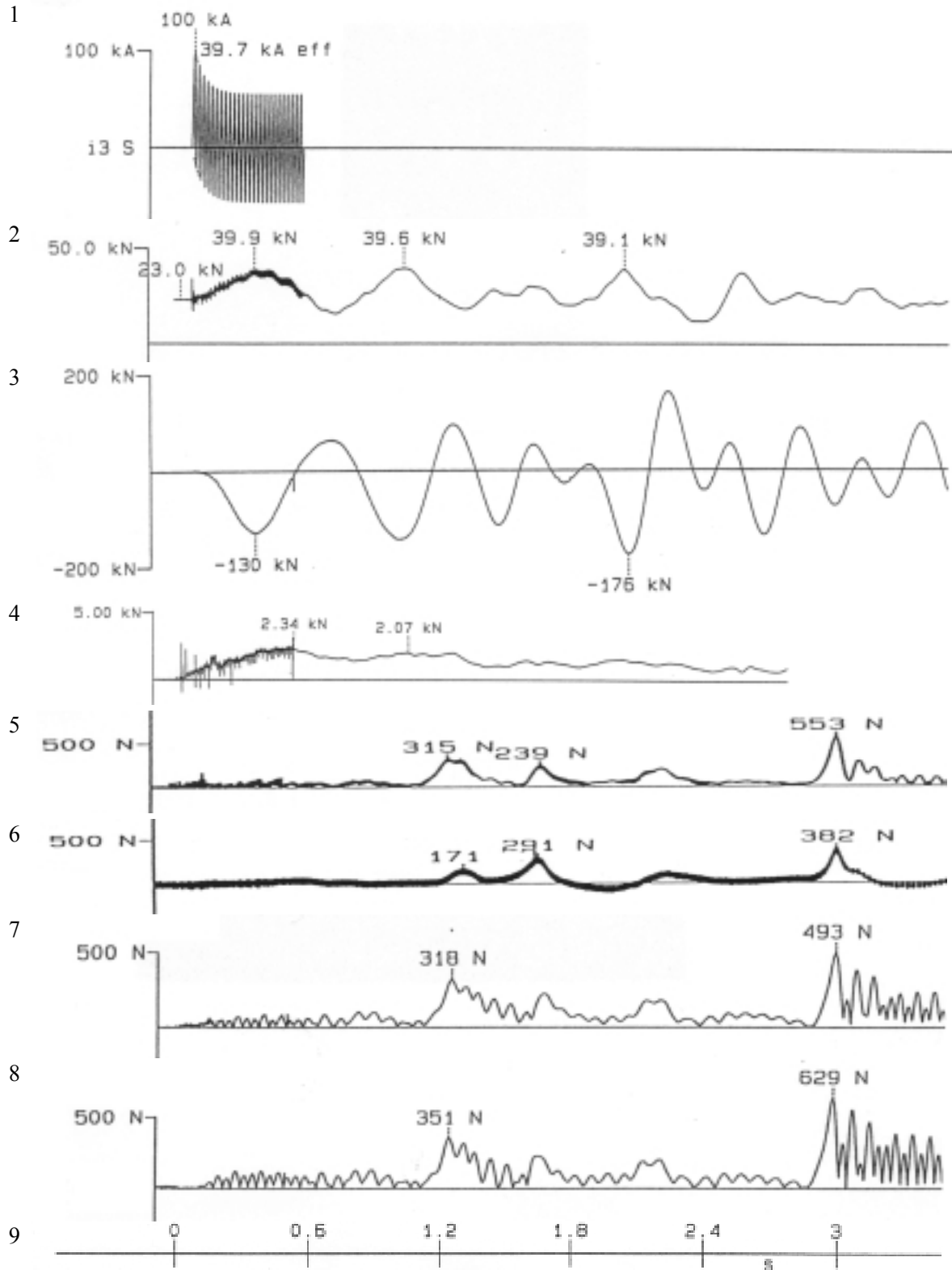
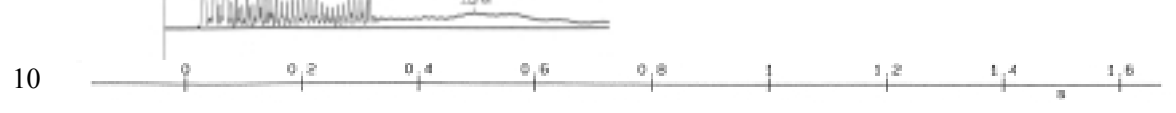
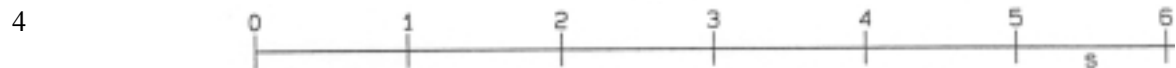
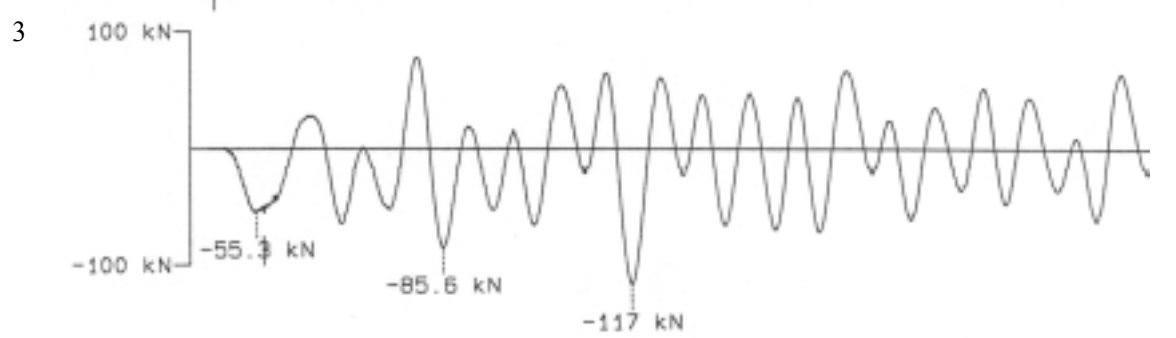
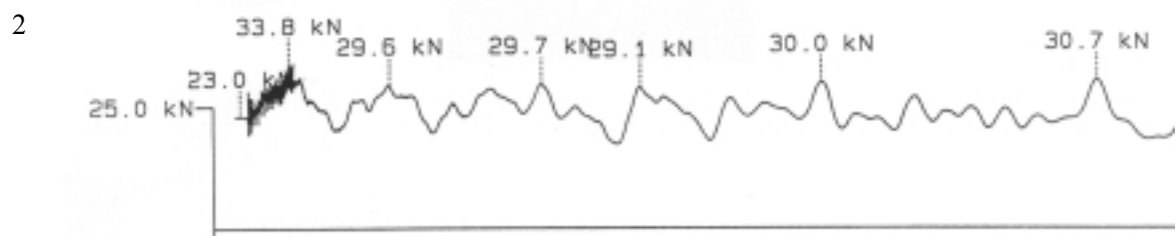
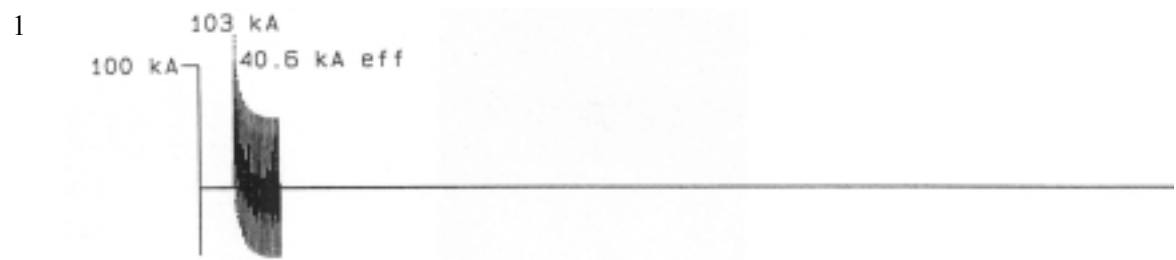


Figure 7.1: Oscillogram of short-circuit test: case B (9 variant); $I_k = 40 \text{ kA}$, $t_k = 0,305 \text{ s}$

- | | |
|---|---|
| <p>1 short-circuit current</p> <p>2 force at the anchoring point of the main conductor</p> <p>3 force at the bottom of the steel support (MAFU2)</p> <p>4 force in the clamp at the upper end of the dropper</p> <p>5 horizontal force at the top of the supporting insulator</p> | <p>6 vertical force at the top of the supporting insulator</p> <p>7 force at the bottom of the supporting insulator</p> <p>8 force at the bottom of the steel support structure</p> <p>9 time scale</p> |
|---|---|



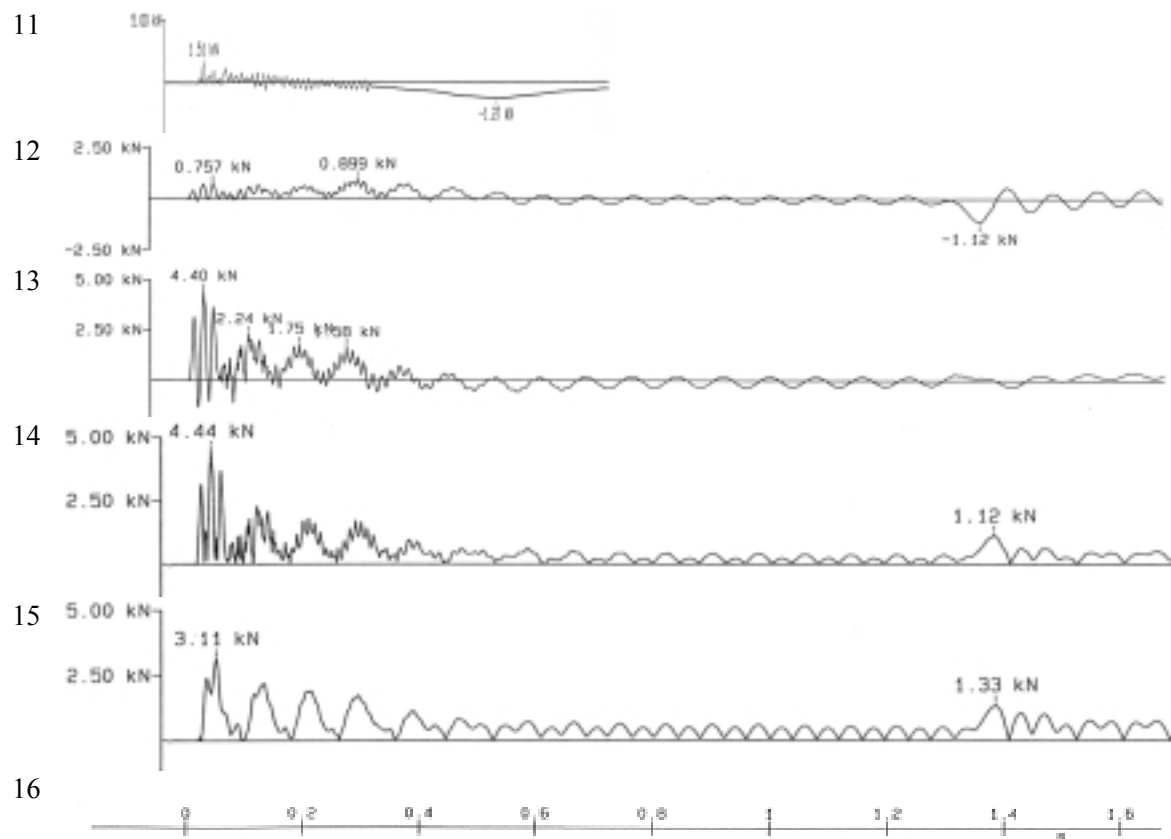


Figure 7.2: Oscillogram of short-circuit test: case C (10 variant); $I_k = 40$ kA, $t_k = 0,305$ s

Traces:

- 1,5 short-circuit current
- 2 force at the anchoring point of the main conductor
- 3 force at the bottom of the steel support (MAFU3)
- 4 time scale for traces 1 to 3
- 6 force in the clamp at the upper end of the dropper
- 7 force in x-axis at the top of the supporting insulator
- 8 force in y-axis at the top of the supporting insulator
- 9 horizontal force at the top of the supporting insulator
- 10,16 time scale for traces 6 to 15
- 11 force in z-axis at the top of the supporting insulator
- 12 force in x-axis at the bottom of the supporting insulator
- 13 force in y-axis at the bottom of the supporting insulator
- 14 horizontal force at the bottom of the supporting insulator
- 15 horizontal force at the bottom of the steel support structure

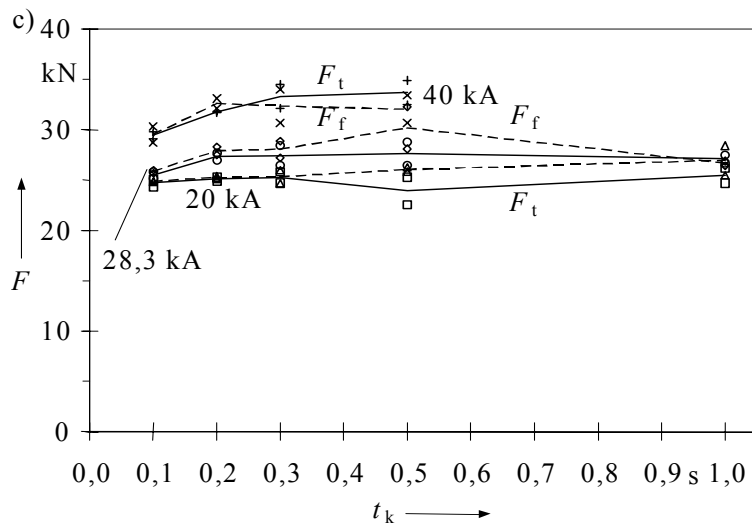
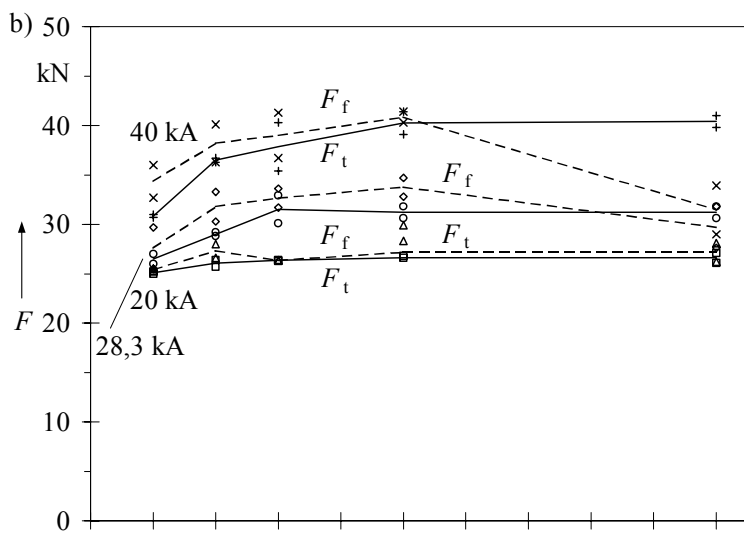
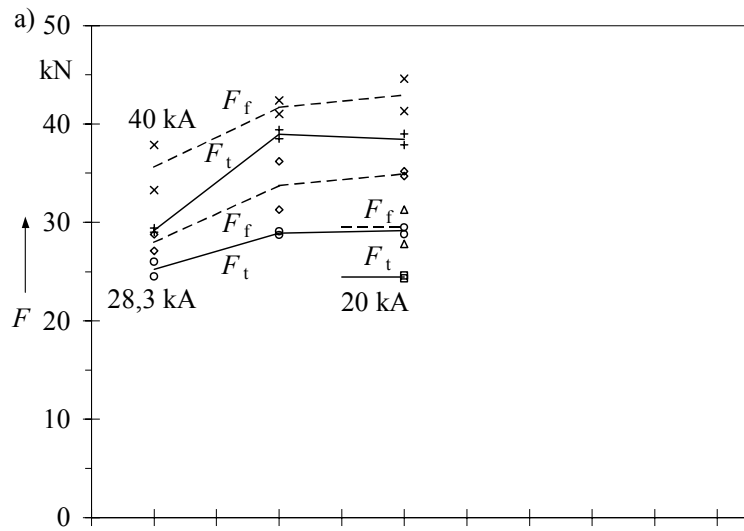


Figure 7.3: Short-circuit tensile force F_t and drop force F_f
 a) Case A b) Case B c) Case C

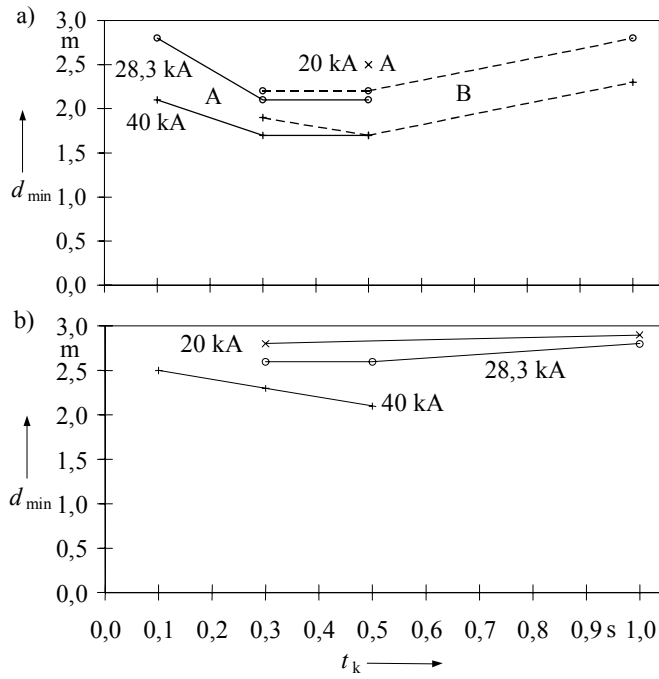


Figure 7.4: Minimum air clearance d_{\min}
 a) Cases A and B b) Case C

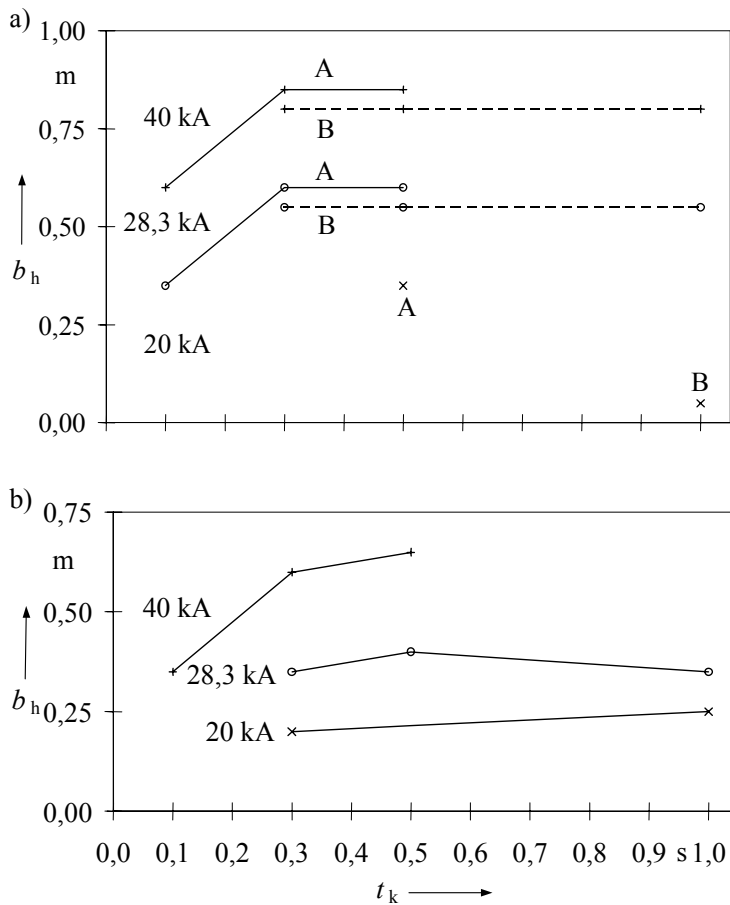


Figure 7.5: Maximum horizontal displacement b_h
 a) Case A and B b) Case C

PART III

Conductor pinch effects

8. CASE 6

Tests performed at Österreichische Elektrizitätswirtschafts-AG (Austria) in 1963
 cross section: ACSR 537/53 mm² twin bundle ($n = 2$)
 short-circuit current: 4 kA eff to 21,5 kA eff
 span length: 12 m

Bus-Bar Geometry

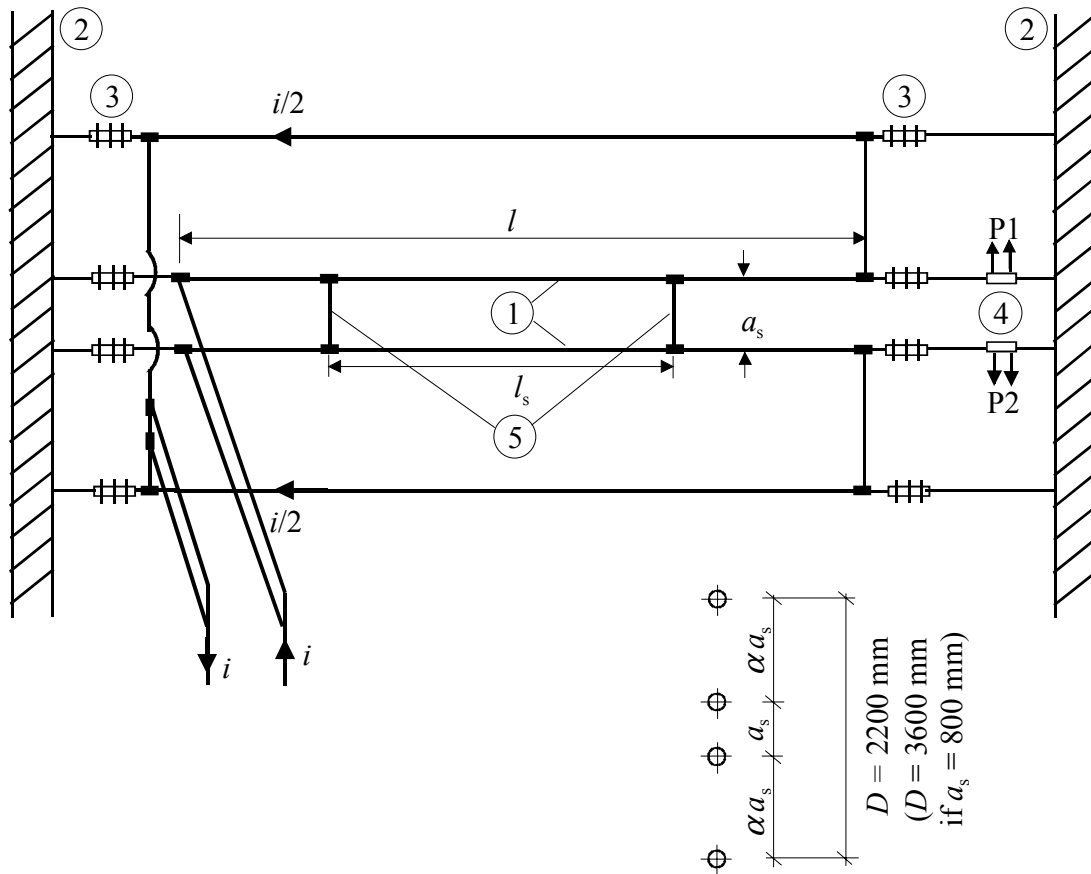


Figure 8.1: Test set-up

- | | |
|-------|--|
| 1 | bundle conductor under test |
| 2 | wall |
| 3 | insulator |
| 4 | strain gage for measuring the forces |
| 5 | spacers |
| l | span length |
| l_s | centre-line distance between spacers |
| D | centre-line distance between return conductors |
| a_s | centre-line distance between subconductors |
| k | number of spacers |

Basic data

Conductors:

	cross-section	diameter	mass per unit length	Young's modulus	temperature coefficient
	A	d	m'	E	α_θ
	mm ²	mm	kg/m	N/mm ²	10 ⁻⁶ /K
ACSR 537/53	590	1,937	32	69000	19,8

bundle configuration: twin bundle ($n = 2$)

number of spacers: 0 ... 11

centre-line distance between subconductors: 35 mm ... 800 mm

centre-line distance between conductors: see Fig. 1

initial static tensile force: 1,2 ... 1,35 kN

initial static stress: 1,0 ... 1,2 N/mm²

short-circuit characteristics: $\kappa < 1,5$

short-circuit duration: $T_k = 0,2$ s

Reference:

- [1] Wagner, E.: Dauer- und Kurzschlußbeanspruchung von Bündelleitern in Hochspannungsschaltanlagen. Österreichische Zeitschrift der Elektrotechnik 18(1965), 18-25.

Results

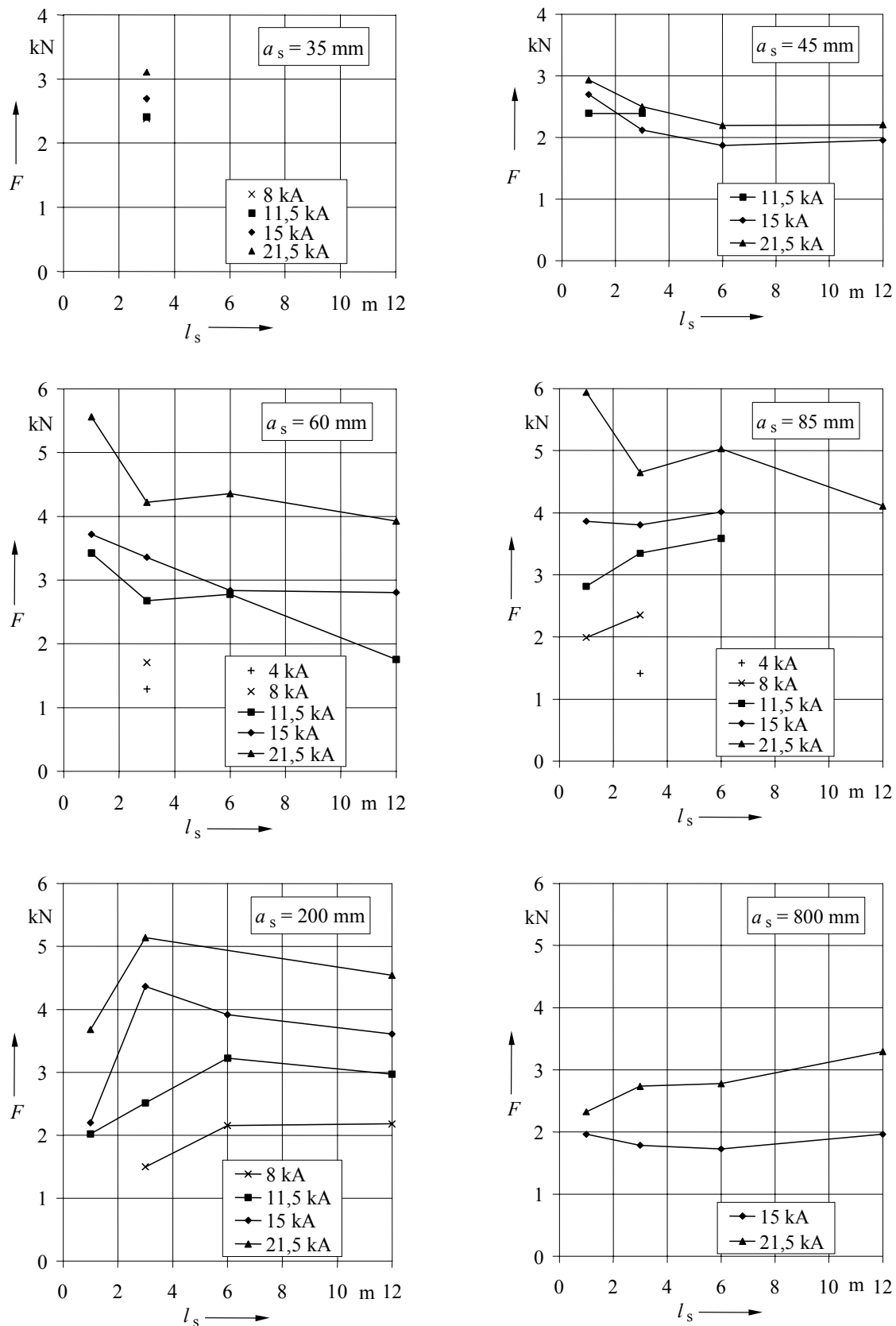


Figure 8.2: Short-circuit tensile force F in the bundle as a function of distance between spacers l_s for different sub-conductor distances a_s

9. CASE 7

Tests performed at Lehrstuhl für Elektrische Energieversorgung (Germany) in 1985
cross section: ACSR 340/30 mm² and ACSR 605/70 mm² twin bundle ($n = 2$)
short-circuit current: 3,5 kA eff to 11 kA eff
span length: 7,6 m

Test arrangement

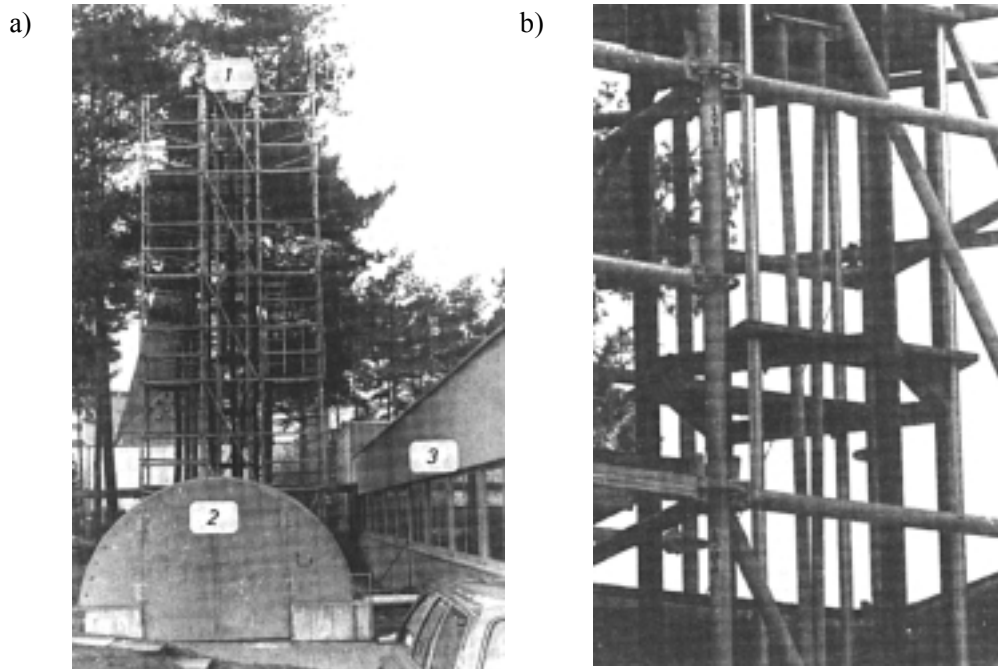


Figure 9.1: Test set-up

- a) Total view
 - 1 tower with bundle; steel frame for fixing the bundle, service frame, height: 10 m
 - 2 house with transformer and a reactor as compensator
 - 3 control center
- b) Close twin bundle
ACSR 605/70 mm²; $F_{st} = 2$ kN; $I_k = 10,6$ kA; one spacer

The arrangement was built up for measuring only the pinch effect. The tested bundles are in vertical position to eliminate the influence of changes in sag. The short-circuit current flows through the bundle and back through four conductors situated in the corners of a quadrate. With this the return current does not induce electromagnetic field inside the quadrate and does not influence the movement of the bundle conductors.

The upper clamp is fixed on a steel frame. The tensile forces are measured at the lower clamp. The static tensile force is adjusted using a turnbuckle.

Basic data

Conductors:

	cross-section	diameter	mass per unit length	Young's modulus	temperature coefficient
	A	d	m'	E	α_θ
	mm ²	mm	kg/m	N/mm ²	10 ⁻⁶ /K
ACSR 340/30	369	25	1,174	62000	20,5
ACSR 605/70	680	33	2,22	68000	19,4

bundle configuration: twin bundle ($n = 2$)

number of spacers: 0 ... 3

centre-line distance between subconductors: 80 mm; 115 mm; 150 mm

initial static tensile force: 0,5 ... 20 kN

initial static stress: 0,4 ... 29 N/mm²

conductor fixation: stiffness: 6 kN/mm
frequency: 87 Hz

short-circuit characteristics: $\kappa = 1,2$ ($\tau = 5,5$ ms)

short-circuit duration: $T_k = 0,245$ s

Results

Figure 9.2 gives the oscillograms of the current and the tensile forces. The time scale of the tensile force shows from its beginning a 100-Hz-component due to the bend between the rotationally symmetric lead-in wires at the lower clamp. This also explains the reduction of the force after initiation of the short-circuit; this had been observed in other tests, too.

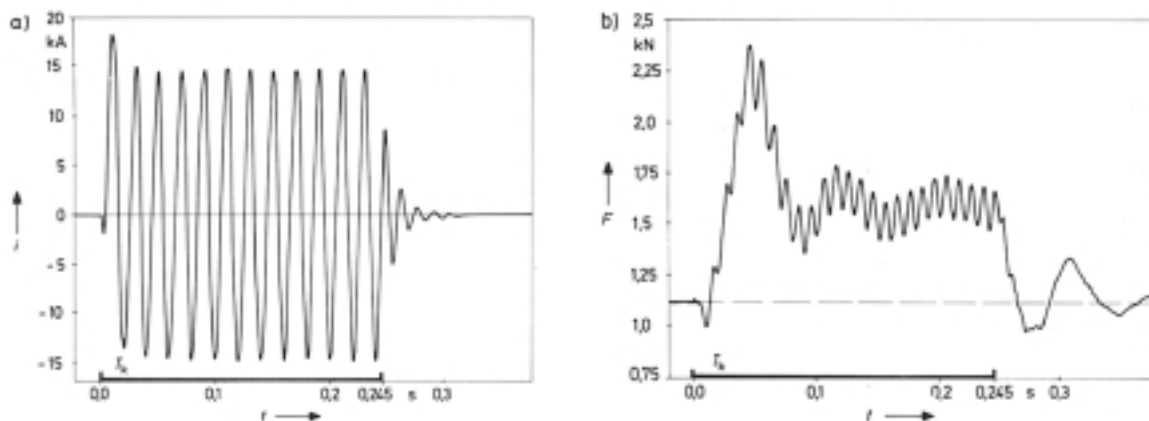


Figure 9.2: Oscillograms. ACSR 605/70 mm²; sub-conductor distance $a_s = 115$ mm; $F_{st} = 1,15$ kN; $I_k = 10,2$ kA; three spacers

a) current

b) tensile force

The measured maximum forces F are represented in the figures 3 and 4 related on the static tensile forces F/F_{st} for the two types of conductors and different short-circuit currents and static tensile forces.

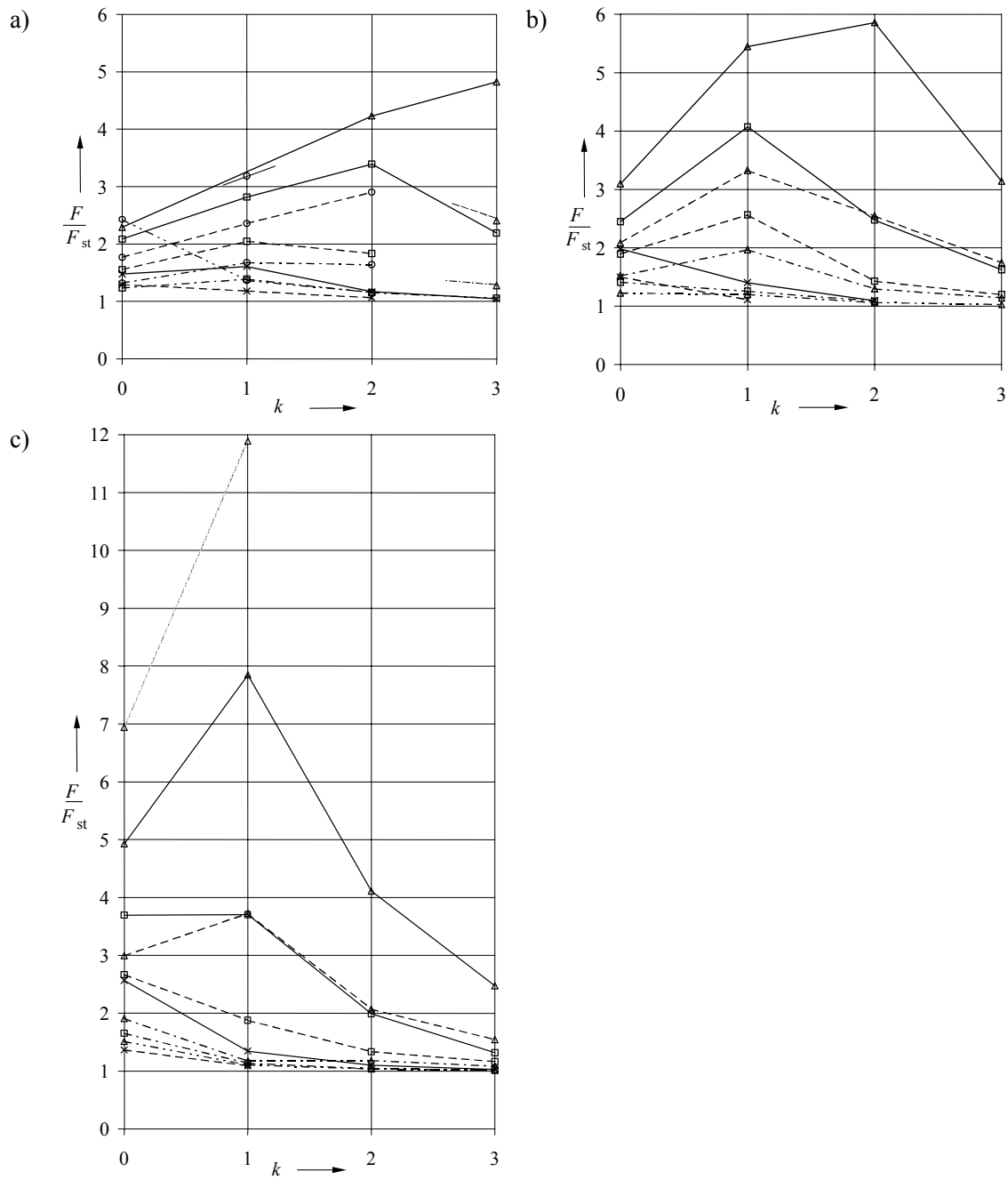


Figure 9.3: Maximum short-circuit tensile force due to pinch effect.

2×ACSR 340/80;

a) $a_s = 80$ mm b) $a_s = 115$ mm c) $a_s = 150$ mm

currents:

× 3,3 kA □ 6,6 kA ○ 7,4 kA △ 9,6 kA

static tensile forces:

——— 0,6 kN ——— 1,0 kN - - - - 2,1 kN
 - · - · - 5,2 kN - · - · - 9,8 kN

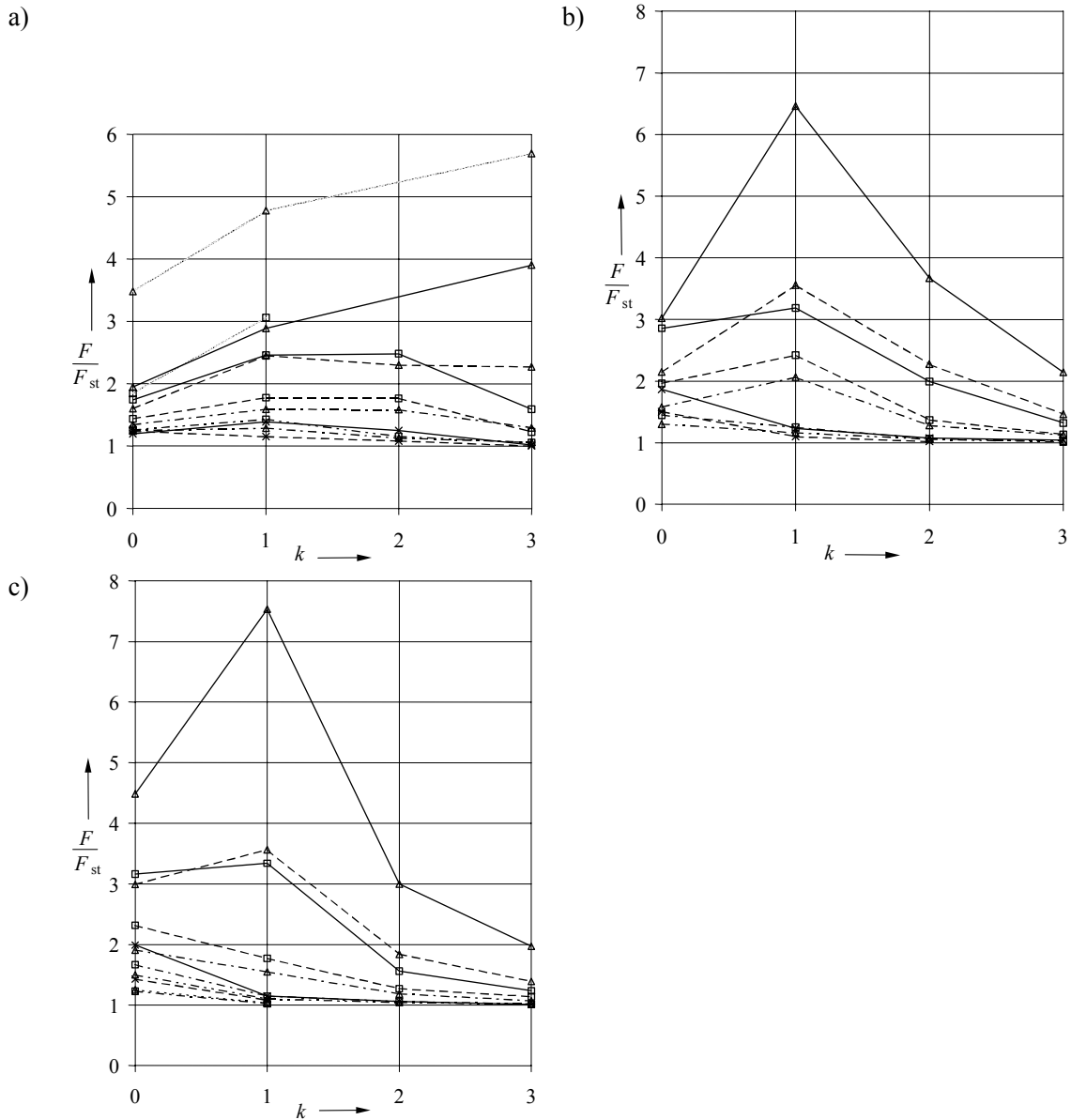


Figure 9.4: Maximum short-circuit tensile force due to pinch effect.

2×ACSR 605/70;

a) $a_s = 80$ mm b) $a_s = 115$ mm c) $a_s = 150$ mm

currents:

× 3,6 kA a,b): □ 6,6 kA c): ○ 7,2 kA △ 10,4 kA

static tensile forces:

———	0,5 kN	—————	1,0 kN	- - - -	2,2 kN
- · - · -	5,1 kN	- · - · - · -	10,1 kN	- - - - -	19,1 kN

References:

- [1] Kießling, G.: Kurzschlußkräfte bei Zweierbündeln – Messungen und analytische Lösung mit dem Parabelmodell. etzArchiv 10 (1988), 53-60.
- [2] Kießling, G.: Die dynamische Kurzschlußbeanspruchung von Seilanlagen – Analytische und numerische Berechnungsverfahren. Dissertation Universität Erlangen-Nürnberg, 1988.

10. CASE 8

Tests performed at VEIKI Laboratories (Hungary) in 1997
cross section: CONDOR 455, twin bundle ($n = 2$)
short-circuit current: 35 kA eff and 48 kA eff
span length: 60 m

10.1. INTRODUCTION

This case provides a set of experimental results collected at the VEIKI Laboratories in April 97. This is not an exhaustive set but we include in this report the most representative results allowing scientists and researchers to well-understand the evolution of tension in sub-conductors, compressive force in rigid spacers depending on subspan length, sagging tension, short-circuit duration or intensity, etc...

10.2. CONFIGURATION CHARACTERISTICS (TWIN HORIZONTAL BUNDLE)

Span length 60 m (subspan length detailed case by case)

- *Sub conductor type* ACSR CONDOR (455 mm², $\phi = 27.7$ mm, 1.52 kg/m, UTS 125 kN)
 - *Spacing* 0.457 m
 - *Current* 35 kA (90 kA peak) ,
- Time constant 33 ms
48 kA (122 kA peak)
- *Duration* 0.17 to 0.2 s, one case 1s.
 - *Sagging tension* 15, 25 or 35 kN
 - Tension is given for one subconductor
 - *All cases one phase fault, return path on the ground*



Figure 10.1 VEIKI test arrangement – 60 m span length – spacer at mid-span. The return path is on the ground.

- *Supporting structure*
- Stiffness: about $8.5 \cdot 10^6$ N/m
First eigen frequency : about 14 Hz

IMPORTANT REMARK

To obtain range of precision, most of the cases have been tested with two spacers at mid-span (separated by 0.5m), each spacer equipped with two full bridges of strain gages. The error on measurements expected is about 10-15 %. It means also that the measured value is only half of the full compression obtained in practice when only one spacer is installed. Only the cases V.1 and VI.1 were tested with a single spacer at mid-span, giving directly the full compression load.



Figure 10.2 Veiki Test arrangement – End span fixations.

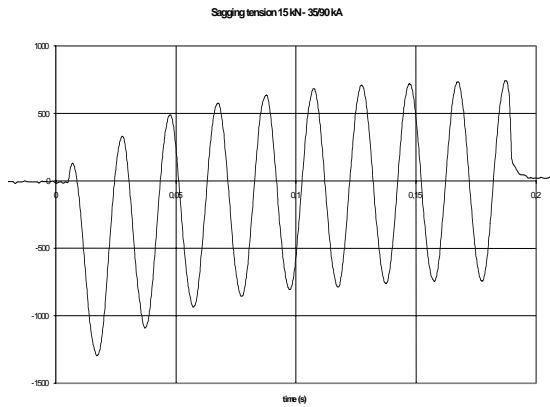
Two sub conductors were separately fixed to the tower

Each set of results includes:

1. Short-circuit wave shape (uncalibrated),
2. Spacer compression on about 1s duration,
3. Sub conductor tension on maximum observation time,
4. Zoom of spacer compression in the first 200 ms,
5. Zoom of sub conductor tension on the first 200 ms.

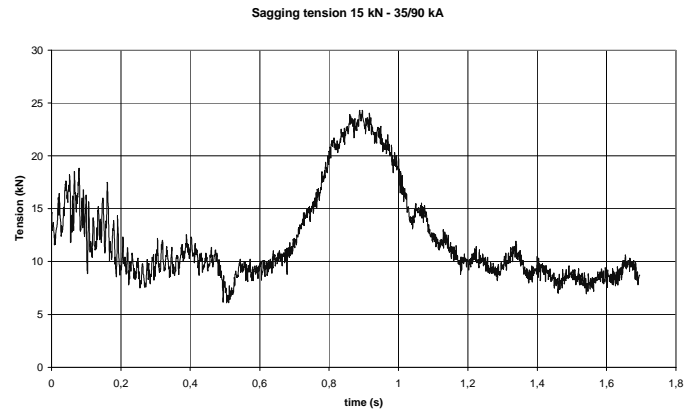
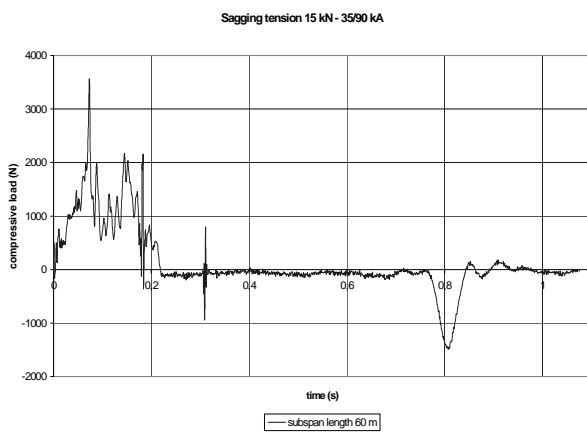
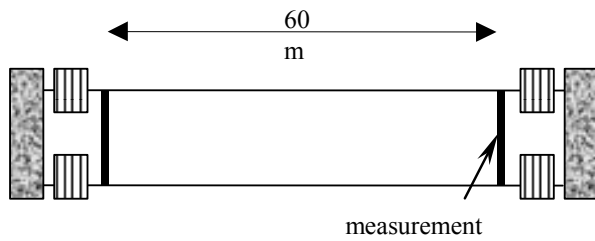
10.3. CASE II.1 – 1 X 60 M – 15 KN – 35/90 KA

- Configuration One subspan 60 m
- Exact tension/subconductor: 13 kN
- Short-circuit level: (rms/peak) 35/90 kA
- Duration: 0.18 s

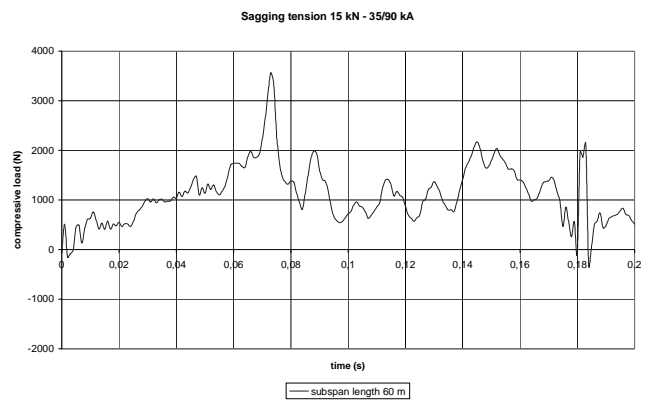
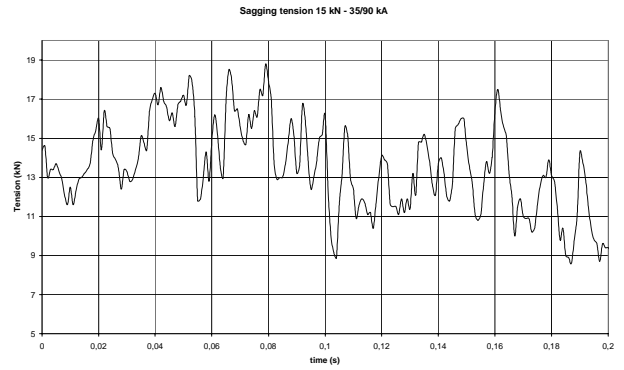


Current wave shape (ordinates not valid)

Configuration :

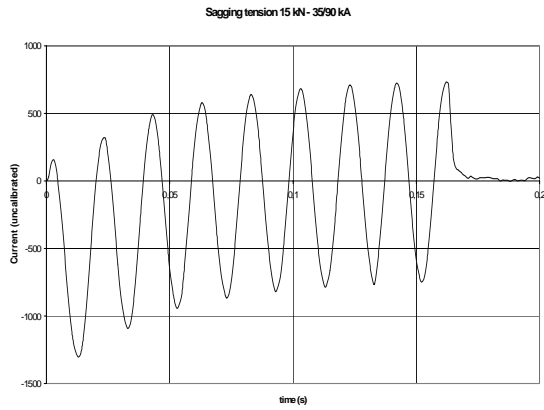


Zoom on spacer compression and tension time evolution

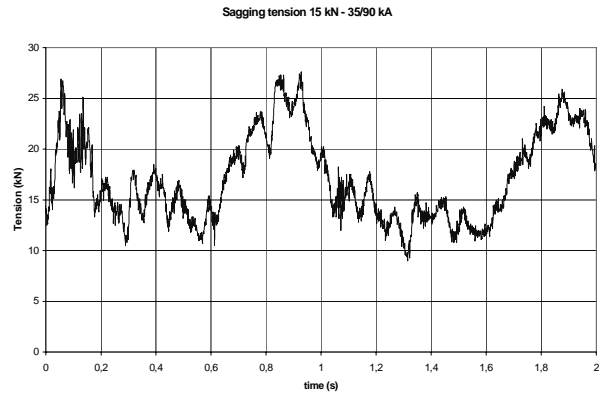
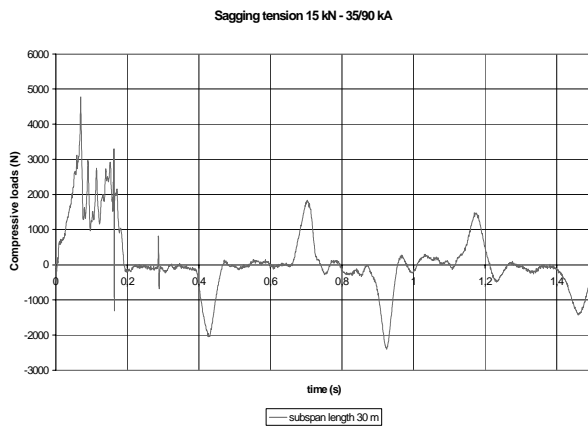
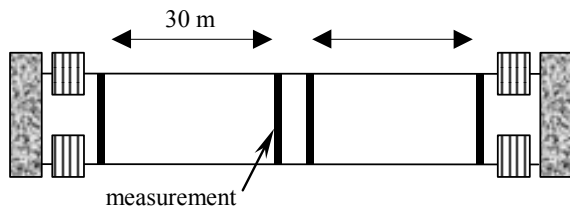


10.4. CASE II.5 – 2 X 30 M – 15 KN – 35/90 KA

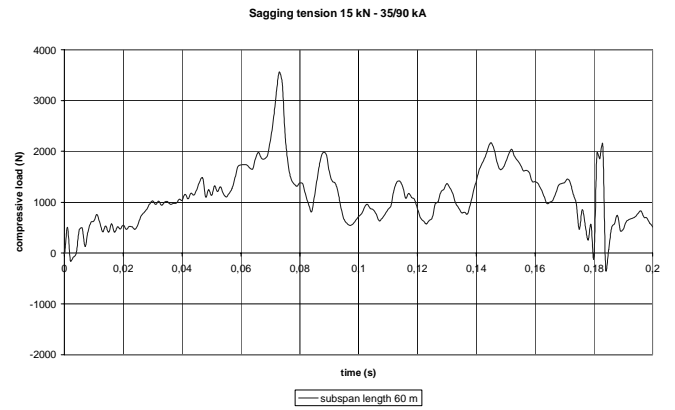
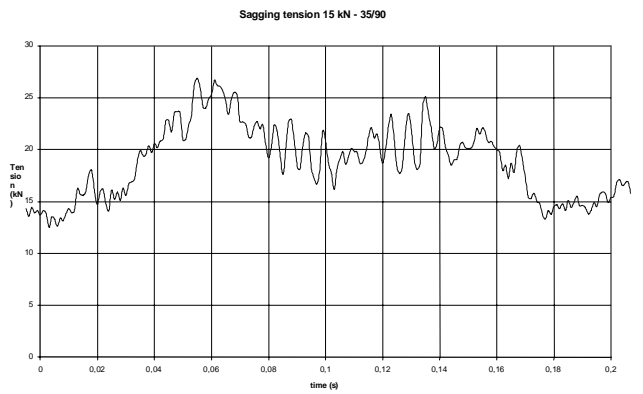
- Configuration One subspan 30 m
- Exact tension/subconductor: 13 kN
- Short-circuit level: 35/90 kA
- Duration: 0.17s



Configuration :

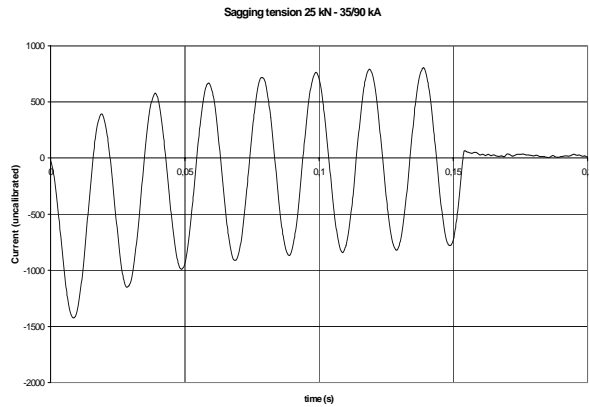


Zoom on spacer compression and tension time evolution

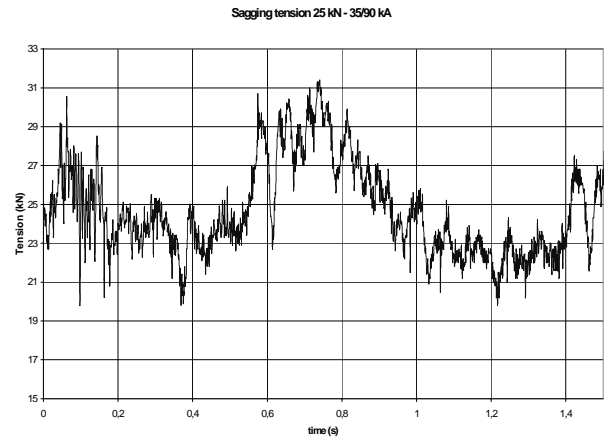
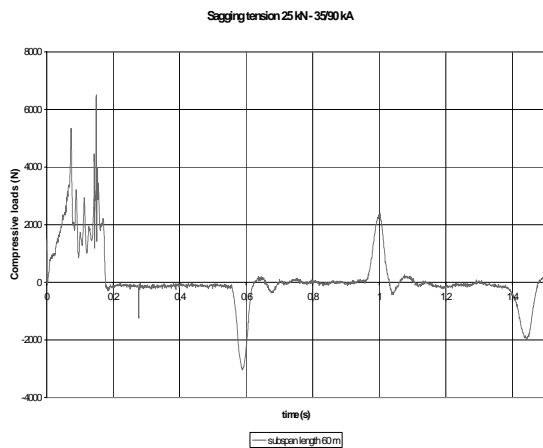
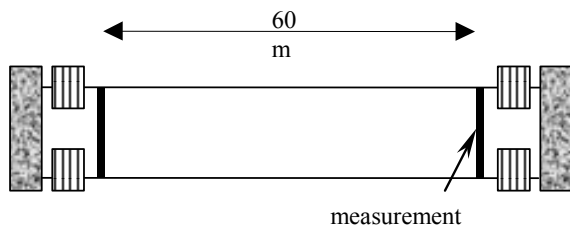


10.5. CASE III.1 – 1 X 60 M – 25 KN – 35/90 KA

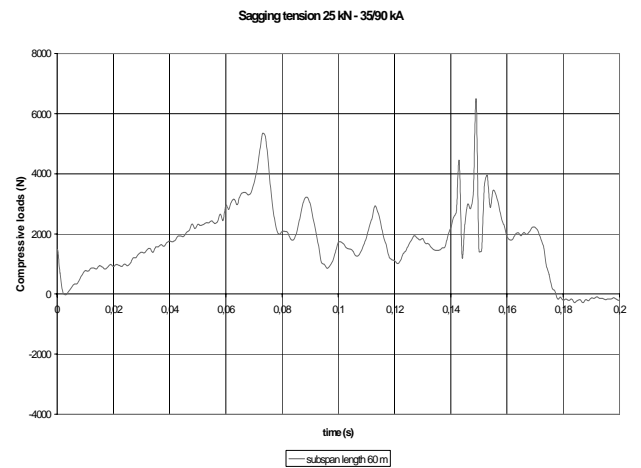
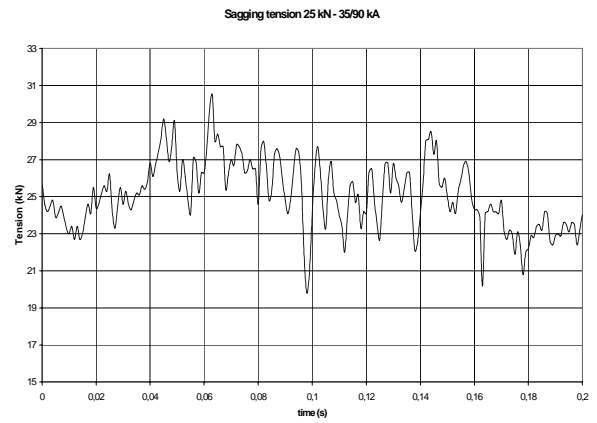
- Configuration One subspan 60 m
- Exact tension/subconductor: 25 kN
- Short-circuit level: 35/90 kA
- Duration: 0.16 s



Configuration :

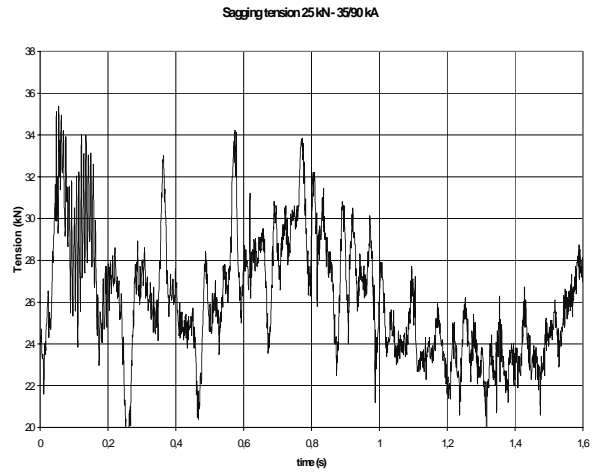
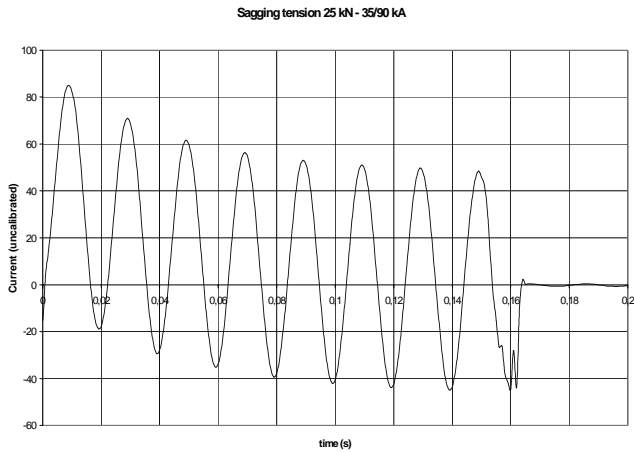


Zoom on spacer compression and tension time evolution



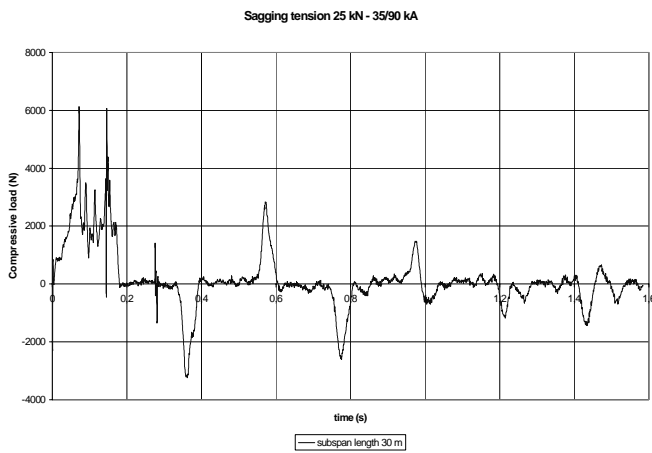
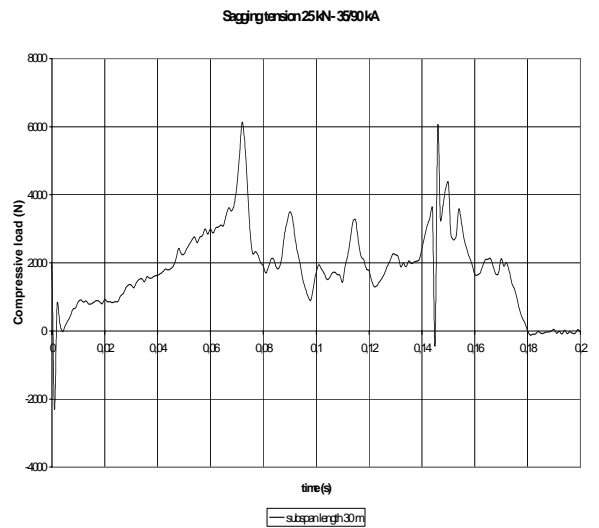
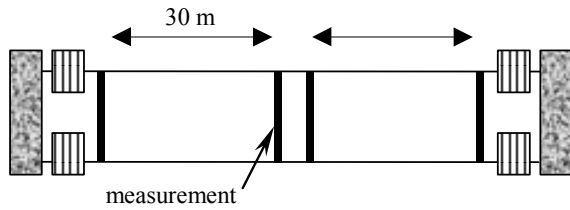
10.6. CASE III.5 – 2 X 30 M – 25 KN – 35/90 KA

- Configuration One subspan 30 m
- Exact tension/subconductor: 25 kN
- Short-circuit level: 35/90 kA
- Duration: 0.16 s



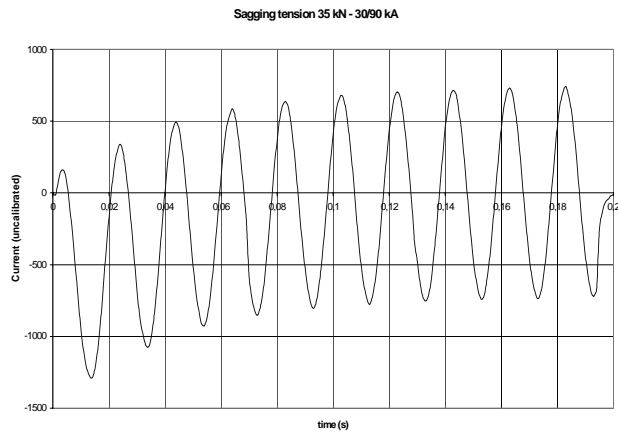
Zoom on spacer compression and tension time evolution :

Configuration :

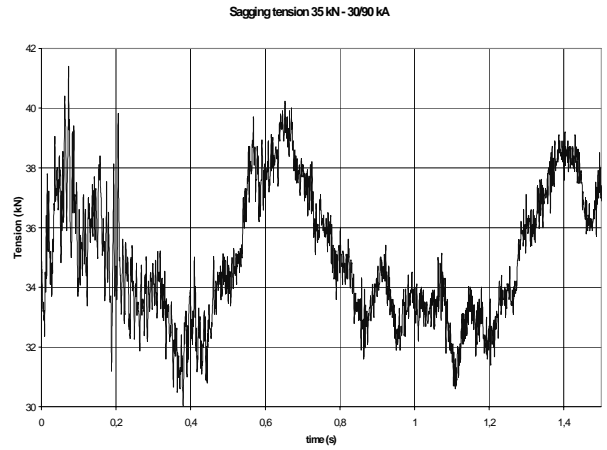
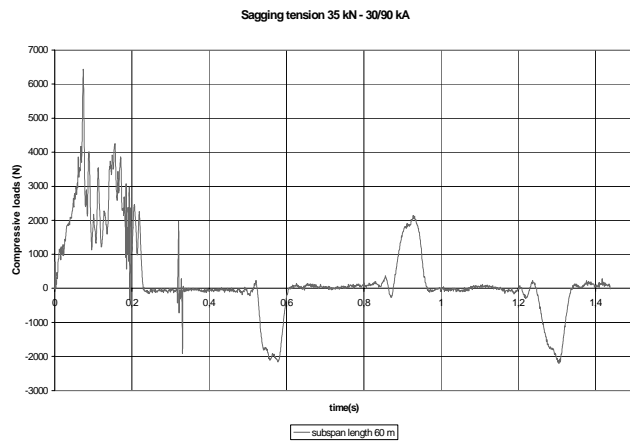
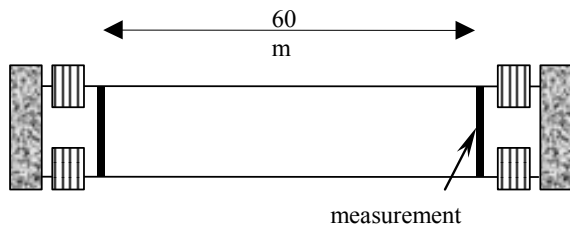


10.7. CASE IV.1 – 1 X 60 M – 35 KN – 35/90 KA

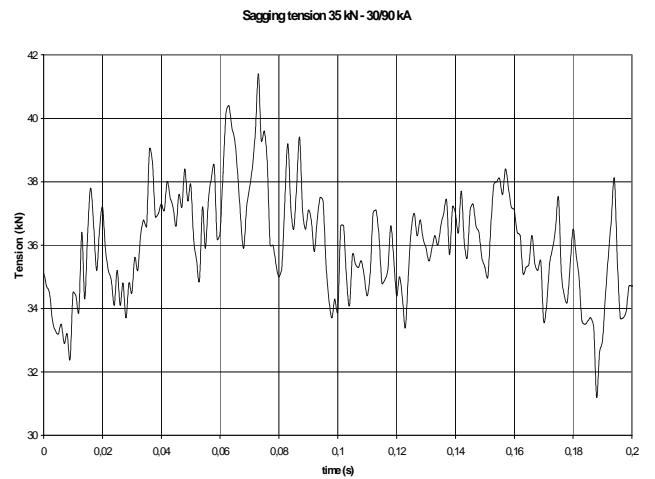
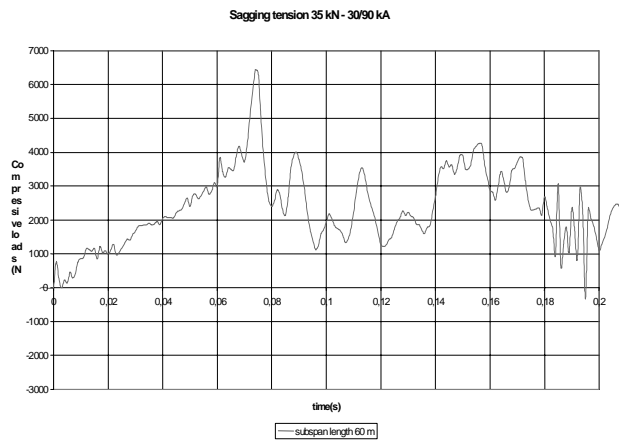
- Configuration One subspan 60 m
- Exact tension/subconductor: 35 kN
- Short-circuit level: 35/90 kA
- Duration: 0.2 s



Configuration :

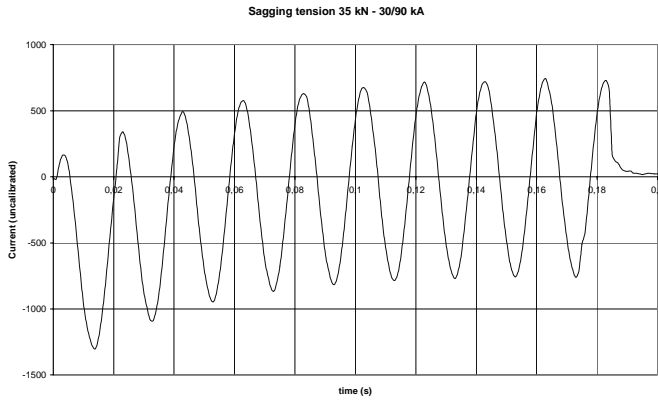


Zoom on spacer compression and tension time evolution

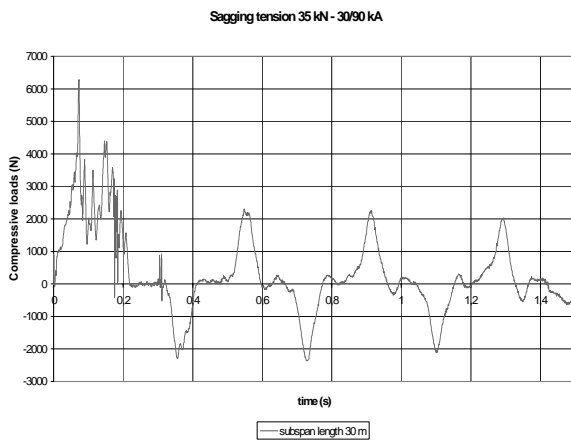
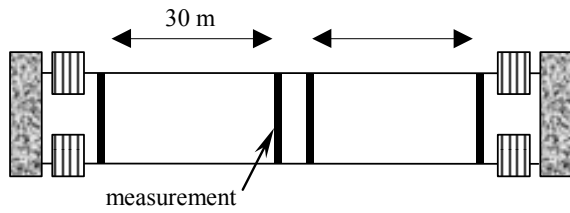


10.8. CASE IV.5 – 2 X 30 M – 35 KN – 35/90 KA

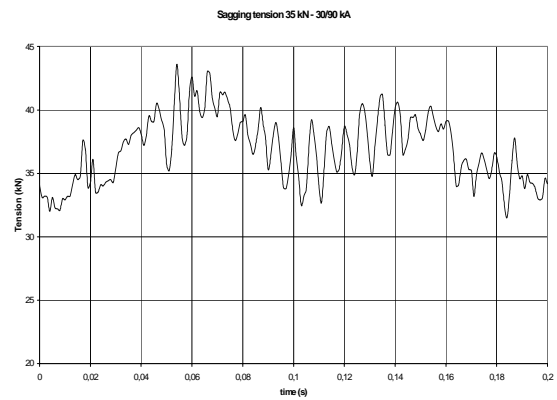
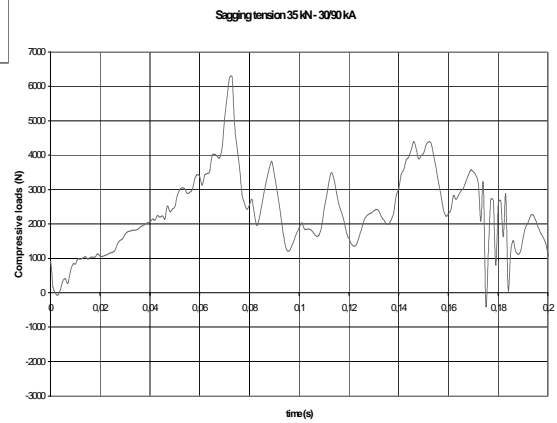
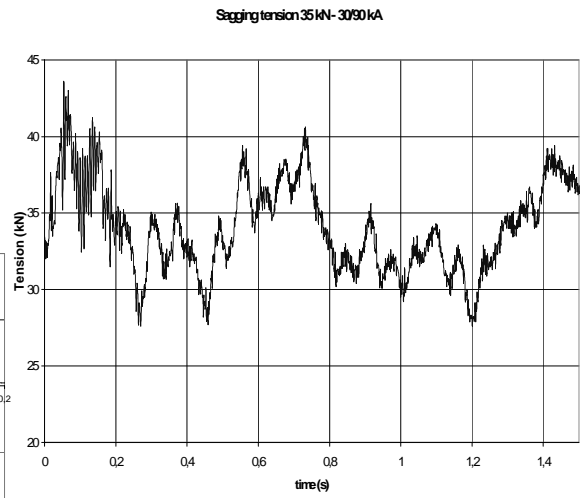
- Configuration One subspan 30 m
- Exact tension/subconductor: 33 kN
- Short-circuit level: 35/90 kA
- Duration: 0.19 s



Configuration :



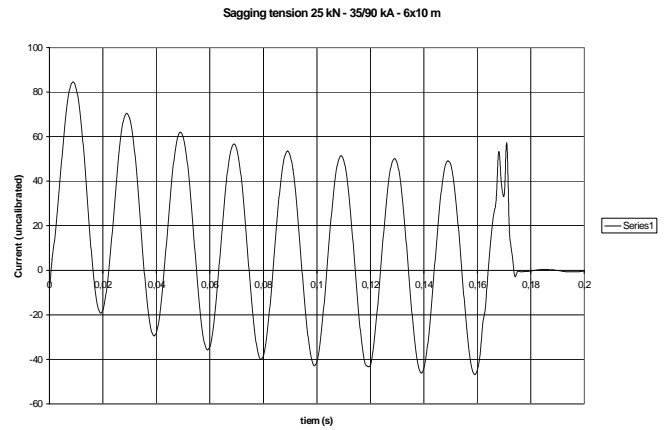
tion :



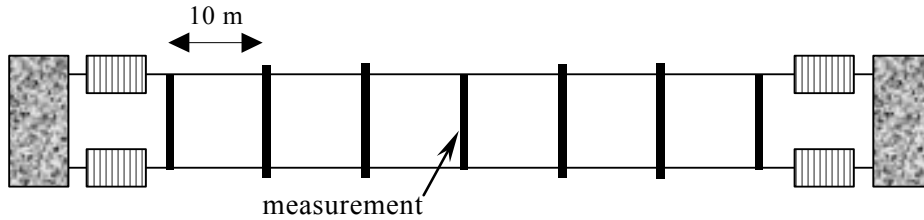
Zoom on spacer compression and tension time evolu-

10.9. CASE V.1 – 6 X 10M – 25 KN – 35/90 KA

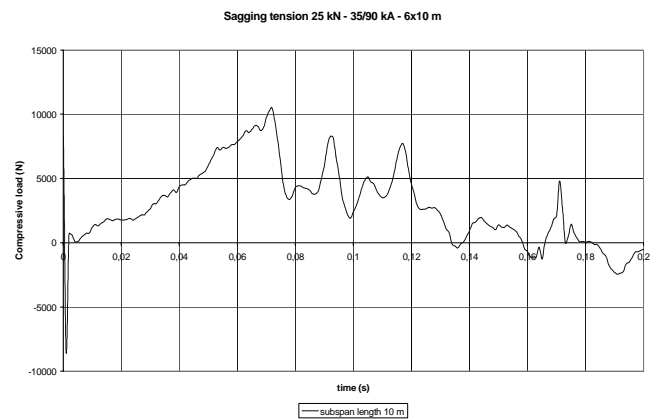
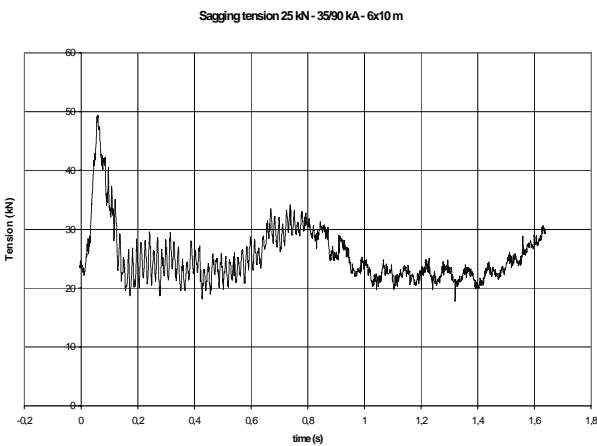
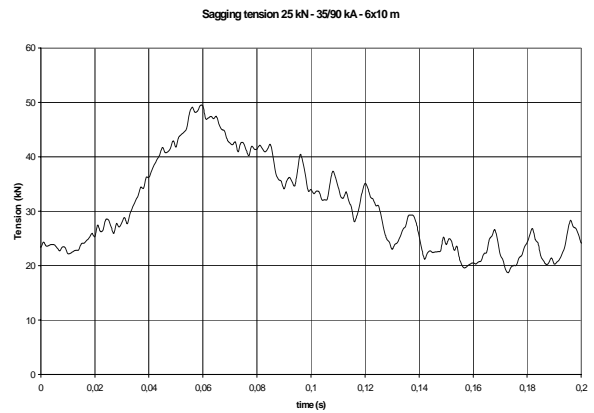
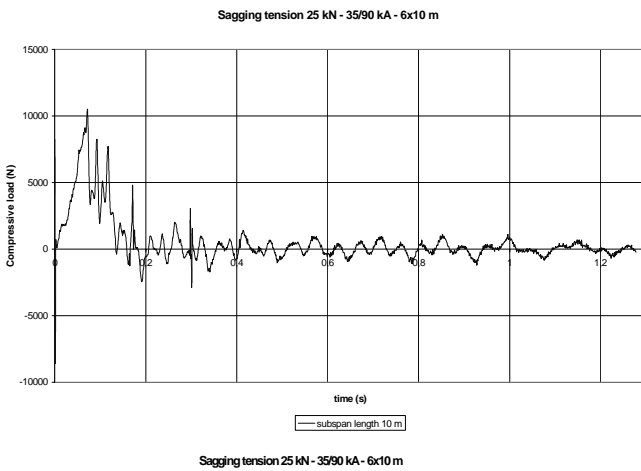
- Configuration One subspan 10 m
- Exact tension/subconductor: 24 kN
- Short-circuit level: 35/90 kA
- Duration: 0.17 s



Configuration :

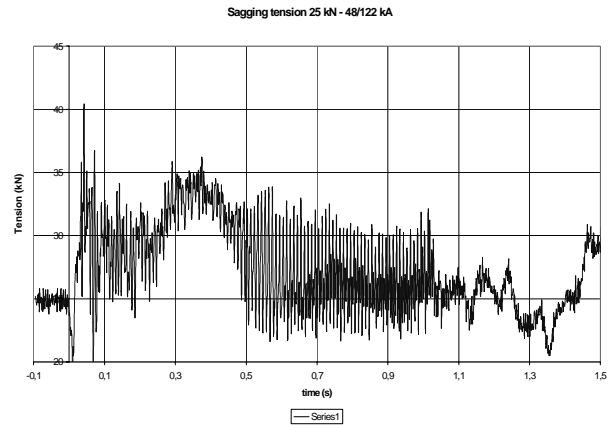
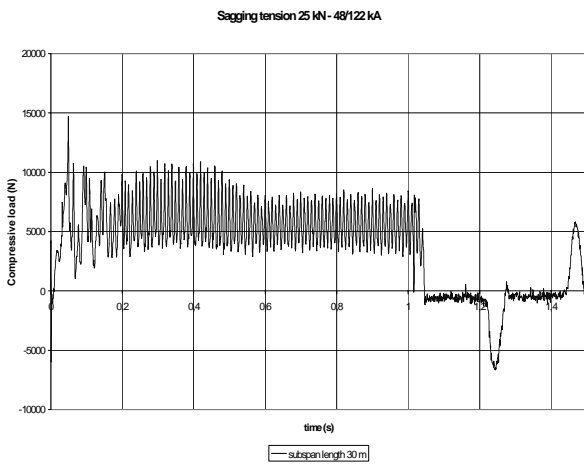
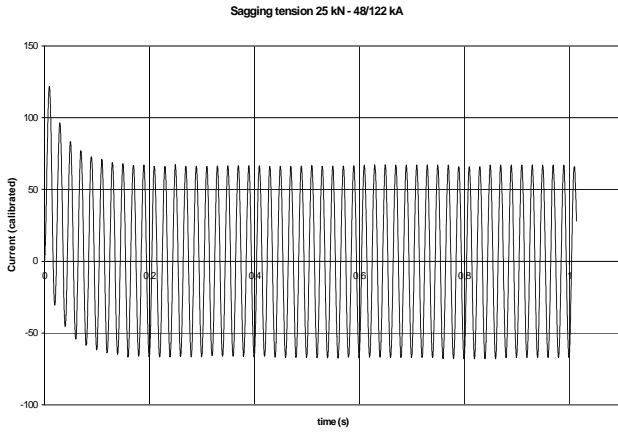


Zoom on spacer compression and tension time evolution :

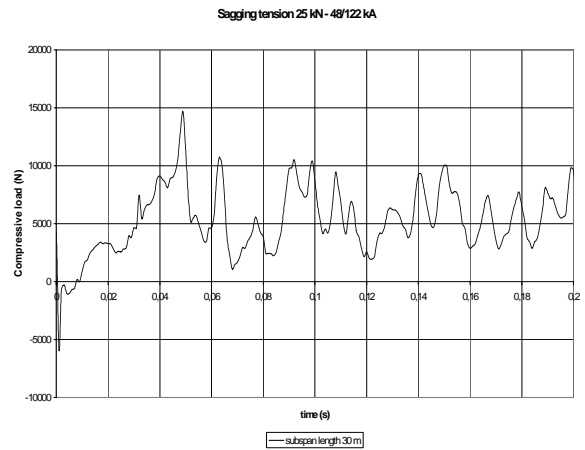
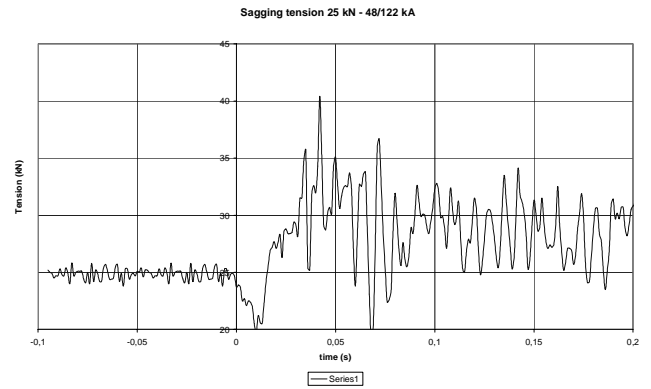


10.10. CASE VI.1 – 2 X 30 M – 25 KN – 48/122 KA

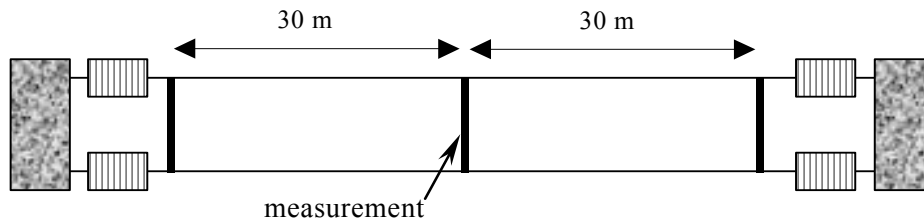
- Configuration One subspan 30 m
- Exact tension/subconductor: 25 kN
- Short-circuit level: 48/ 122 kA
- Duration: 1. S



Zoom on spacer compression and tension time evolution



Configuration :



Copyright © 2002

Tout détenteur d'une publication CIGRE sur support papier ou électronique n'en possède qu'un droit d'usage. Sont interdites, sauf accord express du CIGRE, la reproduction totale ou partielle autre qu'à usage personnel et privé, et toute mise à disposition de tiers, dont la diffusion sur un réseau intranet ou un réseau d'entreprise.

Copyright © 2002

Ownership of a CIGRE publication, whether in paper form or on electronic support only infers right of use for personal purposes. Are prohibited, except if explicitly agreed by CIGRE, total or partial reproduction of the publication for use other than personal and transfer to a third party; hence circulation on any intranet or other company network is forbidden.